STRESS ANALYSIS OF THE ADHESIVE SCARF JOINT BETWEEN DISSIMILAR ADHERENDS

Thesis for the Degree of Ph. D.
MICHIGAN STATE UNIVERSITY
PETHINAIDU SURULINARAYANASAMI
1968

This is to certify that the

thesis entitled

STRESS ANALYSIS OF THE ADHESIVE SCARF JOINT BETWEEN DISSIMILAR ADHERENDS

presented by

Pethinaidu Surulinarayanasami

has been accepted towards fulfillment
of the requirements for

Ph.D. degree in Civil Engineering

James L. Sutton
Major professor

Date 22 July 1968

O-169

ABSTRACT

STRESS ANALYSIS OF THE ADHESIVE SCARF
JOINT BETWEEN DISSIMILAR ADHERENDS

by Pethinaidu Surulinarayanasami

This study determines the adhesive stress distribution in scarf joints between elastically-dissimilar adherends (joined members). Results are presented for five scarf angles; four levels of adherend dissimilarity; three levels of adhesive flexibility in the range appropriate for the bonding of metals and plastics; and for both tensile and bending loading of the joint. The adherends are treated using plane stress, and the adhesive is capable of resisting shear, and normal stress perpendicular to its plane, with strains assumed to be uniform through its (small) thickness. Only linearly elastic behavior is considered.

The Rayleigh-Ritz method is employed to obtain the extensive stress tables presented. Systems of 177 linear equations are solved. This corresponds to the representation of each of the four components of displacement (two elastic bodies) by the sum of all homogeneous polynomials in x and y through the eighth degree. The convergence of the solutions is examined, and the adhesive stress

distributions are discussed exhaustively. Also tabulated are those values of the adhesive combined stresses which are critical for elastic design by some of the common failure criteria. The use of these results in design is outlined.

STRESS ANALYSIS OF THE ADHESIVE SCARF JOINT BETWEEN DISSIMILAR ADHERENDS

By

Pethinaidu Surulinarayanasami

A THESIS

Submitted to
Michigan State University
in partial fulfillment of the requirements
for the degree of

DOCTOR OF PHILOSOPHY

Department of Civil Engineering

1968

ACKNOWLEDGMENTS

The author expresses his sincere appreciation to Dr. James L. Lubkin for suggesting the present research topic, and for his dedicated efforts in advising the author throughout the preparation of this thesis. The author wishes to thank Dr. Robert K. Wen, Dr. William A. Bradley, and Dr. Lawrence E. Malvern for serving on his doctoral guidance committee. Thanks are also extended to the Division of Engineering Research, for supporting the early phases of this research.

TABLE OF CONTENTS

		Page
ACKNOWLEDGMENTS		ii
LIST OF TABLES		v
LIST OF FIGURES		vii
LIST OF APPENDICES		ix
CHAPTER		
I	INTRODUCTION	1
	1.1 General	1
	1.2 Literature Review and Background of the Present Hypotheses	5
	1.2.1 Lap Joints	6
	1.2.2 Scarf Joints	16
	1.2.3 Butt Joints	18
	1.3 The Present Investigation	19
	1.4 Notation	20
II	METHOD OF ANALYSIS	25
	2.1 Formulation of the Problem	25
	2.2 The Rayleigh-Ritz Method	29
	2.2.1 Derivation of Equations	34
	2.3 The Sherman-Lauricella Integral Equation Approach	46
	2.3.1 General	46
	2.3.2 Notation for Integral Equation Method	48
	2.3.3 The Problem Analyzed by Integral Equations	50
	2.4 Numerical Data Assumed in the Calculations	62
	2.5 Computer Programs	65
III	CRITERIA FOR ACCEPTABILITY OF RESULTS; PARTIAL DISCUSSION OF RESULTS	66
	3.1 General	66
	3.1.1 Stress Boundary Condition Check	67

CHAPTER Page

3.1.2 Comparison of Adhesive Stresses Calculated Several Ways From the Results 75
3.1.3 Double-Precision Check of Roundoff Errors 79
3.1.4 Convergence of the Approximating Sequence 81
3.1.5 Overall Equilibrium Check 98

3.2 Confirmation by the Integral Equation Method 104

IV ENGINEERING SIGNIFICANCE OF THE RESULTS . . 107

4.1 Adhesive Normal and Shear Stress Distributions 108
4.1.1 Case of Tensile Loading 110
4.1.2 Case of Bending Load 124
4.1.3 Identical Adherends in Bending . 124
4.1.4 Bending Load (General Case) . . . 135
4.2 Adhesive Combined Stresses 145
4.3 Construction of Design Curves for Scarf Joints with Linearly-Elastic Adhesives 149

V CONCLUSIONS AND SUGGESTIONS FOR FURTHER RESEARCH 154

5.1 Conclusions 154
5.2 Future Research 155

BIBLIOGRAPHY 157

APPENDICES 160

LIST OF TABLES

TABLE		Page
1	Largest boundary condition error (bending)	72
2	Adhesive stresses calculated three ways . .	77
3	Adhesive stresses for 6^{th}-, 7^{th}- and 8^{th}-order polynomials, tensile loading $\alpha = 30°$, $\beta = 20$, $\gamma = 4$	83
4	Tension. $\alpha = 10°$, $\beta = 20$, $\gamma = 4$	84
5	Adhesive stresses for 6^{th}-, 7^{th}- and 8^{th}-order polynomials. Tension. $\alpha = 5°$, $\beta = 20$, $\gamma = 4$	90
6	Bending. $\alpha = 30°$, $\beta = 20$, $\gamma = 4$	90
7	Adhesive stresses for 6^{th}-, 7^{th}- and 8^{th}-order polynomials. Bending. $\alpha = 10°$, $\beta = 20$, $\gamma = 4$	93
8	Bending. $\alpha = 5°$, $\beta = 20°$, $\gamma = 4$	93
9	Disequilibrium of forces and moments	100
10	Sample overall equilibrium checks	103
11	Maximum values of the combined stresses N_1, N_2, T_1 and T_{oy}	147
F1	Adhesive normal and shear stresses	182
F2	Largest values of adhesive normal stress (N_{max}). Locations may be estimated from tables of stress distributions . . .	197
F3	Average difference in adhesive normal and shear stresses between polynomial solutions of orders 8 and 7, or of orders 8 and 6 (latter designated by *) .	198

TABLE Page

F4 Largest difference between 8^{th}- and 7^{th}-order, or 8^{th}- and 6^{th}-order polynomial solutions for adhesive stresses 199

F5 Root-Mean-Square values for percentage differences between 8^{th}-order and lower-order polynomial solutions. 201

LIST OF FIGURES

FIGURE		Page
1a	Lap joint	3
1b	Scarf joint	3
1c	Butt joint	3
1d	Double lap joint	3
2	Adhesive-air boundary in a lap joint . . .	11
3	Mylonas' test	11
4	William's model	11
5	Geometry of Mylonas, McLaren and MacInnes .	11
6	Scarf joint geometry	26
7	Geometry and loading	26
8	Boundary stress errors, tensile loading $\alpha = 10°$, $\beta = 20$, $\gamma = 4$	68
9	Boundary stress errors, bending load $\alpha = 10°$, $\beta = 20$, $\gamma = 4$	69
10	Shear stress (T) by Ritz and integral equation methods	105
11	Normal stress (N) by Ritz and integral equation methods	105
12	Shear stress concentration factor (T_C) in tensile loading	112
13	$(T_C)_{max}$ in tensile loading	112
14	Shear stress concentration factor (T_C) in tensile loading	115

LIST OF FIGURES

FIGURE		Page
1a	Lap joint	3
1b	Scarf joint	3
1c	Butt joint	3
1d	Double lap joint	3
2	Adhesive-air boundary in a lap joint . . .	11
3	Mylonas' test	11
4	William's model	11
5	Geometry of Mylonas, McLaren and MacInnes .	11
6	Scarf joint geometry	26
7	Geometry and loading	26
8	Boundary stress errors, tensile loading $\alpha = 10°$, $\beta = 20$, $\gamma = 4$	68
9	Boundary stress errors, bending load $\alpha = 10°$, $\beta = 20$, $\gamma = 4$	69
10	Shear stress (T) by Ritz and integral equation methods	105
11	Normal stress (N) by Ritz and integral equation methods	105
12	Shear stress concentration factor (T_C) in tensile loading	112
13	$(T_C)_{max}$ in tensile loading	112
14	Shear stress concentration factor (T_C) in tensile loading	115

FIGURE		Page
15	Shear stress concentration factor (T_c) in tensile loading	115
16	Normal stress concentration factor (N_c) in tensile loading	117
17	$(N_c)_{max}$ in tensile loading	117
18	Normal stress concentration factor (N_c) in tensile loading	121
19	Normal stress concentration factor (N_c) in tensile loading	121
20	Normal stress concentration factor (N_c) in tensile loading	123
21	Shear stress (T) in tensile loading	123
22	Shear stress (T) in bending load	126
23	Normal stress (N) in bending load	129
24	Normal stress (N) in bending load	129
25	Shear stress (T) in bending load	136
26	Maximum shear stress (T_{max}) in bending load	136
27	Maximum shear stress (T_{max}) in bending load	138
28	Normal stress concentration factor (N_c) in bending load	140
29	Normal stress concentration factor (N_c) in bending load	143
30	Elastic "design curves" in dimensionless form, for various failure criteria (failure in N_1, N_2, T_1, T_{oy}). Tensile or compressive load	151
31	Elastic "design curves" in dimensionless form, for two failure criteria (N_2, T_{oy}). Bending loads in two senses	153

LIST OF APPENDICES

APPENDIX		Page
A	FORMULATION OF THE EXPRESSION FOR TOTAL POTENTIAL ENERGY	160
B	GENERATION OF RITZ EQUATIONS	162
C	SELF-EQUILIBRATED POLYNOMIAL STRESSES . . .	167
D	DISPLACEMENT DETERMINATION FOR THE INTEGRAL EQUATION APPROACH	170
E	RIGID BODY DISPLACEMENT CONSTANTS	176
F	TABLES OF STRESS DISTRIBUTIONS AND AUXILIARY TABLES	179
G	COMPUTER PROGRAM	202

CHAPTER I

INTRODUCTION

1.1. General

The analysis of adhesive joints has growing importance because of the increasing application of adhesive in industrial and aerospace technology. The applications are usually inconspicuous, but vital to the performance of the bonded objects, whether these be automobile brake linings, the wings of a jet liner, or the ultra-high-strength sheet metal rings of a solid-fuel rocket case. It is essential to pay most attention to the adhesive stresses, because the adhesive is usually the weakest material involved in the joint. With proper design, however, the joint need not necessarily fail in the adhesive.

The adhesive, of course, constitutes a fastening medium between the two adherends (joined members). Some types of adhesive can reasonably be idealized as linearly elastic, and this assumption is used here. This hypothesis is entirely unrealistic[12] for many other adhesives, but even for those with complex rheological behavior, the elastic analysis may offer the designer useful guidance.

Adhesives are employed in many different joint configurations, to bond such materials as metals, plastics, wood and glass to themselves or to each other. The assumptions of the present study make the results applicable primarily to cases where the adherends are considerably more rigid than the adhesive layer, e.g., the bonding of metals and plastics. Some modification of the present approach is required to accommodate glue joints for wood. This might be worthy of study, since the "finger joint" of wood technology is quite similar in geometry to the one considered in this thesis.

The commonest joint configuration is the "lap joint" (Fig. 1a, next page), which is also the easiest one to manufacture. Most previous studies deal with this (see section 1.2, "Literature Review and Background of the Present Hypotheses"). Also of great technical importance is the "scarf joint," with which the present thesis is concerned. The scarf joint connects two bars or sheets on an inclined plane (see Fig. 1b). The scarf angle is usually in the range of 10° to 30°. This joint has the advantage over the lap joint of avoiding the bending action due to the offset of the two members, when the loading is tensile, and the disadvantage of being harder to make. The scarf joint presents a much larger surface area of adhesive for bonding than the conventional "butt joint" (Fig. 1c). The latter is the special case when the "scarf angle" is 90°. A perfect butt joint

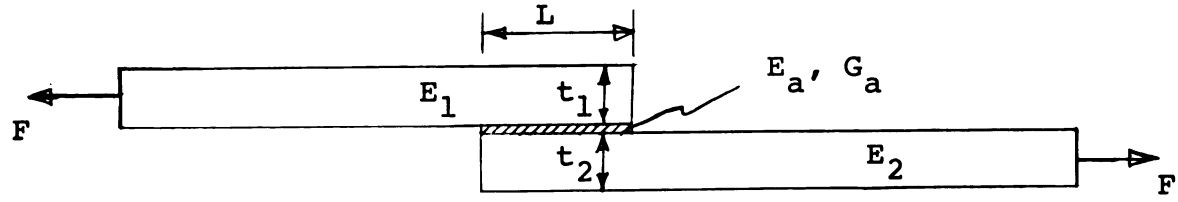

Fig. 1a Lap joint.

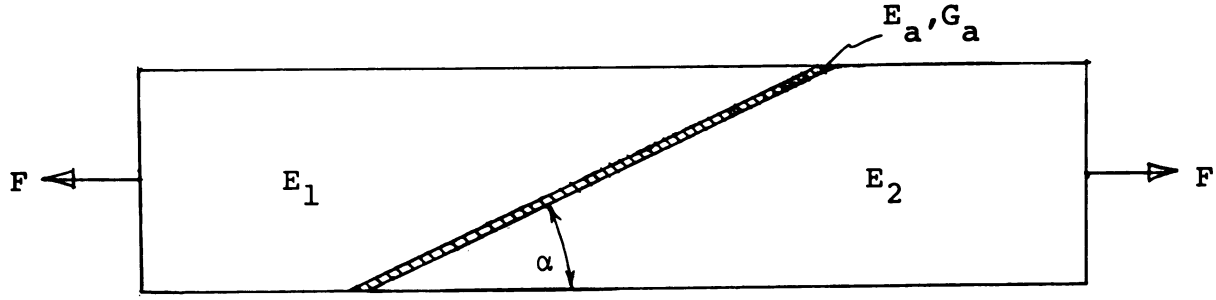

Fig. 1b Scarf joint.

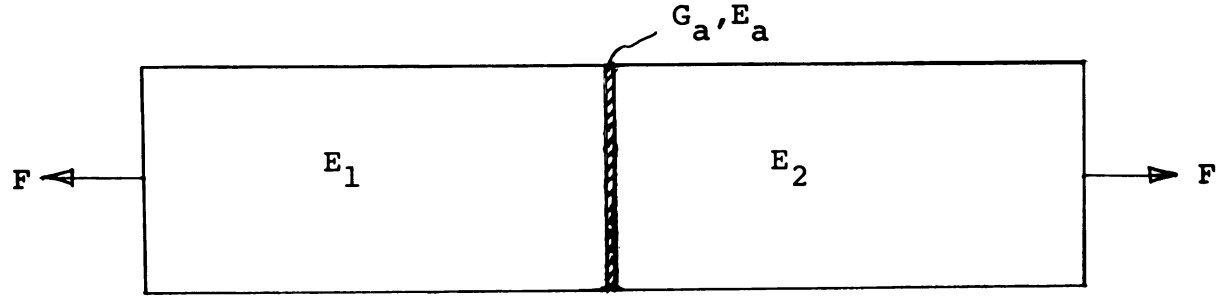

Fig. 1c Butt joint.

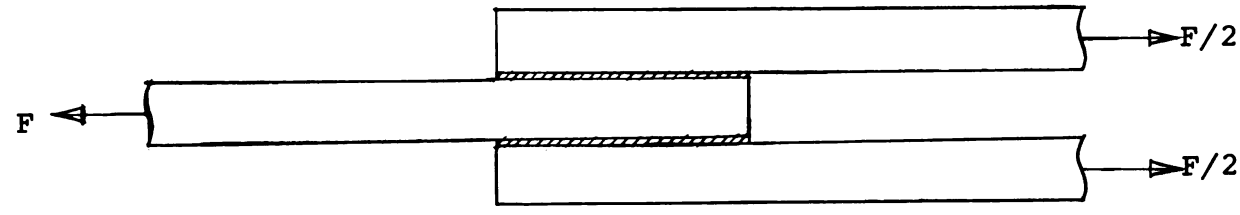

Fig. 1d Double lap joint.

offers a purely tensile loading of the adhesive, but misalignment (which is hard to avoid) can give rise to substantial bending action and corresponding stress concentrations. The scarf joint configuration, with the usual 10°-30° angle, loads the adhesive largely in shear at a moderate stress level.

This thesis follows up a previous study of the scarf joint between identical adherends by investigating the case of dissimilar materials. Prior work, discussed later (Sec. 1.2), indicates that the overall features of the adhesive stress distribution may be obtained by treating the thin adhesive layer as a complex elastic foundation. The latter is assumed to be capable of transmitting shear stress, and normal stress perpendicular to the plane of the adhesive layer. Certain local "edge effects" (stress concentrations) are neglected, as explained subsequently.

The complexity of the present problem, formulated as a boundary-value problem of elasticity theory, appears to preclude an exact solution. Accordingly, the Rayleigh-Ritz method has been used, as the most appropriate for finding answers expeditiously. The method of finite differences is difficult to formulate for this problem, and was abandoned after considerable investigation. An alternate method, described in Muskhelishvili,[4] involves the use of the Sherman-Lauricella integral equation in the complex plane. As utilized here, this approach seems to

require even more computer memory than the considerable amount available in Michigan State University's CDC 3600 computer installation. Thus the method has not been entirely successful, but the computations performed seem to support the results of the Rayleigh-Ritz method.

1.2. Literature Review and Background of the Present Hypotheses

This review is fairly brief because a number of recent surveys are available.[8,9,10,12] Moreover, very little of the work is immediately relevant to the present problem, since it appears that only one previous analysis of scarf jointshas been conducted. There is some literature[12,16, 24,26,30] on experimental work for such joints, mostly from the aerospace field and from wood technology. However most of these involve tests to destruction and it is likely that correlation with the present elastic analysis would only be of the roughest sort.

The studies reviewed, however, serve to validate some of the present hypotheses. They also indicate some of the factors which are neglected in the present type of analysis.

The literature of the "peel test" is not covered here; see References (8,9,10). This test (to destruction) is used for quality control in joint manufacture. It involves large deformations of the adhesive and at least one adherend. The latter is usually peeled off a drum to which

it has been bonded. Since many of the peel test analyses involve the assumption of an elastic adhesive, they are probably not even relevant to the actual peel test, much less to the present study. For convenience, the various past investigations which deal with the stress distribution in adhesive joints have been grouped as follows: a) lap joints, b) scarf joints, and c) butt joints.

1.2.1 Lap Joints

It should be noted that all stress calculations have neglected the adhesive layer thickness in considering the geometry of the problem. This reflects practice; adhesive layers are usually very thin compared to the thickness of the adherends. This sometimes fails to be accurate in the case of the very thin sheets encountered in aircraft construction, but most analyses are readily modified to accommodate the necessary changes. Most theoretical work has been done on the stress distribution in adhesive lap joints. One of the earliest investigators, Volkersen,[11] developed a one-dimensional, elastic-adhesive theory by treating the adhesive joint as an approximate substitute for (limiting case of) the multirow riveted lap joint. He indicates in his analysis, after neglecting the bending of adherends, that the largest adhesive shear stress occurs toward the ends of the overlap region. His analysis includes the case of dissimilar adherends,

and actually applies most accurately to symmetrical double lap joints (Fig. 1d, p. 3), since these involve comparatively little bending. N. A. de Bruyne's[12] analysis is essentially that of Volkersen. Hartman[26] supported some of the theoretical investigations in his tests of double lap joints. N. A. de Bruyne[12] also argues persuasively for the advantages of the bevelled (tapered) lap joint in reducing adhesive shear stress concentration. Sazhin[19] studied the tapered lap joint analytically, and found that it leads to a hypergeometric differential equation. The problem is actually solved using a variational method, but with very few terms and without a discussion of convergence. His reported good agreement with experiments is somewhat suspect, because the experiments are not described and sound suspiciously like ultimate strength tests (in the translation of the original article). It would have to be coincidental that an elastic analysis predicts the behavior of a test to destruction involving the amount of inelastic behavior normally found in adhesive joint failure tests. The tapered lap joint has been investigated experimentally by Hartman,[30] who observed in tests that a tapered lap joint does have a moderately larger ultimate load capacity than the uniform one.

Although the neglect of adherend bending and adhesive normal stress reduces these analytical studies to just one step above "dimensional analysis," they still offer designers considerable guidance as to what to expect. Their

results also explain why adhesive lap joints invariably start failing at the ends, even though, as elastic studies, they cannot be expected to be of much help in studying ultimate strength tests. Nevertheless, these early studies suggested ways of plotting strength test data so as to minimize the total amount of experimental work required to establish system properties (de Bruyne's "joint factor").

Goland and Reissner[13] published a considerably more rigorous analysis. This included the effects of adherend bending, inside and outside the joint, and appears to be the first study to show that large "tearing stresses" arise, concentrating at the ends of the joints. The latter are direct stresses normal to the plane of the adhesive layer. They considered two limiting cases, one of which is relevant to a joint in which the adhesive is much more rigid than the adherends. This applies for certain joints in wood, paper, cardboard, and low modulus plastics. The other limiting case is the one where the adhesive is much more flexible than the adherends, as in metal-to-metal joints. Under this hypothesis, and based upon a consideration of the strain energies of the problem, they argue that it is sufficient to consider only the adhesive shear stress, and the adhesive direct stress normal to the adhesive layer. Most subsequent work (including this thesis) has neglected the longitudinal component of adhesive direct stress, essentially because of the low modulus of the adhesive compared to the adherends.

Their second stress analysis problem was formulated (with minor inconsistencies) as one of cylindrical bending of thin plates (i.e., practically speaking, using elementary beam theory). The first problem, not discussed here because it applies primarily to joints in wood, used plane strain theory. Except for the Goland-Reissner stiff-adhesive (plane strain) case, these investigations all model the adhesive as a uniform elastic foundation capable of transmitting shear (or shear and normal stress) from one adherend to the other.

Plantema[14] modified the Volkersen theory by considering the effect of bending deformation on the adhesive shear stress, arriving at a refined shear stress concentration factor. However, the neglect of normal stress appears undesirable, in view of the results of Goland and Reissner.

Cornell[15] studied the brazed-tab fatigue specimen as a lap joint. His work is closely related to that of Goland and Reissner, although the geometry of the problem is somewhat different. This study constitutes both an extension and a validation of their analysis. His assumption that the two adherends act like beams and that the elastic cement layer behaves like an infinite number of infinitesimal shear and tension springs is simply a restatement of the Goland-Reissner hypothesis. His "cement" was actually a thin layer of braze compound, which perhaps cannot be considered to be flexible enough, relative to metal adherends, to qualify as "much more flexible" than the latter.

His experimental work, however, indicates good agreement with the analysis. This, in turn, simply indicates that Goland and Reissner's energy argument for deciding when the "elastic foundation" model for the adhesive layer will break down is somewhat conservative. It can probably successfully be used for stiffer adhesives than they indicate. Cornell compared his analytical results for adhesive stresses to photoelastic and brittle lacquer experiments.

His study was also one of the first to consider a very significant factor which is entirely neglected in the type of approach used by Goland and Reissner (and in the present thesis). This is the "free-edge effect" at the ends of the joint. The "free-edge effect" is the stress disturbance caused by the complex boundary conditions at the ends of the joint, where adherends and adhesive are adjacent to a stress-free boundary, usually air. Figure 2 (next page), shows such a free boundary in terms of Cornell's geometry. A proper consideration of this problem is enormously complex from the point of view of elasticity theory. This is further complicated by our ignorance of the precise shape of the adhesive-air boundary in practical situations, because the actual boundary shape depends upon the details of the production process, the actual adhesive used, etc. Moreover, the free-edge effect is significant at the point where shear and normal stresses in the adhesive usually take on their largest values, according

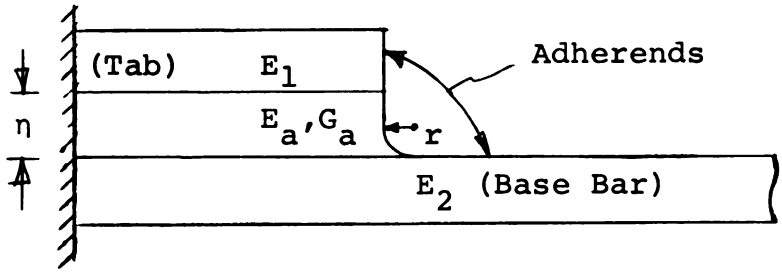

Fig. 2 Adhesive-air boundary in a lap joint.

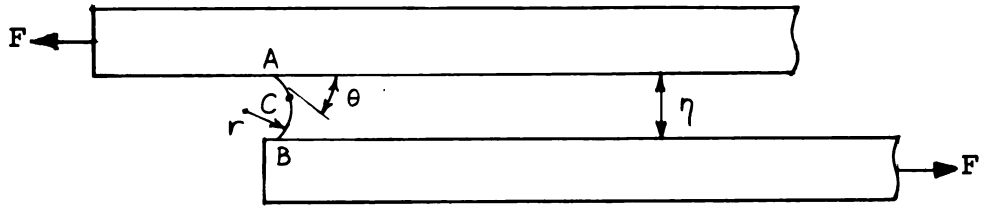

Fig. 3 Mylonas' test.

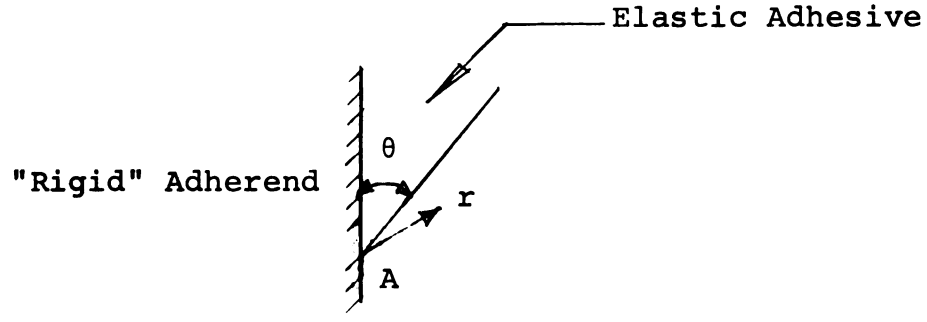

Fig. 4 William's model.

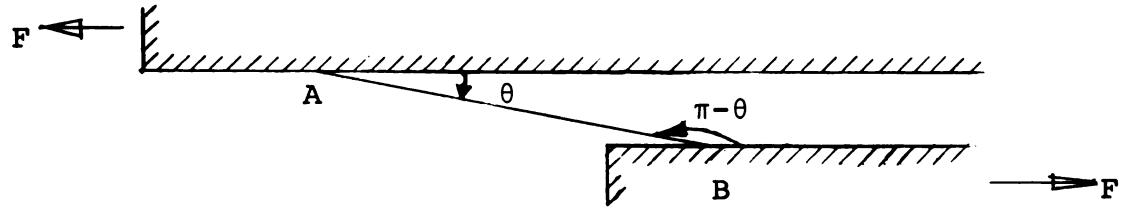

Fig. 5 Geometry of Mylonas; McLaren and MacInnes.

to those approaches which ignore these local effects. As Cornell puts it, the analysis neglecting the free-edge boundary problem has a "built-in fillet," $r > 0$ in Fig. 2. But whether $r = \eta$, 1.7η, 0.2η or any other value depends very much upon manufacturing details. The value of r can of course be investigated statistically for any particular problem important enough to warrant the research costs. We know, at least, that if the adhesive joint is a good one, the fillet radius will be in the sense indicated. This is because a proper bond requires low surface tension: the adhesive must "wet" both of the adherends well.

In Cornell's work, his "adhesive" (brazes and solders) in practice had a radius r about equal to η in Fig. 2, and he bases his discussion on this observation. Though he found fairly good agreement between supporting experiments and the analysis, the main discrepancy was precisely at the free edge. He points out that the stress concentration factor becomes infinite if the tab and the base bar form a right angle, i.e., if the radius of curvature (r in Fig. 2) is zero. This is just another way of saying that stress singularities must be expected at a 90° boundary if shear stress is present on one side and an adjacent edge is stress-free.

To better understand the local effects at free edges, Mylonas[16] conducted photoelastic experiments on transparent plastic layers bonded to "rigid" (steel) plates,

simulating the ends of adhesive lap joints. In effect, his work validates the neglect of free-edge effects, as far as the interior of the joint is concerned. This is what we would also expect from St.-Venant's Principle, since the thickness of the adhesive is normally small compared to the length of overlap. At the joint ends, however, Mylonas finds that the stresses do vary across the thickness of the layer and depend strongly on the shape of the free boundary of the adhesive. He studied models having concave edges in the shape of a circular arc (Fig. 3, p. 11), with ratios of radius r to adhesive thickness η ranging from 0.5 (semicircular edge) to ∞ (straight edge). For the load sense shown, he found that when $r/\eta < 1.25$ ($\theta < 50°$), the maximum stress develops on the adhesive boundary but away from the adhesive-adherend interface ("cohesive failure" expected in the adhesive). For a larger radius, the highest stress level is much larger and develops at the corner, A ("adhesive failure" expected). Generally speaking, his experiments show that the local effects at the free edges are critically dependent upon the shape of these edges.

Mylonas' study correlates well with an investigation, unrelated to adhesive joints, due to Williams.[17] He analyzed thin plates in extension, using generalized plane stress, in order to estimate the strength of the stress singularities which can be expected at the vertex of a semi-infinite triangle (wedge) under various edge boundary

conditions. A typical metal-to-metal joint involves a "nearly-rigid" adherend bonded to a comparatively low-modulus adhesive, so that Fig. 4 (p. 11) approximates the local situation at the adherend-adhesive-air corner in Mylonas' experiments. This corresponds to Williams' boundary-condition case of one edge free and the other edge fixed. He formulated an eigenvalue problem for the rate-of-decay parameter λ, of stress with distance r from point A. All stresses behave as $r^{\lambda-1}$, and all displacements as r^{λ}. The calculations give λ as a function of θ, the wedge angle. According to his results, no stress singularities arise for angles θ less than 63°, but singularities do arise (for general loading) when $\theta > 63°$. This trend is quite similar to what Mylonas found in his experiments. The latter differ in that the steel plates only approximate the ideal "rigid" boundary conditions of Williams.

Misztal[20] studied lap joints in flat sheets loaded by shear flow perpendicular to the plane of the drawing in Fig. 1a (p. 3). He assumed that the shear stress is uniform across the adhesive and adherend thickness, and they deform only in shear, obtaining an adhesive shear stress distribution similar to that of the Volkersen problem. He also examined double lap joints of this type.

McLaren and MacInnes[18] performed photoelastic experiments on lap joints. They found Goland and Reissner's

analytical results to be generally correct, observing an increase in shear and "tearing" stresses towards the ends of the joint. The shear stress, of course, obeys the actual boundary conditions and drops to zero at the ends. They also studied the effect of adhesive-adherend contact angle at the end of the joint, in tests similar to Mylonas'. In this work the adherends are considerably more flexible than in Mylonas' tests (although still stiffer than the adhesive). As "θ," the contact angle, is reduced to about 40°-50° or less, the largest tensile stress moves out of the "leading corner" (adherend-adhesive-air point, A in Fig. 3 (p. 11), on the loaded side) to a point C on the adhesive-to-air boundary. This supports both Mylonas and Williams quite well, considering the somewhat different range of the elastic constants. It is also noted by Mylonas, and by McLaren and MacInnes, that the largest magnitude of stress occurs at B (Fig. 5, p. 11), for the load sense of Figs. 3 and 5. This is compressive in nature, but of course becomes tensile if load F reverses. This is quite consistent with Williams' analytical results, since the stress level exponent $(\lambda-1)$ in $r^{\lambda-1}$ increases with wedge angle. If AB in Fig. 5 is straight and θ is small enough to avoid stress singularities in the adhesive wedge cornering at A, then the obtuse adhesive wedge corner at B is surely large enough for singular stress at B.

Lubkin and Reissner[21] produced an extensive analysis of lap joints between thin, circular, cylindrical shells in axial tension. The investigation was carried out using the linear theory of axisymmetric bending and stretching of thin, isotropic shells. It was again assumed that the adhesive layer is elastic and considerably more flexible than the adherends. The work is basically along the lines of the Goland and Reissner approach, with due allowance for the new geometry. The paper contains considerable discussion of the following: (1) effect of amount of overlap on adhesive stress concentration values, (2) position of maximum adhesive normal and shear stress, and (3) effect of flexibility of adhesive layer on stress concentration values. An instructive comparison is made between tubular and flat-plate lap joint theories.

Sherrer[22] has investigated the stress distribution in lap joints when the adherends are dissimilar, as an extension of Goland and Reissner's analysis. He obtained a series solution for the stresses in the joint, but had difficulties because of slow convergence. Sazhin[19] also studied the lap joint, apparently unaware that he was duplicating the work performed by Goland and Reissner 20 years earlier--at least he does not acknowledge priority.

1.2.2 Scarf Joints

Lubkin[7] considered an adhesive scarf joint between elastically-identical adherends, loaded in tension. With

the assumption that the thickness of the adhesive is negligibly small compared to the depth of the adherends, it is found that the adhesive stress distribution is uniform from end to end. Moreover, the uniformity of adhesive shear and normal stress (both of the latter are considered here) is independent of the scarf angle and of the thickness of adhesive and adherend. The stresses themselves, of course, depend on the scarf angle. This simple state of stress can therefore be calculated directly from equilibrium considerations. Its simplicity arises from the symmetry of the identical adherends, and of the purely tensile load. (If the loading is pure bending, for example, this symmetry is lost and it can be shown that it is impossible for the adhesive stress to vary linearly along the joint.) He presented results useful to the designer within the elastic range. These can probably be applied in the "wood" range of elastic constants also, because both of the adhesive normal stresses have been taken into account. Due to the fortunate uniformity of the adhesive stresses along the adhesive layer, it is possible to speculate that they remain sensibly uniform when the adhesive no longer behaves elastically. The paper therefore had some success in correlating actual failure tests, using what was originally intended to cover only the elastic range. It is not to be expected that the present thesis can be used in this manner, since the stress distributions found here are generally not uniform along the joint.

The present investigation is an extension of Lubkin's work, covering the more complex case of dissimilar adherends.

Cooper[12] measured the adherend strains in a scarf joint with an extensometer. He estimated a stress concentration factor of 1.45 in a joint with a scarf angle of 6° (identical adherends), but the definition of this factor is not clear enough to permit a comparison with Ref. 7. Müller[24] and Hartman[26] performed purely experimental work on scarf joints tested to destruction. Hartman's work was correlated with theory in Ref. 7.

1.2.3 Butt Joints

The "butt" joint is the name given to the special case of the 90° scarf joint (Fig. 1c, p. 3). de Bruyne[27] formulated a relation based on viscous flow theory to indicate that, for very thin adhesive layers, the joint strength is inversely proportional to its thickness. This is found to have good agreement with experimental results, although perhaps not for the theoretical reasons adduced. Shield,[28] using limit analysis, investigated bounds on the joint strength of a butt joint. Norris[29] assumed that the adhesive in the bond is isotropic, and that the strains in the adhesive, parallel to the plane of the bond, are equal to those in the adherends. He developed a method for the determination of the elastic properties of adhesives as they actually exist in bonds. He substituted these properties

in the formula for determination of the stress at which instability becomes general throughout the bond, and this stress is compared with the results of tests.

1.3. The Present Investigation

The purpose of this study is to obtain detailed information on the stress pattern in the adhesive of scarf joints between elastically-dissimilar materials, for a variety of parameters and loading conditions. The problem is treated as one of plane stress, with the assumption (reflecting most practical cases) that the adhesive layer is negligibly thin when compared to the adherends. A considerable number of different approaches have been attempted; only the relatively successful ones are reported.

As formulated here, the problem consists of finding a set of unknown internal boundary conditions for two different plane elastic bodies of trapezoidal shape. It appears that the method of finite differences is not well suited, partly because of the present complexity of shapes and boundary conditions. Of itself, this is not so bad. The major problem is that the model adopted for the adhesive almost demands that the solution be carried out in terms of displacements, which implies four Navier equations in two adherends. Moreover, the nature of the Navier equations is such that interlocking nets of node-points are required in each elastic body. The primary method selected, therefore, is the Rayleigh–Ritz method, a direct approach to

variationally-formulated problems. There is no reason to expect this to yield results inferior to the method of finite differences, and perhaps some reason to expect it to be better.

In addition, the problem has been studied using an elegant approach based upon the Sherman-Lauricella integral equation in the complex plane.[4] This method is so radically different in concept from the Ritz method that good agreement would constitute an independent check on the results of the Ritz method. Unfortunately, just when agreement appears to be getting good, the integral equation formulation exceeds the capacity of the computer. It has, therefore, not been pursued extensively.

The details of the method of analysis, including the mathematical formulation of the problem and the various parameters arising in the investigation, are given in Chapter II. Chapter III is devoted to a discussion of the checks used to validate the results.

1.4. Notation

The symbols used in this thesis are defined in the text while they first appear. For convenience, they are also listed here in alphabetical order, with English letters preceding Greek letters. There are many symbols which are common to both the Rayleigh-Ritz method and the integral equation approach, but these occasionally represent slightly

different quantities. A separate notation section is therefore given for the integral equation method in section 2.3.2. The present section gives the list of all symbols common to both methods, and conveying the same meaning. Other symbols used in Chapters III and IV are also included here.

Subscripts 1 and 2 almost always represent quantities defined for adherends 1 and 2, respectively. Figure 7, p. 26 shows many of the geometric quantities.

$A'_{m,n}$, $B'_{m,n}$, $C'_{m,n}$, $D'_{m,n}$ = Coefficients of displacement functions $(u_1,v_1),(u_2,v_2)$ of 1st and 2nd adherends, respectively.

$A_{m,n}$, $B_{m,n}$, $C_{m,n}$, $D_{m,n}$ = Coefficients of dimensionless displacement functions $(U_1,V_1),(U_2,V_2)$ of 1st and 2nd adherend, respectively.

c = $h(2 + \cot \alpha)$(see Fig. 7).

C = $2 + \cot \alpha$, (dimensionless value of c for $h = 1$).

E = Young's modulus.

E_1, E_2 = Young's moduli.

E_a = Young's modulus of adhesive.

F = Resultant axial tensile force per unit width of adherend (Figs. 1-7).

G_a = Shear modulus of adhesive.

h = Adherend half-thickness.

L_1 = See Fig. 7.

M_0 = Bending moment per unit width of adherend (Figs. 6,7).

M = Highest order of homogeneous polynomials.

n,s = Coordinate directions (Fig. 7).

N = Adhesive normal stress (dimensionless).

N_C = Adhesive normal stress concentration factor.

N_j = N evaluated at X_j,Y_j.

N_1,N_2 = Adhesive principal stresses.

S = $s/h \cot \alpha$ = fraction of joint length along adhesive interface, measured from midpoint (origin).

T = Adhesive shear stress (dimensionless).

T_C = Adhesive shear stress concentration factor.

T_j = T evaluated at X_j,Y_j.

T_1 = Adhesive principal shear stress.

T_{0y} = Adhesive octahedral shearing stress.

$U_s', U_{sa}', U_{s1}', U_{s2}'$ = Strain energy of whole system, adhesive, 1st adherend, 2nd adherend.

U_s, U_{sa},

U_{s1}, U_{s2} = Dimensionless strain energy of whole system, adhesive, 1st adherend, 2nd adherend.

u, v = Displacement components in x- and y- direction.

u_1, v_1,

u_2, v_2 = Displacement components of adherends in x-, y- directions.

U_1, V_1,

U_2, V_2 = Dimensionless displacement components in X-, Y- directions.

W' = Total potential energy of the system.

x, y = Coordinates.

X, Y = x/h, y/h (nondimensional coordinates).

X_j,Y_j = Coordinates of particular points along adhesive interface.

$\bar{X}$, $\bar{Y}$ = Surface tractions in X-, Y- directions.

ν = Poisson's ratio.

ν_1, ν_2 = Poisson's ratios.

α = Scarf angle.

β = $\eta E_1/E_a\ h(1 - \nu_1^2)$ = relative stiffness of adhesive and adherend 1.

γ = $E_2(1 - \nu_1^2)/E_1(1 - \nu_2^2)$ = relative stiffness of adherends.

η = Adhesive film thickness.

Ω' = Total potential energy.

ω = $(1 - \nu_1^2)\Omega'/E_1h^2$ = dimensionless total potential energy.

ε_a, γ_a = Adhesive normal and shear strains.

σ_{XO} = External tensile stress loading adherends (=F/2h), or outer-fiber value of bending stress loading adherends ("M_0h/I").

σ_x, σ_y, τ_{xy} = Usual components of stress.

$\sigma_0(Y)$ = $\sigma_x(\pm c,y)/E_1$ = dimensionless end stresses loading scarf joint system.

σ_n = Adhesive normal stress.

τ_{ns} = Adhesive shear stress.

Miscellaneous

T_0, N_0 = (Eq. 4.1.1).

N_{com} = Any one of the adhesive combined stresses N_1, N_2, T_1, T_{0y}.

$\sum$ = $1/N_{com} = \sigma_{XO}/\sum_a$.

$\sum_a$ = Any allowable (design) value for the adhesive combined stresses.

CHAPTER II

METHOD OF ANALYSIS

This chapter further describes the physical problem and the methods used to investigate it.

2.1. Formulation of the Problem

The scarf joint considered here is shown in Fig. 6 (p. 26). It consists of two elastic adherends, joined together by a thin film of adhesive along the inclined face. The depth of the adherends away from the joint is uniform and equal to 2h, while that of the adhesive is η, also uniform and assumed to be very small compared to 2h. The values of Young's modulus and Poisson's ratio for adherends 1 and 2 are E_1, ν_1, and E_2, ν_2. The adhesive is assumed to be elastic, with Young's modulus E_a and shear modulus G_a. The scarf angle is α, and the joint is subjected to either tensile force F or bending moment M_0, both per unit width. These are typical loadings for this type of joint.

The actual geometry selected for the boundary is shown in Fig. 7 (p. 26). The practical reason for using an adhesive scarf joint is to increase the size of the adhesive area, so that the adhesive--a weak material--can

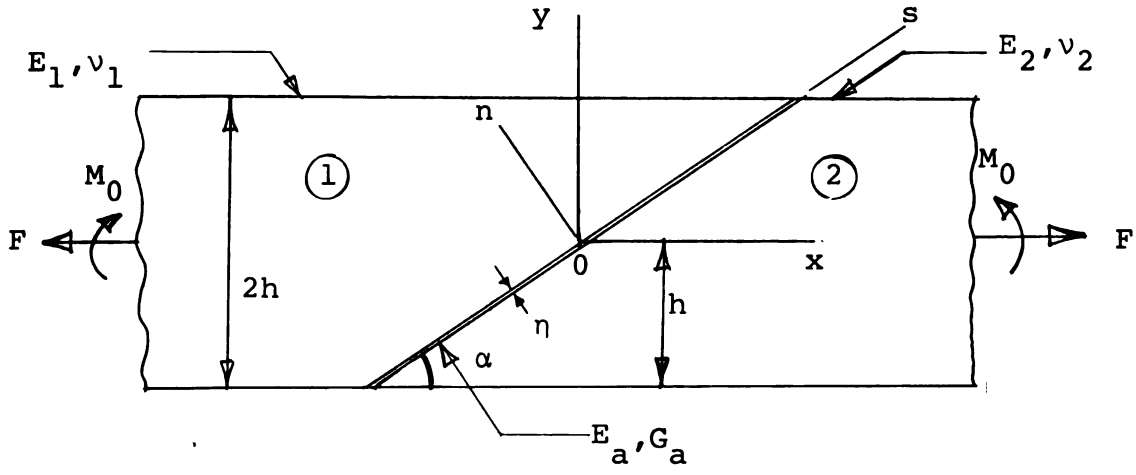

Fig. 6 Scarf joint geometry.

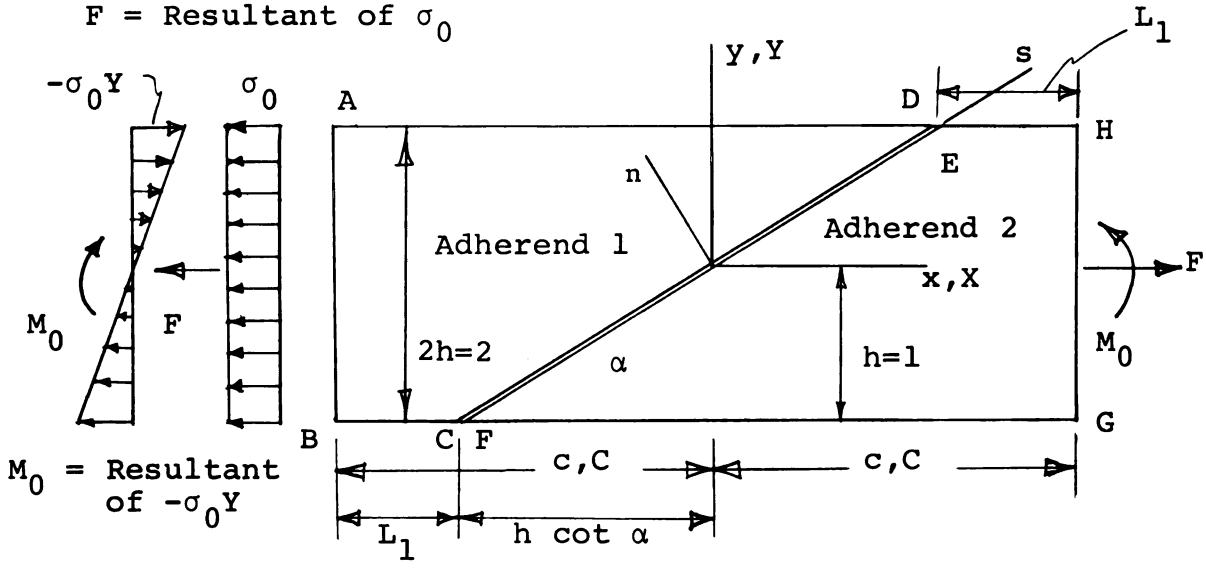

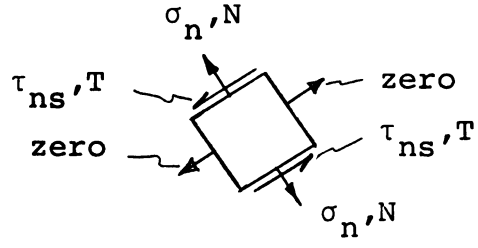

Positive Adhesive Stress Definitions

Fig. 7 Geometry and loading.

sustain lower stresses (stress concentration, of course, can defeat this objective). For this reason α is usually less than 25-30°. The lower limit, perhaps in the range 5-10°, is occasioned by the difficulty of manufacturing straight, finely-tapered edges, especially in thin adherends.

The geometry chosen for the mathematical study of the problem is inherently a compromise. Remote from the joint, there is uniform tension parallel to x. Near the joint, the stress pattern is greatly disturbed, except in the case of identical adherend materials. It is therefore judged important to allow a certain distance L_1 for this disturbance to reduce to the remote uniform bending or tensile field, which is the ultimate end-boundary condition. A trapezoidal shape for each adherend therefore appears to be essential, if the problem is not to be idealized out of existence. The latter would be the case if only triangles adjacent to the adhesive interface were considered ($L_1 = 0$). Conceivably, a parallelogram shape could also be used.

As explained in the introduction, the present type of study attempts only to describe the overall behavior of the joint, and is admittedly imprecise at the free ends of the adhesive. The adhesive-adherends-air boundary must have a clearly-specified geometry before this complex local problem can be attempted. Reasonable assumptions here depend very much upon the actual materials used and precise

manufacturing details. Some of the questions which must then be asked are as follows: Was surplus adhesive wiped off before curing? Machined off after curing? Left alone? Did bonding pressure squeeze any adhesive out? Was there enough adhesive initially? How much adhesive shrinkage was there? At best, these can only be answered statistically, in individual applications whose importance warrants the expense. Nevertheless, the present type of study offers the designer a comparative framework into which he can fit empirically-determined constants (stress at yield, or some such index) for his own particular case. It also offers information about general trends, and the effects of variation of physical parameters.

It is assumed that the adhesive is very thin, and quite flexible compared to the adherends in the metal-to-metal joints at which this study is aimed. The adhesive strains and stresses are therefore taken to be uniform across its thickness, and the direct adhesive stress in the joint axial direction (s - direction in Fig. 7, p. 26) is ignored. To justify this neglect, note that the adhesive is assumed to have a much smaller Young's modulus than that of the adherends. The model used for the adhesive is thus that employed by most previous investigations, and validated by the experiments of Cornell, Mylonas and others. Essentially, it is an elastic foundation, capable of transmitting shear as well as transverse normal stress. The

chief discrepancy in treating the adhesive is the neglect of the local free-edge effects at the ends of the boundary, which is a proper subject of separate study. The idealized problem thus consists of two two-dimensional elastic trapezoids with different elastic moduli, interacting with each other through a complex elastic foundation, the adhesive layer. The exterior boundary conditions (Fig. 7, p. 26) are that the top and bottom surfaces of the system are free of stress ($\sigma_y = \tau_{xy} = 0$). In addition, the ends are loaded by uniform tension (σ_0) or pure bending with linear stress distribution ($-\sigma_0 \cdot y$). The quantities sought are the unknown adhesive shear and normal stress distributions, which constitute a set of unknown interior boundary conditions. This, plus the fact that we are dealing with two different elastic solids of trapezoidal shape, accounts for the peculiar difficulty of obtaining good solutions to this problem.

2.2. The Rayleigh-Ritz Method

Boundary-value problems in the linear theory of elasticity may be solved using the Theorem of Minimum Potential Energy in conjunction with the variational calculus. This theorem states that: "Of all continuous (compatible) displacement fields satisfying the given boundary conditions, the actual, equilibrium state of displacement is such as to minimize the total potential energy of the system." Thus, the input to this theorem must be a compatible displacement

field, satisfying (as forced conditions) internal continuity and any prescribed displacements on the boundary. Then the statement of the theorem itself furnishes the conditions of equilibrium for the problem to which it is applied. For a linear problem, it is known that the single stationary value of total potential energy is a minimum, so that rendering it stationary is equivalent to minimizing it.

In using this theorem, the total potential energy is normally expressed in terms of displacements, which must be differentiated to find the stresses when the latter are sought. The loss of significance associated with differentiation makes it desirable to work with other minimum principles, in most cases where approximate stress solutions are contemplated. Here, however, the stresses sought are those in the adhesive, which will soon be expressed directly as differences in the displacement of the adherends at the adhesive-adherend interfaces. Since no differentiation is required in the present case, the use of the Minimum Potential Energy Theorem appears to be quite appropriate.

The total potential energy Ω' of a region R in plane stress can be expressed as

$$\Omega' = U_s' + W' \qquad 2.2.1$$

where U_s' is the strain energy and W' is the potential energy of the external forces:

$$U_s' = \frac{E}{2(1-\nu^2)} \iint_R \left\{ \left(\frac{\partial u}{\partial x}\right)^2 + \left(\frac{\partial v}{\partial y}\right)^2 + 2\nu \frac{\partial u}{\partial x} \frac{\partial v}{\partial y} + \frac{(1-\nu)}{2} \left(\frac{\partial u}{\partial y} + \frac{\partial v}{\partial x}\right)^2 \right\} dx\, dy \qquad 2.2.2$$

$$W' = \int_{C'} (u\bar{X} + v\bar{Y})\, ds'$$

Here C' represents that portion of the boundary where external forces are specified and displacements are not, and s' is an arc variable on the boundary C' of region R. The notation is otherwise a standard one: u, v are displacements, and $\bar{X}$, $\bar{Y}$ are the x- and y- traction components.

In terms of the calculus of variations, the equilibrium content of the Theorem of Minimum Potential Energy may be expressed as the vanishing of the first variation, $\delta\Omega' = 0$. The Rayleigh-Ritz method is commonly used for finding approximate solutions in such variational problems. It consists of the following steps. First, select a set of functions $f_i(x,y)$ which satisfy the necessary continuity conditions and the essential or forced boundary conditions. This set f_i must be "complete" in the mathematical sense. From the f_i, an "approximating sequence" ϕ_n is constructed. Form:

$$\begin{aligned} \phi_1 &= f_0 + c_1 f_1 \\ \phi_2 &= f_0 + c_1 f_1 + c_2 f_2 \qquad 2.2.4 \\ &- - - - - - - - - - - \\ \phi_n &= f_0 + \sum_{i=1}^{n} c_n f_n \end{aligned}$$

where f_0 is used to satisfy all forced boundary conditions and the rest of the terms of ϕ_n can therefore satisfy homogeneous conditions. The c_i are undetermined parameters. Next, these functions are inserted into the functional to be rendered stationary (here, the total potential energy, Ω'), and any necessary integration is carried out. Finally, the functional is minimized with respect to the parameters c_i. Thus the best approximation possible within the family of ϕ_n is obtained from the minimizing conditions

$$\frac{\partial \Omega'}{\partial c_i} = 0 \qquad i = 1,2,\ldots,n \qquad 2.2.5$$

In a linear problem with a quadratic functional, such as the present one, the above procedure generates a symmetric system of n simultaneous linear equations, if n parameters (c_i) are used. An approximate solution for the given problem is arrived at by substituting the values of the parameters thus determined into the assumed function ϕ_n. The procedure is essentially the same if (as in the present case) the functional being minimized depends upon several functions (four displacement components for two bodies).

The critical question is always one of convergence. It is necessary to check that the desired quantities approach a limit as n is increased, and to verify as well as possible that this limit is theoretically the true solution for the problem in question. It is also important to check

that roundoff errors do not accumulate, in calculations such as these, which may involve large numbers of equations.

Ideally, the approximating sequence in the Ritz method consists of functions orthogonal over the region of interest, to simplify the inevitable integrations. The present problem involves two trapezoidal regions, and suitable orthogonal functions are not easily found. They can be constructed, but it seems more practical to trade simplicity of computer programming and more equations against the substantial difficulties of constructing a set of orthogonal functions. Accordingly, homogeneous xy-polynomials are used below.

In assuming a purely polynomial solution, it is recognized that no account is taken of the possibility of stress singularities at the four adherend "wedge corners" adjacent to the adhesive layer. Singular stresses do not necessarily imply singular displacements, of course. If the proper displacement variation corresponding to stress singularities can be introduced as part of the assumed Ritz function, relatively few equations must be solved. Unfortunately, the eigenfunction method used by Williams[17] does not seem to extend readily to the present case, which is considerably more complex. Where he dealt with a single wedge, the present problem involves two adjacent wedges coupled by an elastic foundation of a complex type. It appears that the elastic foundation model is too distant

an idealization of an elastic solid to permit a treatment along his lines. It has not been possible thus far to deduce the correct stress singularities (if any are present, which the results show to be likely). As a result, very large numbers of polynomial terms have had to be introduced, in order to obtain good approximations for the locally-high displacement gradients which accompany stress singularities.

Other variational methods have been considered, principally the method of Kantorovich.[3] This does not seem well adapted to a trapezoidal region, because it appears to require the solution of a large system of simultaneous, ordinary differential equations with variable coefficients.

2.2.1 Derivation of Equations

Only the principal features are given here; additional details appear in Appendices A and B. Primes are used at first to denote dimensional quantities, and are later removed during the changeover to non-dimensional variables.

The x- and y- displacements of adherend 1 are designated u_1, v_1 (respectively), and for adherend 2, as u_2, v_2 (Fig. 7). When resolved in the n- and s- directions along adherend-adhesive interfaces, the displacement components are referred to as u_{n1}, u_{s1}, u_{n2}, u_{s2}. With the assumption that the two adhesive strains considered are uniform across its thickness

$$\gamma_a = \frac{(u_{s2} - u_{s1})}{\eta} \qquad 2.2.6a$$

$$\varepsilon_a = \frac{(u_{n1} - u_{n2})}{\eta} \qquad 2.2.6b$$

The strain energy of the adhesive, U'_{sa}, is obtained by considering an infinitesimal length ds along the inclined adhesive face. The corresponding volume is = $(\eta \cdot ds)\ 1$, where η is the thickness of the adhesive. Allowing for adhesive transverse normal strain and shear strain, and integrating along the joint from end to end:

$$U'_{sa} = \int_{-s_0}^{s_0} \left(\frac{E_a \varepsilon_a^2}{2} + \frac{G_a \gamma_a^2}{2} \right) \eta \, ds \qquad 2.2.7$$

Substituting equations 2.2.6a, 2.2.6b for γ_a, ε_a into 2.2.7, we obtain

$$U'_{sa} = \frac{1}{2\eta} \int_{-s_0}^{s_0} \left[E_a (u_{n1} - u_{n2})^2 + G_a (u_{s2} - u_{s1})^2 \right] ds \qquad 2.2.8$$

But

$$u_{n1} - u_{n2} = (v_1 - v_2) \cos \alpha - (u_1 - u_2) \sin \alpha \qquad 2.2.9a$$

$$u_{s2} - u_{s1} = (u_2 - u_1) \cos \alpha + (v_2 - v_1) \sin \alpha \qquad 2.2.9b$$

Substitution of equations 2.2.9a-b into 2.2.8 results in

$$U'_{sa} = \frac{1}{2\eta} \int_{-s_0}^{s_0} \Big\{ G_a \Big[(v_2 - v_1)^2 \sin^2\alpha + (u_2 - u_1)^2 \cos^2\alpha + 2(v_2 - v_1)(u_2 - u_1) \cos\alpha \sin\alpha \Big] + E_a \Big[(v_1 - v_2)^2 \cos^2\alpha + (u_1 - u_2)^2 \sin^2\alpha - 2(v_1 - v_2)(u_1 - u_2) \sin\alpha \cos\alpha \Big] \Big\} ds$$

Rearranging and substituting $ds = dy/\sin\alpha$, we get 2.2.10

$$U'_{sa} = \frac{1}{2\eta \sin\alpha} \int_{-h}^{+h} \Big[(u_1 - u_2)^2 (E_a \sin^2\alpha + G_a \cos^2\alpha) + (v_1 - v_2)^2 (E_a \cos^2\alpha + G_a \sin^2\alpha) + 2(u_1 - u_2)(v_1 - v_2) \cdot \cos\alpha \sin\alpha (G_a - E_a) \Big] dy \qquad 2.2.11$$

The remaining strain energy terms consist of two expressions of the form 2.2.2, with subscripts appropriate for adherends 1 and 2.

On the exterior boundary, only tractions are specified: the top and bottom surfaces of the adherends are stress-free, and the outer ends of the trapezoids are loaded by either pure tension or pure bending. Thus there are no forced conditions on displacement, other than the normal requirement that the rigid displacement of the system be properly specified. Therefore, using polynomials, the four unknown displacements are taken in the (dimensional) form

$$u_1 = \sum_{m=0}^{M} \sum_{n=0}^{M-m} A'_{m,n} x^m y^n \qquad 2.2.12a$$

$$v_1 = \sum_{m=0}^{M} \sum_{n=0}^{M-m} B'_{m,n} x^m y^n \qquad 2.2.12b$$

$$u_2 = \sum_{m=0}^{M} \sum_{n=0}^{M-m} C'_{m,n} x^m y^n \qquad 2.2.12c$$

$$v_2 = \sum_{m=0}^{M} \sum_{n=0}^{M-m} D'_{m,n} x^m y^n \qquad 2.2.12d$$

Note that these double sums actually represent the sum of all polynomials homogeneous in x and y, from a constant to the highest order M. If the double sum went to M on both upper limits, a great many additional terms would be included. However, it is likely that these would contribute little to accuracy, and difficulties with Ritz matrix condition could well be anticipated. These displacement functions are next substituted into the total potential energy per unit width of joint in the z- direction. See Appendix A for details; the main item omitted in the derivation to this point is the potential energy of the external loading.

$$\Omega' = \frac{E_1}{2(1-\nu_1^2)} \iint_{①} \left[\left(\frac{\partial u_1}{\partial x}\right)^2 + \left(\frac{\partial v_1}{\partial y}\right)^2 + 2\nu_1 \frac{\partial u_1}{\partial x} \frac{\partial v_1}{\partial y} + \frac{(1-\nu_1)}{2} \left(\frac{\partial u_1}{\partial y} + \frac{\partial v_1}{\partial x}\right)^2 \right] dx\, dy + \frac{E_2}{2(1-\nu_2^2)} \iint_{②} \left[\left(\frac{\partial u_2}{\partial x}\right)^2 + \left(\frac{\partial v_2}{\partial y}\right)^2 + 2\nu_2 \frac{\partial u_2}{\partial x} \frac{\partial v_2}{\partial y} + \frac{(1-\nu_2)}{2} \left(\frac{\partial u_2}{\partial y} + \frac{\partial v_2}{\partial x}\right)^2 \right] dx\, dy$$

$$+ \frac{1}{2\eta \sin\alpha} \int_{-h}^{+h} \Big[(u_1 - u_2)^2 (E_a \sin^2\alpha + G_a \cos^2\alpha)$$

$$+ (v_1 - v_2)^2 (E_a \cos^2\alpha + G_a \sin^2\alpha)$$

$$+ 2(u_1 - u_2)(v_1 - v_2) \sin\alpha \cos\alpha \, (G_a - E_a) \Big] dy$$

$$+ \int_{-h}^{+h} \sigma_x(-c,y) u_1(-c,y) dy - \int_{-h}^{+h} \sigma_x(c,y) u_2(c,y) dy$$

$$c = 2h + h \cot\alpha \qquad 2.2.13$$

The double integrals, one for each adherend, are strain energy expressions of the form 2.2.2; the next integral represents the adhesive strain energy 2.2.11; and the last two terms are the potential energy of the only nonvanishing external tractions, $\sigma_x(\pm c,y)$, at the end boundaries of the joint.

The energy expressions are now converted to a nondimensional form. Let

$$U_i = \frac{u_i}{h} \quad ; \quad V_i = \frac{v_i}{h}$$

$$X = \frac{x}{h} \quad ; \quad Y = \frac{y}{h}$$

$$\frac{\partial u_i}{\partial x} = \frac{\partial U_i}{\partial X} \; ; \; \frac{\partial u_i}{\partial y} = \frac{\partial U_i}{\partial Y} \qquad 2.2.14$$

$$\frac{\partial v_i}{\partial x} = \frac{\partial V_i}{\partial X} \; ; \; \frac{\partial v_i}{\partial y} = \frac{\partial V_i}{\partial Y}$$

$$\sigma_0(Y) = \frac{\sigma_x(\pm c,y)}{E_1} \; ; \; \omega = (1 - \nu_1^2) \frac{\Omega'}{E_1 h^2}$$

The following dimensionless quantities are defined for compact presentation of the long expressions which result. They can all be calculated directly from the primary and secondary parameters governing the physical problem.

$$C = 2 + \cot \alpha \; ; \qquad \gamma = \frac{E_2(1 - \nu_1^2)}{E_1(1 - \nu_2^2)}$$

$$H_1 = (1 - \nu_1^2) \frac{(E_a \sin^2\alpha + G_a \cos^2\alpha)}{E_1} \frac{h}{\eta \cdot \sin \alpha} \qquad 2.2.15$$

$$H_2 = (1 - \nu_1^2) \frac{h}{\eta} \frac{(E_a - G_a)}{E_1} \cos \alpha$$

$$H_h = (1 - \nu_1^2) \frac{(E_a \cos^2\alpha + G_a \sin^2\alpha)}{E_1} \frac{h}{\eta \cdot \sin \alpha}$$

Substituting these quantities into the various energy expressions, we define a dimensionless total potential energy:

$$\omega = \frac{1}{2} \iint_{①} \left[\left(\frac{\partial U_1}{\partial X} \right)^2 + \left(\frac{\partial V_1}{\partial Y} \right)^2 + 2\nu_1 \frac{\partial U_1}{\partial X} \frac{\partial V_1}{\partial Y} + \frac{(1 - \nu_1)}{2} \left(\frac{\partial U_1}{\partial Y} + \frac{\partial V_1}{\partial X} \right)^2 \right] dX \, dY + \frac{\gamma}{2} \iint_{②} \left[\left(\frac{\partial U_2}{\partial X} \right)^2 + \left(\frac{\partial V_2}{\partial Y} \right)^2 + 2\nu_2 \frac{\partial U_2}{\partial X} \frac{\partial V_2}{\partial Y} + \frac{(1 - \nu_2)}{2} \left(\frac{\partial U_2}{\partial Y} + \frac{\partial V_2}{\partial X} \right)^2 \right] dX \, dY + \frac{1}{2} \int_{-1}^{+1} \left[H_1 (U_1 - U_2)^2 \right.$$

$$+ H_h(V_1 - V_2)^2 - 2H_2(U_1 - U_2)(V_1 - V_2)\Big]dY$$

$$+ (1 - \nu_1^2)\int_{-1}^{+1} \sigma_0(Y)U_1(-C,Y)dY$$

$$- (1 - \nu_1^2)\int_{-1}^{+1} \sigma_0(Y)U_2(C,Y)dY \qquad 2.2.16$$

The displacement functions of 2.2.12 a-d, in suitable dimensionless form, are now taken as

$$U_1 = \sum_{m=0}^{M}\sum_{n=0}^{M-m} A_{m,n}X^mY^n \qquad 2.2.17a$$

$$V_1 = \sum_{m=0}^{M}\sum_{n=0}^{M-m} B_{m,n}X^mY^n \qquad 2.2.17b$$

$$U_2 = \sum_{m=0}^{M}\sum_{n=0}^{M-m} C_{m,n}X^mY^n \qquad 2.2.17c$$

$$V_2 = \sum_{m=0}^{M}\sum_{n=0}^{M-m} D_{m,n}X^mY^n \qquad 2.2.17d$$

After substitution of these dimensionless displacements and their derivatives, and the evaluation of all integrals, the expression for total potential energy reduces to a system with $2M(M + 1) - 3$ degrees of freedom. These consist of the 'generalized co-ordinates' (unknown parameters) $A_{m,n}$, $B_{m,n}$, $C_{m,n}$ and $D_{m,n}$. The term -3 appears because plane rigid motion is suppressed by setting certain constants to zero.

The values of $A_{m,n}$, $B_{m,n}$, $C_{m,n}$ and $D_{m,n}$ are determined at this stage by using the principle of minimum

potential energy. The Ritz equations now take the form

$$\frac{\partial \omega}{\partial A_{m,n}} = 0$$

$$\frac{\partial \omega}{\partial B_{m,n}} = 0$$

$$\frac{\partial \omega}{\partial C_{m,n}} = 0 \qquad 2.2.18$$

$$\frac{\partial \omega}{\partial D_{m,n}} = 0$$

These four relations yield four sets of linear equations. On expansion, this produces as many equations as there are undetermined coefficients. The detailed derivation of these equations, which follow, is given in Appendix B:

$$0 = \frac{\partial \omega}{\partial A_{m,n}}$$

$$= \sum_{k=0}^{M} \sum_{j=0}^{M-k} \left\{ A_{k,j} \left[\frac{km}{k+m-1} \left(\phi_0 - (-C)^{k+m-1} f(n+j+1) \right) \right.\right.$$

$$+ \frac{(1-\nu_1)}{2} \frac{nj}{k+m+1} \left(\phi_0 \cot^2 \alpha - (-C)^{k+m+1} f(n+j-1) \right)$$

$$\left. + H_1 \phi_1 \right] + B_{k,j} \left[\left(\frac{\nu_i jm}{k+m} + \frac{1-\nu_1}{2} \frac{kn}{k+m} \right) \left(\phi_0 \cot \alpha \right.\right.$$

$$\left.\left. - (-C)^{k+m} f(n+j) \right) - H_2 \phi_1 \right] - C_{k,j} H_1 \phi_1 + D_{k,j} H_2 \phi_1 \Bigg\}$$

$$+ (1-\nu_1)^2 \int_{-1}^{+1} \sigma_0(Y) (-C)^m Y^n dY \qquad 2.2.19$$

$$0 = \frac{\partial \omega}{\partial B_{m,n}}$$

$$= \sum_{k=0}^{M} \sum_{j=0}^{M-k} \Bigg\{ A_{k,j} \Bigg[\Bigg(\nu_1 \frac{kn}{k+m} + \frac{1-\nu_1}{2} \frac{mj}{k+m} \Bigg) \Big(\phi_0 \cot \alpha - (-C)^{k+m} f(j+n) \Big) - H_2 \phi_1 \Bigg] + B_{k,j} \Bigg[\frac{nj}{k+m+1} \Big(\phi_0 \cot^2 \alpha - (-C)^{k+m+1} f(n+j-1) \Big) + \frac{(1-\nu_1)}{2} \frac{km}{k+m-1} \Big(\phi_0 - (-C)^{k+m-1} f(n+j+1) \Big) + H_h \phi_1 \Bigg] + C_{k,j} H_2 \phi_1 - D_{k,j} H_h \phi_1 \Bigg\} \qquad 2.2.20$$

$$0 = \frac{\partial \omega}{\partial C_{m,n}}$$

$$= \sum_{k=0}^{M} \sum_{j=0}^{M-k} \Bigg\{ -A_{k,j} H_1 \phi_1 + B_{k,j} H_2 \phi_1 + C_{k,j} \Bigg[\gamma \frac{km}{k+m-1} \Big(C^{k+m-1} f(n+j+1) - \phi_0 \Big) + \gamma \frac{(1-\nu_2)}{2} \frac{nj}{k+m+1} \Big(C^{k+m+1} f(n+j-1) - \phi_0 \cot^2 \alpha \Big) + H_1 \phi_1 \Bigg] + D_{k,j} \Bigg[\Big(C^{k+m} f(n+j) - \phi_0 \cot \alpha \Big) \Big(\gamma \nu_2 \frac{mj}{k+m} + \gamma \frac{1-\nu_2}{2} \frac{kn}{k+m} \Big) - H_2 \phi_1 \Bigg] \Bigg\} - (1-\nu_1^2) \int_{-1}^{+1} \sigma_0(Y) C^m Y^n dY \qquad 2.2.21$$

$$0 = \frac{\partial \omega}{\partial D_{m,n}}$$

$$= \sum_{k=0}^{M} \sum_{j=0}^{M-k} \Bigg\{ A_{k,j} H_2 \phi_1 - B_{k,j} H_h \phi_1 + C_{k,j} \Bigg[\gamma \Bigg(\nu_2 \frac{kn}{k+m} + \frac{1-\nu_2}{2} \frac{mj}{k+m} \Bigg) \Big(C^{k+m} f(n+j) - \phi_0 \cot \alpha \Big) - H_2 \phi_1 \Bigg]$$

$$+ D_{k,j} \Bigg[\gamma \frac{nj}{k+m+1} \Big(C^{k+m+1} f(n+j-1) - \phi_0 \cot^2 \alpha \Big)$$

$$+ \gamma \frac{1-\nu_2}{2} \frac{km}{k+m-1} \Big(C^{k+m-1} f(n+j-1) - \phi_0 \Big)$$

$$+ H_h \phi_1 \Bigg] \Bigg\} \qquad 2.2.22$$

The new symbols are defined below:

$$f(R) = \frac{\left[1 - (-1)^R\right]}{R} = \frac{2}{R} : R \text{ odd}$$

$$= 0 : R \text{ even}$$

$$\phi_0 = (\cot \alpha)^{k+m-1} f(k+m+n+j)$$

$$\phi_1 = (\cot \alpha)^{k+m} f(k+m+n+j+1)$$

It can be verified that these equations comprise a symmetric system, in accordance with the general theory of the Ritz procedure for quadratic functionals.

In equations 2.2.19 and 2.2.21 the integrals represent the loading conditions which are to be considered. In case of purely tensile loading at the ends of the adherends we take

$$\sigma_0(Y) = \sigma_0 = \text{constant} \qquad 2.2.23$$

and in pure bending:

$$\sigma_0(Y) = -\sigma_0 Y \qquad 2.2.24$$

with σ_0 also a constant. In the tensile loading case the integral of equation 2.2.19 becomes

$$(1 - \nu_1^2)\sigma_0(-C)^m f(n + 1) \qquad 2.2.25$$

Similarly, the integral of equation 2.2.21 reduces to

$$- (1 - \nu_1^2)\sigma_0(C)^m f(n + 1) \qquad 2.2.26$$

When there is pure bending, the integral of equation 2.2.19 becomes

$$- (1 - \nu_1^2)\sigma_0 \cdot (-C)^m f(n + 2) \qquad 2.2.27$$

and 2.2.21 results in

$$(1 - \nu_1^2)\sigma_0(C)^m f(n + 2) \qquad 2.2.28$$

In the computations σ_0 is always taken as unity, which means that the resulting Ritz coefficients must be multiplied by a factor σ_{X0}/E_1--see last line of equations 2.2.14--to restore true (dimensional) stresses, displacements, etc. The stress σ_{X0} is the actual uniform tensile stress loading the adherends, or the largest value of the bending stress loading the adherends.

Of the undetermined displacement parameters $A_{m,n}$, $B_{m,n}$, $C_{m,n}$, and $D_{m,n}$, three represent rigid-body displacement choices which must be fixed to avoid a singular Ritz matrix. These arbitrary choices are

$$U_1(0,0) = 0 \; ; \; V_1(0,0) = 0 \; ; \; \frac{\partial V_1(0,0)}{\partial X} = 0 \qquad 2.2.29$$

These in turn require that $A_{0,0} = 0$, $B_{0,0} = 0$ and $B_{1,0} = 0$.

The corresponding rows and columns of the Ritz matrix are deleted and the remaining parameters are evaluated by solving the surviving system of simultaneous equations, 2.2.19-2.2.22. After obtaining the displacement coefficients, the (dimensional) adhesive normal (σ_n) and shear (τ_{ns}) stresses are calculated using the strains of equations 2.2.6:

$$\sigma_n = E_a \frac{(u_{n1} - u_{n2})}{\eta}$$

$$\tau_{ns} = G_a \frac{(u_{s2} - u_{s1})}{\eta} \qquad 2.2.30$$

where (as before) u_{s1}, u_{s2} are the displacements of the two adherends along the adhesive film at their respective interfaces and u_{n1}, u_{n2} are the normal displacements at these interfaces. These in turn come from the Ritz coefficients via equations 2.2.9, 2.2.14 and 2.2.17. For user convenience, the actual quantities tabulated later are stresses N and T, corresponding to σ_n and τ_{ns} for unit applied tensile loading, or a bending moment producing an outer-fiber bending stress of unity. Thus the dimensional form of 2.2.30 becomes

$$\sigma_n = \frac{E_a}{\eta} \left[(v_1 - v_2) \cos \alpha - (u_1 - u_2) \sin \alpha\right] \qquad 2.2.31a$$

$$\tau_{ns} = \frac{G_a}{\eta} \left[(v_2 - v_1) \sin \alpha + (u_2 - u_1) \cos \alpha\right] \qquad 2.2.31b$$

and the dimensionless version is

$$N = \frac{E_a h}{E_1 \eta} \left[(V_1 - V_2) \cos \alpha - (U_1 - U_2) \sin \alpha \right] \qquad 2.2.32a$$

$$T = \frac{G_a h}{E_1 \eta} \left[(V_2 - V_1) \sin \alpha + (U_2 - U_1) \cos \alpha \right] \qquad 2.2.32b$$

The factor $(E_a h/E_1 \eta)$ is a primary dimensionless parameter of the tabulated results (discussed later), and the U_i, V_i are found from the Ritz coefficients using 2.2.17. Explicitly, the adhesive normal and shear stresses at points (X_j, Y_j) along the inclined adhesive face are calculated from the relations

$$N_j = \frac{E_a h}{E_1 \eta} \sum_{m=0}^{M} \sum_{n=0}^{M-m} \left[(B_{m,n} - D_{m,n}) \cos \alpha - (A_{m,n} - C_{m,n}) \sin \alpha \right] X_j^m Y_j^n \qquad 2.2.33a$$

$$T_j = \frac{G_a}{E_a} \left(\frac{E_a h}{E_1 \eta} \right) \sum_{m=0}^{M} \sum_{n=0}^{M-m} \left[(D_{m,n} - B_{m,n}) \sin \alpha + (C_{mn} - A_{m,n}) \cos \alpha \right] X_j^m Y_j^n \qquad 2.2.33b$$

On the adhesive line, of course, $X_j = Y_j \tan \alpha$: only one variable is independent.

2.3. The Sherman-Lauricella Integral Equation Approach

2.3.1 General

Integral equations are used quite effectively to formulate many engineering problems. This method of attacking

the fundamental boundary-value problems of plane elasticity appears in several forms in Muskhelishvili[4]. The version used here was initially devised by G. Lauricella[5] and extended by D. I. Sherman.[4] Its power appears in the lack of restrictions on the unknown "weight" function, for which only modest continuity requirements are specified. A similar, real-variable, vector-integral-equation formulation has been discussed by Massonet.[6] A difficulty of the present situation is that the integral equation in question is complex, so that it represents two real, coupled, Fredholm-type equations. Furthermore, this set must be solved simultaneously in each of two regions having different elastic properties. Fortunately, the solution for one region can be made to depend upon the solution for the other. However, once solved, a lengthy numerical integration for displacements must be carried out to complete the solution. In the present case, the results for both regions must be maintained in computer storage at the same time. The problem thus becomes one of computer capacity, and it has been found necessary to relegate this elegant approach to the role of an independent check on the Ritz procedure used for most of the calculations.

Generally speaking, it is out of the question to use analytical methods to solve a linear integral equation. It is usually possible to obtain good answers by solving a large number of simultaneous linear algebraic equations.

The procedure is to write the equation at a set of nodal points, suitably spaced along the boundary, carrying out the integrations numerically.

2.3.2 Notation for Integral Equation Method

The symbols used in the integral equation method development are defined in the text where they first appear. For convenience, those symbols used exclusively for the integral equation method are listed here in alphabetical order, with English letters preceding Greek letters. The symbols having the same meaning in both the present method and the Ritz method are listed in section 1.4. As before, subscripts 1 and 2 normally distinguish quantities defined for adherends 1 and 2. Bars over symbols have the usual "complex conjugate" significance in this section, and in associated appendices.

a_m, b_m = Coefficients of dimensionless, self equilibrated normal and shear stresses on adhesive interface.

C_2, D_2 = Rigid-body translation constants, adherend 2.

$f(t)$ = $f_1(t) + if_2(t)$.

$f_1(t), f_2(t)$ = Known real functions which depend upon the prescribed external loading.

I = Total number of intervals on the boundary of each adherend.

I_1, I_2, I_3, I_4 = Number of intervals on the various boundaries of each adherend.

K = I_1 = number of intervals on inclined adhesive face.

p(t), q(t) = Real and imaginary part of $\omega(t)$.

$U_1^{(1)}$, $V_1^{(1)}$, $U_2^{(1)}$, $V_2^{(1)}$ = Nondimensional displacement components due to unit applied tensile load parallel to X, in X- and Y-directions, for adherends 1 and 2 [part (1) contribution].

$U_1^{(2)}$, $V_1^{(2)}$, $U_2^{(2)}$, $V_2^{(2)}$ = Same as item above, but part (2) contribution associated with self-equilibrated adhesive stress system acting on adhesive interface.

X_n, Y_n = Given tractions on adherend 1 boundary, in the X- and Y- directions.

s,t = Values of the complex variable X + iY on adherend boundary.

S = Distance along the adhesive interface.

z = X + iY = complex variable.

μ_1, μ_2 = Shear moduli of adherends.

σ_n,$\sigma_{n,j}$ = Dimensionless adhesive normal stress, and same when evaluated at points X_j, Y_j.

τ_{ns}, $\tau_{ns,j}$ = Dimensionless adhesive shear stress, and same when evaluated at X_j, Y_j.

$\phi(z)$, $\psi(z)$ = Analytic functions entering governing integral equation.

$\phi(t)$, $\psi(t)$ = Boundary value of functions $\phi(z)$, $\psi(z)$.

χ_1 = $(3 - \nu_1)/(1 + \nu_1)$ for plane stress.

$\omega(t)$ = $p(t) + iq(t)$ = "density function" in definition of $\phi(z)$.

ω_2 = Rigid-body rotation constant of adherend 2.

2.3.3 The Problem Analyzed by Integral Equations

The adhesive scarf joint problem solved here is the tensile loading case described in Section 2.2. All expressions are in the non-dimensional form ultimately used there. The original boundary-value problem is decomposed into two parts, (1) and (2). The first part consists solely of the elementary solution for uniform tension parallel to X in each member, due to a unit applied tensile stress, and the uniform shear and normal stress on the adhesive boundary required to equilibrate the applied stress. Part (2) is then the wholly self-equilibrated residual problem for the "difference" tractions on the adhesive-adherend interfaces, now the only loaded boundary in each adherend. The adhesive normal and shear stresses are still unknown at this stage, and are taken to be polynomials in S, the distance along

the interface, with coefficients to be determined ultimately by the matching of two different expressions for the adhesive stresses at a finite set of points along the adhesive-adherend interface.

In terms of dimensionless quantities, the self-equilibrated adhesive normal and shear stresses [part (2) tractions] along the adhesive inclined face are assumed in the form

$$\sigma_n^{(2)} = \sum_{m=1}^{K} a_m S^m \qquad 2.3.1a$$

$$\tau_{ns}^{(2)} = \sum_{m=1}^{K} b_m S^m \qquad 2.3.1b$$

with undetermined coefficients a_m, b_m $(m = 1,2,...K)$. Here, $S = Y \csc \alpha$ is the dimensionless distance along the inclined adhesive-adherend boundary, measured from the origin of coordinates. The dimensions of (a_m, b_m) are "self-adjusting" as used here, and need not be specified. The integer K is chosen to be odd, as explained later. It would be simple to introduce the appropriate wedge-corner singularities as functions of S at this stage, if these could be determined.

Since this part of the solution is self-equilibrated for force and moment, we constrain the unknown coefficients accordingly. Applying the three static equilibrium conditions for adherend 1, the equations $\sum F_x = 0$, $\sum F_y = 0$ and $\sum M_{xy} = 0$ are used to eliminate the coefficients a_{K-1}, a_K

and b_{K-1}. These are expressed in terms of the remaining total of (2K-3) unknown coefficients (Appendix C), so that

$$\sigma_n^{(2)} = \sum_{m=1,2,3}^{(K-1)/2} a_{2m-1}\left[S^{2m-1} - \frac{(K+2)}{(2m+1)} (\csc \alpha)^{2m-K-1} S^K\right]$$

$$+ \sum_{m=1,2,3}^{(K-3)/2} a_{2m}\left[S^{2m} - \frac{K(\csc \alpha)^{2m-K+1}}{2m+1} S^{K-1}\right] \qquad 2.3.2a$$

$$\tau_{ns}^{(2)} = \sum_{m=1,2,3}^{(K+1)/2} b_{2m-1} S^{2m-1} + \sum_{m=1,2,3}^{(K-3)/2} b_{2m}\left[S^{2m}\right.$$

$$\left. - \frac{K}{2m+1} (\csc \alpha)^{2m-K+1} S^{K-1}\right] \qquad 2.3.2b$$

The boundary conditions of the first fundamental problem (all-traction case), in terms of unknown analytical functions of a complex variable, $\phi(z)$ and $\psi(z)$, is of the following form[4]

$$\phi(t) + t\,\overline{\phi'(t)} + \overline{\psi(t)} = f(t) \qquad 2.3.3$$

where

$\phi(t)$, $\psi(t)$ = boundary values of functions $\phi(z)$, $\psi(z)$

$$f(t) = f_1(t) + i f_2(t)$$

$$= i \int (X_n + iY_n) ds \qquad 2.3.4$$

X_n, Y_n = given tractions on the boundary in the X- and Y- directions

The functions $f_1(t)$ and $f_2(t)$ are known real functions, which depend in a simple way upon the prescribed external loading. Let $\omega(t)$ be an unknown density function ("weight function") for points on the boundary. It is assumed that $\omega(t)$ has a derivative $\omega'(t)$, which satisfies a Hölder's condition. The latter guarantees the continuity of the functions $\phi(z)$, $\phi'(z)$ and $\psi(z)$ up to the boundary. The boundary condition 2.3.3 thus constrains the choice of $\omega(t)$; this constraint is the governing Sherman-Lauricella integral equation of the problem. Following Sherman,[4] let

$$\phi(z) = \frac{1}{2\pi i}\int \frac{\omega(s)}{s - z}\, ds \qquad 2.3.5a$$

$$\psi(z) = \int \frac{\overline{\omega(s)}ds}{s - z} - \frac{1}{2\pi i}\int \frac{\bar{s}\omega'(s)}{s - z}\, ds \qquad 2.3.5b$$

From equation 2.3.5a

$$\phi'(z) = \frac{1}{2\pi i}\int \frac{\omega(s)}{(s - z)^2}\, ds \qquad 2.3.6$$

After using the Plemelj formulae for the boundary values of Cauchy integrals, and an integration by parts in 2.3.6 for $\phi'(z)$, equation 2.3.3 becomes

$$\omega(t) + \frac{1}{2\pi i}\int \omega(s)d \log\frac{s - t}{\bar{s} - \bar{t}} - \frac{1}{2\pi i}\int \overline{\omega(s)}\, d\, \frac{s - t}{\bar{s} - \bar{t}} = f(t) \qquad 2.3.7$$

This may be converted to two real equations by letting

$$s - t = re^{i\theta} \qquad 2.3.8$$

$$r = |s - t|$$

Here θ is the angle between the vector $s - t$ and the x-axis, measured in the positive (CCW) direction. By equation 2.3.8:

$$\log \frac{s - t}{\bar{s} - \bar{t}} = 2i\theta \qquad 2.3.9a$$

$$\frac{s - t}{\bar{s} - \bar{t}} = \cos 2\theta + i \sin 2\theta \qquad 2.3.9b$$

Equation 2.3.5a becomes

$$\omega(t) + \frac{1}{\pi} \int \left(\omega(s) - e^{2i\theta} \bar{\omega}(s) \right) d\theta = f_1(t) + i f_2(t) \qquad 2.3.10$$

Further, writing

$$\omega(t) = p(t) + iq(t) \qquad 2.3.11$$

and separating real and imaginary parts, equation 2.3.10 may be represented in the form of two real, coupled integral equations:

$$p(t) + \frac{1}{\pi} \int [p(s)(1 - \cos 2\theta) - q(s) \sin 2\theta] d\theta = f_1(t) \qquad 2.3.12$$

$$q(t) - \frac{1}{\pi} \int [p(s) \sin 2\theta - q(s)(1 + \cos 2\theta)] d\theta = f_2(t) \qquad 2.3.13$$

Equations 2.3.12 and 2.3.13 are quite simple and readily permit numerical solution. They were derived under the assumption of a continuously-turning tangent for the boundary contour. Muskheliskvili remarks that corners can be included if the contour integrations are interpreted as Stieltjes integrals.

The present contours have at least two critical corners per trapezoidal adherend, those along the inclined face. In failing to interpret the integration in the Stieltjes sense, the trapezoids are implicitly supplied with corner radii which are, roughly speaking, comparable to the interval size chosen for numerical integration. Omitting the Stieltjes interpretation (as in the numerical work here) is probably equivalent to ignoring the singularities of the problem, which is essentially what is done in choosing Ritz trial functions which are exclusively XY-polynomials.

To perform the numerical integration, the boundaries CD, DA, AB and BC of adherend 1 of the scarf joint (Fig. 7, p. 26) are divided into I_1, I_2, I_3 and I_4 intervals, respectively. Care is taken to make $I_1 = K$, the number of points at which adhesive stress expression matching will later take place. Before further discussion of the numerical approach to these equations, the functions $f_1(t)$ and $f_2(t)$ are evaluated. From equation 2.3.4

$$f_1(t) = - \int Y_n ds \; ; \; f_2(t) = \int x_n ds \qquad 2.3.14$$

where

$$X_n = -\sigma_n^{(2)} \sin \alpha - \tau_{ns}^{(2)} \cos \alpha \qquad 2.3.15a$$

$$Y_n = \sigma_n^{(2)} \cos \alpha - \tau_{ns}^{(2)} \sin \alpha \qquad 2.3.15b$$

Substituting equations 2.3.2a and 2.3.2b for $\sigma_n^{(2)}$ and $\tau_{ns}^{(2)}$ into 2.3.15a and 2.3.15b we obtain

$$f_1(t) = -\cos\alpha\left\{\sum_{m=1,2,3}^{(K-1)/2} a_{2m-1}\left[\frac{S^{2m}}{2m} - \frac{(K+2)}{2m+1}(\csc\alpha)^{2m-K-1}\frac{S^{K+1}}{K+1}\right]\right.$$

$$\left. + \sum_{m=1,2,3}^{(K-3)/2} a_{2m}\left[\frac{S^{2m+1}}{2m+1} - \frac{K}{2m+1}(\csc\alpha)^{2m-K+1}\frac{S^{k}}{k}\right]\right\}$$

$$+ \sin\alpha\left\{\sum_{m=1,2,3}^{(K+1)/2} b_{2m-1}\frac{S^{2m}}{2m} + \sum_{m=1,2,3}^{(K-3)/2} b_{2m}\left[\frac{S^{2m+1}}{2m+1}\right.\right.$$

$$\left.\left. - \frac{K}{2m+1}(\csc\alpha)^{2m-K+1}\frac{S^{K}}{K}\right]\right\} \qquad 2.3.16$$

$$f_2(t) = -\sin\alpha\left\{\sum_{m=1,2,3}^{(K-1)/2}\left[a_{2m-1}\frac{S^{2m}}{2m} - \frac{(K+2)}{2m+1}(\csc\alpha)^{2m-k-1}\frac{S^{K+1}}{K+1}\right]\right.$$

$$\left. + \sum_{m=1,2,3}^{(K-3)/2} a_{2m}\left[\frac{S^{2m+1}}{2m+1} - \frac{K}{2m+1}(\csc\alpha)^{2m-K+1}\frac{S^{K}}{K}\right]\right\}$$

$$-\cos\alpha\left\{\sum_{m=1,2,3}^{(K+1)/2} b_{2m-1}\frac{S^{2m}}{2m} + \sum_{m=1,2,3}^{(K-3)/2} b_{2m}\left[\frac{S^{2m+1}}{2m+1}\right.\right.$$

$$\left.\left. - \frac{K}{2m+1}(\csc\alpha)^{2m-K+1}\frac{S^{K}}{K}\right]\right\} \qquad 2.3.16$$

Since the superscript (2) stresses were subjected to the requirements of overall equilibrium, f_1 and f_2 must be continuous and it is possible to verify this directly from the foregoing expressions. The numerical integration is performed on the assumption that p and q vary negligibly in the intervals into which the whole boundary is divided. The p and q terms are extracted and the remaining integrals can be evaluated analytically. Thus, carrying out the integrations described, the two equations 2.3.12 and 2.3.13 are

rewritten in the following form [use $p_j \equiv p(t_j)$, etc.]:

$$p_j + \frac{1}{\pi}\sum_{k=1}^{I}\left[p_k\left(\theta_{+kj} - \theta_{-kj} - \frac{\sin 2\theta_{+kj} - \sin 2\theta_{-kj}}{2}\right)\right.$$

$$\left. + q_k \frac{(\cos 2\theta_{+kj} - \cos 2\theta_{-kj})}{2}\right] = f_{ij} \qquad 2.3.18$$

$$q_j + \frac{1}{\pi}\sum_{k=1}^{I}\left[p_k \frac{(\cos 2\theta_{+kj} - \cos 2\theta_{-kj})}{2} + q_k\left(\theta_{+kj} - \theta_{-kj}\right.\right.$$

$$\left.\left. + \frac{\sin 2\theta_{+kj} - \sin 2\theta_{-kj}}{2}\right)\right] = f_{2j} \qquad 2.3.19$$

where $I = I_1 + I_2 + I_3 + I_4$ = total number of intervals along the boundary,

$$\theta_{\pm kj} = \arg\left(s_k^{\pm} - t_j\right)$$

$$s_k^{\pm} = s_k \pm \frac{H_k}{2}$$

H_k = length of the k^{th} interval

f_{1j}, f_{2j} = values of the function $f_1(t)$, $f_2(t)$ at the j^{th} node (center of j^{th} interval), $t = t_j$.

Upon completion of the numerical integration of equations 2.3.18 and 2.3.19, we have a numerical matrix relating the $(p_j, q_j)(j = 1,2,3,\ldots,I)$ to the still unknown adhesive stress coefficients $(a_k, b_m)(k = 1,2,3,\ldots,K-2;$ $m = 1,2,3,\ldots, K-3, K-2, K)$.

Having established this relation, the expression for the non-dimensional components of displacement $U_1^{(2)}$ and $V_1^{(2)}$ must now be developed.[4] In terms of the functions ϕ and ψ defined previously:

$$2\mu_1(U_1^{(2)} + iV_1^{(2)}) = \chi_1\phi(z) - z\overline{\phi'(z)} - \overline{\psi(z)} \qquad 2.3.20$$

where

μ_1 = Shear modulus of adherend 1.

$\chi_1 = (3 - \nu_1)/(1 + \nu_1)$ for plane stress.

ν_1 = Poisson's ratio for adherend 1.

This equation can be reduced to a contour integration around the boundary of the adherend (Appendix D):

$$\begin{aligned} 2\mu_1\left(U_1^{(2)} + iV_1^{(2)}\right) = {} & \frac{\chi_1}{2\pi i}\int\left\{[p(s) - p(t)] + i[q(s) - q(t)]\right\}\frac{ds}{s - t} \\ & + \frac{1}{2\pi i}\int\left\{[p(s) - p(t)] + i[q(s) - q(t)]\right\}\frac{d\bar{s}}{\bar{s} - \bar{t}} \\ & + \frac{1}{\pi}\int[p(s) + iq(s)]\,\frac{\cos\alpha\ ds}{r} + \tfrac{1}{2}\chi_1[p(t) + iq(t)] \\ & + \tfrac{1}{2}[p(t) + iq(t)] - f_1(t) - if_2(t) \end{aligned} \qquad 2.3.21$$

where

$U_1^{(2)}$, $V_1^{(2)}$ = displacement components of adherend 1.

$\alpha = \alpha(s,t)$ is the angle between the vector s - t and the outward normal at s (unrelated to the scarf angle α used elsewhere).

$r = |s - t|$ 2.3.22

The adjustment of the rigid-body displacement constants is made later.

Equation 2.3.21 is integrated numerically using the trapezoidal formula, with special treatment required at various points, such as corners (Appendix D). The integration is carried out only for the displacements $U_{lj}^{(2)}$, $V_{lj}^{(2)}$, i.e., the X, Y- displacement components of adherend 1 at the j^{th} boundary node point (midpoint of j^{th} interval), of points (X_j, Y_j) on the inclined adherend face. This establishes expressions for $U_{lj}^{(2)}$ and $V_{lj}^{(2)}$ in terms of quantities (p_k, q_k) at all the node points on the boundary, which in turn still depend upon the unknowns (a_m, b_m). Both relations take the form of known numerical matrices. Note that the only elastic constant affecting the right side of 2.3.21 is χ_1. Thus if both adherends have the same Poisson's ratio, the right side of 2.3.21 serves for both. This assumption is made in the calculations.

Next, using the numerical coefficient matrix which relates (p_j, q_j) to the (a_k, b_k), the final displacements of the adherend 1 can be expressed as a single, known numerical matrix multiplying a still unknown column vector of the (a_k, b_k). Careful consideration of the geometry of the second adherend with respect to the first adherend permits us to use the results for the first adherend to write the corresponding $U_2^{(2)}$ and $V_2^{(2)}$ displacement expressions at an equal number (I_1 = K) of points on the inclined face.

The principal adjustment required, if we assume the same Poisson's ratio on both sides, is for the different shear modulus. This affects only the left side of 2.3.21. Some sign changes and "mirror" reflections of coordinates in the origin are also required.

The displacement expressions corresponding to the uniform unit tensile fields in each member [part (1) solutions] are now superposed on those due to the self-equilibrated distributions (superscript 2), to obtain the final displacement expressions for the two adherends.

Rigid-body displacement constants must now be established. This is done by arbitrarily suppressing all translation and rotation at the origin, in the first adherend. The first adherend's final displacement components at the desired points (X_j, Y_j) along the adhesive inclined face are thus taken as (Appendix E):

$$U_{1j} = U_{1j}^{(2)}(X_j,Y_j) + \frac{1}{E_1} X_j - U_{1j}^{(2)}(0,0) \qquad 2.3.23a$$

$$V_{1j} = V_{1j}^{(2)}(X_j,Y_j) - \frac{\nu_1}{E_1} Y_j - V_{1j}^{(2)}(0,0) \qquad 2.3.23b$$

where the terms involving X_j and $-\nu_1 Y_j$ represent the total contribution of the uniform tensile field here. For the second adherend, the solution itself must determine the rigid-displacement constants (c_2, D_2, ω_2 below)--see Appendix E:

$$U_{2j} = U_{2j}^{(2)}(X_j,Y_j) + \frac{1}{E_2} X_j + C_2 - \omega_2 Y_j \qquad 2.3.24a$$

$$V_{2j} = V_{2j}^{(2)}(X_j, Y_j) - \frac{\nu_2}{E_2} Y_j + D_2 + \omega_2 X_j \qquad 2.3.24b$$

where $U_{2j}^{(2)}$, $V_{2j}^{(2)}$ are the displacements of adherends 2 at node point j.

Because of the presence of the three rigid-body constants C_2, D_2 and ω_2, the number of unknowns has increased from the (2K - 3) quantities (a_k, b_k) to 2K (K = I_1). All unknowns are now evaluated by equating two different expressions for the adhesive normal and shear stress. The total stresses are the sum of the part (1) and part (2) contributions. Recalling that part (1) consists of a uniform unit tensile field, and using 2.3.1,

$$\sigma_{n,j} = \sigma_{n,j}^{(1)} + \sigma_{n,j}^{(2)} = \sin^2 \alpha + \sum_{m=1}^{K} a_m S_j^m \qquad 2.3.25a$$

$$\tau_{ns,j} = \tau_{ns,j}^{(1)} + \tau_{ns,j}^{(2)} = \sin \alpha \cos \alpha + \sum_{m=1}^{K} b_m S_j^m \qquad 2.3.25b$$

The sinusoidal terms are the adhesive stresses required to equilibrate a unit tension parallel to X, and subscript j indicates that the stresses are calculated at $S = S_j$. For the part (2) summations, the equations actually used are those of 2.3.2, which show clearly that only 2K - 3 unknowns appear, not the 2K values (a_m, b_m) implied above. The version presented above is more compact and clearer, and conceptually equivalent as long as it is understood that a_{K-1}, a_K and b_{K-1} are linearly related to the rest of the (a_m, b_m). The unknowns C_2, D_2, ω_2 do not appear explicitly in 2.3.25.

The second expression for the stresses is developed from equations 2.2.32, p. 46, rewritten to conform to the demands of the present approach. These equations give the adhesive stresses in terms of the relative displacements of the adherends at the adhesive line. The subscript j implies evaluation at $S = S_j$, or $X_j = Y_j \tan \alpha$:

$$\sigma_{n,j} = \frac{E_a h}{\eta}\left\{ [U_{1,j} - U_{2j}] \sin \alpha - [V_{1j} - V_{2j}] \cos \alpha \right\} \qquad 2.3.26a$$

$$\tau_{ns,j} = \frac{G_a}{E_a}\frac{E_a h}{\eta}\left\{ [U_{2j} - U_{1j}] \cos \alpha + [V_{2j} - V_{1j}] \sin \alpha \right\} \qquad 2.3.26b$$

(The denominator factor of E_1 has been removed from 2.2.32 because the U's and V's as defined in this section contain the adherend moduli already.) Equations 2.3.24 show that 2.3.26 contain the unknown constants C_2, D_2 ω_2 explicitly, as well as the 2K - 3 unknowns (a_m, b_m) implied in 2.3.23 and 2.3.24. The equating of the stress expressions of 2.3.25 and 2.3.26 is therefore sufficient to determine the 2K unknowns, and hence the adhesive stresses.

2.4. Numerical Data Assumed in the Calculations

There are a large number of dimensionless parameters to investigate, so that it becomes necessary to divide them into primary and secondary parameters. The latter are taken as constant throughout the calculations. The primary

parameters are the scarf angle (α); the relative stiffness of the adherends (γ); and the relative stiffness of adhesive and adherends (β). Treated as secondary parameters are the Poisson's ratios of the adhesive and of the adherends. Even so, a great many cases must be studied in order to establish the overall behavior of the dissimilar-adherend scarf joint.

Generally speaking, the parameters are chosen so as to simplify interpolation in the results, either on a linear scale or as equally-spaced values on a logarithmic scale. First of all, reflecting the practical range, the scarf angles are chosen as 5°, 10°, 20°, 30° and 40°. The first and last values are probably outside the usual range, but are explored for completeness and to facilitate interpolation.

The primary dimensionless parameter $\gamma = \dfrac{E_2(1 - \nu_1^2)}{E_1(1 - \nu_2^2)}$ is a measure of the relative stiffness of the adherends. The values selected are 1, 2, 4 and 8; values much larger than 8 are probably quite close to the case of one "rigid" adherend. Adherend 2 is thus always the stiffer of the two, except that when $\gamma = 1$, we have a scarf joint with identical adherends. The successive factors of 2 permit interpolation with respect to this parameter at uniform intervals on a logarithmic scale. We have taken the adherends' Poisson's ratios to be $\nu_1 = \nu_2 = 0.3$ throughout

the major part of the work. This value is intermediate between typical steel and aluminum values.

The next primary dimensionless parameter is the "elastothickness" parameter $\beta = \eta E_1/E_a h(1 - \nu_1^2)$, which is a measure of relative adherend and adhesive stiffness. As used here, large β implies a relatively flexible adhesive. Assuming metal adherends and typical adhesive thickness and moduli for the metal-bonding range, the values for β are set so as to permit interpolation on a logarithmic scale: $\beta = 4$, 20 and 100. The dimensionless ratio (E_a/G_a) of the adhesive's Young's modulus to the shear modulus has been fixed at 8/3 in the present computations. Referring to Fig. 7, the value of L_1 is assumed to be $2h = 2$, so that the uniform portion of each adherend has the same length as its depth. In auxiliary calculations, this length appeared to give the best overall check of the input traction boundary conditions with the polynomial Ritz functions used. It is possible, however, that another choice might be better by some other criterion. This check is described later.

When using the Ritz method, the Ritz matrix is independent of the type of loading used, so that it is expedient to introduce all types of loading considered at the same time. Results are presented here for both pure tension and pure bending.

2.5. Computer Programs

The principal numerical results for this thesis were obtained using the Ritz method of analysis, by means of a computer program developed for the Control Data Corporation 3600 computer at Michigan State University. The program was written in the 3600 Fortran source language. Various auxiliary programs were used to perform checks on the results, described later.

A separate program was developed for the integral equation approach. Both programs allow for full variation of the dimensionless parameters of the problem, including the effects of geometry, material properties and external loading. Upon providing the few input data cards required, the programs calculate and print the adhesive shear and normal stresses at uniformly spaced points along the adhesive's inclined face. In the case of the Ritz program, the Ritz parameters are also punched on cards so that any desired additional calculations can be performed later. Stress distributions on the external boundaries of each adherend are calculated from the approximate Ritz displacement solution, in order to check against the known input boundary conditions.

The format of the input parameters to be supplied by the user of the program (and copies of the programs) appear in Appendix F.

CHAPTER III

CRITERIA FOR ACCEPTABILITY OF RESULTS; PARTIAL DISCUSSION OF RESULTS

3.1. General

In using the Rayleigh-Ritz procedure to arrive at a solution for this problem, the validity of the results always depends upon the convergence of the solution to the correct limit. The few available results of the integral equation method assume only a supporting role here, so that Ritz solutions are the main ones to be checked for acceptability. In this connection, the first and foremost problem is to assess the convergence of the solution.

Since the accuracy acceptable for engineering purposes varies with the demands of the particular problem, it has been considered sufficient to state the indices of accuracy used, and how the results behave in each case. It is left to the reader to decide if this is sufficient for his purposes.

It is worthwhile to note that in every case, the analytical solution obtained by the Ritz method for the case of identical adherends in tension verifies to high accuracy the exact solution of Ref. 7. The identical-adherend

bending solution reported here is new; it is readily shown that the method of Ref. 7 cannot be extended to include the case of the bending of identical adherends.

3.1.1 Stress Boundary Condition Check

For each trapezoidal adherend's external boundary, the input traction conditions are known. The top and bottom surfaces of the system are free of stress, and the ends are loaded by uniform tension, or pure bending with linear stress distribution. Therefore, the ability of the approximate solution to reproduce these is a powerful primary check. This check has been performed for all Ritz solution cases investigated.

In this regard, a more or less intermediate case ($\alpha = 10°$, $\beta = 20$, $\gamma = 4$) is surveyed next for both tensile load (Fig. 8) and bending load (Fig. 9). These figures show the boundary traction error on the exterior boundaries, in the form [(calculated stress, from solution) - (true stress, from boundary conditions)]. The reference level is unity, which is either the value of the uniform tensile load or the maximum value of the applied bending stress. All of the calculated results show these general patterns of boundary-traction error distribution. From this it is possible to select C, and E or F as the critical points, respectively, in adherends 1 and 2. All other errors are either smaller, or much smaller. Point C, in particular,

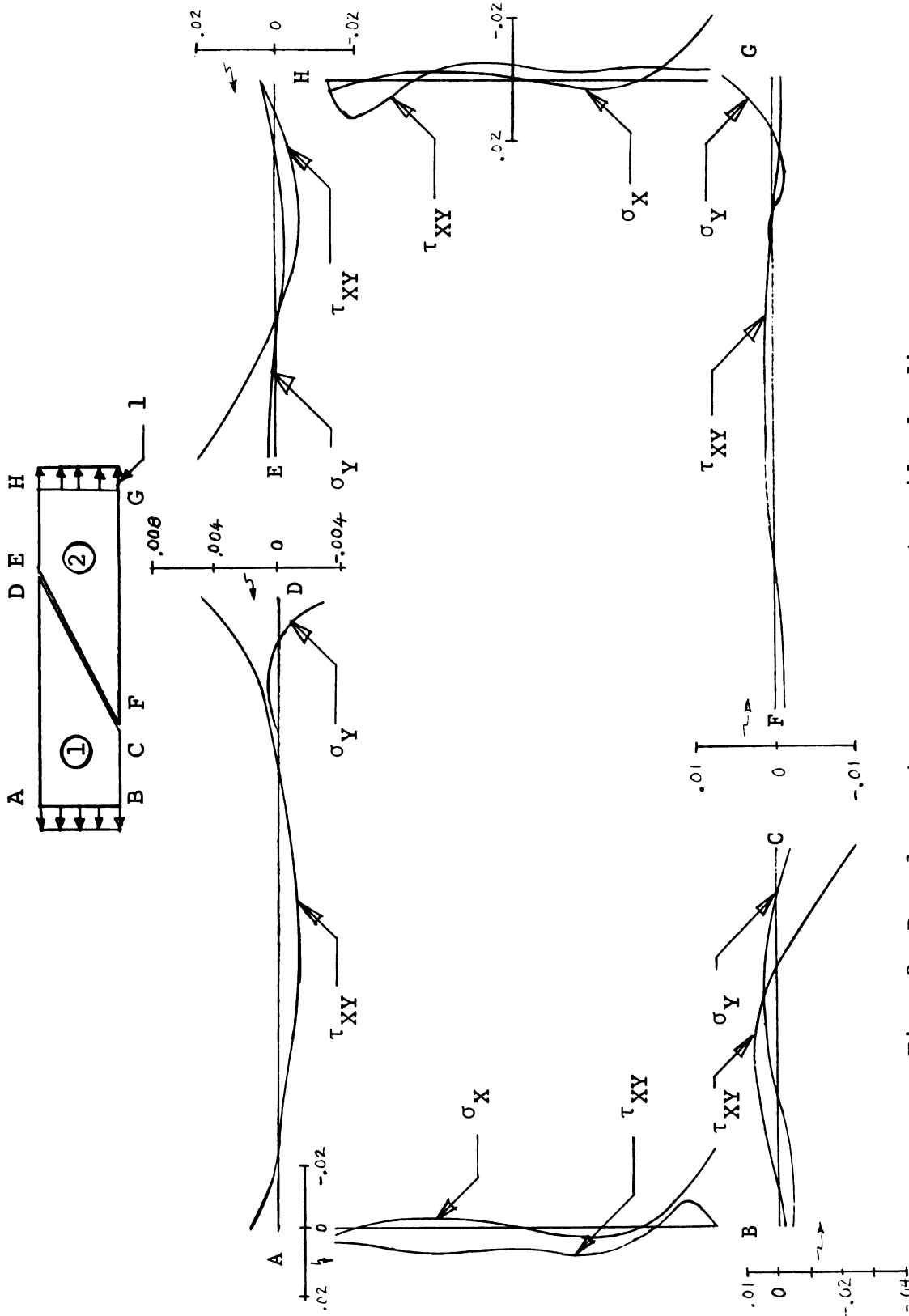

Fig. 8 Boundary stress errors, tensile loading $\alpha = 10°$, $\beta = 20$, $\gamma = 4$.

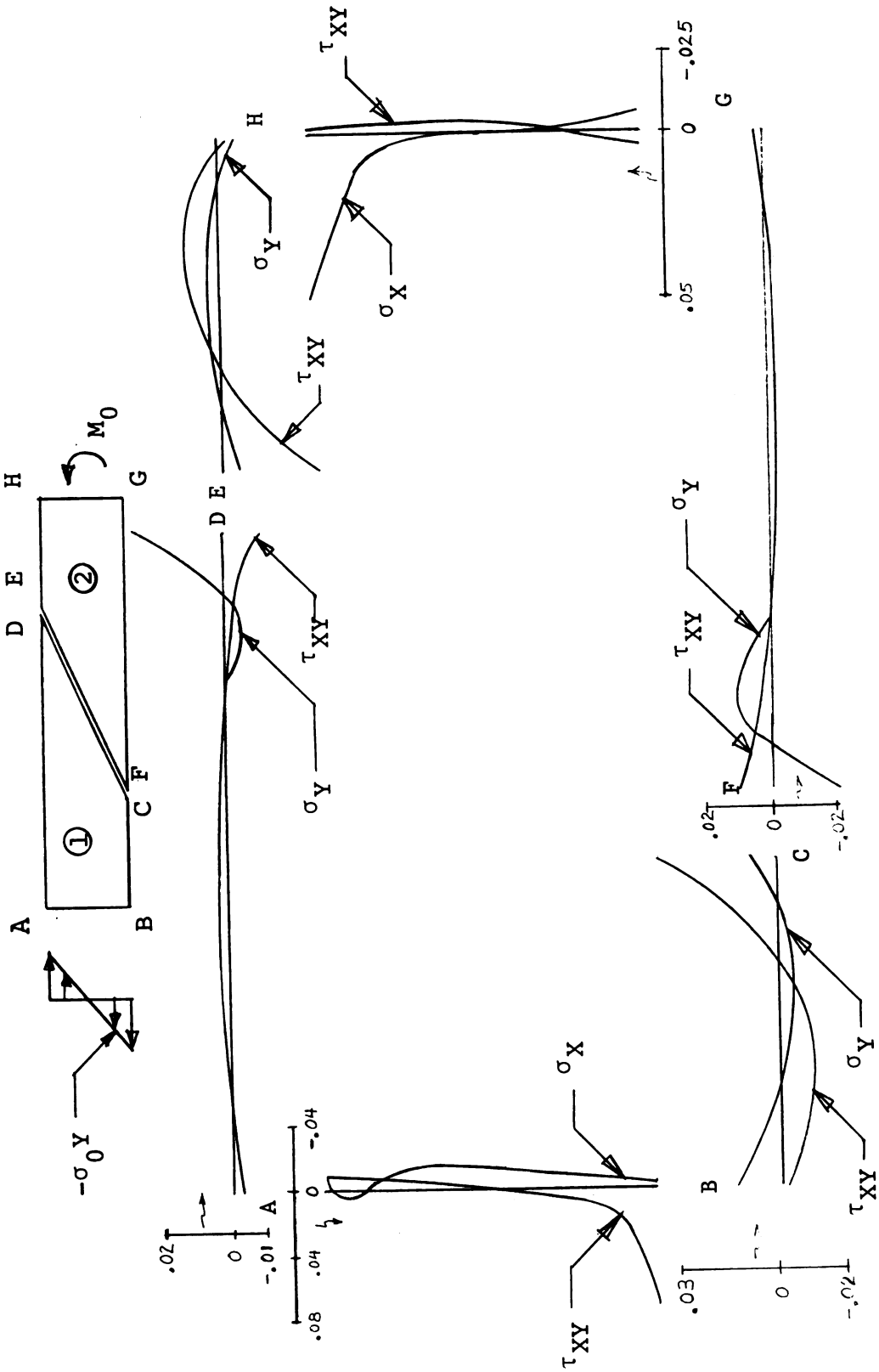

Fig. 9 Boundary stress errors, bending load
$\alpha = 10°$, $\beta = 20$, $\gamma = 4$.

invariably shows the largest error in the case of tensile loading of the joint. For bending load, however, the largest error occurs at point E for the smaller scarf angles and at point F for the larger angles (invariably, the values at E and F are comparable in level). The peaking of the boundary stress errors at the points in question is quite clearly linked to the neglect of singularities in the Ritz trial functions.

The value of the boundary stress errors may be taken as one measure of the merit of the results. In the particular problem of Fig. 8, the point -C error values for tensile loading are -0.029 for shear and -0.005 for normal stress. For Fig. 9--bending load--the corresponding point -E quantities are -0.063 for shear and -0.009 for normal stress.

It is not immediately possible to carry out a comparison of the type just discussed on the adhesive-adherend interface, since we have no "true adhesive stresses" to serve as a reference level. The purpose of the thesis is to find these unknown stresses. Something equivalent has been devised, however, and is discussed in the next section.

In interpreting the present "index of merit" of the calculations, the following should be borne in mind. The desired results in this problem are the adhesive stresses on the inclined boundary. These are calculated using equations 2.2.32 and 2.2.33, i.e., directly from member

displacements. The latter are the direct output of the Ritz method, in the form of the coefficients $A_{m,n}$, $B_{m,n}$, etc. On the other hand, the boundary-stress distributions are much more sensitive to error than the displacements, because these stresses are found using derivatives of displacements. In other words, we anticipate that the Ritz method will produce displacements which are an order of magnitude more accurate than the corresponding stress calculations. This makes the boundary stress an overly-sensitive index, sometimes alarmingly so. The convergence of the adhesive stresses themselves nevertheless appears to be quite good in most cases, as will be seen later.

Speaking generally, then, if the user is satisfied that the boundary stress error is small enough, he can surely be satisfied that the corresponding adhesive stresses are considerably better determined. And a boundary condition error of 20% (0.2 on an applied load scale of unity) may still mean that the corresponding adhesive stresses have been determined to within a few percent. With this as a background we examine Table 1.

Table 1 (next page) gives the largest errors in the boundary stresses for those bending load cases having scarf angles $\alpha = 20°$, 30° and 40°. These stresses have been calculated at 21 equally-spaced points on each of the three external boundaries of each adherend. To emphasize the highly local character of large peak errors, when these

Table 1.--Largest boundary condition error (bending).

$\alpha = 20°$						
β	γ	σ_x Along GH	σ_y Along BC	τ_{xy} BC	τ_{xy} GF	τ_{xy} HE
4	8			0.111		-0.105
				(0.028)		(0.073)
20	2					-0.106
						(0.073)
	4		0.151			-0.115
			(0.040)			(0.079)
	8	0.118			-0.338	-0.120
		(0.043)			(0.093)	(0.083)
100	2			0.117	0.182	0.123
				(0.079)	(0.049)	(0.083)
	4			0.116	0.292	0.126
				(0.078)	(0.080)	(0.087)
	8	0.142	0.103	0.115	0.368	0.128
		(0.030)	(0.067)	(0.077)	(0.012)	(0.088)

$\alpha = 30°$							
β	γ	σ_x GH	σ_y BC	σ_y HE	τ_{xy} AD	τ_{xy} GF	τ_{xy} HE
4	4					0.255	
						(0.010)	
	8		0.146			0.472	0.104
			(0.083)			(0.134)	(0.061)
20	2		0.125			0.290	0.105
			(0.082)			(0.087)	(0.064)
	4		0.155			0.428	
			(0.082)			(0.123)	
	8	0.110	0.174			0.526	0.111
		(0.020)	(0.096)			(0.151)	(0.065)

Table 1 Continued.

$\alpha = 30°$							
β	γ	σ_x GH	σ_y BC	σ_y HE	τ_{xy} AD	τ_{xy} GF	τ_{xy} HE
100	2		0.153	0.134	0.287	0.388	0.104
			(0.079)	(0.066)	(0.030)	(0.112)	(0.058)
	4		0.162	0.131	0.270	0.433	0.105
			(0.085)	(0.062)	(0.016)	(0.125)	(0.058)
	8		0.167	0.129	0.262	0.454	0.105
			(0.089)	(0.062)	(0.076)	(0.132)	(0.059)

$\alpha = 40°$								
β	γ	σ_x GH σ_y AD	σ_y BC	σ_y GP	σ_y HE	τ_{xy} BC	τ_{xy} AD	τ_{xy} GF
4	2		0.128					0.274
			(0.051)					(0.078)
	4			0.128		0.175		0.438
				(0.055)		(0.079)		(0.125)
	8			0.186		0.213		0.573
				(0.048)		(0.103)		(0.164)
20	2		0.190	0.110	0.154		0.299	0.437
			(0.080)	(0.037)	(0.078)		(0.091)	(0.118)
	4		0.209	0.140	0.151		0.278	0.501
			(0.092)	(0.041)	(0.054)		(0.086)	(0.149)
	8		0.220	0.158	0.149		0.268	0.544
			(0.099)	(0.060)	(0.052)		(0.084)	(0.160)
100	2	0.102	0.207	0.122	0.197		0.436	0.479
		(0.038)	(0.089)	(0.045)	(0.082)		(0.132)	(0.144)
	4	0.100	0.212	0.129	0.196		0.430	0.495
		(0.036)	(0.092)	(0.048)	(0.081)		(0.130)	(0.148)
	8		0.214	0.133	0.195		0.427	0.504
			(0.093)	(0.038)	0.080)		(0.129)	(0.150)

occur, the numbers in parentheses give the value of the same stress error at the point next to the peak. When the peak is large, the gradient is always very steep. Errors in boundary stresses are entered only when they exceed 0.10 (where 1.0 is the reference level for applied external stress).

In all tensile load cases these errors are smaller than 0.06, and for all bending cases with $\alpha = 5°$ or $10°$, they are less than 0.10. Hence they are not represented in Table 1 at all.

The largest errors in the boundary stresses are usually observed to be in the shear stresses on side GF of adherend 2 (Fig. 9). For scarf angle $\alpha = 20°$, the largest error is 0.368 when $\beta = 100$, $\gamma = 8$. The largest error for $\alpha = 30°$ is found to be 0.526 when $\beta = 20$, $\gamma = 8$. When $\alpha = 40°$, the largest value is 0.573 for $\beta = 4$ and $\gamma = 8$. These values are observed at the lower tip of the second adherend, point F in Fig. 9. Note from Table 1 that the 0.368 error value for $\alpha = 20°$, $\beta = 100$, $\gamma = 8$ falls to 0.102 in 5% of the distance along GF from G--see value in parentheses. Likewise, the 0.526 local peak for $\alpha = 30°$, $\beta = 20$, $\gamma = 8$ drops to 0.151 in the same distance, and the $\alpha = 40°$, $\beta = 4$, $\gamma = 8$ value of 0.573 falls to 0.164. It is to be anticipated that these local stress errors are associated with much smaller errors in the displacements of the region in question. This, of course, will be revealed by the study

of the convergence of the adhesive stresses themselves. It seems possible to show by direct computation that the stress error functions, separately, contribute displacement errors which are quite small compared to the primary Ritz displacements used to calculate the adhesive stresses. In effect, this would establish the loose "order of magnitude" by which the displacements are more accurately determined than the stresses. However, this hardly seems to be worthwhile, since the study of adhesive stress convergence effectively does the same thing directly for the desired end product.

3.1.2 Comparison of Adhesive Stresses Calculated Several Ways From the Results

The adhesive shear and normal stresses reported here are calculated from equations 2.2.32, i.e., by using displacement differences. Displacement derivatives have been used only to investigate the boundary stresses. It was pointed out in the previous section that the error in calculating adhesive stresses using derivatives is expected to be much greater than when using differences in displacements, since the Ritz method (as employed here) produces accurate displacements, but less accurate strains and stresses. We now suppose that the adhesive stress distributions found using Eqs. 2.2.32 are "exact," and compare them to the same stresses calculated from the displacement derivatives of adherends 1 and 2. We would expect that the

difference between the adhesive stress distributions, as calculated the "exact" and the two "approximate" ways, would be comparable to the boundary stress error. This seems to be the case.

Table 2 (next page) shows the adhesive normal and shear distribution (for $\alpha = 10°$, $\beta = 20$, $\gamma = 4$), calculated three ways: using the displacement derivatives of adherend 1; of adherend 2; and from the differences of the adherend displacements (eq. 2.2.32). The quantity S is the fraction of the joint half-length, measured along the adhesive-adherend interface from the origin (at the center). The value S = -1.0 corresponds to points (C,F) in Figs. 8-9, and S = 1.0 to (D,E). Table 2 gives results for tensile and for bending load. It can be deduced from Table 2, by subtraction, that the characteristic differences between the more accurate and two less accurate methods are of the same order of magnitude as the errors in the satisfaction of the stress boundary conditions. The largest differences occur at the ends of the adhesive joint, corresponding to corners of the adherend trapezoids. These are also the regions of discrepancy on the external boundaries. Such discrepancies are inherent in any approach which fails to account for the stress singularities associated with the acute and obtuse wedge corners of the adherend trapezoids.

Table 2.--Adhesive stresses calculated three ways.

Tensile Loading $\alpha = 10°$ $\beta = 20$ $\gamma = 4$

	Normal Stress			Shear Stress		
S	Difference	Adherend 1 Derivative	Adherend 2 Derivative	Difference	Adherend 1 Derivative	Adherend 2 Derivative
-1.0	0.03881	0.03522	0.04679	0.21817	0.19592	0.22045
-0.9	0.03511	0.03505	0.03382	0.21065	0.20671	0.20871
-0.8	0.02925	0.03083	0.02651	0.20381	0.20821	0.20312
-0.7	0.02428	0.02574	0.02301	0.19787	0.20387	0.19906
-0.6	0.02159	0.02191	0.02208	0.19284	0.19678	0.19469
-0.5	0.02148	0.02054	0.02292	0.18865	0.18935	0.18977
-0.4	0.02354	0.02193	0.02494	0.18509	0.18308	0.18478
-0.3	0.02699	0.02558	0.02768	0.18195	0.17866	0.18037
-0.2	0.03095	0.03047	0.03073	0.17901	0.17598	0.17697
-0.1	0.03457	0.03534	0.03371	0.17606	0.17442	0.17461
0	0.03731	0.03900	0.03694	0.17292	0.17305	0.17310
0.1	0.03872	0.04052	0.03796	0.16950	0.17113	0.17122
0.2	0.03872	0.03970	0.03860	0.16570	0.16786	0.16871
0.3	0.03744	0.03690	0.03802	0.16149	0.16311	0.16469
0.4	0.03521	0.03314	0.03619	0.15690	0.15719	0.15879
0.5	0.03244	0.02977	0.03331	0.15197	0.15085	0.15123
0.6	0.02958	0.02810	0.02980	0.14676	0.14507	0.14295
0.7	0.02700	0.02850	0.02628	0.14138	0.14057	0.13568
0.8	0.02493	0.02945	0.02361	0.13590	0.13710	0.13185
0.9	0.02341	0.02598	0.02277	0.13040	0.13242	0.13440
1.0	0.02228	0.00788	0.02480	0.12495	0.12100	0.14630

Table 2 Continued.

Bending Loading $\alpha = 10°$ $\beta = 20$ $\gamma = 4$

	Normal Stress			Shear Stress		
S	Difference	Adherend 1 Derivative	Adherend 2 Derivative	Difference	Adherend 1 Derivative	Adherend 2 Derivative
-1.0	0.01633	0.02320	-0.00675	0.10098	0.13384	-0.09064
-0.9	0.02549	0.02511	0.02881	0.09104	0.09761	0.09584
-0.8	0.03513	0.03163	0.04270	0.08030	0.07454	0.08286
-0.7	0.04009	0.03720	0.04360	0.06843	0.05999	0.06580
-0.6	0.03866	0.03834	0.03726	0.05554	0.04978	0.05068
-0.5	0.03142	0.03368	0.02737	0.04196	0.04072	0.03868
-0.4	0.02015	0.02364	0.01622	0.02821	0.03083	0.02863
-0.3	0.00712	0.00999	0.00518	0.01479	0.01933	0.01873
-0.2	-0.00549	-0.00469	-0.00490	+0.00219	+0.00648	0.00759
-0.1	-0.01596	-0.01770	-0.01350	-0.00920	-0.00677	-0.00515
0	-0.02320	-0.02682	-0.02231	-0.01911	-0.01902	-0.02346
0.1	-0.02682	-0.03054	-0.02467	-0.02739	-0.02941	-0.03169
0.2	-0.02709	-0.02900	-0.02675	-0.03402	-0.03678	-0.04190
0.3	-0.02478	-0.02350	-0.02636	-0.03910	-0.04113	-0.04764
0.4	-0.02094	-0.01651	-0.02367	-0.04278	-0.04306	-0.04800
0.5	-0.01669	-0.01115	-0.01915	-0.04530	-0.04383	-0.04360
0.6	-0.01298	-0.01003	-0.01370	-0.04689	-0.04493	-0.03695
0.7	-0.01043	-0.01375	-0.00868	-0.04780	-0.04736	-0.03274
0.8	-0.00917	-0.01869	-0.00596	-0.04821	-0.05055	-0.03763
0.9	-0.00884	-0.01423	-0.00784	-0.04828	-0.05080	-0.05969
1.0	-0.00873	+0.00209	-0.01696	-0.04810	-0.03926	-0.10724

3.1.3 Double-Precision Check of Roundoff Errors

In order to check the roundoff error involved in solving the present very large system of simultaneous equations, a few computer runs have been carried out using double precision arithmetic on systems of 141 equations. This corresponds to a sum of homogeneous polynomials, for each of the four displacements, up to and including all 7^{th}-order terms. In all cases checked ($\alpha = 10°$ and $30°$, $\beta = 4$, $\gamma = 2$), it was found that the numerically larger values of adhesive normal and shear stress are affected by roundoff error only in the sixth and seventh significant figures.

Consider, for example, the tension-loaded case of $\alpha = 30°$, $\beta = 4$, $\gamma = 2$. The largest shear stress value at $S = -1.0$ (point C or F of Fig. 7) changes from 0.4723434 (single precision) to 0.4723424 (double precision). The normal stresses are somewhat smaller than the shear stresses for the angle $\alpha = 30°$, but the roundoff contribution must still be comparable to the values found for the shear stress level. This is because the same imperfectly-determined Ritz coefficients are involved in all computations. At $S = -1.0$, the normal stress changes from 0.2687167 (single precision) to 0.2687145 (double precision). Here also it is found that the difference is in the sixth or seventh significant figures.

The final results presented here are for 8^{th}-order polynomials (177 equations). It is estimated that roundoff

error might affect the numerically larger values in the fourth to the sixth significant figure, depending upon the parameters α, β and γ. A precise estimate of roundoff error for 8^{th}-order polynomials is not easily obtained, because the required memory capacity for the double precision version of the program then exceeds the available high-speed memory of the Control Data Corporation 3600 Computer. However, it does not really appear to be necessary to make this check, since in most cases the 7^{th}- and 8^{th}-order (or 6^{th}- and 8^{th}-order) polynomial solutions agree to sufficient significant figures for the latter to be regarded as satisfactory.

Another measure of roundoff is obtainable from a study of a few cases where an exact solution is available, or where considerations of symmetry demand an odd function. Any case involving tensile loading of identical adherends ($\alpha = 1$) should show adhesive stresses uniform along the joint, and independent of the parameter β (this is discussed further, later). From such cases, and from those bending problems where $\alpha = 1$, it is possible to estimate that roundoff error accumulations for 8^{th}-order polynomial Ritz functions (177 equations) consistently affect a few units in the fifth decimal place, ranging occasionally up to 1 unit in the fourth place. This roundoff contribution is independent of the absolute size of the particular stress tabulated. However, it represents a small error in the

significant (i.e., numerically larger) values of any of the tabulated stresses. It is quite clear that imperfect convergence is a far more important source of error than roundoff accumulation. Roundoff error may make it impossible to go to 9^{th}-order polynomials, however, unless double precision arithmetic is used, or some effort is made to "purify" the inverse of the Ritz matrix.

3.1.4 Convergence of the Approximating Sequence

Convergence is studied primarily in the quantities wanted as an end result, the adhesive stresses. From the discussion of the preceding sections, this also amounts to an examination of the convergence of the adherend displacements. To do this, a number of cases are studied in which the adhesive normal and shear stresses are obtained by successively assuming displacement functions consisting of the sum of all homogeneous polynomials through the 6^{th}, 7^{th} and 8^{th} degree. Considering that four displacements are involved and subtracting the three rigid-body constants, this amounts to solving 109, 141 and 177 simultaneous equations, respectively. Typical cases examined include $\beta = 20$ (an intermediate level of flexibility), $\gamma = 4$ (a 4:1, or substantial level of adherend dissimilarity), for $\alpha = 5°$, $10°$, and $30°$, in both tensile and bending load. The tensile loading level here is a unit stress parallel to X, and the

largest bending stress is also unity (Fig. 7). For tensile load, and in most cases for bending load, it is found that the adhesive stresses appear to approach a definite limit.

In using 6^{th}-, 7^{th}- and 8^{th}-degree polynomials, the larger magnitudes of stress are often so close to each other that it is usually not practicable to represent them in terms of tables. Smaller values of stress, of course, are not determined as well as large ones, but they are of less significance precisely because they are small. Tables 3-8 will be used as the framework of this portion of the convergence discussion. Most of the final tabulated results have been treated along the lines of the three samples to be discussed exhaustively in the rest of this section, but in most cases only 6^{th}- order and 8^{th}-order polynomial results have been compared (not the full 6-7-8 sequences as in what follows). In a few cases, only 8^{th}-order results are available. Thus the user usually has one or more indices from which to judge for himself whether he considers the adjacent Ritz solutions to be close enough for the results to be meaningful in his application.

Consider, as a successful example, the tensile load case for the angle $\alpha = 30°$ (upper end of the practical angle range), in Table 3 (next page). The largest shear stress level is of order 0.45, and all orders of polynomial considered give the same stresses to three or more significant figures, usually to better than 0.01%. There appear to be

Table 3.--Adhesive stresses for 6^{th}-, 7^{th}- and 8^{th}-order polynomials (numbers of equations are in parentheses). Tensile loading $\alpha = 30°$, $\beta = 20$, $\gamma = 4$.

	Shear Stress			Normal Stress		
s	6(109)	7(141)	8(177)	6(109)	7(141)	8(177)
-1.0	0.45137	0.45133	0.45131	0.24980	0.25008	0.25024
-0.9	0.44936	0.44932	0.44930	0.24900	0.24904	0.24906
-0.8	0.44741	0.44737	0.44737	0.24861	0.24856	0.24852
-0.7	0.44550	0.44539	0.44539	0.24854	0.24847	0.24844
-0.6	0.44364	0.44364	0.44364	0.24872	0.24868	0.24866
-0.5	0.44180	0.44181	0.44182	0.24908	0.24906	0.24906
-0.4	0.43999	0.44001	0.44002	0.24956	0.24956	0.24957
-0.3	0.43819	0.43822	0.43823	0.25011	0.25012	0.25013
-0.2	0.43642	0.43644	0.43645	0.25067	0.25068	0.25068
-0.1	0.43465	0.43467	0.43468	0.25122	0.25121	0.25120
0	0.43290	0.43289	0.43291	0.25170	0.25168	0.25166
0.1	0.43115	0.43115	0.43115	0.25209	0.25205	0.25203
0.2	0.42941	0.42940	0.42940	0.25234	0.25230	0.25228
0.3	0.42767	0.42765	0.42765	0.25241	0.25238	0.25237
0.4	0.42593	0.42591	0.42590	0.25226	0.25226	0.25227
0.5	0.42418	0.42416	0.42415	0.25183	0.25188	0.25190
0.6	0.42242	0.42241	0.42240	0.25107	0.25116	0.25120
0.7	0.42064	0.42064	0.42064	0.24990	0.25002	0.25007
0.8	0.41882	0.41884	0.41885	0.24825	0.24833	0.24837
0.9	0.41696	0.41700	0.41702	0.24601	0.24596	0.24594
1.0	0.41504	0.41509	0.41510	0.24307	0.24272	0.24257

Table 4.--Adhesive stresses for 6^{th}-, 7^{th}- and 8^{th}-order polynomials (numbers of equations are in parentheses). Tension $\alpha = 10°$, $\beta = 20$, $\gamma = 4$.

	Shear Stress					Normal Stress				
s	6(109)	10^5[7-6]	7(141)	10^5[8-7]	8(177)	6(109)	10^5[7-6]	7(141)	10^5[8-7]	8(177)
-1.0	0.21796	18	0.21814	3	0.21817	0.04209	-249	0.03960	- 79	0.03881
-0.9	0.21058	9	0.21067	- 2	0.21065	0.03472	+ 25	0.03497	+ 14	0.03511
-0.8	0.20394	- 7	0.20387	- 6	0.20381	0.02823	+ 81	0.02904	+ 22	0.02926
-0.7	0.19812	-18	0.19794	-12	0.19786	0.02374	+ 48	0.02422	+ 6	0.02428
-0.6	0.19312	-23	0.19289	- 5	9.19284	0.02165	- 1	0.02164	- 5	0.02159
-0.5	0.18889	-24	0.18865	0	0.18865	0.02186	- 32	0.02154	- 6	0.02148
-0.4	0.18516	-12	0.18504	+ 5	0-18509	0.02392	- 37	0.02355	- 1	0.02354
-0.3	0.18189	- 2	0.18187	+ 8	0.18195	0.02716	- 20	0.02696	+ 3	0.02699
-0.2	0.17884	+ 9	0.17893	+ 8	0.17901	0.03088	+ 4	0.03092	+ 3	0.03095
-0.1	0.17583	+17	0.17600	+ 6	0.17606	0.03440	+ 23	0.03463	- 3	0.03460
0	0.17270	+21	0.17291	+ 1	0.17292	0.03714	+ 28	0.03742	- 11	0.03731
0.1	0.16933	20	0.16953	- 3	0.16950	0.03870	+ 17	0.03887	- 15	0.03872
0.2	0.16561	14	0.16575	- 6	0.16569	0.03891	- 8	0.03883	- 11	0.03872
0.3	0.16150	5	0.16155	- 6	0.16149	0.03777	- 33	0.03744	0	0.03744
0.4	0.15697	- 3	0.15694	- 4	0.15690	0.03553	- 48	0.03505	+ 16	0.03521
0.5	0.15207	-10	0.15197	0	0.15197	0.03257	- 40	0.03217	+ 27	0.03244
0.6	0.14686	-13	0.14672	+ 3	0.14676	0.02940	- 5	0.02935	+ 23	0.02958
0.7	0.14143	-10	0.14133	+ 5	0.14138	0.02655	+ 46	0.02701	- 1	0.02700
0.8	0.13587	0	0.13587	+ 3	0.13590	0.02447	+ 81	0.02528	- 35	0.02493
0.9	0.13031	+ 9	0.13040	0	0.13040	0.02342	+ 31	0.02373	- 32	0.02341
1.0	0.12482	+12	0.12494	1	0.12495	0.02327	-212	0.02115	+113	0.02228

"random" differences in the fourth and fifth significant figures. At some points in the table the stress level goes down slightly with increasing polynomial order; at others, up slightly; and in still others changes very little. For example, at S = -1.0, the value goes from 0.45137 (for 6^{th}-order) to 0.45133 (7^{th}-order) to 0.45131 (8^{th}-order). At S = 0.9, the trend is reversed, and the respective (6,7,8) figures are 0.41696, 0.41700, 0.41702. At S = -0.6, there are no changes at all in any of the figures given. These changes can be shown to be systematic rather than random. The difference between the 7^{th}- order and the 6^{th}-order solutions can be plotted to reveal a 7^{th}-order polynomial of very small maximum amplitude, affecting only the last significant figure of the five given in Table 3. In the same way, the difference between the 8^{th}-order and the 7^{th}-order solutions is an 8^{th}-order polynomial of even smaller maximum amplitude, affecting the last significant figure to a somewhat smaller extent. All differences between adjacent polynomial solutions have this character, so that it is only worthwhile to examine the larger differences. These differences are invariably expressed as a percentage of the highest-order solution, in the discussion which follows. Effectively, it seems fair to say that very good convergence has been achieved for the shear stress in this particular example.

Another measure of convergence has also been examined. It is difficult to inspect the small-amplitude "difference polynomials" just described and decide how much the calculated shear or normal stress function has shifted as a whole with increase in number of terms. To assess this shift, the average shear or normal stress along the length of the joint may be calculated by integration, and the values for adjacent Ritz solutions compared. The most convenient way to do this is to integrate the difference polynomial along the length of the joint. This is a small quantity when convergence is adequate, and its general order of magnitude is about as informative as an accurate absolute value. This index, therefore, has been computed directly from the tabulated output data, using numerical integration and Simpson's rule, rather than by analytical integration. A sample of the "difference polynomials" is given later.

Thus, referring to Table 3, the average difference in shear stress between the 7^{th}-order and 6^{th}-order results is $-2(10^{-7})$, and between the 8^{th}-order and 7^{th}-order is $2(10^{-6})$. For reference, the typical shear stress level is about 0.43. The present index also seems to support the assertion that practical convergence has been obtained for the case under consideration. The fact that the (8-7) difference is larger than the (7-6) difference can probably be ascribed to the rounding of figures to five, for the purposes of tabulation. Some small contribution may also

be present due to accumulated roundoff in the Ritz matrix inversion, which is believed to have a small but measurable effect in the case of 8^{th}-order polynomials.

For this relatively large value of α, the adhesive normal stress is smaller than, but still comparable to, the shear stress. Generally speaking, in all calculations it appears that the normal stress converges more slowly than the shear stress, possibly as a result of different physical mechanisms involved. Joint end-values are particularly uncertain, but these are not always the points of greatest adhesive normal stress. This general behavior is seen to a slight extent in Table 3, where three significant figures are absolutely stable, but the fourth may vary as much as 3.5 units as we sweep through the polynomial orders 6-7-8. Nevertheless, it still seems fair to say that good adhesive normal-stress convergence has been achieved in this particular example (other examples are not nearly as favorable). The (7-6) normal stress difference averages to $-1(10^{-6})$ along the joint, while the (8-7) figure is $5(10^{-7})$, both to be compared to a typical normal stress level of about 0.25. This index also implies that the overall solutions are in good agreement, despite local variations. Thus, even 109 equations deliver average stresses which agree well with the average values for 141 and 177 equations. The index in question is perhaps a good measure of overall equilibrium, but says very little about the accuracy with which distributions have been determined.

The tensile load case in Table 4 ($\alpha = 10°$, $\beta = 20$, $\gamma = 4$), page 83, shows the same general behavior. Here the angle $\alpha = 10°$ is near the lower end of the practical range, and the shear stress is much smaller than for $\alpha = 30°$ (Table 3). The shear stress agreement between 7^{th}- and 8^{th}-order solutions is very good. This is particularly easy to see in Table 4, because the "difference polynomials" have been included in this table as a sample, under such headings as 10^5[7-6]. The normal stress is now 10 times smaller than for the 30° case, and the slower rate of convergence always observed for this stress component means that a good deal more variation is found as the order of the polynomials is increased. Over most of the joint, this still amounts to changes of less than 1% between 7^{th}- and 8^{th}-order results. At or near the ends, as much as 5% change can be detected in going from the 7^{th}-order to the 8^{th}-order solution (e.g., at the end $s = 1.0$). It must be remembered that the normal stress at this point is not the largest value along the adhesive joint, and also that it is always less than one-quarter the size of the shear stress at the same point. A modest uncertainty in its determination does not preclude the general statement that satisfactory convergence seems to have been achieved. This is particularly true if we think in terms of the combined stress picture for the adhesive, which will be dominated by the rather well-determined and much larger shear stress. The (7-6) average adhesive

shear stress difference for this case is $-2(10^{-6})$, and the (8-7) value is the same, both referred to average stresses of about 0.17. The respective data for the normal stress are $-2(10^{-6})$ and $1(10^{-6})$, implying better overall "adjacency" than the local variations at the joint ends might at first appear to indicate.

The tensile load example of Table 5 ($\alpha = 5°$, $\gamma = 4$, $\beta = 20$) page 90, has been included here as a particularly poor example: the Ritz method is approaching the limits of its effectiveness for simple polynomial inputs. (The 5° angle is also probably smaller than normally attempted in most technological applications, since such a scarf joint is hard to make. It has been included primarily to see how far we can push the Ritz method, particularly in connection with bending--discussed later). The shear stress now falls below 0.1 over most of the joint, which means that the changes with polynomial order usually observed in the fourth and fifth decimal place affect the third significant figure rather than the fourth, as before. Nevertheless, the 7^{th}- and 8^{th}-order shear stress results agree to better than 0.5% at all points, and better than 0.35% at all points where the shear stress is large. This is considered to be adequate convergence for most purposes. The corresponding average-difference indices are $-1(10^{-6})$ for (7-6) and $-5(10^{-7})$ for (8-7), on a reference scale of about 0.09 average shear stress.

Table 5.--Adhesive stresses for 6^{th}-, 7^{th}- and 8^{th}-order polynomials.
$\alpha = 5°$, $\beta = 20$, $\gamma = 4$ Tensile Loading

	Shear Stress			Normal Stress		
s	6(109)	7(141)	8(177)	6(109)	7(141)	8(177)
-1.0	0.13756	0.13785	0.13785	0.00121	0.00659	0.01201
-0.9	0.12497	0.12484	0.12493	0.01327	0.01210	0.01019
-0.8	0.11441	0.11395	0.11410	0.01185	0.00923	0.00805
-0.7	0.10625	0.10569	0.10573	0.00609	0.00478	0.00544
-0.6	0.10043	0.10002	0.09988	0.00112	0.00192	0.00328
-0.5	0.09667	0.09654	0.09624	-0.00083	0.00152	0.00242
-0.4	0.09450	0.09466	0.09433	0.00050	0.00316	0.00319
-0.3	0.09337	0.09375	0.09352	0.00417	0.00590	0.00525
-0.2	0.09273	0.09320	0.09317	0.00872	0.00875	0.00794
-0.1	0.09208	0.09249	0.09268	0.01270	0.01093	0.01042
0	0.09098	0.09126	0.09160	0.01499	0.01208	0.01203
0.1	0.08913	0.08925	0.08961	0.01507	0.01217	0.01247
0.2	0.08635	0.08635	0.08661	0.01312	0.01145	0.01183
0.3	0.08261	0.08256	0.08262	0.00990	0.01033	0.01054
0.4	0.07799	0.07796	0.07782	0.00665	0.00917	0.00915
0.5	0.07267	0.07269	0.07242	0.00464	0.00820	0.00807
0.6	0.06690	0.06694	0.06670	0.00481	0.00740	0.00737
0.7	0.06092	0.06090	0.06082	0.00705	0.00658	0.00668
0.8	0.05493	0.05477	0.05491	0.00948	0.00553	0.00553
0.9	0.04897	0.04880	0.04899	0.00757	0.00437	0.00412
1.0	0.04288	0.04329	0.04308	-0.00697	0.00411	0.00488

Table 6.--Bending $\alpha = 30°$, $\beta = 20$, $\gamma = 4$

-1.0	0.05807	0.05899	0.05948	0.29183	0.28525	0.28131
-0.9	0.05451	0.05538	0.05587	0.27289	0.27181	0.27144
-0.8	0.04987	0.05046	0.05074	0.24611	0.24730	0.24808
-0.7	0.04442	0.04466	0.04471	0.21350	0.21518	0.21598
-0.6	0.03838	0.03830	0.03819	0.17770	0.17821	0.17865
-0.5	0.03194	0.03163	0.03143	0.13798	0.13853	0.13863
-0.4	0.02524	0.02477	0.02457	0.09780	0.09782	0.09775
-0.3	0.01840	0.01790	0.01772	0.05759	0.05736	0.05729
-0.2	0.01150	0.01106	0.01093	0.01834	0.01814	0.01820
-0.1	0.00463	0.00432	0.00423	-0.01911	-0.01906	-0.01883
0	-0.00217	-0.00237	-0.00235	-0.05400	-0.05392	-0.05327
0.1	-0.00883	-0.00878	-0.00876	-0.08551	-0.08487	-0.08449
0.2	-0.01530	-0.01508	-0.01501	-0.11302	-0.11232	-0.11203
0.3	-0.02153	-0.02118	-0.02107	-0.13579	-0.13530	-0.13522
0.4	-0.02745	-0.02705	-0.02689	-0.15301	-0.15304	-0.15326
0.5	-0.03296	-0.03260	-0.03245	-0.16383	-0.16461	-0.16514
0.6	-0.03797	-0.03775	-0.03767	-0.16726	-0.16879	-0.16956
0.7	-0.04253	-0.04236	-0.04241	-0.16214	-0.16408	-0.16490
0.8	-0.04589	-0.04624	-0.04646	-0.14716	-0.14860	-0.14910
0.9	-0.04844	-0.04912	-0.04945	-0.12075	-0.12001	-0.11957
1.0	-0.04973	-0.05065	-0.05083	-0.08110	-0.07544	-0.07309

The adhesive normal stress is very small at this angle, which is fortunate, for the Ritz process can hardly be said to have converged. Only the leading figure can be considered significant at many points, and at most of the others there is uncertainty in the second significant figure. If it were of technical importance to determine the adhesive normal stress very accurately, the present methods would have to be abandoned in favor of other approaches. The normal stress average differences here are $6(10^{-6})(7\text{-}6)$ and $7(10^{-6})(8\text{-}7)$, where the reference level is about 0.012.

In general, bending load seems to place a far greater strain on the capabilities of polynomial displacement functions than tensile load, and convergence is not always clearly established. The bending load case of Table 6 ($\alpha = 30°$, $\beta = 20$, $\gamma = 4$), page 90, shows variations affecting the second significant figure of the adhesive shear stress as the order of polynomials is increased, where the corresponding tensile load case is affected in the fourth figure. Since both shear and normal stress change sign for loading by moments, it seems useful to study convergence for the numerically larger positive and negative values of stress only. The largest difference between the 7^{th}- and 8^{th}-order results occurs between $S = -0.9$ and $S = -1.0$, and amounts to less than 0.9%; all other differences represent smaller percentages than this for stress values above the magnitude 0.024 (where 0.059 is the largest

absolute value). The normal stress pattern for this case offers some novelty because larger normal stresses than shear stresses are encountered for the first time. Comparing polynomial orders 7 and 8 for the larger stress range (above 0.119 where 0.28 is the maximum), it is found that the differences are below 0.5% everywhere except at S = -1.0, the joint end. (The difference at S = 1.0 is 3.2%, but this is a point of rather small normal stress.) A difference of 1.4% is observed at the end S = -1.0, where the normal stress level takes on its largest value, 0.281. This probably can be characterized as adequate convergence, depending upon the needs of the user. The average-difference indices for shear stress are $1.4(10^{-5})(7-6)$ and $1.5(10^{-6})(8-7)$, where the largest stress value is about 0.06. The respective results for normal stress difference are $-3(10^{-5})(7-6)$ and $1(10^{-5})(8-7)$, referred to a largest datum level of 0.28.

The bending load case of Table 7 ($\alpha = 10°$, $\beta = 20$, $\gamma = 4$), page 93, shows slightly better convergence of the adhesive shear stress values than the preceding case. For values larger than 0.04 (where 0.1 is maximum), the 8^{th}-order result never differs from the 7^{th}-order result by more than 0.3%. The normal stress calculation convergence is inferior. If attention is confined to values above 0.02 (where 0.04 is the maximum), then the largest difference is less than about 2%. If the lower limit considered is 0.016, however,

Table 7.--Adhesive stresses for 6^{th}-, 7^{th}- and 8^{th}-order polynomials.
Bending $\alpha = 10°$, $\beta = 20$, $\gamma = 4$

	Shear Stress			Normal Stress		
s	6(109)	7(141)	8(177)	6(109)	7(141)	8(177)
-1.0	0.10148	0.10110	0.10098	0.00707	0.01379	0.01632
-0.9	0.09122	0.09106	0.09104	0.02661	0.02599	0.02548
-0.8	0.07998	0.08015	0.08030	0.03812	0.03587	0.03513
-0.7	0.06780	0.06822	0.06843	0.04177	0.04030	0.04009
-0.6	0.05486	0.05538	0.05554	0.03863	0.03847	0.03866
-0.5	0.04150	0.04194	0.04196	0.03039	0.03115	0.03142
-0.4	0.02809	0.02833	0.02821	0.01899	0.02002	0.02015
-0.3	0.01502	0.01500	0.01479	0.00639	0.00715	0.00712
-0.2	0.00268	0.00242	0.00219	-0.00565	-0.00542	-0.00549
-0.1	-0.00860	-0.00903	-0.00920	-0.01574	-0.01599	-0.01595
0	-0.01857	-0.01905	-0.01911	-0.02293	-0.02342	-0.02320
0.1	-0.02708	-0.02745	-0.02739	-0.02677	-0.02715	-0.02682
0.2	-0.03391	-0.03418	-0.03402	-0.02734	-0.02737	-0.02710
0.3	-0.03921	-0.03928	-0.03909	-0.02519	-0.02478	-0.02478
0.4	-0.04305	-0.04292	-0.04278	-0.02123	-0.02054	-0.02094
0.5	-0.04560	-0.04533	-0.04530	-0.01661	-0.01600	-0.01669
0.6	-0.04711	-0.04681	-0.04689	-0.01247	-0.01240	-0.01298
0.7	-0.04784	-0.04766	-0.04770	-0.00974	-0.01048	-0.01043
0.8	-0.04809	-0.04811	-0.04821	-0.00882	-0.01009	-0.00917
0.9	-0.04808	-0.04830	-0.04828	-0.00921	-0.00968	-0.00884
1.0	-0.04797	-0.04819	-0.04810	-0.00914	-0.00576	-0.00873

Table 8.--Bending $\alpha = 5°$, $\beta = 20$, $\gamma = 4$

-1.0	0.09976	0.09976	0.09974	0.01232	0.01159	0.00826
-0.9	0.08395	0.08392	0.08376	0.00704	0.00717	0.00831
-0.8	0.06888	0.06894	0.06876	0.00652	0.00697	0.00761
-0.7	0.05448	0.05462	0.05460	0.00739	0.00769	0.00732
-0.6	0.04079	0.04095	0.04115	0.00781	0.00774	0.00707
-0.5	0.02780	0.02800	0.02839	0.00704	0.00661	0.00622
-0.4	0.01591	0.01593	0.01629	0.00504	0.00447	0.00448
-0.3	0.00499	0.00491	0.00512	0.00223	0.00179	0.00201
-0.2	-0.00474	-0.00489	-0.00491	-0.00079	-0.00087	-0.00069
-0.1	-0.01317	-0.01335	-0.01358	-0.00341	-0.00309	-0.00305
0	-0.02022	-0.02038	-0.02073	-0.00521	-0.00457	-0.00462
0.1	-0.02586	-0.02596	-0.02628	-0.00597	-0.00527	-0.00523
0.2	-0.03011	-0.03013	-0.03031	-0.00575	-0.00529	-0.00508
0.3	-0.03302	-0.03297	-0.03297	-0.00485	-0.00489	-0.00459
0.4	-0.03472	-0.03463	-0.03447	-0.00378	-0.00434	-0.00419
0.5	-0.03535	-0.03526	-0.03505	-0.00303	-0.00390	-0.00414
0.6	-0.03511	-0.03505	-0.03492	-0.00303	-0.00371	-0.00420
0.7	-0.03420	-0.03420	-0.03421	-0.00378	-0.00372	-0.00418
0.8	-0.03283	-0.03288	-0.03298	-0.00466	-0.00369	-0.00332
0.9	-0.03120	-0.03124	-0.03130	-0.00403	-0.00320	-0.00224
1.0	-0.02948	-0.02936	-0.02938	-0.00113	-0.00169	-0.00426

differences of about 4% can be observed, and the values for end S = -1.0 differ by 15.5%. (Again, the stress level here is only 40% of the maximum.) The shear stress difference indices are $2(10^{-6})(7-6)$ and $3(10^{-6})(8-7)$, where 0.1 is the maximum, while for normal stress the respective figures are $3(10^{-6})$ and $-4.5(10^{-6})$, referred to a maximum of about 0.04.

The bending load case ($\alpha = 5°$, $\beta = 20$, $\gamma = 4$) of Table 8, page 93, is an example where the convergence is quite good in the shear stress. The largest error is about 1/4%, if we consider stresses larger than about half the maximum value. The 6^{th}-order polynomial results, surprisingly, seem to agree with the 7^{th}-order results somewhat better than the 8^{th} with the 7^{th}. It is tempting to guess that roundoff has affected the 8^{th}-order results. However, the Ritz matrix inverse is exactly the same for both the bending and tensile loading. In the latter case the 7^{th}-order and 8^{th}-order results are quite close. Hence, questions of convergence rather than of roundoff accumulation seem to be involved here. Overall, the convergence of the shear stress seems reasonably good. The average shear stress difference indices are $3(10^{-7})$ for (7-6) and $7(10^{-7})$ for (8-7), referred to largest a shear stress of about 0.10.

The normal stress is very small for this case (Table 8, p. 93). This is just as well, because the Ritz method produces only one significant figure; at a few points, even this is uncertain. The normal stress difference

averages are $3(10^{-5})$ for (7-6) and $-7(10^{-6})$ for (8-7), on a scale of perhaps 0.008. Since the reference stress is small, these are relatively larger average differences than generally encountered before, so the index in question is not completely insensitive to convergence. To summarize the results, it appears that the Ritz procedure with x-y polynomials produces results ranging from very good to "acceptable," for all cases of tensile loading. The adhesive shear stress is always more reliably determined than the normal stress, but where the latter is not well determined, it is usually small enough to be of no great significance for the overall stress pattern. In tensile loading, convergence seems to improve as the scarf angle increases, while in bending, the trends seems to be opposite.

On the other hand, not all of the bending results are reliable. It becomes necessary to put down some "figure of merit" to characterize these cases for the user. These have been chosen as the largest difference between the results for 7^{th}-order and the 8^{th}-order polynomial solutions, expressed as a percentage of the latter, with attention confined (usually) to the larger levels of stress. Where 7^{th}-order data have not been computed (to limit the total computer time involved), the 6^{th}-order results are compared to the 8^{th}-order ones. This is a considerably rougher version of the index.

The second index of merit is the average difference between "adjacent" Ritz solutions. This consists of the

average along the joint of the difference between the adhesive stress calculated from the 8^{th}-order and the 6^{th}-order polynomial solutions (7^{th}-order substituted where available). This index is provided for both the adhesive shear stress and the normal stress. All of these indices are in App. F tables, since there is no room to place them on the sheets tabulating the raw results (Appendix F). As a supplementary warning to the user, an asterisk is placed on each table in Appendix F where the local error in the satisfaction of the stress boundary conditions exceeds 0.1 on a scale of "largest applied stress" = 1.0. As mentioned in section 3.1.1, this is a considerably less reliable indicator than the "percentages" of App. F. It may be of some interest to note how the boundary stress error behaves as the order of the Ritz polynomials is increased. The discussion here is confined to the vicinity of the peak errors in the stress component showing the largest error.

Consider, for example, the tension-loaded case corresponding to Table 4 ($\alpha = 10°$, $\beta = 20$, $\gamma = 4$). The largest shear stress boundary errors at C (Fig. 8) are -0.0256, -0.0247 and -0.0246 for 6^{th}-, 7^{th}- and 8^{th}-order polynomials respectively. (The reference level is a largest applied stress of unity.) This clearly indicates that the boundary stress errors do not decrease very rapidly as the polynomial order increases. What is interesting is that the gradient down from the peak gets larger with polynomial

order, i.e., the error effect becomes more localized. The Ritz solution is attempting to conform to the local stress singularity ignored in the analysis, as well as a polynomial can while still satisfying the remaining boundary conditions of a stress-free edge. Possibly, if the order of the polynomials could increase greatly and a solution could still be obtained, the error "spike" would grow to very large values, but becomes very narrow.

The shear stress boundary condition errors for the bending-load case at E (Fig. 9) are -0.0676 for the 6^{th}-order, -0.0654 for the 7^{th}-order and -0.0629 for the 8^{th}-order polynomial. This indicates that the level of error for the bending load case likewise does not decrease much in magnitude as the degree of the polynomials used is increased. As in the case of tensile loading, the significant trend observed is a steeper gradient in the shear stress boundary condition error with increasing polynomial order.

At the same points, the normal stress σ_Y is much smaller and thus closer to the desired zero boundary values. Its general behavior is similar. In the case of tensile loading, the point-C values are -0.00343 (6^{th}-order), -0.00353 (7^{th}-order), -0.00337 (8^{th}-order). For the bending load case, at E the values are -0.00999, -0.00946 and -0.00914 (6^{th}-, 7^{th}- and 8^{th}-order polynomials respectively).

3.1.5 Overall Equilibrium Check

As another check of the results, a few sample cases have been examined for various aspects of overall equilibrium. In one approach, this involves finding the resultant forces produced on each of the four trapezoidal boundaries of adherend 1, and writing the three equations of static equilibrium. In each case, the stresses used are the actual ones produced by differentiating the polynomial solution, not the exact input boundary conditions. On the inclined adhesive interface, the stresses chosen are also the less exact ones produced by differentiation, for consistency. All integrations reported here are carried out analytically, using the 8^{th}-order polynomial solutions.

Since these calculations have the error level of the stresses, which is substantially larger than that of the displacements, no great perfection of the results is anticipated. The integration process for finding resultants may improve the situation somewhat, however. The resultant forces should theoretically be zero, of course, so that a reference level has to be devised to help evaluate the numbers representing resultant force and moment. For tensile loading of the adherends, the logical reference level is the input force derived from the unit stress acting on a member height of $2h = 2.0$. The representative length required for examining overall moment equilibrium is somewhat more of a puzzle. As one possibility, it could

be thought of as the adherend height 2h = 2, producing a moment of 2(2) = 4 units. However, since error tractions act on long sides of the adherends, as well as the short sides, a better choice (perhaps) might be the average length of the adherend in the X-direction, (2 + cot α), making the reference level for moment angle-dependent. The latter length ranges to about 10 for the smallest α considered (5°), producing a reference level for moment of 2(10) = 20; it is 2(3.73) $\simeq$ 7.5 for α = 30°.

For bending load, a suitable force and moment reference level are about as hard to choose. For moment, the applied moment could be used. The input bending stress for this case varies from +1 to -1 as y ranges from -h to +h (nondimensional Y goes from -1 to +1). The resultant force from Y = 0 to 1 can be chosen as a reference level for force (= 1/2 unit). The corresponding applied moment is then 1/2(4/3) = 2/3. However, the argument about error tractions acting on the long sides is just as valid here as before, in which case the reference levels for moment become angle-dependent values perhaps (1/2)/2.0 = 1/4 as large as those estimated for the tensile-loaded system. With these uncertainties in mind, we examine a few sample cases which have been tabulated below. The calculations are carried out using the separate stress distributions for adherends 1 and 2, in bending and tensile load. Also tabulated are the resultants for the overall equilibrium

Table 9.--Disequilibrium of forces and moments.

			Adherend 1			Adherend 2			Overall		
α	β	γ	X-Force	Y-Force	Moment	X-Force	Y-Force	Moment	X-Force	Y-Force	Moment
Tension											
10°	20	4	0.00452	0.00439	0.05370	-0.00253	0.00268	0.00315	0.01167	-0.00593	-0.05298
20°	20	4	0.00223	0.00045	-0.00200	0.01113	-0.00161	-0.00389	-0.00764	0.00352	0.00590
30°	20	4	-0.00694	0.00843	-0.00939	0.00699	0.00139	-0.00037	-0.01385	0.00770	0.00814
Bending											
10°	20	4	-0.00163	0.00928	0.00259	-0.00292	-0.00689	-0.00603	-0.01218	0.01416	0.11792
20°	20	4	0.00383	0.01079	-0.00105	-0.02880	0.00022	0.03580	0.02055	0.00056	-0.00744
30°	20	4	0.00952	-0.00137	-0.03130	-0.04970	-0.00266	0.04130	0.05387	-0.02122	-0.09050

of the two joined members, with the interior adhesive interfaces making no contribution at all.

Considering the tensile load case, with datum force 2.0, the force resultants tabulated seem generally good. No error exceeds 1/2% significantly, and most values are a good deal smaller. Moment equilibrium discrepancies are comparably small, in adherends 1 and 2 taken separately, if the angle-dependent reference level criterion is adopted. For example, the 10° (adherend 1) figure of 0.0537 is small on a scale of 20, and not even too bad on the more conservative scale of 4 units. The "overall" columns seem to provide the same sort of error level also, but perhaps here the moment reference level at 10° can be enlarged to 40, since the largest dimension of the system doubled.

Bending-load force resultants are not quite as good, for a reference level of 0.5, but this is to be expected from the rather large boundary stress errors in Table 1, and the generally less satisfactory results observed for the bending solution. Even so, no error is as large as 10% of the nominal datum level in either adherend considered alone. This 10% level occurs for $\alpha = 30°$, $\beta = 20$, $\gamma = 4$. The Table 1 data for this case shows a largest stress error of 0.428 (on a scale of unity, or 42.8%) in the shear stress which directly affects the present error quantity. Thus there appears to be some gain in the process of integrating to resultants. The "overall" columns do not change the pattern appreciably.

Moment equilibrium in bending is again hard to interpret because of the uncertainty regarding the reference level. If the angle-dependent length is chosen, the reference level for moment becomes (1/2)(10) = 5 for individual adherends with $\alpha = 10°$, and perhaps twice this for the overall case. On this optimistic basis, even the worst cases appear to be fairly satisfactory.

Another sort of overall check is possible, one where significance should be very much greater. The tabulated adhesive stresses of this thesis are presumably much more accurate than the stresses calculated by differentiating displacements (discussed in Section 3.1.1). Therefore, it is reasonable for us to test how well they hold the exact input boundary tractions in equilibrium. The tractions are the pure tensile stress at the end of each adherend, or the linearly-distributed stresses at the same ends (bending load case). To be explicit, these should be supplemented by the vanishing of stress at the top and bottom of each adherend, and of the shear stress on the extreme ends. Tabulated in Table 10, for the cases treated in the preceding table, are the resultant forces and moment produced when the "more exact" adhesive stress resultants are equilibrated against the input forces and moments.

Table 10.--Sample overall equilibrium checks

			Either Adherend		
α	β	γ	X-Force	Y-Force	Moment
Tension*					
10	20	4	0.0000055	0.0000054	0.000029
20	20	4	0.000025	-0.0000080	-0.0000005
30	20	4	-0.0000048	0.0000047	-0.0000004
Bending**					
10	20	4	0.0000016	-0.0000025	0.00022
20	20	4	-0.0000025	0.0000017	0.00246
30	20	4	0.0000031	0.0000011	0.00631

*Force reference ≃ 2.0; Moment reference ≃ 4.0, or larger, angle-dependent values.

**Force reference ≃ 0.5; Moment reference = 2/3 (applied) or angle-dependent from ≃ 1.85(30°) to 5(10°).

For results of this caliber, it is probably not important which of the many possible reference levels discussed before are used, with possible exception of the moment imbalance for bending load. Even using the most conservative reference level of 2/3, the applied moment, the worst error is now less than 1% (α = 30°, β = 20, γ = 4, bending). This, incidentally, is for a case showing very large boundary-stress errors in Table 1. Whatever else may be said about the precision with which the adhesive stress curves are determined by the Ritz process, the

overall resultants of these stresses seem to equilibrate the input forces in satisfactory fashion.

3.2. Confirmation by the Integral Equation Method

The approach outlined in Section 2.3 is quite complex and radically different from the Ritz method. Any reasonable degree of agreement between solutions obtained these two ways constitutes a further useful check on the present results. As noted before, the largest problem which can be run in the high-speed memory of the CDC 3600 computer involves just enough boundary points to begin to support the Ritz method. The character of the solution, however, is such that it does not seem worthwhile to explore larger-sized problems, by attempting to utilize the slow-speed computer memory. It appears that the integral equation approach is more sensitive to the neglect of wedge-corner singularities than the Ritz method.

This is seen in Figs. 10 and 11, comparing the adhesive shear and normal stresses obtained by the Ritz and the integral equation methods. Over most of the length of the adhesive joint, the agreement is quite good. Near the ends, the integral equation method shows large sudden departures from the general trend of the curves (and from the Ritz results). These are believed to be associated with the neglect of stress singularities, or to treating the sharp direction changes at the corners as continuously

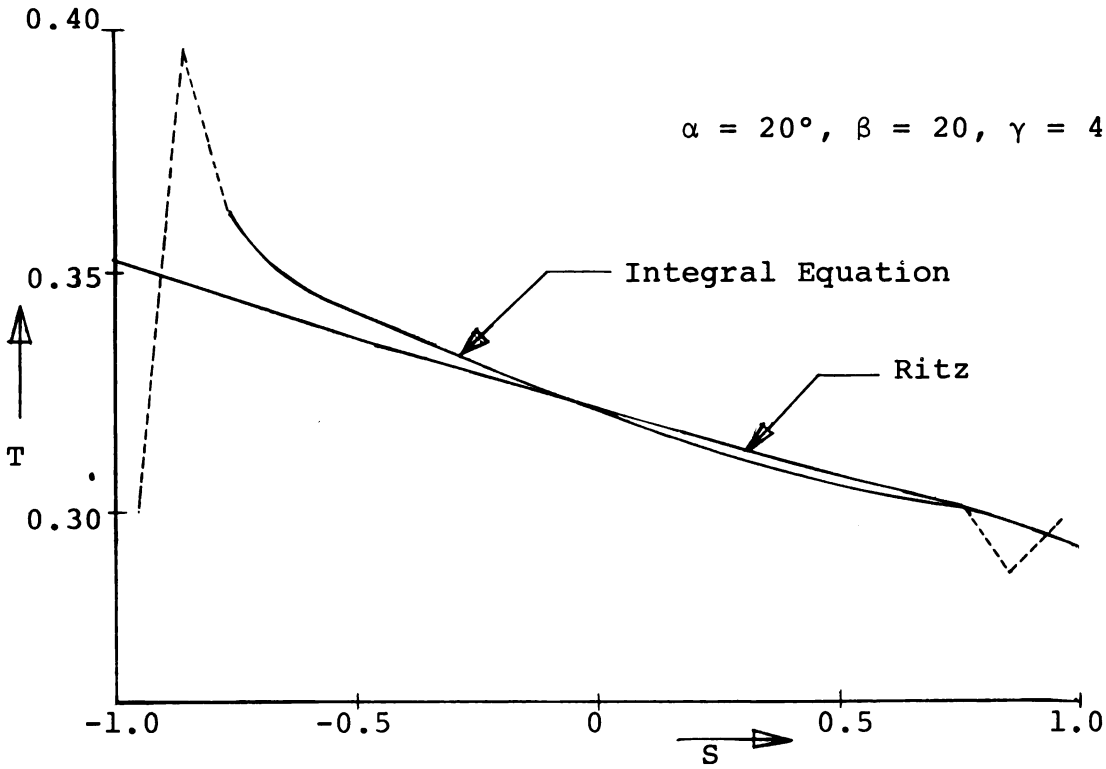

Fig. 10 Shear stress (T) by Ritz and integral equation methods.

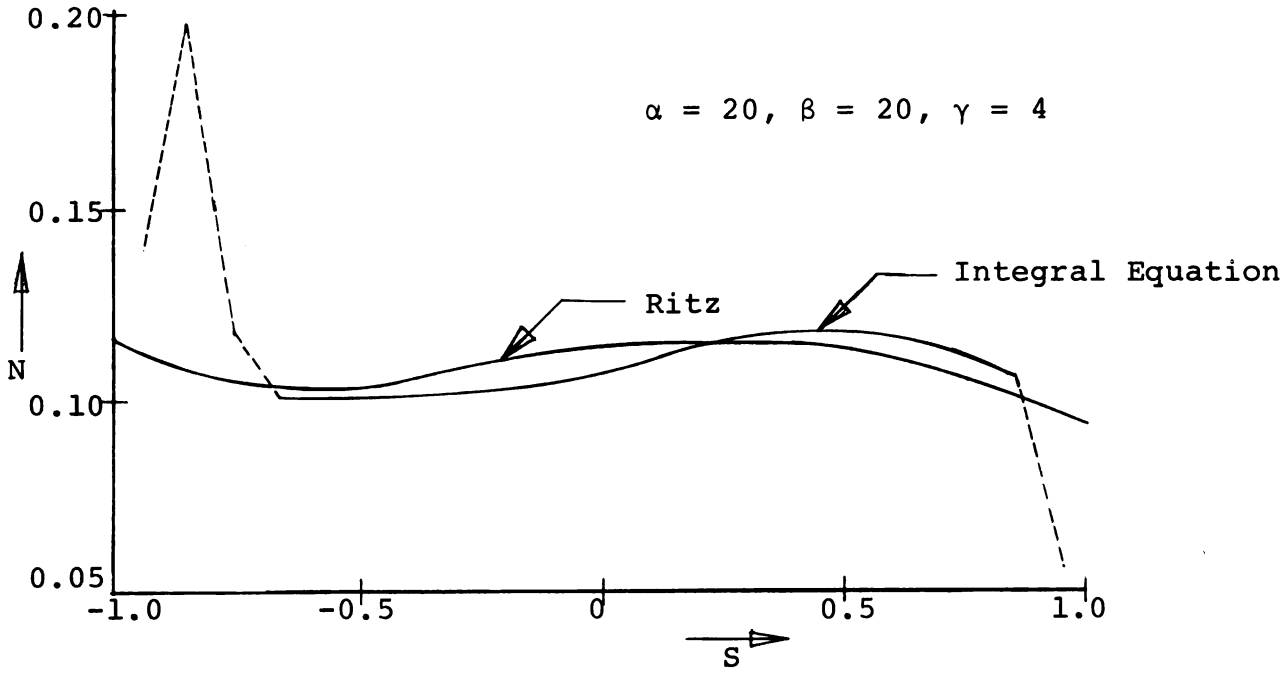

Fig. 11 Normal stress (N) by Ritz and integral equation methods.

turning tangents (which may amount to the same thing as neglecting singularity stresses). It is considered possible (but not likely) that these effects would be reduced if larger-sized problems could be explored. The overall agreement is adjudged sufficient for us to be able to say that the integral equation method does support the Ritz method, despite the substantial differences in the two approaches.

CHAPTER IV

ENGINEERING SIGNIFICANCE OF THE RESULTS

A considerable amount of discussion of the results has necessarily taken place in Chapter III, with primary emphasis on evaluating their quality. Here, attention is centered on their physical and engineering significance. When the scarf joint consists of elastically-dissimilar members, which is the general case here, it becomes important to take account of the sense of the applied loading. Reversal of the loading may cause a numerically-smaller stress component to become the critical one for design purposes. In the following treatment of stress distributions, we will assume that the loading is in the sense pictured in Fig. 7, p. 26. The emphasis will then be on one set of largest stresses, and these will form the basis for the diagrams presented, and their discussion. If the loading were reversed, a different set of largest stresses would become the center of interest. This second discussion has been omitted for brevity. The corresponding material could be drawn from the raw data of Appendix F. When attention is finally focused on principal stresses and the design aspects of the present results, the question of sense of loading is taken into account properly.

4.1 Adhesive Normal and Shear Stress Distributions

The discussion here concerns the general character of the adhesive normal stress (N) and shear stress (T) distribution calculations as a whole. Because of the large number of cases studied, it is impractical to attempt to plot and crossplot all of the results, and the discussion is carried out in terms of representative sample cases. Even here it has been necessary to reduce the presentation of figures to a bare minimum, in order to keep the total number within reasonable bounds.

Primary calculated results for all cases are tabulated in Appendix F, and any desired crossplots may be constructed from these. In addition, the computed Ritz coefficients for each case are available in punched-card form if any further processing of the raw data appears desirable in the future. The stresses T and N are already dimensionless quantities, in the sense that they are the result of a unit applied stress. To recover actual, dimensional adhesive stresses, the user must calculate for his case the values of the parameters α, β and γ. Their definitions can be found in sections 1.4, 2.4 and section 4.3. Interpolation three ways in the tables is then required. Finally, he must multiply the tabulated values by a "load stress." In the case of tensile loading of the joint, the load stress is the actual tensile stress (σ_{X0}) in the

adherends at points remote from the adhesive joint. For pure bending, the "load stress" is the maximum value of the bending stress σ_{X0} at remote points in the adherends (i.e., the usual "Mc/I").

This describes one use of the raw results; advice on interpolation appears in Appendix F. For a discussion of the physical significance of most of the data, however, it is most useful to convert the raw dimensionless stress distributions into an even more meaningful dimensionless form: stress concentration distributions. A primary result of Ref. 7 is that in the case of tensile loading of a scarf joint the adhesive normal and shear stresses are independent of adhesive properties and thickness, and uniform along the joint. Hence they can be calculated from equilibrium alone for each angle α. Thus they comprise a convenient stress reference level for discussion of the influence of adherend dissimilarity and other parameters--the principal goal of this thesis. For tensile loading, then, we take

$$N_C = N/N_0 \qquad T_C = T/T_0 \tag{4.1.1}$$

where

$$N_0 = \sigma_{X0} \sin^2 \alpha \qquad T_0 = \sigma_{X0} \sin \alpha \cos \alpha \tag{4.1.2}$$

are the identical-adherend results for tensile loading. Equations 4.1.1 produce a stress concentration factor of 1, uniform along the joint and independent of the value of β, for the case of identical adherends.

We continue to use the position variable "S," the fraction of the joint half-length, to locate points along the adhesive joint. Since the origin of the coordinate system is fixed at the midpoint of the inclined joint (S = 0 here), the location of (C,F) in Fig. 7 is S = -1.0, and (D,E) correspond to S = 1.0. For bending, not covered by prior theory, the stresses in the adhesive are neither uniform along the joint nor linear, even for the case of identical adherends. Moreover, even these distributions are now β-dependent. Thus the treatment of bending does not benefit greatly from the method of non-dimensionalization now under discussion, and it will be handled differently.

To convert the "stress concentration factor" type of dimensionless stress (N_0, T_0) back to dimensional form, it is necessary to multiply by N_0 or T_0, as well as the "load stress" σ_{X0}.

In discussing the results to follow, we attempt to follow the rule that any behavior pattern pointed out holds for other cases of similar type, unless otherwise noted. The difference for other cases is thus one of degree, not of general trend.

4.1.1 Case of Tensile Loading

Some representative samples of the adhesive shear stress distribution T_C defined in the preceding section are plotted in the main portion of Fig. 12 (the smaller

inset is mentioned later). This shows the stresses due to tensile loading for scarf angle $\alpha = 10°$, for $\beta = 20$ (an intermediate level of adhesive flexibility), and for three of the four values of the dissimilarity parameter: $\gamma = 1$, 2 and 8 (essentially, ratio of adherend 2 Young's modulus to that of adherend 1). Thus only the dissimilarity parameter γ changes. A curve is sometimes omitted, $\gamma = 4$ in this case, when it is so close to another as to confuse the diagrams. Figure 12 indicates that the shear stress is not uniform when the adherends are dissimilar, with the departure from uniformity increasing smoothly as γ increases. This seems reasonable on a physical basis. The omitted curve for $\gamma = 4$ lies between the cases pictured for $\gamma = 2$ and $\gamma = 8$, but closer to $\gamma = 8$ than to $\gamma = 2$. This implies, perhaps, that $\gamma = 8$ is probably rather near the limiting case $\gamma = \infty$ (adherend 2 "rigid"). Note that the largest stress concentration factor is about 1.35, for $\gamma = 8$.

The largest shear stress for all cases of tensile loading follows the pattern shown: it is always at $S = -1$. This can be supported by physical reasoning, because of the simple model adopted here for adhesive strains in terms of relative displacement of the adherend-adhesive interfaces. At $S = -1$, adherend 2 has its smallest stiffness, because it has a sharp point. It therefore deforms very readily. In the same region, adherend 2 is at its stiffest and deforms less readily, by

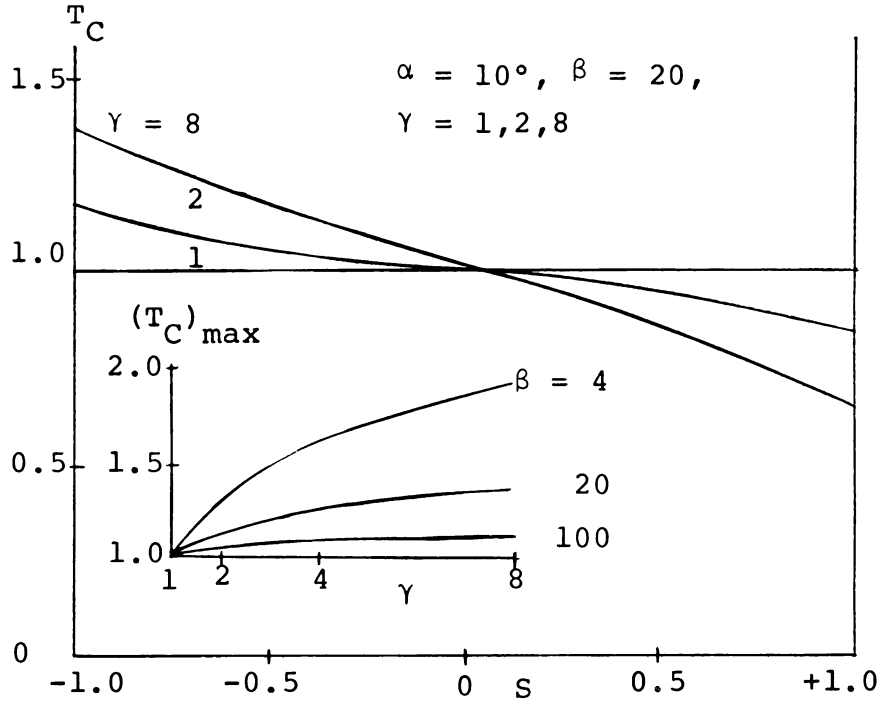

Fig. 12 Shear stress concentration factor (T_C) in tensile loading.

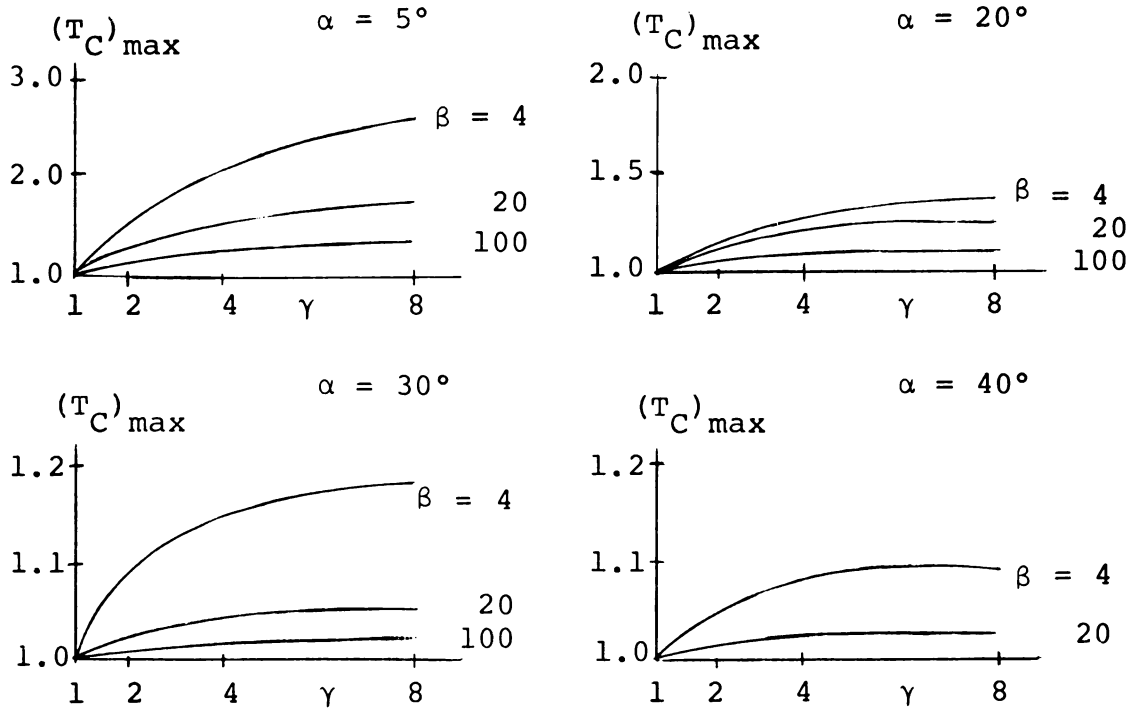

Fig. 13 $(T_C)_{max}$ in tensile loading.

contrast. The situation is geometrically identical but elastically different at the other end. Since the adhesive acquires stress on the basis of relative displacements of adherends, it follows that the local stiffness of tip regions dominates end-region stress generation in the adhesive. Flexible tips yield readily if the opposing member displaces, and do not allow the local relative displacement to become very large. The tip of adherend 2 is the stiffer one whenever $\gamma > 1$, since $\gamma = E_2/E_1$ (essentially). Hence the largest shear stresses are invariably found at this tip, or S = -1. This reasoning should apply to bending load as well as tensile load, and it is offered to account for the asymmetry of the adhesive stresses when the adherends are dissimilar. A few exceptions are discussed later, in connection with bending load cases.

The same pattern is observed with a relatively more flexible adhesive ($\beta = 100$), except that there is much less stress concentration and the adhesive shear stress is almost uniform along the joint for all values of γ: $T_C \simeq 1$. This behavior is found in all prior studies of the stresses in adhesive joints: a very flexible interlayer permits smooth and uniform load transfer. On the other hand, a relatively stiff adhesive layer ($\beta = 4$) results in a substantial exaggeration of the trends of Fig. 12, with the largest shear stress concentration factor (for $\gamma = 8$) reaching 1.84 at the same scarf angle. This number comes from the tables in Appendix F, and can also be deduced from

the small inset diagram in Fig. 12. The latter shows how the maximum shear stress $(T_C)_{max}$, which always occurs at S = -1.0, varies with dissimilarity γ for the fixed value β = 20 of Fig. 12. Also shown are the behavior of $(T_C)_{max}$ for the other values of β at the same scarf angle, $\alpha = 10°$. This simply restates the foregoing discussion pictorially, for the special case of the largest shear stress. The similar diagrams which obtain for the other scarf angles all appear in Fig. 13.

If dissimilarity γ is held fast, adhesive shear stress concentration drops off rapidly with increase in adhesive flexibility, β. This is seen in Fig. 14, for $\alpha = 10°$, $\gamma = 4$, and $\beta = 4, 20, 100$. No inset diagrams of $(T_C)_{max}$ are used here, because the rapid drop off of the maximum shear stress with β is readily visualized from the inset of Fig. 12 and the four parts of Fig. 13.

Figure 15 shows what happens to the adhesive shear stress distribution T_C, for intermediate $\beta(=20)$ and $\gamma(=4)$, when the scarf angle α is varied. It is found that stress concentration increases smoothly but suddenly when α is reduced below 20° (30° and 40° curves conform to the pattern, but are omitted for clarity). Remember, however, that the absolute value of the shear stress T becomes very small as α is made small. Therefore, the stress concentration factor T_C of about 1.59 for $\alpha = 5°$ is applied to a reference stress of small magnitude, $T_0 = \sin \alpha \cos \alpha$.

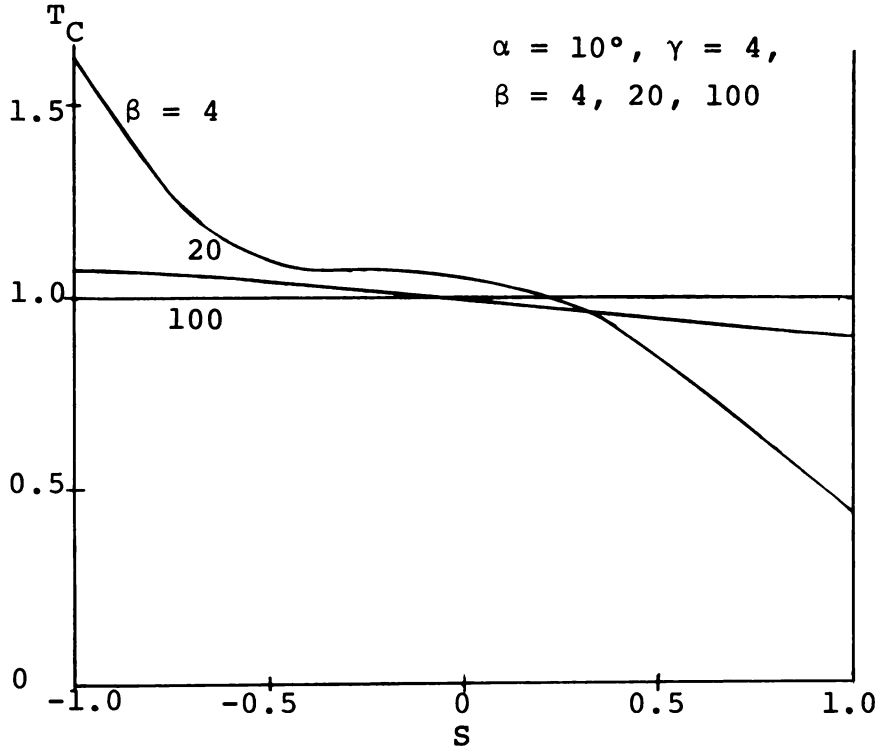

Fig. 14 Shear stress concentration factor (T_C) in tensile loading.

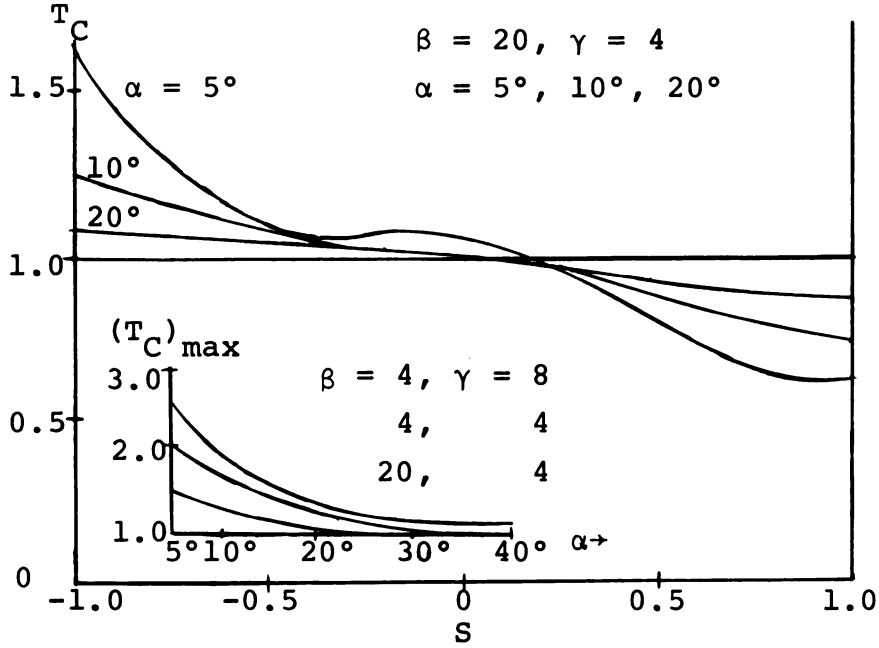

Fig. 15 Shear stress concentration factor (T_C) in tensile loading.

This means that the halving of angle α from 10° to 5° has a much larger effect on the stress magnitudes than the change in local end-stress concentration from 1.59 to 1.28 exhibited at S = -1.0. Within the "manufacturable" range, we are always gaining ground if we reduce the scarf angle, apparently. Figure 15's trend applies to all other cases of α-variation at constant β and γ. The inset diagram of Figure 15 shows some typical variations of $(T_C)_{max}$ with α, for the constant β and γ of the main part of the figure, and the two other sets of β and γ which give the worst shear stress concentration in tensile loading.

The most obvious feature of the adhesive normal stresses of Fig. 16 is their wavy pattern (case of α = 10°; β = 20; γ = 2,4,8). This phenomenon has been observed in the results of prior studies[21] and probably arises from the very nature of the model used for the adhesive. The latter has been treated as an elastic foundation. It is well known that a uniform beam on an elastic foundation (which adheres when the beam attempts to lift) will exhibit a damped sinusoidal displacement pattern if the foundation modulus is large enough. The present problem is complicated by the fact that the "beams" are tapered, but this explanation appears to account for the wavy distribution of normal stress. When the "foundation modulus" decreases (β increases here), the waves become longer and the effect less noticeable. However, when β = 4 the waves shorten and the

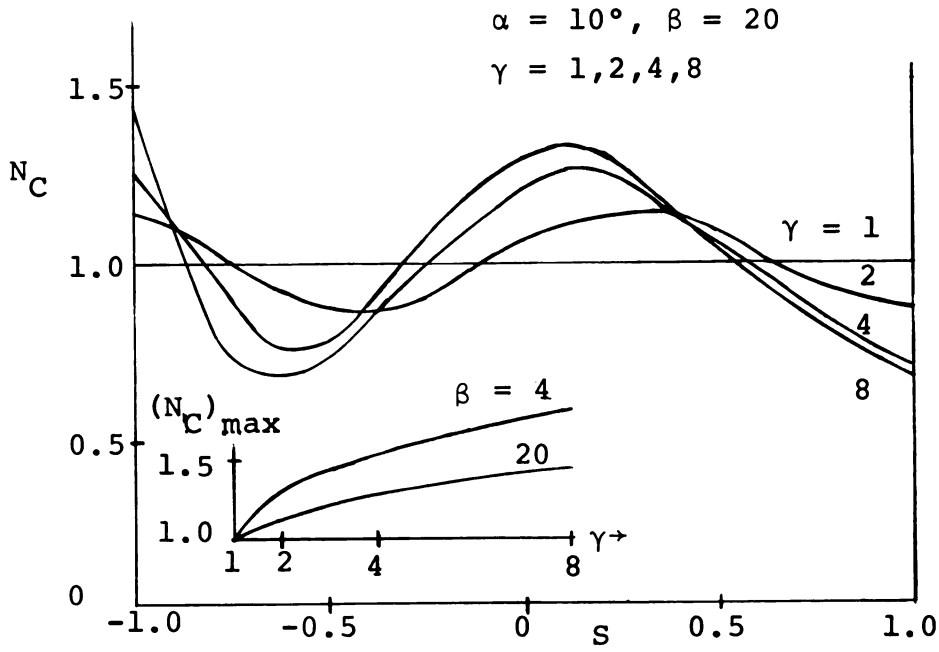

Fig. 16 Normal stress concentration factor (N_C) in tensile loading.

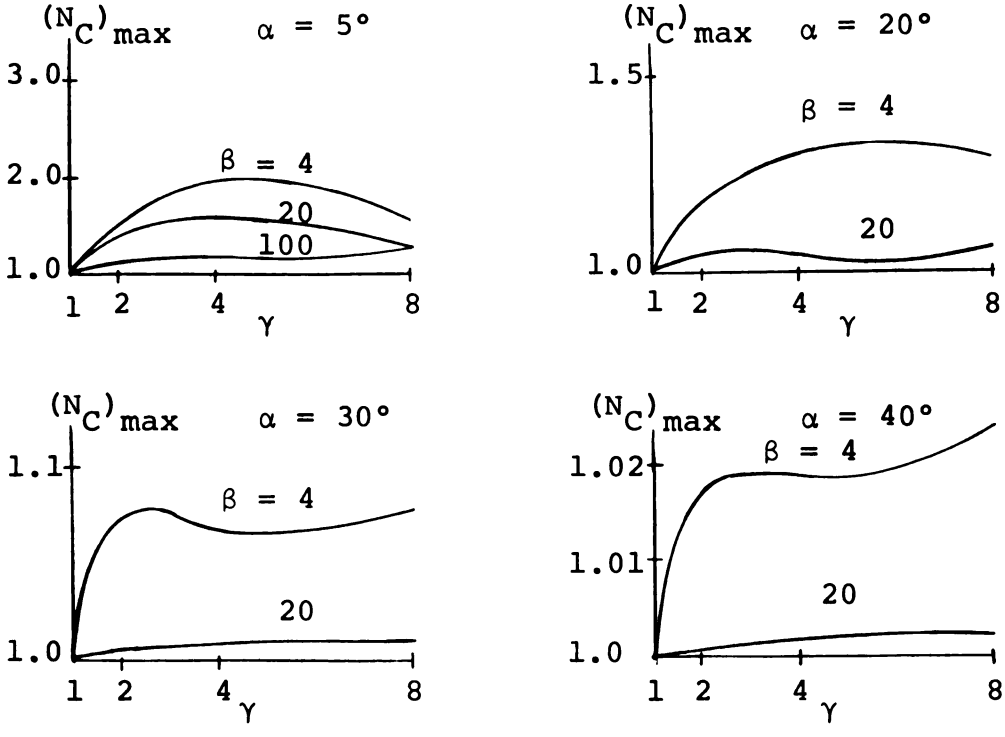

Fig. 17 $(N_C)_{max}$ in tensile loading.

normal stress oscillates very rapidly. This occurs to such a degree that high-order polynomial interpolation in the stress distribution tables of Appendix F is sometimes required, because the 21 points at which the adhesive stresses have been tabulated are not always sufficient to define the normal stress curve properly for the user. Waviness is not observed in shear stress distributions. A crude explanation is as follows: Shear stress is governed by "axial" displacement of the tapered adherend "beams" or, in another analytical formulation, by second-order differential equations for displacement. Normal stress is governed by the bending of these "beams," i.e., by fourth-order differential equations in displacement. The latter can be expected to show damped quasi-sinusoidal waves.

The dimensionless presentation of Figure 16, p. 117, hides the fact that the normal stress is much smaller than the shear stress when α is small, as in the 10° case plotted. It should also be observed that increasing dissimilarity (γ) causes an increase in the largest values of normal stress (wave amplitude). Figure 16 also illustrates the difficulty of stating where the peak normal stress is found. Often it is at or near S = -1, but a secondary peak occurs in the ranges S = 0 to 0.4 (considering all results, not just those pictured). In many cases the differences between the peaks are so small that imperfection of convergence, or even the estimated roundoff error in the calculations, could affect

a decision as to the location of N_{max} or $(N_C)_{max}$. In other cases, N_{max} can be located fairly distinctly. For the large value $\beta = 100$, the normal stress is often so nearly uniform that the location of a peak value is of no great significance.

For practical stress calculations, the significant factor is the adhesive combined-stress situation. This resolves the difficulty, because the relatively large adhesive shear stress usually dominates all types of combined stress of engineering interest, and its location is always at $S = -1$. The uncertainty in N_{max} does complicate any attempt to crossplot normal stress maxima. To aid the user, Appendix F has an auxiliary table giving the values of N_{max}.

The inset diagram in Figure 16 shows a plot of $(N_C)_{max}$ as a function of dissimilarity γ, for the values $\beta = 20$ and $\alpha = 10°$ governing the main part of the diagram. Also shown is the curve for $\beta = 4$ ($\beta = 100$ is close to $N_C \equiv 1$, and is omitted). Remember that N_C has been normalized with respect to $N_0 = \sin^2 \alpha$, which tends to distort the fact that 5° cases exhibit absolute stresses basically 1/4 as large as 10° cases (ignoring the stress concentration effects exhibited in the inset). Values of $(N_C)_{max}$ are plotted without regard to location S. Figure 17 furnishes the same information as the inset diagram just mentioned, for the other four scarf angles.

Figure 18 shows (for fixed $\alpha = 10°$ and $\gamma = 4$) the expected result that the normal stresses become much more nearly uniform as adhesive flexibility β is increased. Finally, Figure 19 shows that normal stress "waves" acquire increasing amplitude (at constant $\beta = 20$, $\gamma = 4$) as scarf angle α is reduced below 20° (same behavior as adhesive shear stress). The 30° and 40° angles are scarcely distinguishable from $N_C = 1$ on this scale. Note once again that the absolute stress level N goes down with α as $\sin^2 \alpha$, so that the modest effect of increasing stress concentration is normally overwhelmed by the gross decrease in magnitude. For example, the 5°, 10° and 20° intercepts on an N basis (not N_C, as in Figure 19), are actually 0.01201, 0.03881, 0.12285, respectively, from the tables in Appendix F. The 30° and 40° results are 0.25024 and 0.41293. Thus the stress concentration type of presentation in this case reveals the increased amplitude of oscillation with decreasing α, but distorts the picture of the magnitude of the stresses.

Before going on to the discussion of the sample bending load cases, one additional set of results is presented, for the case of the butt joint in tension ($\alpha = 90°$). This puts in perspective the enormous influence which the adhesive's relatively large flexibility exerts in the case of metal-to-metal bonds. Figure 20 shows the adhesive normal stress in a butt joint for the stiffest adhesive considered

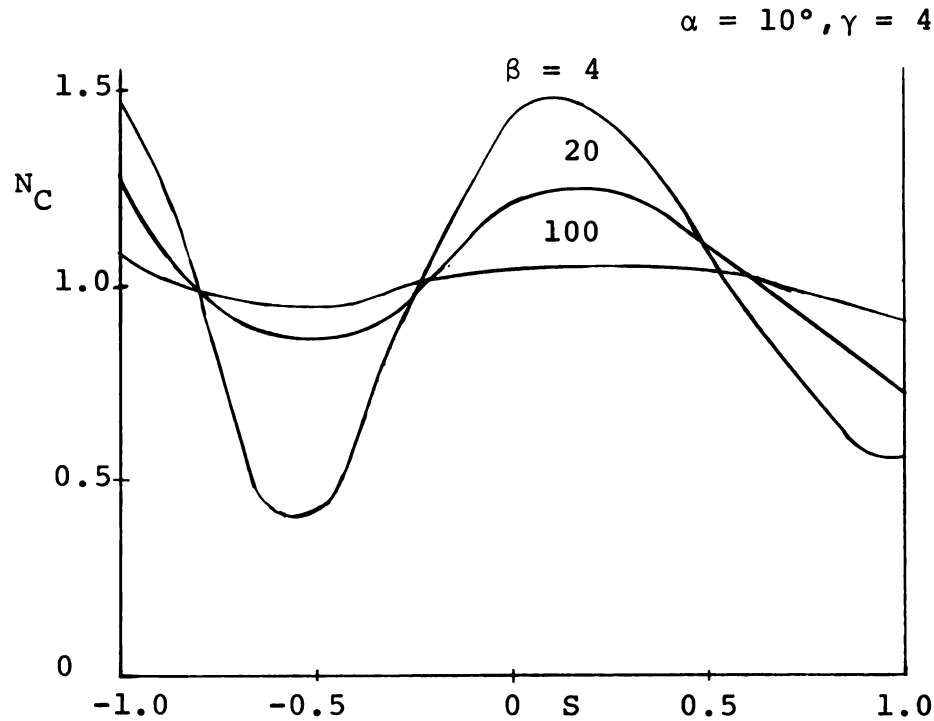

Fig. 18 Normal stress concentration factor (N_C) in tensile loading.

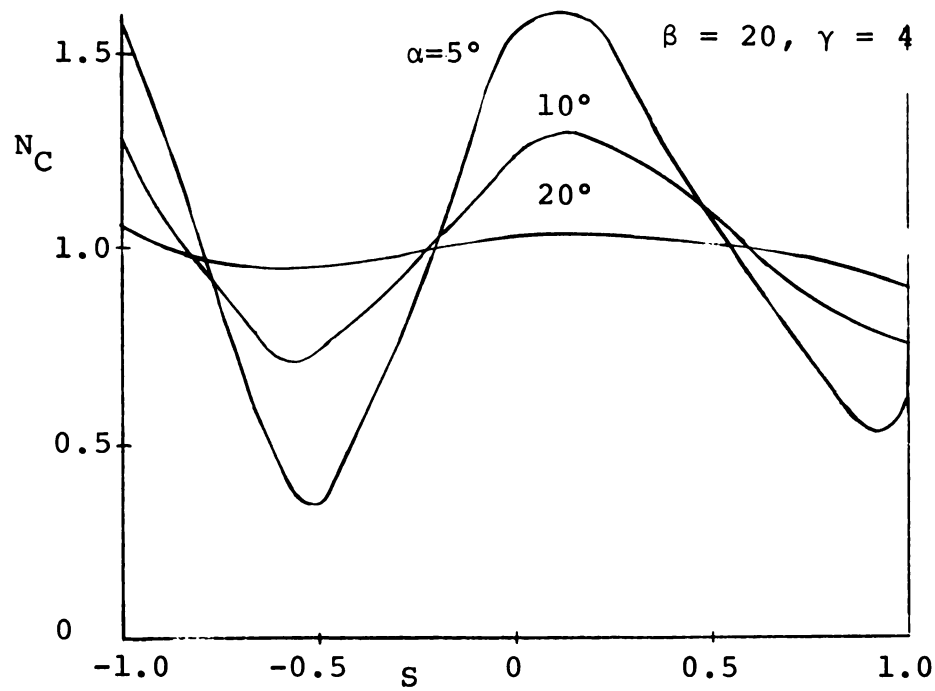

Fig. 19 Normal stress concentration factor (N_C) in tensile loading.

($\beta = 4$), and the case of identical ($\gamma = 1$) and maximally-dissimilar adherends ($\gamma = 8$). It is apparent that the two extremes differ very little. The comparatively flexible adhesive readily accommodates the different lateral contractions of the equally-stressed adherends, and indeed, Figure 21 shows that it acquires very little shear stress in doing so; the shear stresses are nearly linear functions. This diagram covers the same two cases as Figure 20. Here it is necessary to plot dimensionless shear stresses T (actual magnitudes for adherend tensile stress = unity), rather than T_c, since $T_0 = 0$ in this case. The latter is the curve labeled $\gamma = 1$. Symmetry dictates that the adhesive shear stress be an odd function of S for the butt joint, and the normal stress an even function. It is easily verified from first principles, by consideration of the lateral displacements of the two axially-loaded adherends, that this very small shear stress is of the correct order of magnitude.

In view of the results, it is probably sufficient to simply state here the maximum shear and normal stresses for the butt joint cases omitted from the diagram ($\alpha = 90°$, $\beta = 4$):

$$\left.\begin{array}{lll} \gamma = 2 : & |N_{max}| = 1.0011 & |T_{max}| = 0.0126 \\ \gamma = 4 : & |N_{max}| = 1.0027 & |T_{max}| = 0.0196 \end{array}\right\} \text{at } S = \pm 1$$

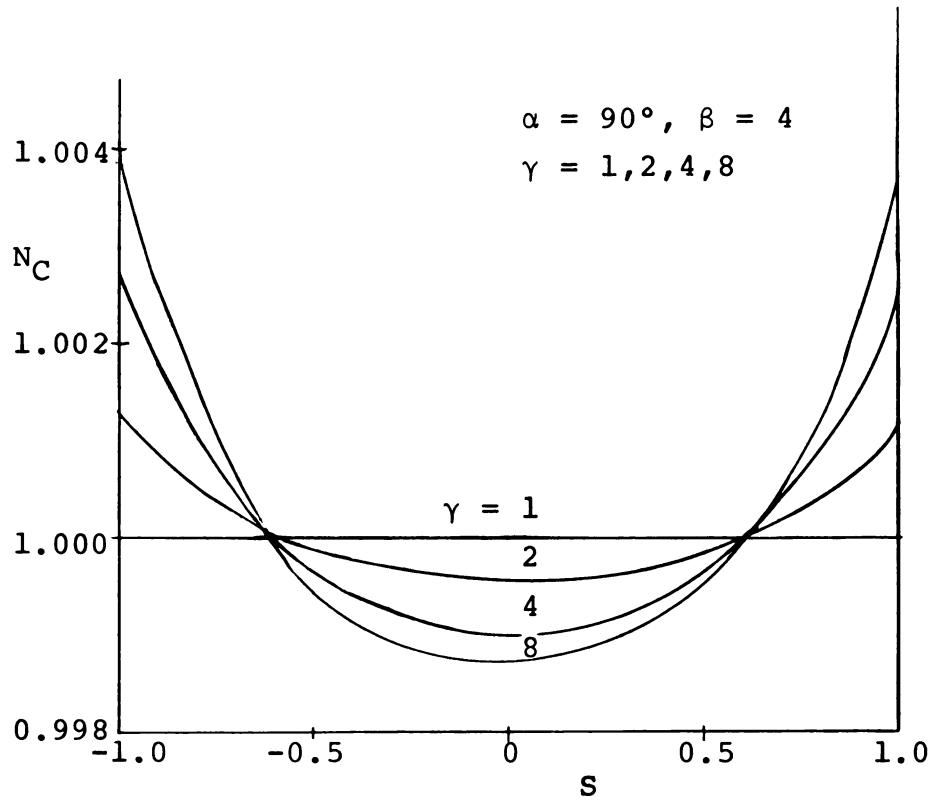

Fig. 20 Normal stress concentration factor (N_C) in tensile loading.

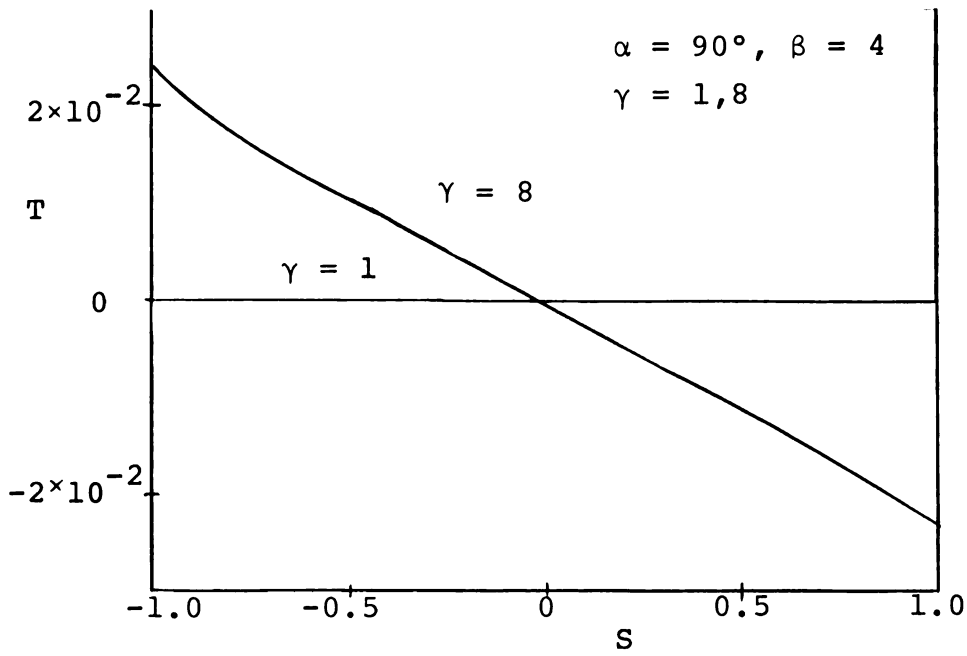

Fig. 21 Shear stress (T) in tensile loading.

4.1.2 Case of Bending Load

The general conclusions from Chapter III are that the Ritz method (as used here) finds adhesive normal stresses with less certainty than shear stresses, and converges better for tensile load than bending load. The confidence level is therefore high for all tensile loadings, especially in the shear stresses, which are the most significant ones. It is less high for bending cases, particularly for normal stresses. The discussion of the latter is somewhat more tentative, because some of the trends observed may be fictitious due to incomplete convergence.

4.1.3 Identical Adherends in Bending

Even for identical adherends ($\gamma = 1$) in pure bending, we still have a two-parameter family of results to consider. Adhesive flexibility (β) and scarf angle (α) are the parameters. The corresponding adhesive stresses must be plotted as T- and N- type rather than as the more instructive concentration factors. This is because, unlike the case of tensile loading, there is no analytical solution other than the present one to serve as a reference level. To obtain true, dimensional stresses from the figures to follow, or the tables of Appendix F, multiply by the "load stress" σ_{X0} of Section 4.1: the adhesive shear and normal stresses tabulated and diagrammed are based on an outer-fiber bending stress ("Mc/I"), remote from the joint, of unity. The

bending moment per unit width of adherend, in the sense of Figures 6 and 7, is then 2/3.

Figure 22 shows the adhesive shear stress T for a bending case with $\alpha = 10°$, $\gamma = 1$ (identical members), and $\beta = 4, 20, 100$. The roundoff error level seems to affect about one unit in the fourth decimal place, or less, regardless of the magnitude of the stress. A typical value at $S = 0$, where an odd function should be zero, is $1(10^{-4})$ units on a reference scale of unit applied stress. (This is not bad roundoff for "one-pass" solution of 177 equations.) Within this error level, the tables and the figures indicate that these stresses are odd functions of the distance parameter S. The odd property can also be deduced from a consideration of the symmetries of the identical-adherend case. It is evident that these stresses are not linear functions of S, in general, but this was not really to be expected, despite the linearity of the applied bending stress.

The shear stress maximum is always at $S = \pm 1$. The expected decrease of stress level with increase of adhesive flexibility (β increasing) is evident. It is interesting that the stiffest adhesive ($\beta = 4$) represents the straightest line. It may be speculated that as the adhesive becomes very stiff, the identical-adherend configuration approaches the state of a single uniform beam, with the adhesive interface behaving like the imaginary line one passes to

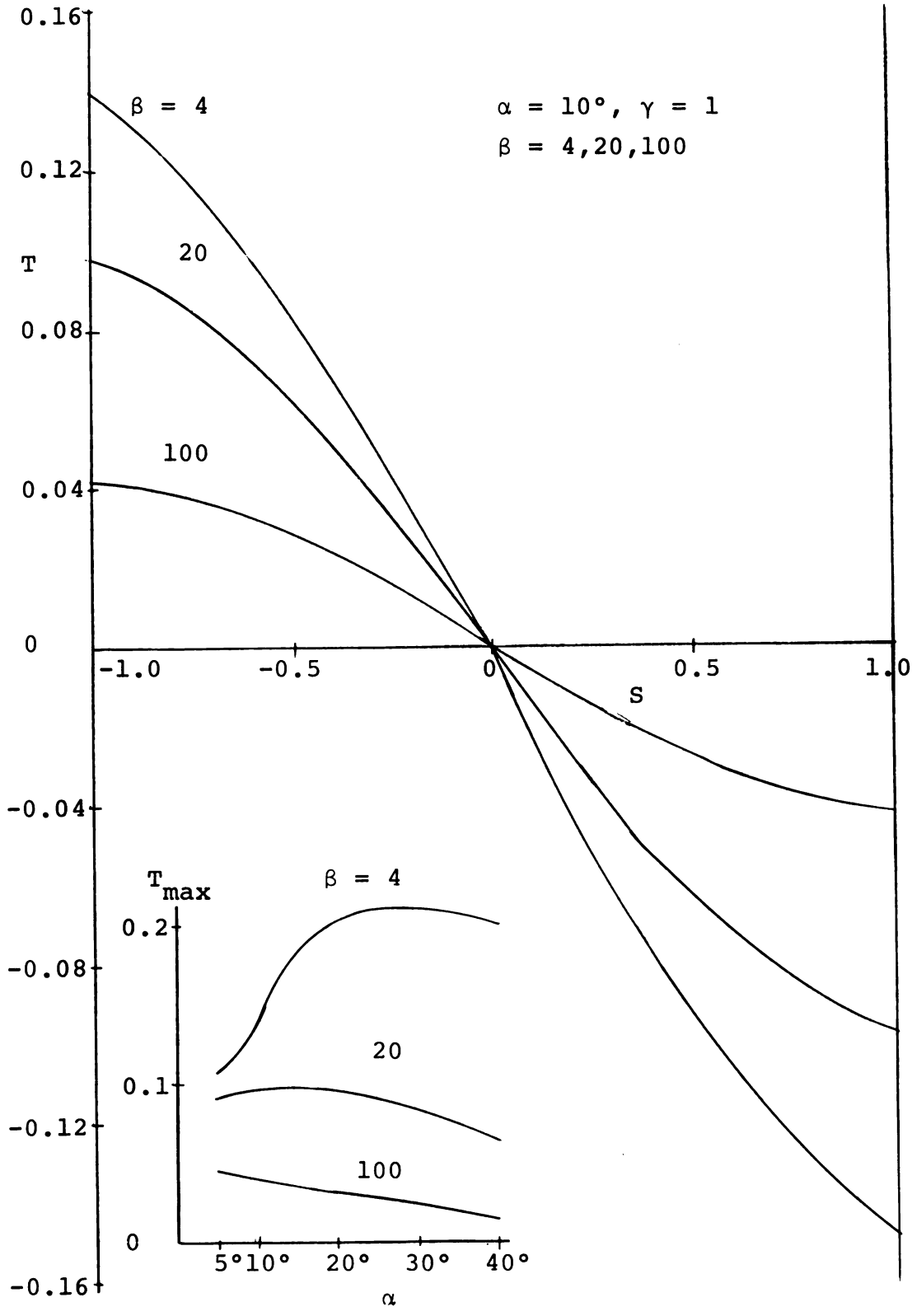

Fig. 22 Shear stress (T) in bending load.

calculate stresses under rotation of axes. That is, the adhesive is "not there," and the stresses can be calculated from simple beam theory. This may not be too far from the true situation when $\beta = 4$, for small angles α, since the largest shear stress (at $S = \pm 1$) is 80% of the theoretical value $\sin \alpha \cos \alpha$ which one would calculate from beam theory. As another indication that the present physical interpretation may be a good one for a "stiff adhesive," the tangent to the $\beta = 4$ curve of Figure 22, as estimated over the interval $S = -0.1$ to $S = 0$, would project to $S = -1.0$ as an intercept of 0.144. The value of $\sin \alpha \cos \alpha$ for $\alpha = 10°$ is 0.171. The behavior of the normal stress distributions also supports this interpretation; these are discussed later. However, this explanation must not be pushed too far, because there may be some questions about the validity of the adhesive model when the adhesive is anything but relatively "flexible."

All identical-adherend shear stresses in the bending case follow the general pattern of Figure 22, but the level of stress changes with angle α. Indeed the inset diagram in Figure 22 shows that the maximum shear stress (at $S = \pm 1$) goes up with α and then falls off, if β is small to moderate, but decreases uniformly with α if β is large (100, very flexible).

The adhesive normal stress pattern for identical adherends ($\gamma = 1$) also shows the odd-function behavior

expected from symmetry. Otherwise, it is difficult to make general statements about N, since the pattern keeps changing with the parameters. The explanations given below, however, seem to account well enough for the calculated behavior.

Figure 23 shows the normal stresses N for $\alpha = 10°$; $\gamma = 1$; $\beta = 4, 20, 100$. Here the stiffest adhesive ($\beta = 4$) shows no oscillation, and the most flexible the largest wave amplitudes. One would usually expect the "elastic foundation" (adhesive) to be associated with shorter, larger-amplitude waves as it gets stiffer, but the opposite trend is seen here. In this case the maximum normal stress occurs at the ends $S = \pm 1$ for $\beta = 4$ only; it is found in the interior for the other values of β.

It is likely that the oscillations of Figure 24 are not solely related to the idea of a beam on an elastic foundation, but that other mechanisms are also involved. The following is offered as a possible interpretation of the behavior observed. As in the case of the shear stresses, for $\beta = 4$ (relatively stiff adhesive) the joint is not far from being vanishingly thin and infinitely stiff ($\beta = 0$), which we interpret as being the case of the homogeneous, joint-free beam. In the latter situation, the "adhesive" normal stress, calculated from elementary theory, should be linearly distributed and have the largest value $\sin^2 \alpha$ for the present unit "load stress." When β is allowed to

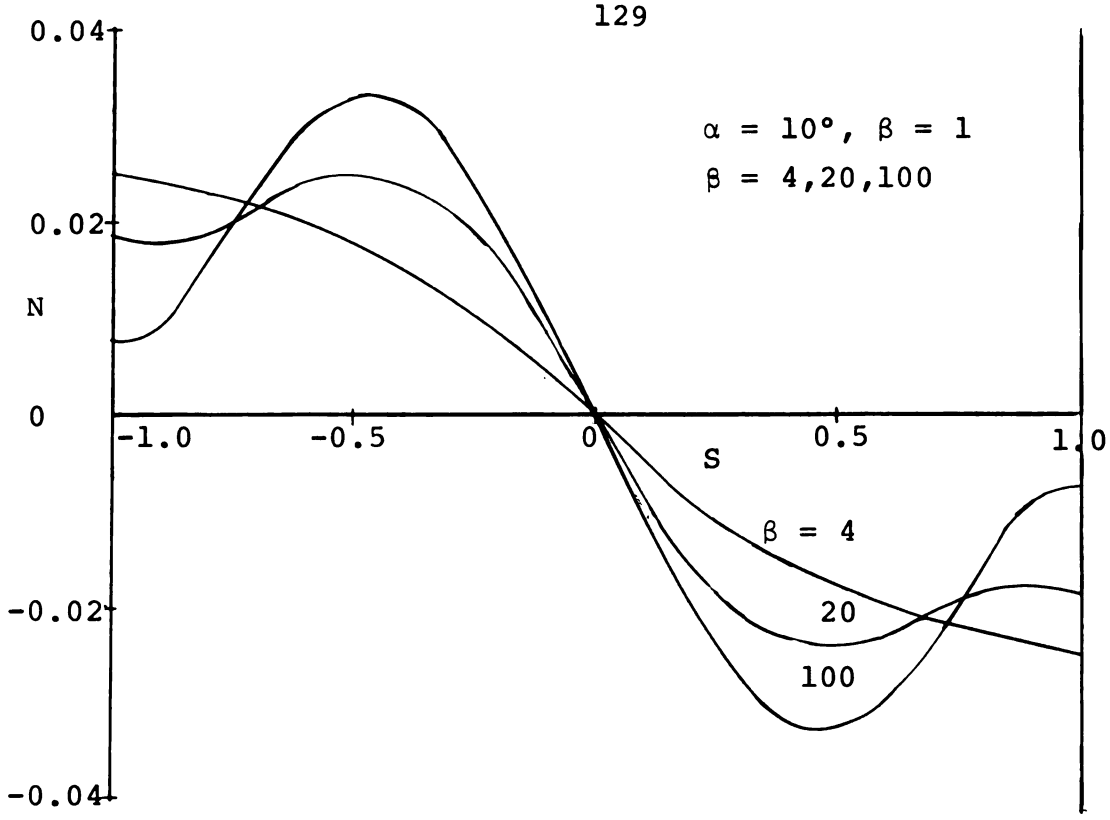

Fig. 23 Normal stress (N) in bending load.

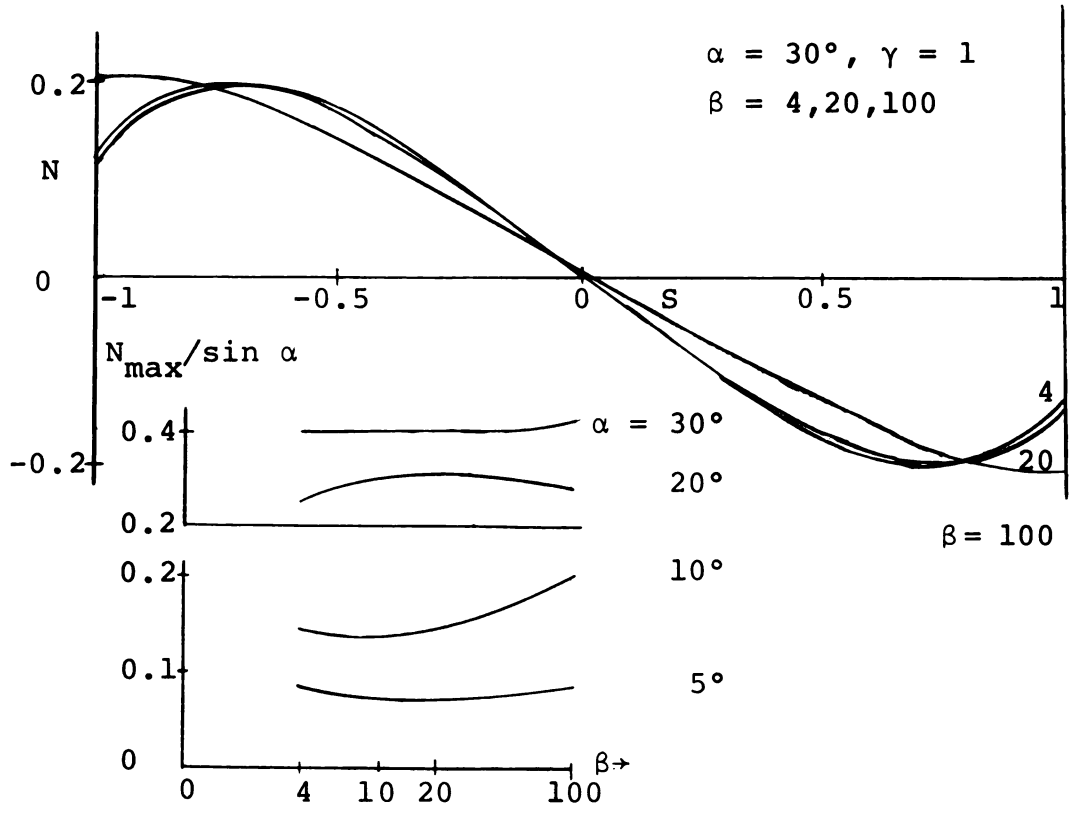

Fig. 24 Normal stress (N) in bending load.

have a finite elasticity, we must consider the mode of deformation of the adherends and adhesive. The adherends are regarded as tapered beams in this argument, and since they taper to a point, their bending stiffness drops off rapidly as the tip is approached. In the vicinity of a tip, the adjacent adherend beam has its maximum section and is therefore very stiff. Adhesive normal stress is developed by relative transverse displacement of the two beams, one locally very stiff and the other very flexible. When the adhesive itself is nothing but an imaginary line, the linear stress distribution is of course transmitted without difficulty. But when a flexible adhesive is present, it is incapable of actually transmitting a linear stress variation. This is because the beam tip is too flexible to offer enough resistance to its full share of the normal stress, precisely at the point where the latter tends to take on its largest values. It is simply too compliant, and displaces too readily. Relative to the stiff adjacent member, the corresponding adhesive interface is not displaced as much as a linear distribution of stress would demand. Thus the normal stress simply falls off from the $\sin^2 \alpha$ value. To satisfy moment equilibrium, a readjustment of the adhesive stress distribution must take place. It acquires larger values than the linear distribution in the interior region of the joint, to compensate for the dropoff at the tip. Following up on this model a little

further, the more flexible the adhesive, the smaller the normal stress which the joint end is likely to experience. Loosely speaking, a softer "spring" (the adhesive) cannot develop a given level of stress near the tip without deforming the tip more, which in turn requires higher transverse stress level. Instead, the actual stress developed falls off as adhesive flexibility β increases. The argument fails when the scarf angle increases to the point that the elastic solids become compact bodies rather than slender tapered beams. Then the load should be transferred as if the two adherends were rigid bodies, at least when the adhesive is very flexible. It follows that we should find the adhesive normal stress almost linear along the joint, at large scarf angles and large β. The transitional behavior from one model to the other should be smooth and gradual.

This interpretation is supported by the relative positions of the curves, and the calculated numbers. For the stiffest adhesive in Figure 23 ($\beta = 4$), $\sin^2 10° = 0.03022$, yet the value of N_{max} at $S = -1$ is the somewhat smaller 0.0252. To compensate for this, the convex-up shape of the curve for $\beta = 4$ must develop. It starts out from $S = 0$, where $N = 0$, with a slope which would project to $S = -1$ at a value $N_{max} = 0.045$ (based on the interval $S = 0$ to $S = -0.1$).

Considering these data, the present argument implies that $\beta = 4$ is not too far from the "rigid" condition, as indicated at the start of the discussion. For the much greater adhesive flexibilities $\beta = 20$ and $\beta = 100$, the effect described should be increasingly exaggerated, and the central region of the joint must transmit an increasing proportion of the overall bending moment. In addition, as the value of β increases, the intercept at $S = \pm 1$ drops off. The foregoing mechanism, of itself, may or may not be sufficient to make the maximum normal stress actually occur toward the interior of the joint as adhesive flexibility increases. It does seem sufficient to account for the curve for $\beta = 4$ in Figure 23. There is another mechanism operating which may also have an effect: the "beam-on-an-elastic-foundation" idea. The oscillatory behavior of the curves for $\beta = 20$ and $\beta = 100$ may be associated with a superposition of these two mechanisms.

The picture for $\alpha = 5°$ (not shown) is entirely consistent with the first explanation attempted above, but in this case there is also a very clear-cut indication of wavy behavior in the curves for $\beta = 20$ and $\beta = 100$. As the scarf angle increases, the adherends become less and less like tapered beams. At $\alpha = 20°$ there is only a small tendency for the curve for $\beta = 4$ (not shown) to exhibit oscillations, and little evidence of it for the other values of β, or for any values of β at larger scarf angles.

Where one would expect to see wavy behavior and it does not actually occur, this may be due to a coincidence of parameters, a special gradient of the normal stress, or some aspect of symmetry. It is later found that identical-adherend cases often do not show expected oscillations, but that the introduction of some dissimilarity brings them out strongly.

Besides attempting to account for the shapes of the calculated stress distributions, there is another point to justify this lengthy discussion. Some sort of explanation is demanded by a situation which has occurred very rarely in the adhesive joint literature (if at all): the increase of a stress component as the flexibility of the adhesive β is increased. The trend is normally the opposite. Indeed, the usual smoothing effect of increasing β may have its influence here, as yet a third mechanism interacting with the "flexible tip" and "elastic foundation" interpretations. The fourth factor is the question of Ritz process convergence, which may be significant because the adhesive stresses in bending load are not as well determined as for tensile load. The fact remains that (in these calculations) the maximum normal stress does appear to increase with adhesive flexibility in some cases, as shown in the inset diagram of Figure 24.

Figure 24 is for $\alpha = 30°$, $\gamma = 1$, and $\beta = 4, 100$; the case $\beta = 20$ is not distinguishable from $\beta = 100$ on this scale.

The interchange of shape of the stress distributions for $\beta = 4$ and 100, between Figures 23 and 24, is noteworthy and in line with the expectation that as α increases the large-β curves will begin to straighten out. The interchange mentioned is another example of the difficulty of making general statements about the normal stresses for bending load. For an even larger scarf angle, $\alpha = 40°$ (not shown), the pattern is similar but all curves are more nearly linear in the interior of the joint, and the maxima are closer to the ends $S = \pm 1$. In this case the stresses for $\beta = 100$ are almost linear from end to end, with no downturn at all. Even the $\beta = 20$ curve has begun to straighten out.

The inset diagrams in Figure 24, incidentally, cross-plot the values of $N_{max}/\sin \alpha$ against a logarithmic scale of adhesive flexibility β, for the various scarf angles. It would theoretically be desirable to plot $N_{max}/\sin^2 \alpha$, but then all values lie in the range 0.77 to 1.08 and the various curves become quite confused. A plot in the present manner separates them well. A plot of N_{max} itself shows too large a range to appear on a single diagram, since it varies essentially as $\sin^2 \alpha$.

Before leaving the case of identical adherends, the bending of the butt joint configuration ($\alpha = 90°$) should be mentioned. For all values of β, with these compact adherend shapes the adhesive normal stresses are perfectly linear and are the same as those calculated from beam theory. This is to be expected.

The adhesive shear stress is identically zero, as symmetry would demand.

4.1.4 Bending Load (General Case)

Here there is a full three-parameter family again: α, β, γ all vary. Figure 25 illustrates the variation of the shear stress for $\alpha = 20°$, $\beta = 20$, and $\gamma = 1, 8$. The curves for $\gamma = 2$ and 4 fall smoothly between the $\gamma = 1, 8$ values and are omitted for clarity. The stress curves becomes increasingly asymmetric as the dissimilarity (γ) increases; it is an odd curve for identical adherends ($\gamma = 1$). The explanation of the asymmetry was taken up in section 4.1.1 and applies here also. According to the argument there, we would normally expect the shear stress to be largest at $S = -1$. This seems to hold for most of the results now under consideration. There are, however, a few anomalous cases where the computations find T_{max} slightly larger at $S = +1$. These all have the following character: scarf angle α is large (30°, 40° only), and adhesive flexibility β is moderate (20) or large (100). In all such cases, the adhesive normal stress is much larger than the shear stress and the discrepancy is very small compared to either the "load stress" of unity or the somewhat smaller local value of normal stress. It is therefore felt that the argument mentioned above remains valid, but that other factors intrude to produce an opposing effect. These could

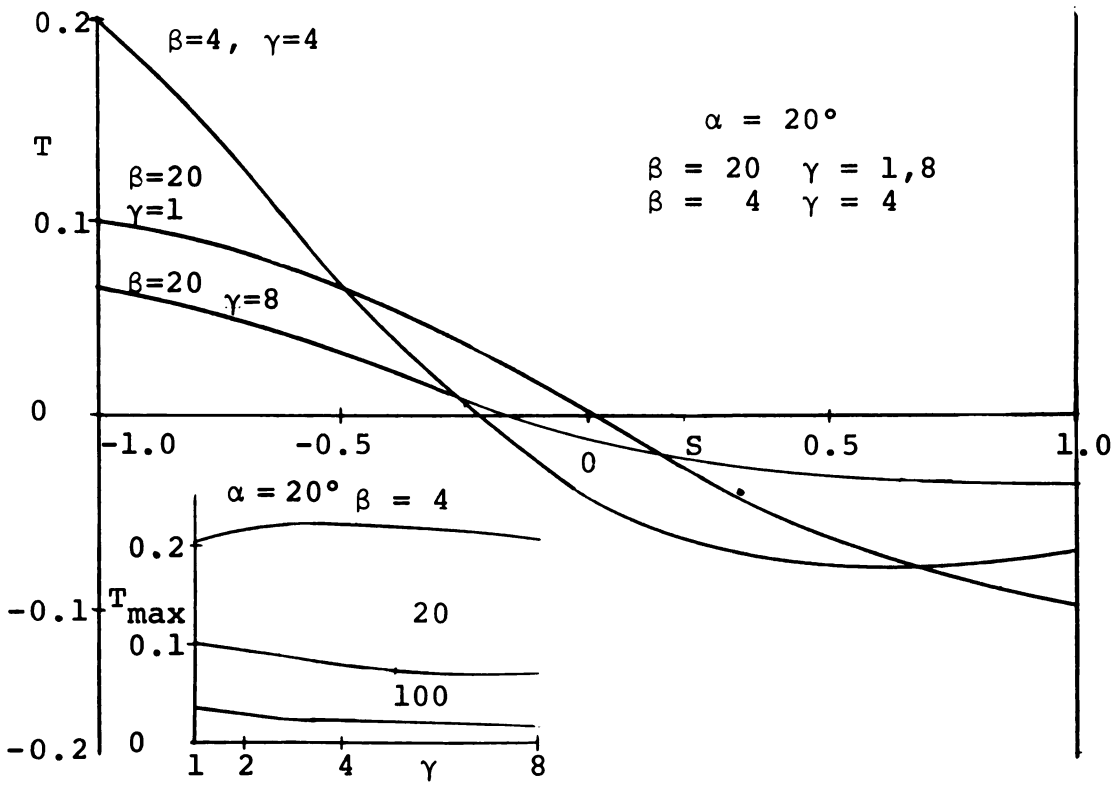

Fig. 25 Shear stress (T) in bending load.

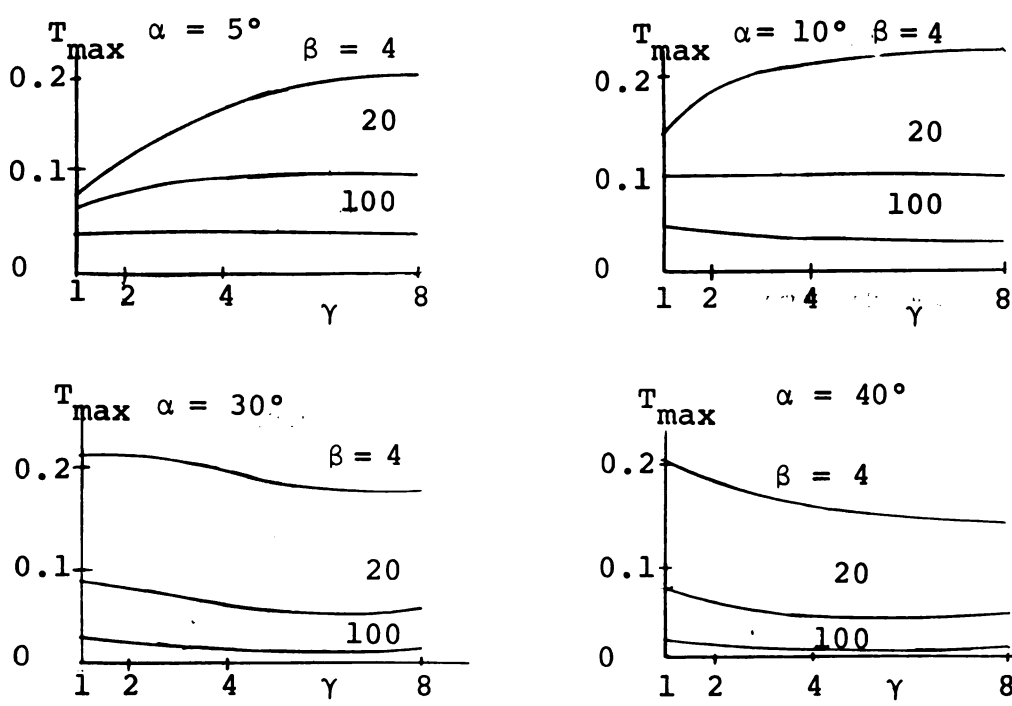

Fig. 26 Maximum shear stress (T_{max}) in bending load.

include roundoff error accumulation, another physical phenomenon, or more likely, a question of convergence. It should be emphasized that the effect is very small, whatever the source. For example, the Appendix F tables show ($\alpha = 40°$, $\beta = 20$, $\gamma = 8$) $T = 0.0372$ at $S = -1$, and $T = -0.0396$ at $S = 1$, where $N = -0.2526$. In bending, it is not believed likely that the stresses are always so well determined as to make a discrepancy of 0.0024 significant.

The extra curve in Figure 25 is for the same scarf angle of 20°, but $\beta = 4$ and $\gamma = 8$. It is introduced to show that on many diagrams, the effect of dissimilarity ($\gamma > 1$) is to produce a curve of this concave-up character. It is also interesting that an increase in dissimilarity γ may produce a decrease in the largest shear stress level (as in Figure 25), or sometimes an increase, or even no appreciable change. This is seen in the inset diagram of Figure 25, for $\alpha = 20°$ and the three values of β. Thus T_{max} decreases uniformly with increase of adhesive flexibility β, but has varying behavior with change of γ. Figure 26 shows the same information as the inset diagram of Figure 25 for the rest of the scarf angles, and produces similar conclusions.

Figure 27 shows how the maximum shear stress in bending varies with scarf angle α. Each diagram holds adhesive flexibility β constant, and allows dissimilarity γ to vary. The interaction is quite complex.

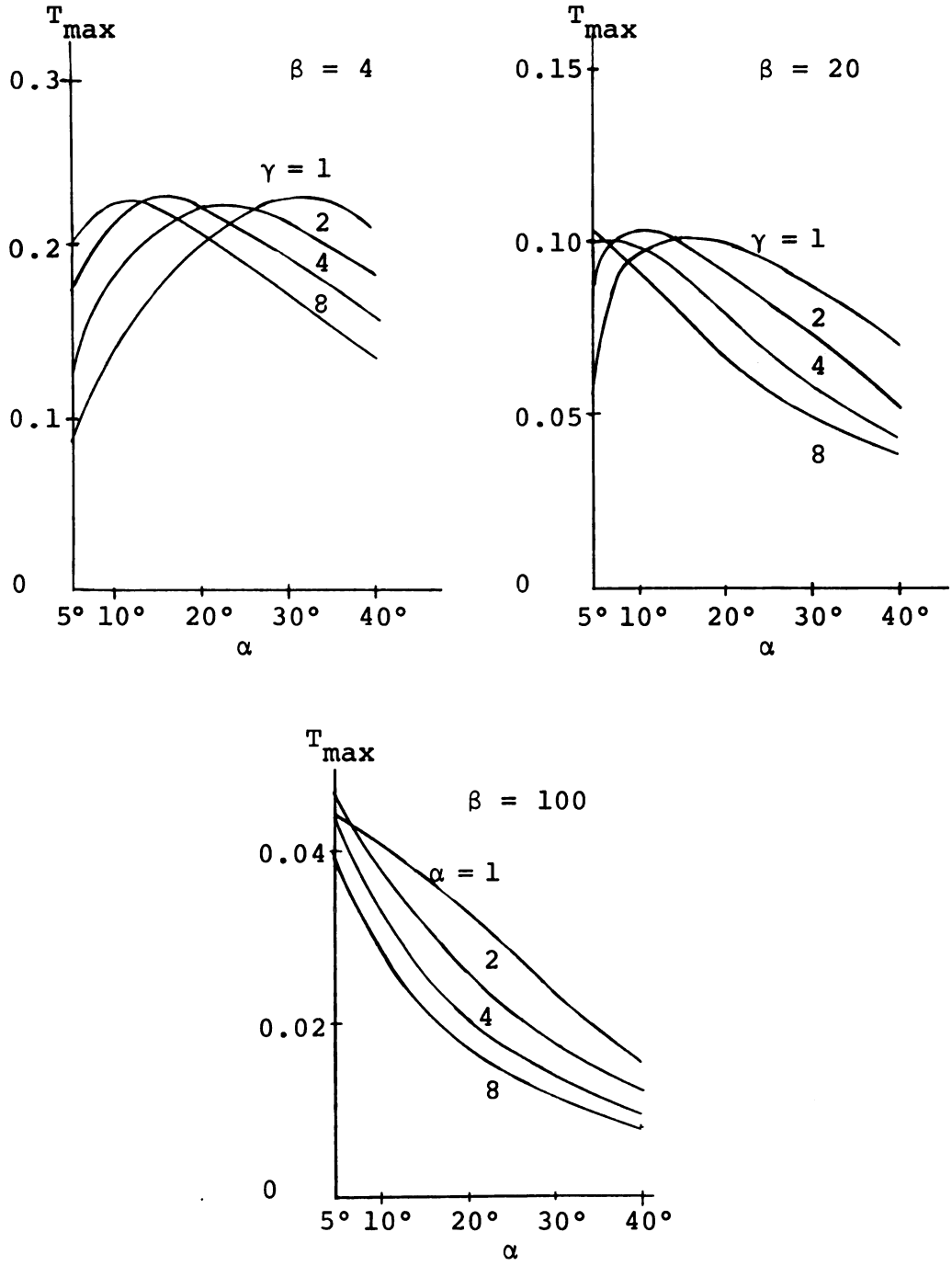

Fig. 27 Maximum shear stress (T_{max}) in bending load.

The normal stresses in bending are shown in Figure 28, for $\alpha = 10°$, $\beta = 20$, and $\gamma = 1,2,4,8$. The curve for $\gamma = 1$ was discussed in the previous section; it represents an odd function. For increasing adherend dissimilarity, the curves become increasingly asymmetric. For $\gamma > 1$, all show the largest stress N_{max} toward the end $S = -1$, but still on the interior of the joint. There is strong evidence of oscillatory behavior, of "elastic foundation" type. All this is to be expected, in the light of previous discussion: for small scarf angles, wavy behavior is expected; N_{max} tends to be toward $S = -1$ with the present elastic asymmetry; and N_{max} does not appear at the end of the joint for small scarf angles and moderate to large adhesive flexibility. The diagram shows that increase of dissimilarity raises the peak value of N_{max}. Going to a larger value of adhesive flexibility ($\beta = 100$, not shown) leaves the general pattern of stress much the same. For a stiffer adhesive ($\beta = 4$), the curves are slightly different in character toward $S = -1$. Figure 23 shows the $\gamma = 1$ case for $\beta = 4$, and the $\gamma = 2$ curves for this value of β are somewhat similar (i.e., monotomic increasing as 5 approaches -1). The latter two show a slight upturn toward the end, with N_{max} there. Only the case of $\gamma = 8$ shows the downturn at $S = -1$, with a maximum still on the interior of the joint. The inset diagram of Figure 28 shows how N_{max} varies with dissimilarity γ. On this small scale, the curves for $\beta = 4$, 100 are hard to

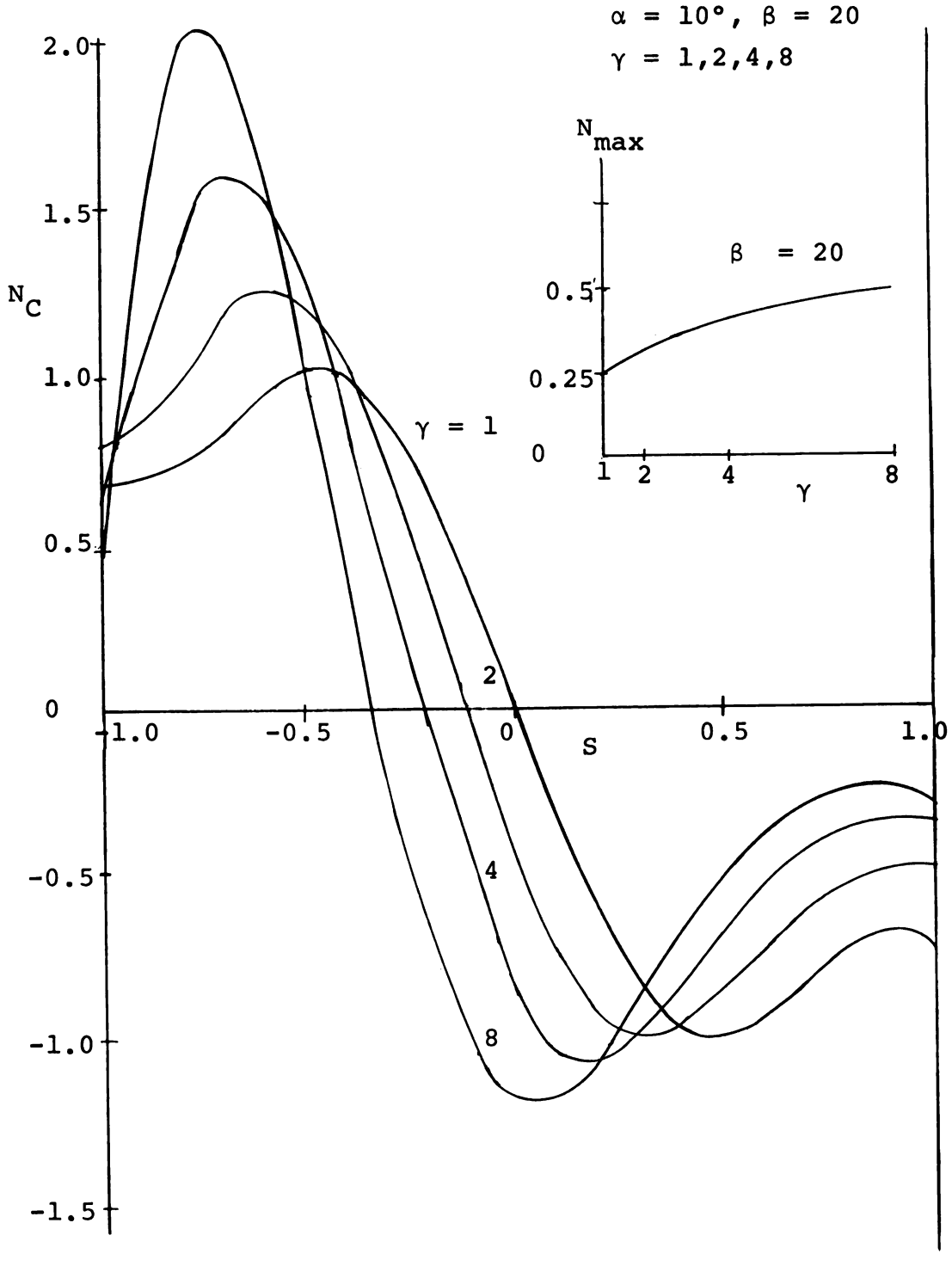

Fig. 28 Normal stress concentration factor (N_C) in bending load.

distinguish and have been omitted. The trend with γ in this inset holds for every case tabulated, but the slope of the curve may become very small.

If α is reduced to 5° and the "tapered beams" become more slender, the stress distribution for the stiff adhesive ($\beta = 4$) and identical adherends ($\gamma = 1$) is roughly linear and shows little waviness. As γ is increased to 2, 4, 8, violent oscillations of increasing amplitude and rather short wavelength are superimposed upon the $\gamma = 1$ case, and the asymmetry of the stresses increases. Also at 5°, the wavelength of the oscillations gets longer as β is increased to 20 and 100 ("foundation" becomes more flexible). All this is much as one might expect, and this further indicates that the identical adherend cases ($\gamma = 1$, Section 4.1.2) which show little evidence of waviness probably do so as a result of special symmetry or a coincidence of parameters. For $\alpha = 20°$, $\beta = 4$ and 20, the stress distributions (not shown) also have the general character of Figure 28, although a gradual transition to new behavior is observable. When adhesive flexibility is increased to $\beta = 100$, the normal stresses have evolved until they are quite similar to Figure 29. The latter shows the normal stresses for $\alpha = 30$, $\beta = 20$, and $\gamma = 1,2,4,8$. For large dissimilarity γ, the maximum no longer occurs on the interior of the joint, and there is little evidence of elastic foundation waviness. There is still asymmetry for $\gamma > 1$,

of course, and all values of N_{max} occur at or near S = -1. Some of the curves are beginning to straighten out, a trend anticipated in Section 4.1.2 for large scarf angles α and moderate to large β. If β is reduced to 4 (not shown), the pattern of Figure 29 still holds. However, for β = 100 (not shown), all curves are quite close to each other for all γ, and nearly straight, with just a small tendency to curve toward the ends. The large scarf angle $\alpha = 40°$ still shows similarity to Figure 29 when β = 4 (stiff adhesive). The stresses for the case of $\alpha = 40°$ with β = 20 behave much like the γ = 8 case of Figure 29, but generally straighter and with more sudden end changes in curvature. Finally, for $\alpha = 40°$ and the large flexibility β = 100, the transition is nearly complete. All curves are nearly linear from end to end, independent of dissimilarity γ, as befits "compact" adherends in bending with a highly flexible adhesive. These features could largely be deduced from the general discussion of the normal stresses in the case of identical adherends.

For the bending of butt joints between dissimilar adherends, it is still found that the adhesive normal stress is the linear distribution one would calculate from elementary beam theory, to four or more significant figures. When $\gamma \neq 1$, small shear stresses are induced in the adhesive. The distributions are self-equilibrated and even in S, as demanded by considerations of symmetry in geometry

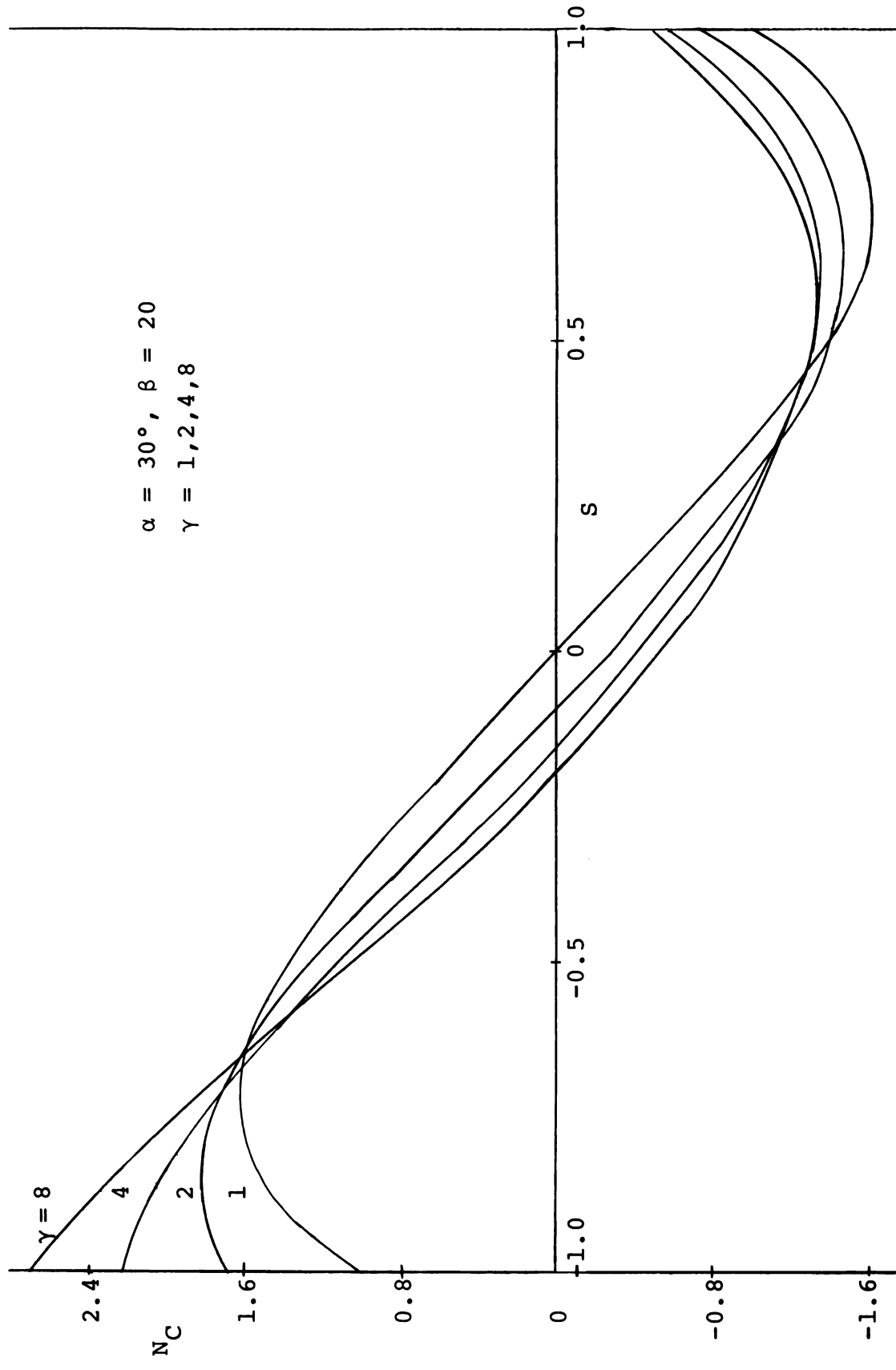

Fig. 29 Normal stress concentration factor (N_C) in bending load.

and loading. The largest such value found ($\beta = 4$, $\gamma = 8$), at $S = \pm 1$, is 0.00851 for the unit "load stress" in bending. Some of the other values of T_{max} are:

β	γ	T_{max}
4	4	0.00725
4	2	0.00477
20	8	0.00178
20	4	0.00152
100	8	0.00036

4.2. Adhesive Combined Stresses

Since the adhesive is in a known state of combined stress (shear and one component of normal stress), we can at every point find the corresponding maximum principal stresses (N_1,N_2), the maximum shear stress T_1, and the octahedral shear stress T_{oy}. All of these are quantities which commonly enter into engineering design criteria, in one form or another. They are found by using the standard relations:

$$N_1 = N/2 + \sqrt{(N/2)^2 + T^2} \qquad 4.2.1$$

$$N_2 = N/2 - \sqrt{(N/2)^2 + T^2} \qquad 4.2.2$$

$$T_1 = \sqrt{(N/2)^2 + T^2} \qquad 4.2.3$$

$$T_{oy} = \sqrt{(6T^2 + 2N^2)/9} \qquad 4.2.4$$

The principal stress $N_1 \geq N_2$ and is always the governing tensile stress for tensile loading of the joint. When the loading is compressive, N_2 becomes the largest tensile stress. For bending moments in the sense of Fig. 7, the N_1 stress is the critical tensile value, and if the moments are reversed, the N_2 stress takes on this role.

From a design viewpoint, there is no need to examine entire distributions of the combined stresses. Accordingly, the largest values of the combined stresses have been extracted from the calculated distributions by suitable interpolation techniques, and only these are tabulated. In

Table 11 (next page), the signs given correspond to the loading senses of Figure 7, p. 26. The "load stress" σ_{X0}, labeled σ_0 in Figure 7, is always unity in Table 11.

The variation of the combined stresses is fairly simple for tensile loading. Table 11 shows that all quantities have the following behavior, with minor exception ascribable to roundoff or other computational (rather than physical) cause:

1. All increase monotonically with increase in dissimilarity of the adherends, γ (at constant α, β).
2. All decrease monotonically with increase in adhesive flexibility, β(at constant α, γ).
3. All decrease monotonically with decrease in scarf angle α (at constant β, γ).

The last item indicates that the function of a scarf joint is being accomplished (if the loading is tensile): as the scarf angle decreases, the combined stresses which are likely to be critical for failure decrease, which means that 'more load can be applied' for smaller scarf angles.

General statements cannot easily be made for bending load; there is a complex interaction of parameters. To keep the length of the present discussion within reasonable bounds, the bending problem will not be treated here. The user may deduce all the necessary information from Table 11.

Table 11.--Maximum values of the combined stresses N_1, N_2, T_1, T_{oy}. Signs correspond to the loading sense of Fig. 7, p. 26, with adherend 2 assumed to be the stiffer one.

			Tension				Bending			
α	β	γ	N_1	$-N_2$	T_1	T_{oy}	N_1	$-N_2$	T_1	T_{oy}
5	4	1	0.0907	0.0831	0.0869	0.0710	0.0853	0.0853	0.0818	0.0668
		2	0.1450	0.1331	0.1390	0.1135	0.1318	0.1239	0.1278	0.1044
		4	0.1971	0.1820	0.1895	0.1548	0.1745	0.1672	0.1708	0.1395
		8	0.2343	0.2226	0.2284	0.1865	0.2061	0.1970	0.2015	0.1646
	20	1	0.0907	0.0831	0.0869	0.0710	0.0728	0.0728	0.0670	0.0571
		2	0.1215	0.1103	0.1159	0.0947	0.0921	0.0858	0.0889	0.0726
		4	0.1440	0.1320	0.1380	0.1127	0.1040	0.0957	0.0998	0.0815
		8	0.1591	0.1492	0.1541	0.1259	0.1085	0.0979	0.1032	0.0843
	100	1	0.0907	0.0831	0.0869	0.0710	0.0469	0.0681	0.0457	0.0373
		2	0.1041	0.0953	0.0997	0.0814	0.0485	0.0447	0.0466	0.0381
		4	0.1127	0.1037	0.1082	0.0884	0.0468	0.0416	0.0442	0.0361
		8	0.1188	0.1090	0.1139	0.0930	0.0415	0.0385	0.0400	0.0327
10	4	1	0.1868	0.1566	0.1717	0.1404	0.1557	0.1557	0.1431	0.1170
		2	0.2532	0.2133	0.2332	0.1907	0.2034	0.1699	0.1867	0.1526
		4	0.3035	0.2589	0.2812	0.2298	0.2341	0.1941	0.2141	0.1750
		8	0.3421	0.2900	0.3161	0.2584	0.2452	0.2050	0.2251	0.1840
	20	1	0.1868	0.1566	0.1717	0.1404	0.1080	0.1080	0.0990	0.0809
		2	0.2171	0.1826	0.1999	0.1634	0.1142	0.0940	0.1041	0.0851
		4	0.2384	0.1996	0.2190	0.1791	0.1095	0.0931	0.1013	0.0828
		8	0.2538	0.2102	0.2320	0.1897	0.1048	0.0878	0.0941	0.0769
	100	1	0.1868	0.1566	0.1717	0.1404	0.0464	0.0463	0.0425	0.0348
		2	0.1968	0.1649	0.1808	0.1479	0.0514	0.0406	0.0380	0.0310
		4	0.2025	0.1696	0.1861	0.1521	0.0536	0.0356	0.0332	0.0290
		8	0.2051	0.1729	0.1890	0.1545	0.0573	0.0325	0.0335	0.0295
20	4	1	0.3852	0.2682	0.3267	0.2681	0.2443	0.2442	0.2067	0.1697
		2	0.4519	0.3132	0.3826	0.3141	0.2618	0.1857	0.2238	0.1836
		4	0.4979	0.3435	0.4207	0.3454	0.2710	0.1837	0.2245	0.1843
		8	0.5222	0.3699	0.4460	0.3659	0.2878	0.1560	0.2174	0.1799
	20	1	0.3852	0.2682	0.3267	0.2681	0.1463	0.1463	0.1013	0.0841
		2	0.4076	0.2842	0.3459	0.2839	0.1537	0.1197	0.0976	0.0835
		4	0.4183	0.2955	0.3569	0.2928	0.1645	0.1043	0.0978	0.0856
		8	0.4218	0.3042	0.3630	0.2977	0.1875	0.0966	0.1052	0.0942
	100	1	0.3852	0.2682	0.3267	0.2681	0.1028	0.1028	0.0548	0.0501
		2	0.3901	0.2726	0.3314	0.2720	0.1121	0.0901	0.0585	0.0540
		4	0.3923	0.2753	0.3338	0.2739	0.1317	0.0831	0.0676	0.0630
		8	0.3932	0.2768	0.3350	0.2749	0.1572	0.0797	0.0796	0.0746

Table 11 Continued.

			Tension				Bending			
α	β	γ	N_1	$-N_2$	T_1	T_{oy}	N_1	$-N_2$	T_1	T_{oy}
30	4	1	0.5758	0.3257	0.4507	0.3727	0.3140	0.3140	0.2253	0.1873
		2	0.6256	0.3566	0.4911	0.4060	0.3391	0.2526	0.2285	0.1926
		4	0.6494	0.3821	0.5756	0.4257	0.3704	0.2150	0.2320	0.1998
		8	0.6554	0.4046	0.5300	0.4367	0.4317	0.1947	0.2500	0.2214
	20	1	0.5757	0.3257	0.4507	0.3727	0.2256	0.2255	0.1258	0.1129
		2	0.5882	0.3363	0.4623	0.3821	0.2480	0.1949	0.1333	0.1215
		4	0.5935	0.3432	0.4683	0.3869	0.2934	0.1778	0.1527	0.1412
		8	0.5955	0.3475	0.4715	0.3894	0.3410	0.1693	0.1742	0.1625
	100	1	0.5757	0.3257	0.4507	0.3727	0.2108	0.2107	0.1066	0.1000
		2	0.5783	0.3282	0.4533	0.3748	0.2457	0.1950	0.1235	0.1161
		4	0.5795	0.3296	0.4546	0.3758	0.2681	0.1868	0.1344	0.1265
		8	0.5801	0.3303	0.4552	0.3763	0.2804	0.1826	0.1405	0.1323
40	4	1	0.7406	0.3274	0.5340	0.4467	0.4109	0.4109	0.2490	0.2167
		2	0.7683	0.3476	0.5580	0.4662	0.4523	0.3445	0.2598	0.2306
		4	0.7791	0.3636	0.5713	0.4766	0.5286	0.3047	0.2874	0.2608
		8	0.7820	0.3750	0.5785	0.4820	0.6146	0.2837	0.3221	0.2970
	20	1	0.7406	0.3274	0.5340	0.4467	0.3506	0.3506	0.1816	0.1683
		2	0.7470	0.3334	0.5402	0.4517	0.4109	0.3160	0.2090	0.1954
		4	0.7499	0.3369	0.5434	0.4542	0.4595	0.2977	0.2318	0.2176
		8	0.7511	0.3389	0.5450	0.4555	0.4882	0.2884	0.2455	0.2308
	100	1	0.7406	0.3274	0.5340	0.4467	0.3905	0.3905	0.1956	0.1843
		2	0.7419	0.3287	0.5353	0.4478	0.4133	0.3786	0.2069	0.1949
		4	0.7426	0.3294	0.5360	0.4483	0.4256	0.3724	0.2129	0.2007
		8	0.7429	0.3298	0.5363	0.4486	0.4319	0.3693	0.2161	0.2037

4.3. Construction of Design Curves for Scarf Joints with Linearly-Elastic Adhesives

If the adhesive is assumed to fail when a certain combined stress attains some specified allowable value, presumably determined empirically, it is possible to use Table 11 in design. Let $\sum_a$ be this allowable stress, whether it is a maximum normal stress, a principal shear or an octahedral shear. Designate the four combined-stress quantities in Table 11, collectively, by N_{com}. It is up to the user to decide which "law of failure" he wishes to select, and to determine the appropriate value of $\sum_a$ for his chosen law. Recall that the "load stress" σ_{X0} is the actual applied tensile stress for tensile loading, or the maximum bending stress ("Mc/I"). Since Table 11 is constructed for $\sigma_{X0} = 1$, when the adhesive combined stress is equal to the "allowable" we must have

$$\sum_a = \sigma_{X0} N_{com} \qquad 4.3.1$$

Since $\sum_a$ is a known constant, the external loading σ_{X0} which the designer is allowed to introduce can be computed from this equation. A dimensionless load quantity, convenient for design, is

$$\sum = \sigma_{X0}/\sum_a = 1/N_{com} \qquad 4.3.2$$

Curvesof $\sum$ can readily be constructed from Table 11, by crossplotting quantities as desired. It is always

necessary to interpolate three ways in α, β, γ, since we have tabulated a three-parameter family. Some sample "design curves" are shown in Figure 30 for tensile loading. In one diagram, $N_{com} = N_1$; in a second, $N_{com} = N_2$; etc. The values actually plotted are not $\sum$ but $\sum \sin \alpha$, since these particular samples are plotted against scarf angle α. The α-dependence of $\sum$ is such that the curves plot over a convenient range of ordinates when multiplied by $\sin \alpha$ or $\sin \alpha \cos \alpha$. The parameters chosen represent a random sampling. Note that all cases of $\gamma = 1$ are independent of β, a result from Ref. 7. For actual design use, more extensive families of curves would be needed, and systematic interpolation schemes are necessary. It may prove simplest to interpolate directly in Table 11, and not work with design curves at all.

For bending load, some of the curves can be plotted on the $\sin \alpha / N_{com}$ basis of Figure 30, and others cannot, depending upon the parameter values. The large-β cases in particular show a very large peak near $\alpha = 10\text{-}15°$, shifting toward 20° for intermediate values of β. This implies that certain scarf angles should be favored by designers in particular flexibility ranges. The device of using a log-log scale permits a smoother plot with all curves treated on the same basis; further study would probably reveal an even better device. A few samples of the log-log plot for bending load are shown in Figure 31, for two failure criteria.

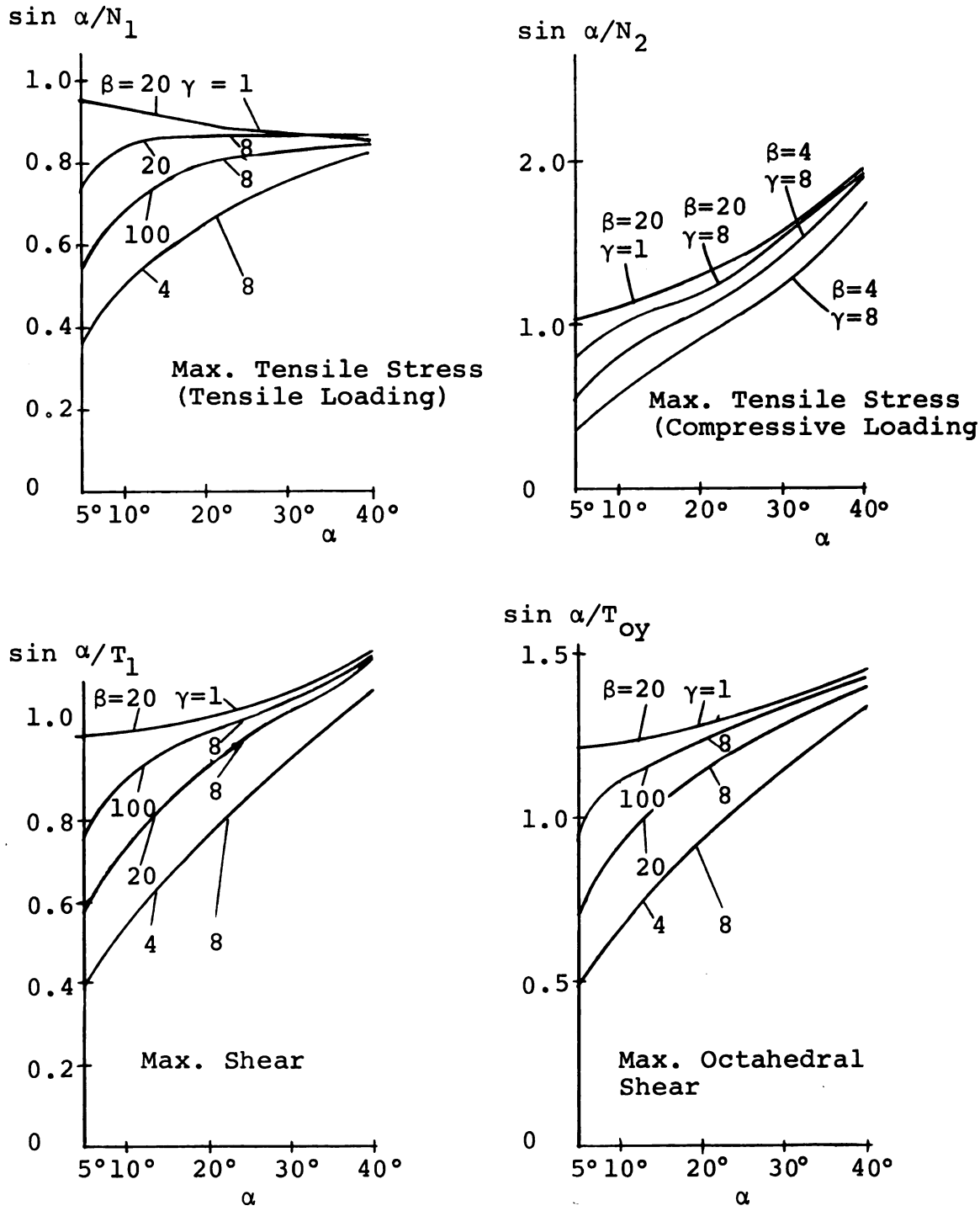

Fig. 30 Elastic "design curves" in dimensionless form, for various failure criteria (failure in N_1, N_2, T_1, T_{oy}). Tensile or compressive load.

The discussion of design is an appropriate place to review the use of both Table 11 and the primary results of Appendix F. It is necessary to align the geometry and loading so that it coincides with Figure 7, p. 26, with adherend 2 made the stiffer one. All tabulated quantities assume that the applied loading has the sense of Figure 7. The parameters

$$\beta = \frac{E_1 \eta}{E_a h(1 - \nu_1^2)}, \qquad \gamma = \frac{E_2(1 - \nu_1^2)}{E_1(1 - \nu_2^2)}$$

are calculated, using the actual values. Interpolation is then carried out as needed. The tabulated values of β (4,20,100) and γ (1,2,4,8) are uniformly spaced on a logarithmic scale, permitting 3- and 4-point Lagrangean interpolation formulas. The angles α = 5, 10, 20, 30, 40° permit linear interpolation (omit 5°) or logarithmic interpolation (omit 30°) by 4-point formulas.

The Poisson's ratios $\nu_1 = \nu_2 = 0.3$, together with the ratio $E_a/G_a = 8/3$ (implying an adhesive Poisson's ratio of 1/3), are inextricably incorporated into the Ritz matrix and thus into all the results. To this extent the user cannot make any adjustments. No calculations have been performed, but the errors are not believed to be very large if the user's Poisson's ratios differ slightly. To the extent that Poisson's ratio affects γ and β, it can be accounted for exactly.

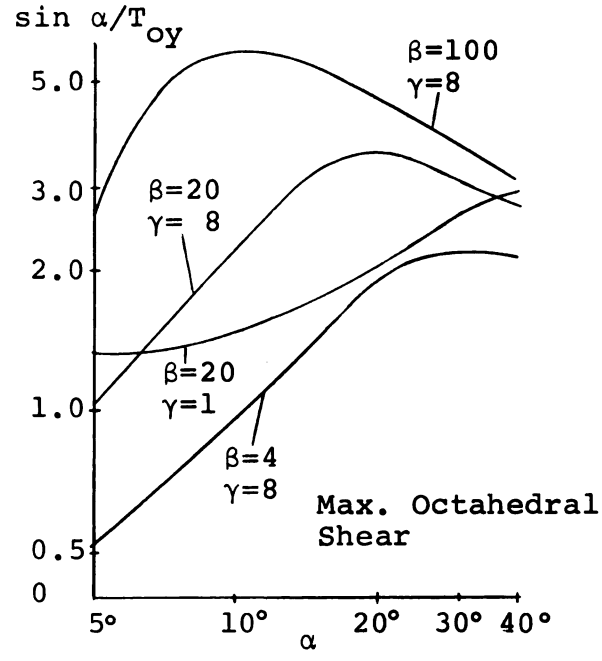

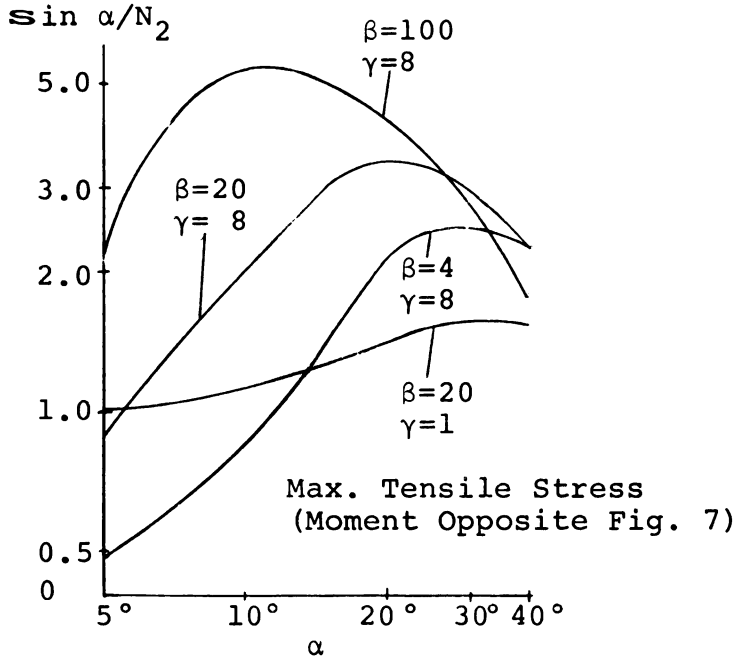

Fig. 31 Elastic "design curves" in dimensionless form, for two failure criteria (N_2, T_{oy}). Bending loads in two senses.

CHAPTER V

CONCLUSIONS AND SUGGESTIONS FOR FURTHER RESEARCH

5.1. Conclusions

The Rayleigh-Ritz method, all in all, appears to have handled the present complex problem with quite good results for the case of tensile loading, and fair to good results for most of the bending load cases. It has been possible to account for many of the phenomena observed in the calculations by physical arguments, and the large range of primary variables explored is probably adequate to give the user a good idea of the overall adhesive stress distribution for any case encountered in practice. The results are valid for a linearly elastic adhesive only, but there are enough adhesives for which this is a fair approximation to make the present results useful. How to employ these results in design has been outlined in sufficient detail that the next steps required are well within the grasp of most stress analysts.

While most of the practical information a user needs has been tabulated and analyzed here, any additional data desired in the future may be calculated from the basic

Ritz matrix coefficients for the two types of loading considered. The latter are available in punched-card form. The computer program in Appendix G can be used for further studies along the present lines, and with minor changes can cope with other types of loading. It is easily possible to alter some of the geometric assumptions about the shape of the adherends.

The nature of the results indicates a large stress disturbance in the adherends, at the ends of the scarf joint. The singularities characteristic for the adherend shapes have been activated by a formulation of the problem which introduces a finite shear stress on the inclined adhesive interface, but leaves the top and bottom adherend faces ("around the corner") stress free. Some alternate formulation, which avoids this difficulty in a manner consistent with the way scarf joints are actually manufactured, would probably greatly improve the rate of convergence of the Ritz method.

5.2. Future Research

Several interesting possibilities can be explored within the present framework; these were not studied here to keep the amount of computer time within reasonable bounds. One useful item would be to examine the effects of varying the Poisson's ratios of adherends and adhesive. A few additional cases might also be computed to facilitate

interpolation in the bending load problem for the smaller scarf angles.

The most interesting research centers around the stress singularities characteristic of the adherend-adhesive corners at the joint ends. If these can be correctly deduced, it seems likely that the Ritz method's convergence could be greatly accelerated, and far fewer equations would be required to calculate any given case. This would open the possibility of dispensing entirely with design tables and curves. It would also make the Sherman-Lauricella integral approach a practical computing tool for this problem.

Another interesting study would circumvent the problem of stress singularities entirely, and yet still be a practical computing tool for scarf joints in the practical (10-30°) range of scarf angles. This would be to treat each adherend as a beam of variable cross section, in extension, bending and shear. The adhesive model could be the same as at present, and there would be little difficulty in allowing for the component of adhesive normal stress not considered here, in the simpler proposed problem. The latter could be tested against the present results to delimit its range of validity. An additional consideration motivating this study is the following: it would be highly desirable to have available a workable, simpler model of the scarf joint for the purposes of studying adhesives with complex rheological behavior.

BIBLIOGRAPHY

1. Langhaar, H. L., Energy Methods in Applied Mechanics, John Wiley, New York, 1962.

2. Courant, R., and Hilbert, D., Methods of Mathematical Physics, Interscience, New York, 1953, pp. 175-176.

3. Kantorovich, L. V., and Krylov, V. I., Approximate Methods of Higher Analysis, Interscience, 1964.

4. Muskhelishvili, N. I., Some Basic Problems of the Mathematical Theory of Elasticity, P. Noordhoff, Holland, 1963, pp. 418-422.

5. Lauricella, G., "Sur l'intégration de l'equation relative á l'équilibre des plaques élastiques encastrées" Acta Math. Vol. 32 (1909), pp. 201-256.

6. Flügge, W., Handbook of Engineering Mechanics, McGraw-Hill, 1962, Section 37, p. 28-29.

7. Lubkin, J. L., "A Theory of Adhesive Scarf Joints," Journal of Applied Mechanics, June, 1957.

8. Eley, D. D., Editor, Adhesion, Oxford University Press, 1961.

9. Bikerman, J. J., The Science of Adhesive Joints, Academic Press, 1961, Chapter 7.

10. Benson, N. K., "The Mechanics of Adhesive Bonding," Applied Mechanics Surveys, Spartan Books, Washington, D. C., 1966.

11. Volkersen, O., Luftfahrtforchung 15, 1938, p. 41.

12. de Bruyne, N. A., and Houwink, R., Adhesion and Adhesives, Elsevier Publishing Company, New York, 1951, Chapter 4 (by Mylonas and de Bruyne).

13. Goland, M. and Reissner, E., "The Stresses in Cemented Joints," Journal of Applied Mechanics, Trans. A.S. M.E., Volume 66, 1944, p. A-17.

14. Plantema, F. J., and Hartman, A. M., Rept. M. 1181, Nat. Luchtvaartlaboratorium, Amsterdam, 1947.

15. Cornell, R. W., "Determination of Stresses in Cemented Lap Joints," Journal of Applied Mechanics, Trans. A.S.M.E., Vol. 75, 1953, pp. 355-364.

16. Mylonas, C., "Experiments with Composite Models," Proceedings of the SESA. XII, 1955, pp. 129-142.

17. Williams, M. L., "Stress Singularities Resulting From Various Boundary Conditions in Angular Corners of Plates in Extension," J. Appl. Mech., 19:4, Dec. 1952, pp. 526-528; also 20:4, Dec. 1953, p. 590.

18. McLaren, A. S. and MacInnes, I., "The influence on the stress distribution in an adhesive lap joint of bending of the adhering sheets," British Journal of Applied Physics, 9, 1958, p. 72; AMR, 12, 1959, Rev. 1280.

19. Sazhin, A. M., "Determining the Stresses in Glued Joints Between Metal Plates," Russian Engineering Journal, 1964, No. 11, pp. 45-49.

20. Misztal, F., "Stress Distribution in Glued Single and Multi-Joints of Sheets Subjected to Shear Along the Splice Line," Bull. DE L'ACADEMIE POLONAISE DES SCIENCES, Cl, IV - Vol. IV, No. 1, 1956, pp. 21-27.

21. Lubkin, J. L., and Reissner, E., "Stress Distribution and Design Data for Adhesive Lap Joints Between Circular Tubes," Trans. ASME, Vol. 78, 1956, pp. 1213-1221.

22. Sherrer, R. E., Rept. 1864, U. S. Forest Products Laboratory, Madison, Wisconsin, 1957; AMR, 12, 1959, Rev. 1897.

23. Timoshenko, S., and Goodier, J. N., Theory of Elasticity, McGraw-Hill, New York, 1951.

24. Müller, G., Dr.-Ing Thesis, Technische Universität, Berlin-Charlottenburg, 1959.

25. Sokolnikoff, I. S., Mathematical Theory of Elasticity, McGraw-Hill, New York, 1956.

26. Hartman, A., Rept. M. 1275, Nat. Luchtvaartlaboratorium Amsterdam, 1948.

27. de Bruyne, N. A., Aero Research Technical Note No. 61, February, 1948.

28. Shield, R. T., Quarterly of Applied Mathematics, 15, July, 1957; AMR, 11, 1958, Rev. 128.

29. Norris, C. B., "Plastic Flow Throughout the Volume of Thin Adhesive Bonds," U.S. FPL Rept. No. 2092, Mar. 1958.

30. Hartman, A., Rept. M. 1475, Nat. Luchtvaartlaboratorium, Amsterdam, 1949.

APPENDIX A

FORMULATION OF THE EXPRESSION FOR TOTAL POTENTIAL ENERGY

For the case of plane stress, the strain energy per unit width in each adherend takes the standard form ($i = 1,2$):

$$U'_{si} = \frac{E_i}{2(1 - \nu_i^2)} \iint_{A_i} \left[\left(\frac{\partial u_i}{\partial x} \right)^2 + \left(\frac{\partial v_i}{\partial y} \right)^2 + 2\nu_1 \frac{\partial u_i}{\partial x} \frac{\partial v_i}{\partial y} + \frac{1 - \nu_i}{2} \left(\frac{\partial u_i}{\partial y} + \frac{\partial v_i}{\partial x} \right)^2 \right] dx\, dy \qquad \text{A-1}$$

where A_i is the area of the i^{th} adherend, the E_i and ν_i are the usual elastic constants, and the u_i and the v_i are (respectively) the x- and y- components of displacement.

The total potential energy of the scarf joint is

$$\Omega' = U'_{s1} + U'_{s2} + U'_{sa} + W' \qquad \text{A-2}$$

where U'_{sa} = strain energy of the adhesive film

W' = potential energy of the external forces

The strain energy of the adhesive is derived in Section 2.2.

$$U'_{sa} = \frac{1}{2\eta \sin \alpha} \int_{-h}^{+h} \Big[(u_1 - u_2)^2 (E_a \sin^2 \alpha + G_a \cos^2 \alpha) + (v_1 - v_2)(E_a \cos^2 \alpha + G_a \sin^2 \alpha) + 2(u_1 - u_2)(v_1 - v_2) \sin \alpha \cos \alpha \, (G_a - E_a) \Big] dy \qquad \text{A-3}$$

The only nonvanishing external loading consists of the pure tensile or bending stress $\sigma_x(\pm c, y)$ on $x = \pm c = \pm h(2 + \cot \alpha)$, the extreme ends of the joint (Fig. 7, p. 26). The potential energy due to loading is thus

$$W' = -\int_{-h}^{h} \sigma_x(c,y) u_2(c,y) dy + \int_{-h}^{h} \sigma_x(-c,y) u_1(-c,y) dy \qquad \text{A-4}$$

This accounts for all terms needed for equation A-2, which is the same as 2.2.13. Using the nondimensionalization of 2.2.14, the dimensionless total potential energy ω of 2.2.16 is produced.

APPENDIX B

GENERATION OF RITZ EQUATIONS

The total potential energy expression in its dimensionless form is given by equation 2.2.16, p. 39. The four principal equations are derived from the following four relations

$$\frac{\partial \omega}{\partial A_{m,n}} = 0 \qquad \text{B - 1}$$

$$\frac{\partial \omega}{\partial B_{m,n}} = 0 \qquad \text{B - 2}$$

$$\frac{\partial \omega}{\partial C_{m,n}} = 0 \qquad \text{B - 3}$$

$$\frac{\partial \omega}{\partial D_{m,n}} = 0 \qquad \text{B - 4}$$

Note that U_1 contains only $A_{m,n}$, V_1 contains only $B_{m,n}$, U_2 only $C_{m,n}$ and V_2 only $D_{m,n}$.

$$\frac{\partial \omega}{\partial A_{m,n}} = 0 = \int\int_{①} \left[\left(\frac{\partial U_1}{\partial X} \right) \frac{\partial}{\partial A_{m,n}} \left(\frac{\partial U_1}{\partial X} \right) + \nu_1 \left(\frac{\partial V_1}{\partial Y} \right) \frac{\partial}{\partial A_{m,n}} \left(\frac{\partial U_1}{\partial X} \right) \right.$$

$$\left. + \frac{1}{2} (1 - \nu_1) \left(\frac{\partial U_1}{\partial Y} + \frac{\partial V_1}{\partial X} \right) \frac{\partial}{\partial A_{m,n}} \left(\frac{\partial U_1}{\partial Y} \right) \right] dX \, dY$$

$$+ \int_{-1}^{1} \left[H_1 (U_1 - U_2) \frac{\partial U_1}{\partial A_{m,n}} - H_2 (V_1 - V_2) \frac{\partial U_1}{\partial A_{m,n}} \right] dY$$

$$+ (1 - \nu_1^2) \int_{-1}^{1} \sigma_0(Y) \left[\frac{\partial U_1(-C,Y)}{\partial A_{m,n}}\right] dY \qquad \text{B-5}$$

Here and below, ① and ② indicate integrations over adherends 1 and 2.

$$\frac{\partial \omega}{\partial B_{m,n}} = 0 = \int\int_{①} \left[\left(\frac{\partial V_1}{\partial Y}\right) \frac{\partial}{\partial B_{m,n}} \left(\frac{\partial V_1}{\partial Y}\right) + \nu_1 \left(\frac{\partial U_1}{\partial X}\right) \frac{\partial}{\partial B_{m,n}} \left(\frac{\partial V_1}{\partial Y}\right) \right.$$

$$\left. + \frac{1}{2} (1 - \nu_1) \left(\frac{\partial U_1}{\partial Y} + \frac{\partial V_1}{\partial X}\right) \frac{\partial}{\partial B_{m,n}} \left(\frac{\partial V_1}{\partial X}\right)\right] dX\, dY$$

$$+ \int_{-1}^{1} \left[H_h (V_1 - V_2) \frac{\partial V_1}{\partial B_{m,n}} - H_2 (U_1 - U_2) \frac{\partial V_1}{\partial B_{m,n}}\right] dY$$

B-6

$$\frac{\partial \omega}{\partial C_{m,n}} = 0 = \gamma \int\int_{②} \left[\left(\frac{\partial U_2}{\partial X}\right) \frac{\partial}{\partial C_{m,n}} \left(\frac{\partial U_2}{\partial X}\right) + \nu_2 \left(\frac{\partial V_2}{\partial Y}\right) \frac{\partial}{\partial C_{m,n}} \left(\frac{\partial U_2}{\partial X}\right) \right.$$

$$\left. + \frac{1}{2} (1 - \nu_2) \left(\frac{\partial U_2}{\partial Y} + \frac{\partial V_2}{\partial X}\right) \frac{\partial}{\partial C_{m,n}} \left(\frac{\partial U_2}{\partial Y}\right)\right] dX\, dY$$

$$+ \int_{-1}^{1} \left[-H_1 (U_1 - U_2) \frac{\partial U_2}{\partial C_{m,n}} + H_2 (V_1 - V_2) \frac{\partial U_2}{\partial C_{m,n}}\right] dY$$

$$- (1 - \nu_2^2) \int_{-1}^{+1} \sigma_0(Y) \left[\frac{\partial U_2(C,Y)}{\partial C_{m,n}}\right] dY \qquad \text{B-7}$$

$$\frac{\partial \omega}{\partial D_{m,n}} = 0 = \gamma \int\int_{②} \left[\left(\frac{\partial V_2}{\partial Y}\right) \frac{\partial}{\partial D_{m,n}} \left(\frac{\partial V_2}{\partial Y}\right) + \nu_2 \left(\frac{\partial U_2}{\partial X}\right) \frac{\partial}{\partial D_{m,n}} \left(\frac{\partial V_2}{\partial Y}\right) \right.$$

$$\left. + \frac{1}{2} (1 - \nu_2) \left(\frac{\partial U_2}{\partial Y} + \frac{\partial V_2}{\partial X}\right) \frac{\partial}{\partial D_{m,n}} \left(\frac{\partial V_2}{\partial X}\right)\right] dX\, dY$$

$$+ \int_{-1}^{1} \left[- H_h (V_1 - V_2) \frac{\partial V_2}{\partial D_{m,n}} + H_2 (U_1 - U_2) \frac{\partial V_2}{\partial D_{m,n}} \right] dY$$

B-8

Substituting the explicit double sums for U_1, V_1 and their derivatives into the equation B-5, it becomes

$$0 = \sum_{k=0}^{M} \sum_{j=0}^{M-k} \int_{-1}^{1} \int_{-C}^{Y} \cot \alpha \left[A_{k,j}\ k\ m\ X^{k+m-2}\ Y^{n+j} \right.$$

$$+ \nu_1\ B_{k,j}\ j\ m\ X^{k+m-1}\ Y^{n+j-1} + \frac{1}{2} (1 - \nu_1) nj\ A_{k,j} X^{k+m} Y^{n+j-2}$$

$$\left. + \frac{1}{2} (1 - \nu_1)\ B_{k,j}\ k\ n\ X^{k+m-1}\ Y^{n+j-1} \right] dX\ dY + \int_{-1}^{1} \left[H_1 (A_{k,j} \right.$$

$$\left. - C_{k,j}) - H_2 (B_{k,j} - D_{k,j}) \right] X^{k+m}\ Y^{n+j}\ dY +$$

$$+ (1 - \nu_1^2) \int_{-1}^{1} \sigma_0 (Y) (-C)^m\ Y^n\ dY \qquad \text{B-9}$$

In all the double integrals of equation B-9, integration is carried out first with respect to X. The result is

$$0 = \sum_{k=0}^{M} \sum_{j=0}^{M-k} \int_{-1}^{1} \left\{ A_{k,j} \frac{km}{k + m - 1} \left[Y^{k+m+n+j-1} (\cot \alpha)^{k+m-1} \right. \right.$$

$$\left. - Y^{n+j} (-C)^{k+m-1} \right] + \nu_1\ B_{k,j} \frac{jm}{k + m} \left[Y^{k+m+n+j-1} (\cot \alpha)^{k+m} \right.$$

$$\left. - Y^{n+j-1} (-C)^{k+m} \right] + \frac{(1 - \nu_1)}{2}\ A_{k,j} \frac{nj}{k + m + 1} \cdot$$

$$\cdot \left[Y^{k+m+n+j-1}\ (\cot \alpha)^{k+m+1} - Y^{n+j-2}\ (-C)^{k+m+1} \right]$$

$$+ \frac{(1 - \nu_1)}{2} B_{k,j} \frac{nk}{k + m} \left[Y^{k+m+n+j-1} (\cot \alpha)^{k+m} - Y^{n+j-1} (-C)^{k+m} \right] \Bigg\} dY + \int_{-1}^{1} \left[H_1 (A_{k,j} - C_{k,j}) - H_2 (B_{k,j} - D_{k,j}) \right] X^{k+m} Y^{j+n} dY$$

$$+ (1 - \nu_1^2) \int_{-1}^{1} \sigma_0(Y) (-C)^m Y^n dY \qquad \text{B-10}$$

Equation B-10 is now integrated with respect to Y. The final equation is in the form

$$0 = \sum_{k=0}^{M} \sum_{j=0}^{M-k} \Bigg\{ A_{k,j} \frac{km}{k + m - 1} \left[f(k+m+n+j) (\cot \alpha)^{k+m-1} - (-C)^{k+m-1} f(n+j+1) \right]$$

$$+ \nu_1 B_{k,j} \frac{jm}{k + m} \left[f(k+m+n+j) (\cot \alpha)^{k+m} - (-C)^{k+m} f(j+n) \right]$$

$$+ \frac{(1 - \nu_1)}{2} \frac{nj}{k+m+1} A_{k,j} \left[f(k+m+n+j) (\cot \alpha)^{k+m+1} - (-C)^{k+m+1} f(n+j-1) \right]$$

$$+ \frac{(1 - \nu_1)}{2} B_{k,j} \frac{kn}{k + m} \left[f(k+m+n+j) (\cot \alpha)^{k+m} - (-C)^{k+m} f(j+n) \right] + \left[H_1 (A_{k,j} - C_{k,j}) - H_2 (B_{k,j} - D_{k,j}) \right] (\cot \alpha)^{k+m} f(k+m+n+j+1)$$

$$+ (1 - \nu_1^2) \int_{-1}^{1} \sigma_0(Y) (-C)^m Y^n dY \qquad \text{B-11}$$

where

$$C = 2 + \cot \alpha$$

$$f(R) = \frac{1 - (-1)^R}{R} = \begin{cases} 0 : R \text{ even} \\ 2/R : R \text{ odd} \end{cases}$$

Other quantities are now defined as follows

$$\phi_0 = (\cot \alpha)^{k+m-1} f(k+m+n+j)$$

$$\phi_1 = (\cot \alpha)^{k+m} f(k+m+n+j+1)$$

After rearrangement, first set of Ritz equations, corresponding to B-1, becomes

$$\begin{aligned} 0 = \sum_{k=0}^{M} \sum_{j=0}^{M-k} \Bigg\{ & A_{k,j} \Bigg[\frac{km}{k+m-1} \left(\phi_0 - (-C)^{k+m-1} f(n+j+1) \right) \\ & + \frac{1 - \nu_1}{2} \frac{nj}{k+m+1} \left(\phi_0 \cot^2 \alpha - (-C)^{k+m+1} f(n+j-1) \right) \\ & + H_1 \phi_1 \Bigg] + B_{k,j} \Bigg[\left(\frac{\nu_1 jm}{k+m} + \frac{1 - \nu_1}{2} \frac{kn}{k+m} \right) \left(\phi_0 \cot \alpha \right. \\ & \left. - (-C)^{k+m} f(n+j) \right) - H_2 \phi_1 \Bigg] - C_{k,j} H_1 \phi_1 + D_{k,j} H_2 \phi_1 \Bigg\} \\ & + (1 - \nu_1^2) \int_{-1}^{+1} \sigma_0(Y) (-C)^m Y^n \, dY \end{aligned} \qquad \text{B-12}$$

Equation B-12 corresponds to 2.2.19. The other three basic Ritz equations are derived similarly. Note that the foregoing reflects the contribution of the $A_{m,n}$ coefficients to the corresponding row of the final Ritz matrix. Each of equations B-2 through B-4 makes a similar contribution, and these appear in equations 2.2.20-2.2.22.

APPENDIX C

SELF-EQUILIBRATED POLYNOMIAL STRESSES

In equation 2.3.1, the part (2) contribution to the adhesive normal and shear stresses is assumed to have the form

$$\sigma_n^{(2)} = \sum_{m=1}^{K} a_m S^m \qquad \text{C-1}$$

$$\tau_{ns} = \sum_{m=1}^{K} b_m S^m \qquad \text{C-2}$$

in undetermined coefficients a_m, b_m. Here S is the dimensionless distance along the inclined adhesive boundary, or s/h in terms of Fig. 7, and is measured from the origin of coordinates. From the diagram cited, S ranges from $-\csc\alpha$ to $\csc\alpha$. The integer K must be odd.

The purpose of this derivation is to eliminate three coefficients from the set (a_m, b_m), by enforcing the requirement that C-1 and -2 represent a wholly self-equilibrated stress distribution. Of the three static equilibrium conditions, the vanishing of the resultant force in the X-direction (by integration and taking components) yields:

$$\sum_{m=1}^{K} (a_m \sin\alpha + b_m \cos\alpha) \frac{S^{m+1}}{m+1} \Bigg|_{-\csc\alpha}^{\csc\alpha} = 0 \quad (m \text{ even}) \qquad C\text{-}3$$

Similarly, the vanishing of the Y- resultant gives

$$\sum_{m=1}^{K} (-a_m \cos\alpha + b_m \sin\alpha) \frac{S^{m+1}}{m+1} \Bigg|_{-\csc\alpha}^{\csc\alpha} = 0 \quad (m \text{ even}) \qquad C\text{-}4$$

The vanishing of the resultant moment about the origin produces:

$$\sum_{m=1}^{K} a_m S^{m+2} \Bigg|_{-\csc\alpha}^{\csc\alpha} = 0 \quad (m \text{ odd}) \qquad C\text{-}5$$

After entering the limits, equations C-3 and C-4 may be solved to obtain

$$\sum_{m=1}^{K} a_m \frac{(\csc\alpha)^{m+1}}{m+1} = 0 \quad (m \text{ even}) \qquad C\text{-}6$$

$$\sum_{m=1}^{K} b_m \frac{(\csc\alpha)^{m+1}}{m+1} = 0 \quad (m \text{ even}) \qquad C\text{-}7$$

After substitution of these two relations equation C-5 becomes

$$\sum_{m=1}^{K} a_m \frac{(\csc\alpha)^{m+1}}{m+2} = 0 \quad (m \text{ odd}) \qquad C\text{-}8$$

Equations C-6, C-7 and C-8 give the desired expressions for eliminating a_{K-1}, b_{K-1} and a_K, respectively:

$$a_{K-1} = - K \sum_{m \text{ even}}^{K-3} a_m \frac{(\csc\alpha)^{m-K+1}}{m + 1} \qquad \text{C-9}$$

$$b_{K-1} = - K \sum_{m \text{ even}}^{K-3} b_m \frac{(\csc\alpha)^{m-K+1}}{m + 1} \qquad \text{C-10}$$

$$a_K = - (K + 2) \sum_{m \text{ odd}}^{K-2} a_m \frac{(\csc\alpha)^{m-K}}{m + 2} \qquad \text{C-11}$$

Expanding C-1 and C-2

$$\tau_{ns}^{(2)} = \sum_{m=1,2,3\ldots}^{K-2} b_m S^m + b_{K-1} S^{K-1} + b_K S^K \qquad \text{C-12}$$

$$\sigma_n^{(2)} = \sum_{m=1}^{K-2} a_m S^m + a_{K-1} S^{K-1} + a_K S^K \qquad \text{C-13}$$

These become, after substitution from C-9, -10 and -11:

$$\sigma_n^{(2)} = \sum_{m=1,2,3,\ldots}^{(K-1)/2} a_{2m-1} \left[S^{2m-1} - \frac{(K + 2)}{(2m + 1)} (\csc\alpha)^{2m-K-1} S^K \right]$$

$$+ \sum_{m=1,2,3,\ldots}^{(K-3)/2} a_{2m} \left[S^{2m} - \frac{K(\csc\alpha)^{2m-k+1}}{2m + 1} S^{K-1} \right] \qquad \text{C-14}$$

$$\tau_{ns}^{(2)} = \sum_{m=1,2,3,\ldots}^{(K+1)/2} b_{2m-1} S^{2m-1} + \sum_{m=1,2,3,\ldots}^{(K-3)/2} b_{2m} \left[S^{2m} - \frac{K(\csc\alpha)^{2m-K+1}}{2m + 1} S^{K-1} \right] \qquad \text{C-15}$$

Equations C-14 and -15 are the same as 2.3.2.

APPENDIX D

DISPLACEMENT DETERMINATION FOR THE INTEGRAL EQUATION APPROACH

The displacement components U_1, V_1 of the first adherend are related to the analytic functions $\phi(z)$, and $\psi(z)$ of the complex variable $z = X + iY$ by the following equation[4]

$$2\mu_1(U_1 + iV_1) = \chi_1\phi(z) - z\overline{\phi'(z)} - \overline{\psi(z)} \qquad \text{D-1}$$

where

μ_1 = shear modulus

$\chi_1 = (3 - \nu_1)/(1 + \nu_1)$ for plane stress

ν_1 = Poisson's ratio

and the values of the functions $\phi(z)$, $\phi'(z)$ and $\psi(z)$ are defined below in terms of a "density function" $\omega(t)$, presumed known at this stage. With the $\omega(t)$ actually used, the displacements calculated are the contributions $U_1^{(2)}$ and $V_1^{(2)}$ of section 2.3.

$$\phi(z) = \frac{1}{2\pi i}\int \frac{\omega(s)}{s - z}\, ds \qquad \text{D-2}$$

$$\phi'(z) = \frac{1}{2\pi i}\int \frac{\omega'(s)}{s - z}\, ds \qquad \text{D-3}$$

$$\psi(z) = \frac{1}{2\pi i}\int \frac{\overline{\omega(s)}}{s - z}\, ds - \frac{1}{2\pi i}\int \frac{\bar{s}\,\omega'(s)}{s - z}\, ds \qquad \text{D-4}$$

where all integrations are around the boundary of adherend 1. Substituting the limiting (boundary) values of the functions $\phi(z)$ and $\psi(z)$ into equation D-1 (Plemelj formulas):

$$2\mu_1(U_1 + iV_1) = \frac{\chi_1}{2\pi i}\int \frac{\omega(s)}{s - t}\, ds + \frac{1}{2\pi i}\int \frac{t\overline{\omega'(s)}}{\bar{s} - \bar{t}}\, d\bar{s}$$

$$+ \frac{1}{2\pi i}\int \frac{\omega(s)}{\bar{s} - \bar{t}}\, d\bar{s} - \frac{1}{2\pi i}\int \frac{s\,\overline{\omega'(s)}}{\bar{s} - \bar{t}}\, d\bar{s} \qquad \text{D-5}$$

Adding and subtracting $\frac{\chi_1}{2\pi i}\int \frac{\omega(t)}{s - t}\, ds$ and $\frac{1}{2\pi i}\int \frac{\omega(t)}{\bar{s} - \bar{t}}\, d\bar{s}$ respectively in the first and third integrals, and rearranging:

$$2\mu_1(U_1 + iV_1) = \frac{\chi_1}{2\pi i}\int \frac{\omega(s)}{s - t}\, ds + \frac{1}{2\pi i}\int \overline{\omega'(s)}\,\frac{s - t}{\bar{s} - \bar{t}}\, d\bar{s}$$

$$+ \frac{1}{2\pi i}\int \frac{\omega(s) - \omega(t)}{\bar{s} - \bar{t}} + \frac{\chi_1}{2\pi i}\,\omega(t)\int \frac{ds}{s - t}$$

$$+ \frac{\omega(t)}{2\pi i}\int \frac{d\bar{s}}{\bar{s} - \bar{t}} - \frac{\chi_1}{2\pi i}\,\omega(t)\int \frac{ds}{s - t} \qquad \text{D-6}$$

But

$$\frac{\omega(t)}{2\pi i}\int \frac{d\bar{s}}{\bar{s} - \bar{t}} = \text{conjugate of } \left[- \frac{\overline{\omega(t)}}{2\pi i}\int \frac{ds}{s - t} \right]$$

$$= - \omega(t)/2 \qquad \text{D-7}$$

$$\chi_1\,\omega(t)\int \frac{ds}{s - t} = \chi_1\,\omega(t)/2 \qquad \text{D-8}$$

$$- \frac{1}{2\pi i}\int \overline{\omega'(s)}\ \frac{s - t}{\bar{s} - \bar{t}}\, d\bar{s} = - \frac{1}{2\pi i}\ \text{conj}\int \omega'(s)\ \frac{\bar{s} - \bar{t}}{s - t}\, ds \qquad \text{D-9}$$

The terms of equation D-9 reduce, upon integration by parts, to

$$- \frac{1}{2\pi i}\ \text{conj}\left[\frac{\bar{s} - \bar{t}}{s - t}\ \omega(s)\right]\Bigg|_{s_0}^{s_0} - \int \omega(s)\ d\left(\frac{\bar{s} - \bar{t}}{s - t}\right)$$

$$= \frac{1}{2\pi i}\int \overline{\omega(s)}\ d\left(\frac{\bar{s} - \bar{t}}{s - t}\right) \qquad \text{D-10}$$

since the first term vanishes. Let

$$s - t = re^{i\theta}$$

$$\bar{s} - \bar{t} = re^{-i\theta}$$

$$\frac{s - t}{\bar{s} - \bar{t}} = e^{2i\theta} \quad ; \quad d\left(\frac{s - t}{\bar{s} - \bar{t}}\right) = i2e^{2i\theta}d\theta$$

The term in equation D-10 now becomes

$$\frac{1}{\pi}\int \overline{\omega(s)}\ e^{2i\theta}d\theta \qquad \text{D-11}$$

But, from the basic integral equation of the problem, 2.3.14, the expression of equation D-11 is also

$$\omega(t) + \frac{1}{\pi}\int \omega(s)d\theta - f(t) \qquad \text{D-12}$$

Upon substitution of relations D-7, D-8 and D-12 into equation D-6,

$$2\mu_1(U_1 + iV_1) = \frac{\chi_1}{2\pi i}\int \frac{\omega(s) - \omega(t)}{s - t}\, ds + \frac{1}{2\pi i}\int \frac{\omega(s) - \omega(t)}{\bar{s} - \bar{t}}\, \frac{d\bar{s}}{\bar{s}-\bar{t}}$$

$$+ \frac{1}{\pi}\int \omega(s)d\theta - f(t) + \tfrac{1}{2}\chi_1\omega(t) + \tfrac{1}{2}\omega(t) \qquad \text{D-13}$$

now write

$$\omega(s) = p(s) + iq(s) \qquad \text{D-14}$$

and convert the integration in θ to s by the relation

$$d\theta = \frac{\partial\theta}{\partial s}\, ds \qquad \text{D-15}$$

Since[4]

$$\frac{\partial\theta}{\partial s} = \frac{\cos\alpha}{r} \quad ,$$

$$d\theta = \frac{\cos\alpha}{r}\, ds \qquad \text{D-16}$$

where α is the angle between the vector s - t and the outward normal at s (unrelated to the scarf angle α used elsewhere).

After substitution of D-14 and D-16, equation D-13 becomes

$$2\mu_1(U_1 + iV_1) = \frac{\chi_1}{2\pi i}\int \Big\{[p(s) - p(t)] + i[q(s) - q(t)]\Big\}\, \frac{ds}{s - t}$$

$$+ \frac{1}{2\pi i}\int \Big\{[p(s) - p(t)] + i[q(s) - q(t)]\Big\}\, \frac{d\bar{s}}{\bar{s} - \bar{t}}$$

$$+ \frac{1}{\pi}\int [p(s) + iq(s)]\, \frac{\cos\alpha}{r}\, ds + \tfrac{1}{2}\chi_1[p(t) + iq(t)]$$

$$+ \tfrac{1}{2}[\, p(t) + iq(t)] - f_1(t) - if_2(t) \qquad \text{D-17}$$

For numerical integration to find the displacement components, the boundaries AB, BC, CD and DA in Fig. 7 are divided into

I_1, I_2, I_3 and I_4 intervals, respectively. Equation D-17 is rewritten as a sum of integrals over each interval along the boundary.

$$2\mu_1(U_{1j} + iV_{1j}) = \frac{1}{\pi}\sum_{k=1}^{I}\int\left[p_k(s) + iq_k(s)\right]\frac{\cos\alpha_{jk}}{r_{jk}}\,ds - f_{1j} - if_{2j} + \tfrac{1}{2}\chi_1[p_j + iq_j] - \frac{i}{2\pi}\sum_{k=1}^{I}\int\left\{\left[p_k(s) - p_j\right] + i\left[q_k(s) - q_j\right]\right\}\left(\chi_1\frac{ds}{s_k - t_j} + \frac{d\bar{s}}{\bar{s}_k - \bar{t}_j}\right) + \tfrac{1}{2}(p_j + iq_j) \qquad \text{D-18}$$

where

$I = I_1 + I_2 + I_3 + I_4$ = total number of intervals along the boundary of each adherend

$p_k(s)$, $q_k(s)$ = functions p(s), q(s) on the k^{th} interval

U_{1j}, V_{1j} = X,Y-displacement components of adherend 1 at j^{th} boundary node point (midpoint of j^{th} interval)

α_{jk} = angle between the vector $s_k - t_j$ and the outward normal at s

$r_{jk} = |s_k - t_j|$; $p_j, q_j = p(t_j), q(t_j)$

Equation D-18 is symbolic of the numerical integration; the details had to be carried out differently because of the nature of the integrand. Special treatment is

required when k = j, and at the ends of each side of the adherend. At all other points, the integration is by the trapezoidal rule, from the center of each boundary interval to the center of the next, or node to node. When k = j, the last integral term in D-18 is interpreted in terms of the first derivatives of p and q (the nominal singularity is removable). These are evaluated using a central difference formula at the node points adjacent to $s_k = t_j$.

For the half intervals at each end of each side, the special treatment is as follows. Lagrange's three-point interpolation formula is used to compute the values of p and q at special points, such as the corners and ends of the first and last interval along each side, in terms of the values at the nodal points. The values of p and q at corners of the adherend are evaluated by taking the average of the extrapolated values for the corner from the adjacent adherend sides. The derivative treatment is more involved when j = k involves the end half-intervals, but it is along similar lines.

APPENDIX E

RIGID BODY DISPLACEMENT CONSTANTS

The net displacement components U_1, V_1 of the first adherend are

$$U_1 = U_1^{(1)} + U_1^{(2)}$$
$$V_1 = V_1^{(1)} + V_1^{(2)} \qquad \text{E-1}$$

where $U_1^{(1)}$, $V_1^{(1)}$ are the displacement components due to an applied tensile stress parallel to X which is assumed to be equal to unity, and $U_1^{(2)}$, $V_1^{(2)}$ are the displacements due to the self-equilibrated stresses of equations 2.3.1. In terms of rigid translation constants C_1, D_1 and rotation ω_1,

$$U_1^{(1)} = \frac{1}{E_1} X + C_1 - \omega_1 Y$$
$$V_1^{(1)} = -\frac{\nu_1 Y}{E_1} + D_1 + \omega_1 X \qquad \text{E-2}$$

The totals are thus

$$U_1 = \frac{1}{E_1} X + C_1 - \omega_1 Y + U_1^{(2)}$$
$$V_1 = -\frac{\nu_1 Y}{E_1} + D_1 + \omega_1 X + V_1^{(2)} \qquad \text{E-3}$$

An arbitrary rigid-body displacement choice is possible for one adherend. Accordingly, adherend 1 is assumed not to translate or rotate at the origin, or $U_1(0,0) = 0 = V_1(0,0)$ in equation E-3. Thus

$$C_1 = - U_1^{(2)}(0,0) \quad \text{and} \quad D_1 = - V_1^{(2)}(0,0)$$

The suppression of rigid-body rotation, finally requires $\omega_1 = 0$. Thus the net displacement components of the first adherend are

$$U_1 = U_1^{(2)} + \frac{X}{E_1} - U_1^{(2)}(0,0)$$
$$V_1 = V_1^{(2)} - \nu_1 \frac{Y}{E_1} - V_1^{(2)}(0,0) \qquad \text{E-4}$$

The displacement components of the second adherend, also due to a unit applied tensile stress parallel to X, are

$$U_2^{(1)} = \frac{X}{E_2} + C_2 - \omega_2 Y$$
$$V_2^{(1)} = - \nu_2 \frac{Y}{E_2} + D_2 + \omega_2 x \qquad \text{E-5}$$

The net displacement components of adherend 2, including the contribution due to the self-equilibrated stresses of equation 2.3.1 acting at the adhesive interface, can be expressed as,

$$U_2 = \frac{X}{E_2} + C_2 - \omega_2 Y + U_2^{(2)}$$
$$V_2 = - \frac{\nu_2}{E_2} Y + D_2 + \omega_2 X + V_2^{(2)} \qquad \text{E-6}$$

In section 2.3, it is noted that the last terms in E-6 are constructed from $U_1^{(2)} - U_1^{(2)}(0,0)$ and $V_1^{(2)} - V_1^{(2)}(0,0)$, which appear in E-4. Actually, these expressions are symbolic; the displacements in question are related by a numerical matrix to still-undetermined coefficients (a_m, b_m), 2K-3 in number. As explained in section 2.3, the main adjustment required to construct $U_2^{(2)}$ and $V_2^{(2)}$ is simply to multiply the numerical matrix by μ_1/μ_2, the ratio of adherend shear moduli. Since it is assumed that both adherends have the same Poisson's ratio, this is equivalent to multiplying by E_1/E_2. Thus the factor $1/E_1$ and $1/E_2$ are actually present implicitly in $U_2^{(2)}$ and $V_2^{(2)}$, but do not appear explicitly in E-6.

APPENDIX F

TABLES OF STRESS DISTRIBUTIONS, AND AUXILIARY TABLES

The primary results of this thesis are the following tables. Table F1 gives adhesive normal stress distribution (N), which acts perpendicular to the plane of the adhesive layer, and the shear stress distribution (T). The positive senses of these stresses are shown in Figure 7, p. 26.

The tables are based on a uniform applied tensile stress of unity, or a linearly-varying bending stress with outer-fiber value unity. This unit stress corresponds to $\sigma_0 = 1$ in Figure 7; it also corresponds to the stress $\sigma_{X0} = 1$ (a name used elsewhere in the text). It is also referred to as the "load stress." The corresponding force resultants, F and M_0 in Figure 7, are positive as shown in the figure.

The stress distributions are tabulated against the variable S, which is the fraction of the joint half-length, measured from its center (the origin in Figure 7). At joint end D in Figure 7, S = 1.0, and at joint end C, S = -1.0. The cases covered include both tension and bending load; for five scarf angles (α = 5, 10, 20, 30, 40°); for

three values of relative adhesive-adherend flexibility (β = 4,20,100); and for four values of the dissimilarity parameter (γ = ratio of adherend stiffnesses = 1,2,4,8). The tabulated stresses represent exact 8^{th}-order polynomials in S. Advice on interpolation (with respect to α, β, γ) appears in section 4.3.

To save the user the trouble of interpolating for maximum values of the normal stress N, an auxiliary table (F2) gives the maximum values N_{max} for every distribution in the primary tables. The shear stress maxima T_{max} are usually at S = -1.0, except for a few cases noted in the main discussion of Chapter 4 (large α and medium to large β, in bending).

Two auxiliary tables offer the user some assistance in deciding for himself whether the present tables are accurate enough for his purposes. In all cases tabulated here, 177 Ritz equations have been solved by matrix inversion, using a standard symmetric-matrix computer subroutine. This solution is referred to as an 8^{th}-order polynomial solution. In many cases, a 7^{th}-order solution is also available for comparison (141 equations). In other cases, only a 6^{th}-order solution is available for comparison (109 equations). In some cases, no comparison is available. Where available, the two solutions are compared in the manner described in section 3.1.4. Thus one auxiliary table in this Appendix (F3) gives the average difference

between the 8^{th}-order and the 7^{th}-order solutions (averaged over the length of the joint). The 8^{th}-order is compared to the 6^{th}-order where no 7^{th}-order result is available.

Another auxiliary table (F4) presents a much sharper test of Ritz convergence. The primary tables of N and T are examined for all stresses ranging from one-half the largest value up to the largest value. The largest percentage difference between the 8^{th}- and 7^{th}-order results is tabulated, for the "large-stress" range considered. Orders 8 and 6 are compared where 7 is not available. (The latter check is often not as favorable as one may wish, because the 7^{th}-order results are frequently quite close to the 8^{th}-order ones when the 6^{th}-order is still far away.) Sometimes the "half-the-maximum" criterion distorts the picture too favorably, and additional entries in the auxiliary table show that by going a little below half the maximum, a much larger difference may appear.

Table F1.--Adhesive normal and shear stresses.

ALPHA=5 DEGREES, BETA=4

S	GAMMA=1 TENSION N	GAMMA=1 TENSION T	GAMMA=1 BENDING N	GAMMA=1 BENDING T	GAMMA=2 TENSION N	GAMMA=2 TENSION T	GAMMA=2 BENDING N	GAMMA=2 BENDING T
-1.0	0.0076	0.0868	0.0071	0.0817	0.0119	0.1389	0.0079	0.1277
-0.9	0.0076	0.0868	0.0066	0.0745	0.0097	0.1197	0.0098	0.1013
-0.8	0.0076	0.0868	0.0060	0.0672	0.0075	0.1046	0.0064	0.0789
-0.7	0.0076	0.0868	0.0054	0.0596	0.0061	0.0941	0.0039	0.0608
-0.6	0.0076	0.0868	0.0047	0.0517	0.0056	0.0878	0.0034	0.0463
-0.5	0.0076	0.0868	0.0040	0.0435	0.0055	0.0849	0.0038	0.0341
-0.4	0.0076	0.0868	0.0033	0.0351	0.0056	0.0844	0.0039	0.0233
-0.3	0.0076	0.0868	0.0025	0.0265	0.0059	0.0853	0.0032	0.0131
-0.2	0.0076	0.0868	0.0017	0.0177	0.0064	0.0871	0.0016	0.0032
-0.1	0.0076	0.0868	0.0009	0.0089	0.0072	0.0890	-0.0001	-0.0064
0.0	0.0076	0.0868	-0.0000	-0.0000	0.0082	0.0906	-0.0015	-0.0154
0.1	0.0076	0.0868	-0.0009	-0.0089	0.0093	0.0915	-0.0024	-0.0236
0.2	0.0076	0.0868	-0.0017	-0.0177	0.0101	0.0915	-0.0027	-0.0310
0.3	0.0076	0.0868	-0.0025	-0.0265	0.0105	0.0903	-0.0029	-0.0373
0.4	0.0076	0.0868	-0.0033	-0.0351	0.0101	0.0876	-0.0035	-0.0425
0.5	0.0076	0.0868	-0.0040	-0.0435	0.0091	0.0836	-0.0046	-0.0465
0.6	0.0076	0.0868	-0.0047	-0.0517	0.0079	0.0782	-0.0058	-0.0491
0.7	0.0076	0.0868	-0.0054	-0.0596	0.0069	0.0717	-0.0062	-0.0502
0.8	0.0076	0.0868	-0.0060	-0.0672	0.0066	0.0646	-0.0049	-0.0496
0.9	0.0076	0.0868	-0.0066	-0.0745	0.0061	0.0570	-0.0032	-0.0478
1.0	0.0076	0.0868	-0.0071	-0.0817	0.0025	0.0490	-0.0071	-0.0461

S	GAMMA=4 TENSION N	GAMMA=4 TENSION T	GAMMA=4 BENDING N	GAMMA=4 BENDING T	GAMMA=8 TENSION N	GAMMA=8 TENSION T	GAMMA=8 BENDING N	GAMMA=8 BENDING T
-1.0	0.0151	0.1893	0.0073	0.1708	0.0117	0.2283	0.0091	0.2015
-0.9	0.0114	0.1469	0.0131	0.1220	0.0145	0.1666	0.0149	0.1347
-0.8	0.0063	0.1163	0.0065	0.0844	0.0039	0.1252	0.0069	0.0853
-0.7	0.0032	0.0975	0.0023	0.0572	-0.0032	0.1026	0.0025	0.0507
-0.6	0.0022	0.0883	0.0025	0.0375	-0.0036	0.0943	0.0034	0.0268
-0.5	0.0028	0.0860	0.0046	0.0225	0.0005	0.0946	0.0059	0.0095
-0.4	0.0042	0.0878	0.0056	0.0100	0.0058	0.0989	0.0064	-0.0041
-0.3	0.0058	0.0913	0.0044	-0.0012	0.0099	0.1035	0.0038	-0.0154
-0.2	0.0075	0.0949	0.0013	-0.0116	0.0123	0.1062	-0.0009	-0.0250
-0.1	0.0092	0.0974	-0.0022	-0.0210	0.0132	0.1060	-0.0056	-0.0327
0.0	0.0108	0.0981	-0.0046	-0.0290	0.0136	0.1026	-0.0081	-0.0379
0.1	0.0122	0.0969	-0.0052	-0.0352	0.0140	0.0966	-0.0077	-0.0405
0.2	0.0130	0.0935	-0.0043	-0.0393	0.0143	0.0883	-0.0052	-0.0406
0.3	0.0128	0.0881	-0.0031	-0.0415	0.0138	0.0786	-0.0026	-0.0388
0.4	0.0115	0.0809	-0.0029	-0.0422	0.0120	0.0678	-0.0017	-0.0358
0.5	0.0092	0.0723	-0.0043	-0.0416	0.0086	0.0567	-0.0034	-0.0324
0.6	0.0068	0.0628	-0.0064	-0.0399	0.0048	0.0460	-0.0063	-0.0289
0.7	0.0052	0.0531	-0.0068	-0.0372	0.0024	0.0363	-0.0068	-0.0251
0.8	0.0050	0.0440	-0.0036	-0.0333	0.0033	0.0282	-0.0023	-0.0209
0.9	0.0049	0.0355	0.0005	-0.0287	0.0049	0.0215	0.0032	-0.0164
1.0	-0.0010	0.0267	-0.0101	-0.0257	-0.0054	0.0138	-0.0129	-0.0144

ALPHA=5 DEGREES, BETA=20

GAMMA=1

S	TENSION N	TENSION T	BENDING N	BENDING T
-1.0	0.0076	0.0868	0.0056	0.0699
-0.9	0.0076	0.0868	0.0060	0.0651
-0.8	0.0076	0.0868	0.0057	0.0599
-0.7	0.0076	0.0868	0.0052	0.0544
-0.6	0.0076	0.0868	0.0049	0.0482
-0.5	0.0076	0.0868	0.0046	0.0415
-0.4	0.0076	0.0868	0.0042	0.0341
-0.3	0.0076	0.0868	0.0036	0.0262
-0.2	0.0076	0.0868	0.0026	0.0177
-0.1	0.0076	0.0868	0.0014	0.0089
0.0	0.0076	0.0868	0.0000	0.0000
0.1	0.0076	0.0868	-0.0014	-0.0089
0.2	0.0076	0.0868	-0.0026	-0.0177
0.3	0.0076	0.0868	-0.0036	-0.0262
0.4	0.0076	0.0868	-0.0042	-0.0341
0.5	0.0076	0.0868	-0.0046	-0.0415
0.6	0.0076	0.0868	-0.0049	-0.0482
0.7	0.0076	0.0868	-0.0052	-0.0544
0.8	0.0076	0.0868	-0.0057	-0.0599
0.9	0.0076	0.0868	-0.0061	-0.0651
1.0	0.0076	0.0868	-0.0056	-0.0699

GAMMA=2

S	TENSION N	TENSION T	BENDING N	BENDING T
-1.0	0.0113	0.1158	0.0063	0.0889
-0.9	0.0087	0.1086	0.0077	0.0777
-0.8	0.0081	0.1023	0.0065	0.0669
-0.7	0.0074	0.0971	0.0056	0.0565
-0.6	0.0064	0.0932	0.0053	0.0462
-0.5	0.0054	0.0905	0.0051	0.0360
-0.4	0.0050	0.0890	0.0046	0.0258
-0.3	0.0053	0.0884	0.0035	0.0157
-0.2	0.0063	0.0883	0.0018	0.0058
-0.1	0.0077	0.0885	-0.0002	-0.0036
0.0	0.0089	0.0887	-0.0020	-0.0123
0.1	0.0098	0.0884	-0.0034	-0.0201
0.2	0.0101	0.0876	-0.0042	-0.0268
0.3	0.0098	0.0862	-0.0045	-0.0324
0.4	0.0091	0.0840	-0.0046	-0.0369
0.5	0.0084	0.0812	-0.0046	-0.0404
0.6	0.0077	0.0778	-0.0047	-0.0430
0.7	0.0072	0.0739	-0.0048	-0.0446
0.8	0.0067	0.0697	-0.0045	-0.0455
0.9	0.0060	0.0652	-0.0040	-0.0457
1.0	0.0052	0.0607	-0.0045	-0.0455

GAMMA=4

S	TENSION N	TENSION T	BENDING N	BENDING T
-1.0	0.0120	0.1378	0.0083	0.0997
-0.9	0.0102	0.1249	0.0083	0.0838
-0.8	0.0080	0.1141	0.0076	0.0688
-0.7	0.0054	0.1057	0.0073	0.0546
-0.6	0.0033	0.0999	0.0071	0.0412
-0.5	0.0024	0.0962	0.0062	0.0284
-0.4	0.0032	0.0943	0.0045	0.0163
-0.3	0.0053	0.0935	0.0020	0.0051
-0.2	0.0079	0.0932	-0.0007	-0.0049
-0.1	0.0104	0.0927	-0.0030	-0.0136
0.0	0.0120	0.0916	-0.0046	-0.0207
0.1	0.0125	0.0896	-0.0052	-0.0263
0.2	0.0118	0.0866	-0.0051	-0.0303
0.3	0.0105	0.0826	-0.0046	-0.0330
0.4	0.0092	0.0778	-0.0042	-0.0345
0.5	0.0081	0.0724	-0.0041	-0.0351
0.6	0.0074	0.0667	-0.0043	-0.0349
0.7	0.0067	0.0608	-0.0042	-0.0342
0.8	0.0055	0.0549	-0.0033	-0.0330
0.9	0.0041	0.0490	-0.0022	-0.0313
1.0	0.0049	0.0431	-0.0043	-0.0294

GAMMA=8

S	TENSION N	TENSION T	BENDING N	BENDING T
-1.0	0.0099	0.1540	0.0106	0.1031
-0.9	0.0120	0.1374	0.0090	0.0841
-0.8	0.0064	0.1241	0.0103	0.0662
-0.7	0.0010	0.1145	0.0109	0.0494
-0.6	-0.0012	0.1081	0.0094	0.0337
-0.5	0.0003	0.1043	0.0062	0.0194
-0.4	0.0041	0.1020	0.0021	0.0067
-0.3	0.0086	0.1004	-0.0019	-0.0041
-0.2	0.0124	0.0986	-0.0048	-0.0129
-0.1	0.0145	0.0961	-0.0064	-0.0196
0.0	0.0149	0.0927	-0.0066	-0.0244
0.1	0.0138	0.0881	-0.0059	-0.0274
0.2	0.0119	0.0826	-0.0048	-0.0290
0.3	0.0099	0.0764	-0.0039	-0.0294
0.4	0.0084	0.0698	-0.0035	-0.0290
0.5	0.0075	0.0629	-0.0035	-0.0280
0.6	0.0069	0.0562	-0.0037	-0.0267
0.7	0.0059	0.0497	-0.0033	-0.0251
0.8	0.0043	0.0434	-0.0022	-0.0232
0.9	0.0028	0.0373	-0.0012	-0.0211
1.0	0.0046	0.0314	-0.0036	-0.0189

ALPHA=5 DEGREES, BETA=100

	GAMMA=1				GAMMA=2			
	TENSION		BENDING		TENSION		BENDING	
S	N	T	N	T	N	T	N	T
-1.0	0.0076	0.0868	0.0024	0.0456	0.0088	0.0996	0.0039	0.0466
-0.9	0.0076	0.0868	0.0047	0.0432	0.0084	0.0977	0.0045	0.0430
-0.8	0.0076	0.0868	0.0044	0.0405	0.0080	0.0958	0.0052	0.0392
-0.7	0.0076	0.0868	0.0043	0.0375	0.0075	0.0942	0.0067	0.0350
-0.6	0.0076	0.0868	0.0051	0.0340	0.0068	0.0927	0.0083	0.0302
-0.5	0.0076	0.0868	0.0063	0.0299	0.0063	0.0914	0.0090	0.0249
-0.4	0.0076	0.0868	0.0072	0.0250	0.0061	0.0903	0.0083	0.0191
-0.3	0.0076	0.0868	0.0071	0.0195	0.0063	0.0894	0.0062	0.0129
-0.2	0.0076	0.0868	0.0057	0.0134	0.0069	0.0886	0.0029	0.0065
-0.1	0.0076	0.0868	0.0032	0.0068	0.0076	0.0879	-0.0009	0.0002
0.0	0.0076	0.0868	0.0000	0.0000	0.0084	0.0872	-0.0043	-0.0057
0.1	0.0076	0.0868	-0.0032	-0.0068	0.0089	0.0864	-0.0067	-0.0111
0.2	0.0076	0.0868	-0.0057	-0.0134	0.0091	0.0855	-0.0078	-0.0157
0.3	0.0076	0.0868	-0.0071	-0.0195	0.0090	0.0845	-0.0076	-0.0197
0.4	0.0076	0.0868	-0.0072	-0.0250	0.0086	0.0833	-0.0064	-0.0229
0.5	0.0076	0.0868	-0.0063	-0.0299	0.0080	0.0819	-0.0049	-0.0254
0.6	0.0076	0.0868	-0.0051	-0.0340	0.0075	0.0805	-0.0037	-0.0274
0.7	0.0076	0.0868	-0.0043	-0.0375	0.0072	0.0790	-0.0031	-0.0289
0.8	0.0076	0.0868	-0.0044	-0.0405	0.0070	0.0774	-0.0032	-0.0302
0.9	0.0076	0.0868	-0.0047	-0.0432	0.0068	0.0758	-0.0033	-0.0311
1.0	0.0076	0.0868	-0.0024	-0.0456	0.0062	0.0742	-0.0019	-0.0319
	GAMMA=4				GAMMA=8			
-1.0	0.0090	0.1081	0.0052	0.0441	0.0098	0.1138	0.0030	0.0400
-0.9	0.0091	0.1050	0.0046	0.0400	0.0090	0.1100	0.0078	0.0355
-0.8	0.0079	0.1021	0.0078	0.0355	0.0066	0.1065	0.0131	0.0305
-0.7	0.0063	0.0995	0.0109	0.0305	0.0047	0.1035	0.0152	0.0250
-0.6	0.0052	0.0972	0.0119	0.0249	0.0040	0.1008	0.0134	0.0191
-0.5	0.0049	0.0953	0.0105	0.0190	0.0046	0.0984	0.0086	0.0132
-0.4	0.0054	0.0936	0.0069	0.0129	0.0061	0.0962	0.0024	0.0075
-0.3	0.0065	0.0920	0.0023	0.0069	0.0079	0.0942	-0.0034	0.0022
-0.2	0.0078	0.0906	-0.0023	0.0011	0.0095	0.0921	-0.0077	-0.0023
-0.1	0.0090	0.0891	-0.0060	-0.0040	0.0106	0.0900	-0.0099	-0.0061
0.0	0.0098	0.0876	-0.0081	-0.0085	0.0110	0.0877	-0.0100	-0.0091
0.1	0.0102	0.0860	-0.0086	-0.0122	0.0107	0.0853	-0.0086	-0.0112
0.2	0.0099	0.0841	-0.0078	-0.0150	0.0100	0.0827	-0.0064	-0.0128
0.3	0.0093	0.0821	-0.0063	-0.0172	0.0090	0.0800	-0.0043	-0.0138
0.4	0.0086	0.0800	-0.0046	-0.0188	0.0081	0.0773	-0.0028	-0.0144
0.5	0.0078	0.0778	-0.0033	-0.0200	0.0074	0.0745	-0.0021	-0.0148
0.6	0.0072	0.0754	-0.0026	-0.0208	0.0069	0.0717	-0.0019	-0.0151
0.7	0.0068	0.0731	-0.0024	-0.0213	0.0065	0.0689	-0.0019	-0.0152
0.8	0.0065	0.0707	-0.0022	-0.0217	0.0061	0.0662	-0.0014	-0.0152
0.9	0.0061	0.0683	-0.0019	-0.0219	0.0056	0.0634	-0.0009	-0.0151
1.0	0.0057	0.0659	-0.0023	-0.0220	0.0055	0.0607	-0.0024	-0.0149

ALPHA=10 DEGREES, BETA=4

GAMMA=1

S	TENSION N	TENSION T	BENDING N	BENDING T
-1.0	0.0301	0.1709	0.0252	0.1425
-0.9	0.0301	0.1710	0.0240	0.1323
-0.8	0.0301	0.1710	0.0228	0.1216
-0.7	0.0302	0.1710	0.0215	0.1099
-0.6	0.0302	0.1710	0.0200	0.0971
-0.5	0.0302	0.1710	0.0181	0.0831
-0.4	0.0302	0.1710	0.0156	0.0680
-0.3	0.0302	0.1710	0.0125	0.0519
-0.2	0.0302	0.1710	0.0087	0.0351
-0.1	0.0302	0.1710	0.0045	0.0177
0.0	0.0302	0.1710	-0.0000	-0.0000
0.1	0.0302	0.1710	-0.0045	-0.0177
0.2	0.0302	0.1710	-0.0087	-0.0351
0.3	0.0302	0.1710	-0.0125	-0.0519
0.4	0.0302	0.1710	-0.0156	-0.0680
0.5	0.0302	0.1710	-0.0181	-0.0831
0.6	0.0302	0.1710	-0.0200	-0.0971
0.7	0.0302	0.1710	-0.0215	-0.1099
0.8	0.0302	0.1710	-0.0228	-0.1216
0.9	0.0302	0.1710	-0.0240	-0.1323
1.0	0.0302	0.1710	-0.0252	-0.1425

GAMMA=2

S	TENSION N	TENSION T	BENDING N	BENDING T
-1.0	0.0399	0.2324	0.0335	0.1859
-0.9	0.0367	0.2158	0.0290	0.1608
-0.8	0.0320	0.2016	0.0258	0.1372
-0.7	0.0272	0.1904	0.0236	0.1146
-0.6	0.0235	0.1823	0.0216	0.0928
-0.5	0.0216	0.1771	0.0190	0.0715
-0.4	0.0218	0.1743	0.0154	0.0506
-0.3	0.0238	0.1734	0.0107	0.0303
-0.2	0.0270	0.1736	0.0054	0.0108
-0.1	0.0307	0.1743	-0.0003	-0.0077
0.0	0.0341	0.1748	-0.0058	-0.0249
0.1	0.0366	0.1746	-0.0105	-0.0404
0.2	0.0379	0.1733	-0.0142	-0.0541
0.3	0.0379	0.1707	-0.0168	-0.0657
0.4	0.0367	0.1665	-0.0183	-0.0751
0.5	0.0347	0.1609	-0.0190	-0.0824
0.6	0.0320	0.1539	-0.0192	-0.0876
0.7	0.0291	0.1456	-0.0190	-0.0909
0.8	0.0260	0.1364	-0.0184	-0.0924
0.9	0.0232	0.1266	-0.0174	-0.0924
1.0	0.0211	0.1167	-0.0157	-0.0912

GAMMA=4

S	TENSION N	TENSION T	BENDING N	BENDING T
-1.0	0.0446	0.2803	0.0400	0.2131
-0.9	0.0420	0.2499	0.0332	0.1763
-0.8	0.0302	0.2251	0.0308	0.1426
-0.7	0.0188	0.2067	0.0292	0.1115
-0.6	0.0123	0.1945	0.0261	0.0826
-0.5	0.0120	0.1875	0.0210	0.0558
-0.4	0.0167	0.1843	0.0140	0.0310
-0.3	0.0242	0.1835	0.0060	0.0086
-0.2	0.0325	0.1834	-0.0019	-0.0113
-0.1	0.0394	0.1829	-0.0088	-0.0285
0.0	0.0439	0.1812	-0.0140	-0.0428
0.1	0.0456	0.1776	-0.0173	-0.0541
0.2	0.0448	0.1719	-0.0189	-0.0625
0.3	0.0422	0.1642	-0.0191	-0.0681
0.4	0.0387	0.1547	-0.0185	-0.0713
0.5	0.0347	0.1438	-0.0176	-0.0725
0.6	0.0306	0.1319	-0.0167	-0.0719
0.7	0.0260	0.1192	-0.0155	-0.0699
0.8	0.0210	0.1061	-0.0138	-0.0668
0.9	0.0166	0.0930	-0.0117	-0.0627
1.0	0.0170	0.0807	-0.0105	-0.0578

GAMMA=8

S	TENSION N	TENSION T	BENDING N	BENDING T
-1.0	0.0520	0.3150	0.0402	0.2242
-0.9	0.0417	0.2759	0.0409	0.1796
-0.8	0.0206	0.2452	0.0415	0.1388
-0.7	0.0053	0.2238	0.0381	0.1015
-0.6	0.0012	0.2104	0.0302	0.0678
-0.5	0.0074	0.2030	0.0190	0.0379
-0.4	0.0198	0.1994	0.0068	0.0118
-0.3	0.0336	0.1972	-0.0045	-0.0102
-0.2	0.0452	0.1947	-0.0133	-0.0280
-0.1	0.0523	0.1906	-0.0190	-0.0418
0.0	0.0543	0.1842	-0.0217	-0.0516
0.1	0.0522	0.1754	-0.0218	-0.0579
0.2	0.0475	0.1645	-0.0203	-0.0611
0.3	0.0419	0.1519	-0.0183	-0.0619
0.4	0.0367	0.1384	-0.0164	-0.0609
0.5	0.0323	0.1243	-0.0149	-0.0585
0.6	0.0279	0.1102	-0.0135	-0.0552
0.7	0.0226	0.0962	-0.0120	-0.0512
0.8	0.0162	0.0824	-0.0097	-0.0468
0.9	0.0112	0.0692	-0.0075	-0.0418
1.0	0.0159	0.0572	-0.0079	-0.0364

ALPHA=10 DEGREES, BETA=20

	GAMMA=1				GAMMA=2			
	TENSION		BENDING		TENSION		BENDING	
S	N	T	N	T	N	T	N	T
-1.0	0.0301	0.1710	0.0181	0.0985	0.0345	0.1991	0.0203	0.1036
-0.9	0.0301	0.1710	0.0173	0.0933	0.0340	0.1945	0.0190	0.0955
-0.8	0.0301	0.1710	0.0183	0.0876	0.0315	0.1902	0.0236	0.0868
-0.7	0.0301	0.1710	0.0207	0.0810	0.0286	0.1863	0.0288	0.0771
-0.6	0.0301	0.1710	0.0233	0.0731	0.0263	0.1830	0.0316	0.0661
-0.5	0.0301	0.1710	0.0249	0.0640	0.0251	0.1803	0.0306	0.0540
-0.4	0.0301	0.1710	0.0245	0.0533	0.0251	0.1781	0.0257	0.0409
-0.3	0.0301	0.1710	0.0215	0.0414	0.0263	0.1763	0.0176	0.0273
-0.2	0.0301	0.1710	0.0160	0.0283	0.0282	0.1747	0.0076	0.0136
-0.1	0.0301	0.1710	0.0085	0.0143	0.0304	0.1733	-0.0027	0.0002
0.0	0.0301	0.1710	0.0000	-0.0001	0.0326	0.1718	-0.0121	-0.0125
0.1	0.0301	0.1710	-0.0085	-0.0143	0.0342	0.1703	-0.0193	-0.0241
0.2	0.0301	0.1710	-0.0160	-0.0283	0.0351	0.1685	-0.0237	-0.0343
0.3	0.0301	0.1710	-0.0215	-0.0414	0.0351	0.1664	-0.0253	-0.0431
0.4	0.0301	0.1710	-0.0245	-0.0533	0.0342	0.1639	-0.0243	-0.0503
0.5	0.0301	0.1710	-0.0249	-0.0640	0.0327	0.1611	-0.0216	-0.0560
0.6	0.0301	0.1710	-0.0233	-0.0731	0.0308	0.1579	-0.0182	-0.0604
0.7	0.0301	0.1710	-0.0207	-0.0810	0.0290	0.1545	-0.0151	-0.0636
0.8	0.0301	0.1710	-0.0183	-0.0876	0.0274	0.1509	-0.0132	-0.0660
0.9	0.0301	0.1710	-0.0173	-0.0933	0.0262	0.1471	-0.0126	-0.0678
1.0	0.0301	0.1710	-0.0181	-0.0985	0.0254	0.1433	-0.0123	-0.0692
	GAMMA=4				GAMMA=8			
-1.0	0.0388	0.2182	0.0163	0.1010	0.0436	0.2309	0.0125	0.0938
-0.9	0.0351	0.2107	0.0255	0.0910	0.0323	0.2219	0.0396	0.0826
-0.8	0.0293	0.2038	0.0351	0.0803	0.0237	0.2139	0.0512	0.0704
-0.7	0.0243	0.1979	0.0401	0.0684	0.0193	0.2069	0.0499	0.0572
-0.6	0.0216	0.1928	0.0387	0.0555	0.0189	0.2009	0.0396	0.0436
-0.5	0.0215	0.1887	0.0314	0.0420	0.0215	0.1957	0.0243	0.0300
-0.4	0.0235	0.1851	0.0201	0.0282	0.0261	0.1911	0.0076	0.0171
-0.3	0.0270	0.1819	0.0071	0.0148	0.0312	0.1867	-0.0078	0.0052
-0.2	0.0309	0.1790	-0.0055	0.0022	0.0360	0.1824	-0.0197	-0.0053
-0.1	0.0346	0.1761	-0.0160	-0.0092	0.0395	0.1779	-0.0273	-0.0140
0.0	0.0373	0.1729	-0.0232	-0.0191	0.0413	0.1732	-0.0304	-0.0210
0.1	0.0387	0.1695	-0.0268	-0.0274	0.0414	0.1681	-0.0297	-0.0263
0.2	0.0387	0.1657	-0.0271	-0.0340	0.0400	0.1626	-0.0263	-0.0301
0.3	0.0374	0.1615	-0.0248	-0.0391	0.0375	0.1568	-0.0213	-0.0325
0.4	0.0352	0.1569	-0.0209	-0.0428	0.0344	0.1508	-0.0162	-0.0340
0.5	0.0324	0.1520	-0.0167	-0.0453	0.0311	0.1446	-0.0118	-0.0347
0.6	0.0296	0.1468	-0.0130	-0.0469	0.0280	0.1382	-0.0087	-0.0349
0.7	0.0270	0.1414	-0.0104	-0.0478	0.0253	0.1319	-0.0069	-0.0347
0.8	0.0249	0.1359	-0.0092	-0.0482	0.0231	0.1255	-0.0061	-0.0343
0.9	0.0234	0.1304	-0.0088	-0.0483	0.0214	0.1193	-0.0060	-0.0338
1.0	0.0223	0.1249	-0.0087	-0.0481	0.0204	0.1131	-0.0066	-0.0331

ALPHA=10 DEGREES, BETA=100

	GAMMA=1				GAMMA=2			
	TENSION		BENDING		TENSION		BENDING	
S	N	T	N	T	N	T	N	T
-1.0	0.0301	0.1710	0.0077	0.0423	0.0320	0.1801	0.0034	0.0380
-0.9	0.0301	0.1710	0.0088	0.0406	0.0311	0.1791	0.0154	0.0358
-0.8	0.0301	0.1710	0.0153	0.0386	0.0302	0.1780	0.0264	0.0332
-0.7	0.0301	0.1710	0.0231	0.0360	0.0295	0.1770	0.0339	0.0300
-0.6	0.0301	0.1710	0.0295	0.0327	0.0290	0.1761	0.0366	0.0262
-0.5	0.0301	0.1710	0.0327	0.0287	0.0289	0.1752	0.0347	0.0218
-0.4	0.0301	0.1710	0.0322	0.0239	0.0289	0.1743	0.0287	0.0169
-0.3	0.0301	0.1710	0.0279	0.0185	0.0293	0.1735	0.0197	0.0119
-0.2	0.0301	0.1710	0.0206	0.0126	0.0297	0.1727	0.0091	0.0067
-0.1	0.0301	0.1710	0.0109	0.0064	0.0302	0.1719	-0.0021	0.0015
0.0	0.0301	0.1710	-0.0001	0.0000	0.0307	0.1711	-0.0125	-0.0035
0.1	0.0301	0.1710	-0.0109	-0.0064	0.0311	0.1703	-0.0213	-0.0082
0.2	0.0301	0.1710	-0.0206	-0.0126	0.0314	0.1694	-0.0275	-0.0125
0.3	0.0301	0.1710	-0.0279	-0.0185	0.0315	0.1686	-0.0307	-0.0163
0.4	0.0301	0.1710	-0.0322	-0.0239	0.0314	0.1677	-0.0308	-0.0196
0.5	0.0301	0.1710	-0.0327	-0.0287	0.0311	0.1668	-0.0278	-0.0224
0.6	0.0301	0.1710	-0.0295	-0.0327	0.0306	0.1659	-0.0224	-0.0245
0.7	0.0301	0.1710	-0.0231	-0.0360	0.0300	0.1649	-0.0156	-0.0261
0.8	0.0301	0.1710	-0.0153	-0.0386	0.0293	0.1639	-0.0089	-0.0272
0.9	0.0301	0.1710	-0.0088	-0.0406	0.0288	0.1629	-0.0047	-0.0280
1.0	0.0301	0.1710	-0.0077	-0.0423	0.0286	0.1619	-0.0061	-0.0288
	GAMMA=4				GAMMA=8			
-1.0	0.0329	0.1853	0.0061	0.0331	0.0322	0.1883	0.0234	0.0281
-0.9	0.0308	0.1837	0.0276	0.0305	0.0297	0.1864	0.0430	0.0255
-0.8	0.0294	0.1821	0.0388	0.0275	0.0284	0.1845	0.0483	0.0222
-0.7	0.0286	0.1806	0.0418	0.0239	0.0280	0.1827	0.0442	0.0187
-0.6	0.0283	0.1792	0.0384	0.0200	0.0282	0.1810	0.0346	0.0149
-0.5	0.0285	0.1778	0.0305	0.0157	0.0288	0.1793	0.0222	0.0111
-0.4	0.0289	0.1764	0.0199	0.0114	0.0296	0.1777	0.0090	0.0074
-0.3	0.0296	0.1751	0.0082	0.0070	0.0305	0.1760	-0.0034	0.0038
-0.2	0.0304	0.1738	-0.0034	0.0028	0.0313	0.1744	-0.0140	0.0005
-0.1	0.0311	0.1724	-0.0136	-0.0012	0.0319	0.1728	-0.0221	-0.0025
0.0	0.0317	0.1711	-0.0219	-0.0049	0.0324	0.1711	-0.0275	-0.0051
0.1	0.0321	0.1698	-0.0274	-0.0082	0.0326	0.1695	-0.0301	-0.0074
0.2	0.0322	0.1684	-0.0301	-0.0110	0.0326	0.1678	-0.0298	-0.0093
0.3	0.0321	0.1671	-0.0299	-0.0134	0.0323	0.1661	-0.0272	-0.0107
0.4	0.0318	0.1656	-0.0271	-0.0153	0.0317	0.1644	-0.0228	-0.0117
0.5	0.0311	0.1642	-0.0222	-0.0168	0.0309	0.1626	-0.0171	-0.0125
0.6	0.0304	0.1627	-0.0161	-0.0179	0.0300	0.1609	-0.0111	-0.0129
0.7	0.0295	0.1612	-0.0098	-0.0185	0.0290	0.1591	-0.0057	-0.0131
0.8	0.0286	0.1597	-0.0047	-0.0189	0.0281	0.1573	-0.0020	-0.0131
0.9	0.0279	0.1582	-0.0023	-0.0192	0.0275	0.1555	-0.0010	-0.0132
1.0	0.0277	0.1567	-0.0048	-0.0195	0.0273	0.1538	-0.0038	-0.0132

ALPHA=20 DEGREES, BETA=4

GAMMA=1

S	TENSION N	TENSION T	BENDING N	BENDING T
-1.0	0.1170	0.3214	0.0752	0.2032
-0.9	0.1170	0.3214	0.0766	0.1937
-0.8	0.1170	0.3214	0.0833	0.1819
-0.7	0.1170	0.3214	0.0888	0.1673
-0.6	0.1170	0.3214	0.0899	0.1496
-0.5	0.1170	0.3214	0.0854	0.1292
-0.4	0.1170	0.3214	0.0754	0.1063
-0.3	0.1170	0.3214	0.0607	0.0814
-0.2	0.1170	0.3214	0.0424	0.0551
-0.1	0.1170	0.3214	0.0218	0.0278
0.0	0.1170	0.3214	-0.0000	-0.0000
0.1	0.1170	0.3214	-0.0218	-0.0278
0.2	0.1170	0.3214	-0.0424	-0.0551
0.3	0.1170	0.3214	-0.0607	-0.0814
0.4	0.1170	0.3214	-0.0754	-0.1063
0.5	0.1170	0.3214	-0.0854	-0.1292
0.6	0.1170	0.3214	-0.0899	-0.1496
0.7	0.1170	0.3214	-0.0888	-0.1673
0.8	0.1170	0.3214	-0.0832	-0.1819
0.9	0.1170	0.3214	-0.0766	-0.1937
1.0	0.1170	0.3214	-0.0752	-0.2032

GAMMA=2

TENSION N	TENSION T	BENDING N	BENDING T
0.1387	0.3763	0.0760	0.2205
0.1275	0.3659	0.0945	0.2033
0.1170	0.3569	0.1075	0.1836
0.1092	0.3494	0.1113	0.1613
0.1047	0.3432	0.1054	0.1366
0.1035	0.3383	0.0911	0.1101
0.1050	0.3343	0.0704	0.0826
0.1084	0.3310	0.0458	0.0548
0.1129	0.3282	0.0197	0.0273
0.1179	0.3255	-0.0059	0.0007
0.1225	0.3228	-0.0293	-0.0245
0.1264	0.3199	-0.0494	-0.0478
0.1292	0.3167	-0.0652	-0.0690
0.1303	0.3130	-0.0762	-0.0878
0.1298	0.3087	-0.0821	-0.1039
0.1272	0.3037	-0.0829	-0.1172
0.1227	0.2979	-0.0790	-0.1277
0.1164	0.2912	-0.0714	-0.1354
0.1090	0.2838	-0.0622	-0.1405
0.1021	0.2757	-0.0547	-0.1433
0.0981	0.2671	-0.0549	-0.1445

GAMMA=4

S	TENSION N	TENSION T	BENDING N	BENDING T
-1.0	0.1544	0.4136	0.0815	0.2207
-0.9	0.1260	0.3971	0.1250	0.1983
-0.8	0.1071	0.3832	0.1403	0.1727
-0.7	0.0971	0.3717	0.1345	0.1451
-0.6	0.0943	0.3622	0.1143	0.1164
-0.5	0.0969	0.3542	0.0853	0.0873
-0.4	0.1031	0.3475	0.0524	0.0589
-0.3	0.1112	0.3415	0.0194	0.0316
-0.2	0.1197	0.3359	-0.0110	0.0061
-0.1	0.1276	0.3303	-0.0370	-0.0172
0.0	0.1339	0.3246	-0.0574	-0.0379
0.1	0.1381	0.3184	-0.0718	-0.0558
0.2	0.1399	0.3116	-0.0802	-0.0709
0.3	0.1392	0.3042	-0.0829	-0.0830
0.4	0.1357	0.2959	-0.0807	-0.0922
0.5	0.1297	0.2869	-0.0744	-0.0989
0.6	0.1212	0.2770	-0.0651	-0.1030
0.7	0.1109	0.2663	-0.0544	-0.1051
0.8	0.1000	0.2548	-0.0445	-0.1054
0.9	0.0904	0.2429	-0.0383	-0.1043
1.0	0.0858	0.2306	-0.0402	-0.1022

GAMMA=8

TENSION N	TENSION T	BENDING N	BENDING T
0.1523	0.4395	0.1228	0.2086
0.1136	0.4198	0.1692	0.1830
0.0939	0.4034	0.1714	0.1542
0.0878	0.3896	0.1470	0.1243
0.0909	0.3780	0.1087	0.0945
0.0993	0.3678	0.0656	0.0658
0.1102	0.3587	0.0238	0.0389
0.1214	0.3502	-0.0130	0.0143
0.1315	0.3419	-0.0428	-0.0076
0.1394	0.3336	-0.0648	-0.0266
0.1446	0.3249	-0.0790	-0.0427
0.1469	0.3158	-0.0860	-0.0556
0.1463	0.3060	-0.0867	-0.0656
0.1427	0.2956	-0.0823	-0.0727
0.1364	0.2845	-0.0739	-0.0773
0.1276	0.2728	-0.0629	-0.0797
0.1168	0.2604	-0.0509	-0.0803
0.1046	0.2475	-0.0396	-0.0796
0.0924	0.2342	-0.0308	-0.0778
0.0823	0.2206	-0.0266	-0.0754
0.0777	0.2069	-0.0293	-0.0722

ALPHA=20 DEGREES, BETA=20

S	GAMMA=1 TENSION N	GAMMA=1 TENSION T	GAMMA=1 BENDING N	GAMMA=1 BENDING T	GAMMA=2 TENSION N	GAMMA=2 TENSION T	GAMMA=2 BENDING N	GAMMA=2 BENDING T
-1.0	0.1169	0.3214	0.0295	0.1002	0.1234	0.3404	0.0456	0.0918
-0.9	0.1169	0.3214	0.0594	0.0964	0.1192	0.3380	0.0891	0.0865
-0.8	0.1169	0.3213	0.0830	0.0910	0.1163	0.3359	0.1119	0.0792
-0.7	0.1169	0.3213	0.0981	0.0838	0.1146	0.3338	0.1184	0.0705
-0.6	0.1169	0.3213	0.1040	0.0750	0.1138	0.3319	0.1125	0.0606
-0.5	0.1169	0.3213	0.1010	0.0647	0.1138	0.3300	0.0974	0.0499
-0.4	0.1169	0.3213	0.0903	0.0531	0.1143	0.3282	0.0761	0.0387
-0.3	0.1169	0.3213	0.0733	0.0406	0.1151	0.3265	0.0510	0.0273
-0.2	0.1169	0.3213	0.0515	0.0274	0.1161	0.3248	0.0241	0.0159
-0.1	0.1169	0.3213	0.0265	0.0138	0.1173	0.3231	-0.0030	0.0045
0.0	0.1169	0.3213	-0.0002	-0.0001	0.1184	0.3215	-0.0286	-0.0066
0.1	0.1169	0.3213	-0.0265	-0.0138	0.1194	0.3198	-0.0516	-0.0172
0.2	0.1169	0.3213	-0.0515	-0.0274	0.1201	0.3181	-0.0708	-0.0272
0.3	0.1169	0.3213	-0.0733	-0.0406	0.1205	0.3164	-0.0850	-0.0365
0.4	0.1169	0.3213	-0.0903	-0.0531	0.1205	0.3146	-0.0935	-0.0450
0.5	0.1169	0.3213	-0.1010	-0.0647	0.1200	0.3128	-0.0955	-0.0524
0.6	0.1169	0.3213	-0.1040	-0.0750	0.1190	0.3109	-0.0904	-0.0586
0.7	0.1169	0.3213	-0.0981	-0.0838	0.1173	0.3089	-0.0786	-0.0635
0.8	0.1169	0.3213	-0.0830	-0.0910	0.1151	0.3068	-0.0608	-0.0671
0.9	0.1169	0.3213	-0.0594	-0.0964	0.1124	0.3046	-0.0393	-0.0694
1.0	0.1169	0.3213	-0.0295	-0.1002	0.1095	0.3024	-0.0182	-0.0708

S	GAMMA=4 N	GAMMA=4 T	GAMMA=4 BENDING N	GAMMA=4 BENDING T	GAMMA=8 N	GAMMA=8 T	GAMMA=8 BENDING N	GAMMA=8 BENDING T
-1.0	0.1228	0.3516	0.0935	0.0800	0.1176	0.3582	0.1580	0.0682
-0.9	0.1172	0.3480	0.1273	0.0741	0.1136	0.3539	0.1652	0.0623
-0.8	0.1140	0.3446	0.1362	0.0663	0.1119	0.3499	0.1529	0.0548
-0.7	0.1127	0.3415	0.1280	0.0573	0.1119	0.3461	0.1288	0.0465
-0.6	0.1126	0.3384	0.1089	0.0477	0.1129	0.3424	0.0983	0.0378
-0.5	0.1133	0.3355	0.0833	0.0378	0.1145	0.3388	0.0654	0.0291
-0.4	0.1147	0.3326	0.0546	0.0279	0.1164	0.3352	0.0327	0.0206
-0.3	0.1162	0.3298	0.0253	0.0181	0.1184	0.3317	0.0022	0.0124
-0.2	0.1179	0.3270	-0.0029	0.0086	0.1202	0.3283	-0.0250	0.0046
-0.1	0.1195	0.3242	-0.0297	-0.0005	0.1217	0.3248	-0.0480	-0.0028
0.0	0.1209	0.3215	-0.0509	-0.0091	0.1229	0.3214	-0.0662	-0.0096
0.1	0.1219	0.3187	-0.0688	-0.0171	0.1237	0.3180	-0.0793	-0.0157
0.2	0.1225	0.3159	-0.0817	-0.0244	0.1239	0.3145	-0.0871	-0.0212
0.3	0.1226	0.3131	-0.0892	-0.0310	0.1235	0.3110	-0.0894	-0.0259
0.4	0.1220	0.3102	-0.0909	-0.0367	0.1224	0.3075	-0.0863	-0.0299
0.5	0.1208	0.3073	-0.0867	-0.0414	0.1206	0.3040	-0.0781	-0.0329
0.6	0.1188	0.3043	-0.0768	-0.0451	0.1180	0.3003	-0.0654	-0.0351
0.7	0.1161	0.3011	-0.0620	-0.0477	0.1148	0.2966	-0.0494	-0.0364
0.8	0.1128	0.2979	-0.0439	-0.0493	0.1111	0.2928	-0.0321	-0.0370
0.9	0.1091	0.2946	-0.0255	-0.0500	0.1070	0.2889	-0.0164	-0.0369
1.0	0.1053	0.2913	-0.0112	-0.0503	0.1031	0.2850	-0.0069	-0.0366

ALPHA=20 DEGREES, BETA=100

GAMMA=1

S	TENSION N	TENSION T	BENDING N	BENDING T
-1.0	0.1169	0.3214	0.0470	0.0324
-0.9	0.1169	0.3214	0.0758	0.0310
-0.8	0.1169	0.3214	0.0912	0.0286
-0.7	0.1169	0.3214	0.0963	0.0258
-0.6	0.1169	0.3214	0.0938	0.0225
-0.5	0.1169	0.3213	0.0854	0.0190
-0.4	0.1169	0.3213	0.0728	0.0154
-0.3	0.1169	0.3213	0.0570	0.0116
-0.2	0.1169	0.3213	0.0391	0.0078
-0.1	0.1169	0.3213	0.0199	0.0039
0.0	0.1169	0.3213	-0.0002	0.0000
0.1	0.1169	0.3213	-0.0199	-0.0039
0.2	0.1169	0.3213	-0.0391	-0.0078
0.3	0.1169	0.3213	-0.0570	-0.0116
0.4	0.1169	0.3213	-0.0728	-0.0154
0.5	0.1169	0.3213	-0.0854	-0.0190
0.6	0.1169	0.3213	-0.0938	-0.0225
0.7	0.1169	0.3213	-0.0963	-0.0258
0.8	0.1169	0.3213	-0.0912	-0.0286
0.9	0.1169	0.3213	-0.0758	-0.0310
1.0	0.1169	0.3214	-0.0470	-0.0324

GAMMA=2

TENSION N	TENSION T	BENDING* N	BENDING* T
0.1175	0.3261	0.0898	0.0260
0.1171	0.3256	0.1044	0.0245
0.1168	0.3251	0.1072	0.0224
0.1167	0.3247	0.1019	0.0198
0.1167	0.3242	0.0909	0.0170
0.1167	0.3237	0.0761	0.0141
0.1167	0.3233	0.0589	0.0112
0.1168	0.3228	0.0404	0.0082
0.1169	0.3223	0.0212	0.0052
0.1171	0.3219	0.0021	0.0023
0.1172	0.3214	-0.0164	-0.0007
0.1173	0.3209	-0.0339	-0.0036
0.1173	0.3205	-0.0498	-0.0064
0.1174	0.3200	-0.0637	-0.0092
0.1174	0.3195	-0.0749	-0.0119
0.1174	0.3191	-0.0828	-0.0145
0.1173	0.3186	-0.0865	-0.0169
0.1171	0.3181	-0.0850	-0.0191
0.1168	0.3177	-0.0768	-0.0210
0.1164	0.3172	-0.0604	-0.0225
0.1157	0.3167	-0.0333	-0.0234

GAMMA=4

TENSION N	TENSION T	BENDING* N	BENDING* T
0.1171	0.3286	0.1283	0.0209
0.1167	0.3279	0.1268	0.0196
0.1166	0.3271	0.1177	0.0177
0.1166	0.3264	0.1036	0.0156
0.1166	0.3257	0.0863	0.0133
0.1167	0.3250	0.0673	0.0110
0.1169	0.3242	0.0475	0.0086
0.1170	0.3235	0.0276	0.0062
0.1172	0.3228	0.0083	0.0039
0.1173	0.3221	-0.0102	0.0015
0.1174	0.3214	-0.0273	-0.0008
0.1176	0.3207	-0.0427	-0.0030
0.1176	0.3200	-0.0561	-0.0053
0.1176	0.3193	-0.0672	-0.0074
0.1176	0.3185	-0.0753	-0.0095
0.1175	0.3178	-0.0801	-0.0114
0.1173	0.3171	-0.0810	-0.0132
0.1170	0.3164	-0.0770	-0.0149
0.1165	0.3157	-0.0673	-0.0163
0.1159	0.3150	-0.0504	-0.0173
0.1150	0.3142	-0.0249	-0.0178

GAMMA=8

TENSION N	TENSION T	BENDING* N	BENDING* T
0.1165	0.3299	0.1552	0.0176
0.1164	0.3290	0.1416	0.0164
0.1164	0.3282	0.1239	0.0148
0.1165	0.3273	0.1039	0.0130
0.1166	0.3264	0.0826	0.0112
0.1168	0.3256	0.0611	0.0092
0.1170	0.3247	0.0399	0.0072
0.1172	0.3239	0.0194	0.0052
0.1174	0.3230	0.0001	0.0032
0.1175	0.3222	-0.0177	0.0012
0.1177	0.3214	-0.0338	-0.0007
0.1177	0.3205	-0.0478	-0.0026
0.1178	0.3197	-0.0596	-0.0045
0.1178	0.3189	-0.0689	-0.0063
0.1177	0.3180	-0.0752	-0.0079
0.1175	0.3172	-0.0782	-0.0096
0.1173	0.3164	-0.0774	-0.0111
0.1169	0.3155	-0.0721	-0.0124
0.1163	0.3147	-0.0615	-0.0135
0.1156	0.3138	-0.0446	-0.0143
0.1146	0.3130	-0.0202	-0.0147

ALPHA=30 DEGREES, BETA=4

	GAMMA=1				GAMMA=2			
	TENSION		BENDING		TENSION		BENDING	
S	N	T	N	T	N	T	N	T
-1.0	0.2501	0.4330	0.1227	0.2165	0.2690	0.4723	0.1612	0.2125
-0.9	0.2500	0.4330	0.1668	0.2080	0.2558	0.4664	0.2179	0.1992
-0.8	0.2500	0.4330	0.1928	0.1950	0.2475	0.4612	0.2383	0.1810
-0.7	0.2500	0.4330	0.2018	0.1780	0.2430	0.4567	0.2324	0.1594
-0.6	0.2500	0.4330	0.1960	0.1578	0.2413	0.4527	0.2085	0.1356
-0.5	0.2500	0.4330	0.1782	0.1350	0.2416	0.4491	0.1730	0.1105
-0.4	0.2500	0.4330	0.1515	0.1102	0.2432	0.4457	0.1307	0.0849
-0.3	0.2500	0.4330	0.1183	0.0838	0.2455	0.4425	0.0854	0.0591
-0.2	0.2500	0.4330	0.0809	0.0564	0.2482	0.4393	0.0397	0.0336
-0.1	0.2500	0.4330	0.0410	0.0284	0.2510	0.4363	-0.0047	0.0085
0.0	0.2500	0.4330	-0.0000	-0.0000	0.2537	0.4333	-0.0465	-0.0158
0.1	0.2500	0.4330	-0.0410	-0.0284	0.2560	0.4302	-0.0845	-0.0390
0.2	0.2500	0.4330	-0.0809	-0.0564	0.2579	0.4271	-0.1178	-0.0610
0.3	0.2500	0.4330	-0.1183	-0.0838	0.2592	0.4239	-0.1453	-0.0816
0.4	0.2500	0.4330	-0.1515	-0.1102	0.2595	0.4205	-0.1658	-0.1003
0.5	0.2500	0.4330	-0.1782	-0.1350	0.2586	0.4169	-0.1779	-0.1170
0.6	0.2500	0.4330	-0.1960	-0.1578	0.2562	0.4131	-0.1802	-0.1313
0.7	0.2500	0.4330	-0.2018	-0.1780	0.2519	0.4089	-0.1716	-0.1429
0.8	0.2500	0.4330	-0.1928	-0.1950	0.2456	0.4043	-0.1516	-0.1515
0.9	0.2499	0.4330	-0.1667	-0.2080	0.2371	0.3993	-0.1215	-0.1571
1.0	0.2499	0.4330	-0.1226	-0.2165	0.2267	0.3937	-0.0847	-0.1594
	GAMMA=4				GAMMA=8			
-1.0	0.2671	0.4980	0.2484	0.1947	0.2508	0.5149	0.3633	0.1718
-0.9	0.2499	0.4887	0.2834	0.1792	0.2390	0.5037	0.3499	0.1559
-0.8	0.2409	0.4807	0.2787	0.1590	0.2346	0.4939	0.3082	0.1364
-0.7	0.2374	0.4735	0.2486	0.1362	0.2351	0.4849	0.2509	0.1149
-0.6	0.2377	0.4670	0.2037	0.1123	0.2385	0.4766	0.1871	0.0928
-0.5	0.2403	0.4609	0.1517	0.0880	0.2435	0.4688	0.1229	0.0708
-0.4	0.2442	0.4551	0.0977	0.0640	0.2491	0.4614	0.0621	0.0494
-0.3	0.2486	0.4495	0.0452	0.0408	0.2546	0.4541	0.0070	0.0290
-0.2	0.2530	0.4441	-0.0037	0.0184	0.2595	0.4470	-0.0412	0.0098
-0.1	0.2571	0.4387	-0.0477	-0.0028	0.2637	0.4400	-0.0819	-0.0081
0.0	0.2606	0.4333	-0.0859	-0.0227	0.2669	0.4330	-0.1148	-0.0245
0.1	0.2633	0.4279	-0.1176	-0.0412	0.2690	0.4260	-0.1399	-0.0393
0.2	0.2651	0.4224	-0.1425	-0.0580	0.2698	0.4189	-0.1571	-0.0524
0.3	0.2656	0.4168	-0.1600	-0.0731	0.2690	0.4117	-0.1661	-0.0637
0.4	0.2646	0.4110	-0.1692	-0.0863	0.2665	0.4043	-0.1668	-0.0731
0.5	0.2617	0.4050	-0.1697	-0.0974	0.2619	0.3968	-0.1591	-0.0805
0.6	0.2567	0.3986	-0.1610	-0.1061	0.2549	0.3889	-0.1433	-0.0860
0.7	0.2491	0.3919	-0.1433	-0.1126	0.2454	0.3807	-0.1205	-0.0895
0.8	0.2390	0.3847	-0.1180	-0.1166	0.2332	0.3722	-0.0929	-0.0910
0.9	0.2264	0.3770	-0.0879	-0.1183	0.2188	0.3631	-0.0645	-0.0909
1.0	0.2119	0.3688	-0.0589	-0.1179	0.2031	0.3536	-0.0418	-0.0891

ALPHA=30 DEGREES, BETA=20

	GAMMA=1				GAMMA=2			
	TENSION		BENDING		TENSION		BENDING	
S	N	T	N	T	N	T	N	T
-1.0	0.2500	0.4330	0.1281	0.0882	0.2520	0.4448	0.2078	0.0727
-0.9	0.2500	0.4330	0.1750	0.0844	0.2504	0.4434	0.2282	0.0688
-0.8	0.2500	0.4330	0.1971	0.0781	0.2495	0.4422	0.2274	0.0628
-0.7	0.2500	0.4330	0.2007	0.0702	0.2490	0.4410	0.2119	0.0556
-0.6	0.2500	0.4330	0.1906	0.0613	0.2489	0.4398	0.1865	0.0477
-0.5	0.2500	0.4330	0.1706	0.0517	0.2490	0.4387	0.1546	0.0395
-0.4	0.2500	0.4330	0.1433	0.0417	0.2492	0.4375	0.1189	0.0312
-0.3	0.2500	0.4330	0.1112	0.0315	0.2495	0.4364	0.0812	0.0228
-0.2	0.2500	0.4330	0.0758	0.0210	0.2499	0.4352	0.0430	0.0144
-0.1	0.2500	0.4330	0.0383	0.0105	0.2503	0.4341	0.0051	0.0062
0.0	0.2500	0.4330	-0.0003	-0.0001	0.2507	0.4330	-0.0316	-0.0020
0.1	0.2500	0.4330	-0.0383	-0.0105	0.2510	0.4319	-0.0662	-0.0101
0.2	0.2500	0.4330	-0.0758	-0.0210	0.2513	0.4307	-0.0982	-0.0180
0.3	0.2500	0.4330	-0.1112	-0.0315	0.2514	0.4296	-0.1267	-0.0257
0.4	0.2500	0.4330	-0.1433	-0.0417	0.2515	0.4285	-0.1506	-0.0332
0.5	0.2500	0.4330	-0.1706	-0.0517	0.2514	0.4273	-0.1686	-0.0405
0.6	0.2500	0.4330	-0.1906	-0.0613	0.2510	0.4262	-0.1792	-0.0473
0.7	0.2500	0.4330	-0.2007	-0.0702	0.2504	0.4251	-0.1801	-0.0535
0.8	0.2500	0.4330	-0.1971	-0.0781	0.2493	0.4239	-0.1687	-0.0590
0.9	0.2500	0.4330	-0.1749	-0.0844	0.2477	0.4227	-0.1415	-0.0631
1.0	0.2500	0.4330	-0.1281	-0.0882	0.2455	0.4214	-0.0942	-0.0653
	GAMMA=4				GAMMA=8			
-1.0	0.2502	0.4513	0.2813	0.0595	0.2480	0.4549	0.3335	0.0505
-0.9	0.2491	0.4493	0.2714	0.0559	0.2477	0.4525	0.3005	0.0472
-0.8	0.2485	0.4474	0.2481	0.0507	0.2478	0.4502	0.2606	0.0428
-0.7	0.2484	0.4455	0.2160	0.0447	0.2482	0.4479	0.2171	0.0378
-0.6	0.2487	0.4436	0.1787	0.0382	0.2488	0.4457	0.1720	0.0323
-0.5	0.2491	0.4418	0.1386	0.0314	0.2494	0.4435	0.1270	0.0266
-0.4	0.2496	0.4400	0.0978	0.0246	0.2501	0.4414	0.0832	0.0208
-0.3	0.2501	0.4382	0.0573	0.0177	0.2508	0.4392	0.0414	0.0150
-0.2	0.2507	0.4365	0.0182	0.0109	0.2514	0.4371	0.0023	0.0092
-0.1	0.2512	0.4347	-0.0188	0.0042	0.2520	0.4350	-0.0338	0.0034
0.0	0.2517	0.4329	-0.0533	-0.0023	0.2524	0.4328	-0.0665	-0.0022
0.1	0.2520	0.4311	-0.0845	-0.0088	0.2528	0.4307	-0.0953	-0.0076
0.2	0.2523	0.4294	-0.1120	-0.0150	0.2529	0.4287	-0.1199	-0.0129
0.3	0.2524	0.4276	-0.1352	-0.0211	0.2529	0.4266	-0.1397	-0.0180
0.4	0.2523	0.4259	-0.1533	-0.0269	0.2526	0.4245	-0.1541	-0.0229
0.5	0.2519	0.4241	-0.1651	-0.0324	0.2521	0.4224	-0.1623	-0.0275
0.6	0.2512	0.4224	-0.1696	-0.0377	0.2511	0.4203	-0.1631	-0.0318
0.7	0.2501	0.4206	-0.1649	-0.0424	0.2497	0.4183	-0.1553	-0.0357
0.8	0.2484	0.4189	-0.1491	-0.0465	0.2476	0.4162	-0.1371	-0.0390
0.9	0.2459	0.4170	-0.1196	-0.0495	0.2448	0.4140	-0.1065	-0.0414
1.0	0.2426	0.4151	-0.0731	-0.0508	0.2409	0.4118	-0.0608	-0.0424

ALPHA=30 DEGREES, BETA=100

	GAMMA=1				GAMMA=2			
	TENSION		BENDING		TENSION		BENDING	
S	N	T	N	T	N	T	N	T
-1.0	0.2500	0.4330	0.2059	0.0234	0.2501	0.4357	0.2444	0.0175
-0.9	0.2500	0.4330	0.2076	0.0223	0.2500	0.4354	0.2303	0.0166
-0.8	0.2500	0.4330	0.1995	0.0204	0.2500	0.4351	0.2106	0.0152
-0.7	0.2500	0.4330	0.1844	0.0181	0.2499	0.4349	0.1870	0.0135
-0.6	0.2500	0.4330	0.1643	0.0155	0.2499	0.4346	0.1609	0.0117
-0.5	0.2500	0.4330	0.1408	0.0129	0.2499	0.4343	0.1332	0.0098
-0.4	0.2500	0.4330	0.1148	0.0103	0.2500	0.4341	0.1045	0.0079
-0.3	0.2500	0.4330	0.0873	0.0077	0.2500	0.4338	0.0754	0.0060
-0.2	0.2500	0.4330	0.0587	0.0051	0.2500	0.4335	0.0461	0.0040
-0.1	0.2500	0.4330	0.0295	0.0025	0.2500	0.4333	0.0170	0.0021
0.0	0.2500	0.4330	-0.0003	0.0000	0.2501	0.4330	-0.0118	0.0002
0.1	0.2500	0.4330	-0.0295	-0.0025	0.2501	0.4327	-0.0399	-0.0018
0.2	0.2500	0.4330	-0.0587	-0.0051	0.2501	0.4325	-0.0671	-0.0037
0.3	0.2500	0.4330	-0.0873	-0.0077	0.2501	0.4322	-0.0933	-0.0057
0.4	0.2500	0.4330	-0.1148	-0.0103	0.2501	0.4319	-0.1180	-0.0077
0.5	0.2500	0.4330	-0.1408	-0.0129	0.2501	0.4317	-0.1407	-0.0097
0.6	0.2500	0.4330	-0.1643	-0.0155	0.2501	0.4314	-0.1608	-0.0117
0.7	0.2500	0.4330	-0.1844	-0.0181	0.2500	0.4312	-0.1773	-0.0138
0.8	0.2500	0.4330	-0.1995	-0.0204	0.2500	0.4309	-0.1888	-0.0156
0.9	0.2500	0.4330	-0.2076	-0.0223	0.2498	0.4306	-0.1934	-0.0171
	GAMMA=4				GAMMA=8			
1.0	0.2500	0.4330	-0.2059	-0.0234	0.2497	0.4304	-0.1888	-0.0180
-1.0	0.2499	0.4371	0.2673	0.0140	0.2498	0.4378	0.2799	0.0121
-0.9	0.2499	0.4367	0.2434	0.0133	0.2498	0.4373	0.2505	0.0115
-0.8	0.2499	0.4362	0.2167	0.0122	0.2498	0.4368	0.2200	0.0106
-0.7	0.2499	0.4358	0.1882	0.0110	0.2499	0.4363	0.1888	0.0096
-0.6	0.2499	0.4354	0.1587	0.0096	0.2499	0.4358	0.1574	0.0084
-0.5	0.2500	0.4350	0.1286	0.0081	0.2500	0.4354	0.1261	0.0072
-0.4	0.2500	0.4346	0.0984	0.0066	0.2500	0.4349	0.0951	0.0059
-0.3	0.2500	0.4342	0.0684	0.0050	0.2501	0.4344	0.0647	0.0046
-0.2	0.2501	0.4338	0.0388	0.0035	0.2501	0.4339	0.0350	0.0032
-0.1	0.2501	0.4334	0.0099	0.0019	0.2501	0.4335	0.0061	0.0018
0.0	0.2501	0.4330	-0.0183	0.0003	0.2502	0.4330	-0.0218	0.0004
0.1	0.2501	0.4326	-0.0456	-0.0013	0.2502	0.4325	-0.0486	-0.0010
0.2	0.2502	0.4322	-0.0717	-0.0029	0.2502	0.4321	-0.0741	-0.0024
0.3	0.2502	0.4318	-0.0965	-0.0045	0.2502	0.4316	-0.0981	-0.0039
0.4	0.2502	0.4314	-0.1196	-0.0062	0.2502	0.4311	-0.1203	-0.0054
0.5	0.2501	0.4310	-0.1405	-0.0079	0.2502	0.4307	-0.1403	-0.0069
0.6	0.2501	0.4306	-0.1587	-0.0096	0.2501	0.4302	-0.1575	-0.0085
0.7	0.2500	0.4302	-0.1732	-0.0114	0.2500	0.4297	-0.1710	-0.0101
0.8	0.2499	0.4298	-0.1827	-0.0130	0.2498	0.4293	-0.1795	-0.0116
0.9	0.2497	0.4294	-0.1856	-0.0143	0.2496	0.4288	-0.1815	-0.0128
1.0	0.2494	0.4290	-0.1794	-0.0150	0.2493	0.4283	-0.1744	-0.0134

ALPHA=40 DEGREES, BETA=4

	GAMMA=1				GAMMA=2			
	TENSION		BENDING		TENSION		BENDING	
S	N	T	N	T	N	T	N	T
-1.0	0.4132	0.4924	0.2509	0.2036	0.4207	0.5168	0.3589	0.1823
-0.9	0.4132	0.4924	0.3089	0.1950	0.4147	0.5136	0.3869	0.1719
-0.8	0.4132	0.4924	0.3303	0.1808	0.4114	0.5107	0.3791	0.1567
-0.7	0.4132	0.4924	0.3250	0.1630	0.4098	0.5081	0.3473	0.1384
-0.6	0.4132	0.4924	0.3007	0.1426	0.4094	0.5057	0.3006	0.1184
-0.5	0.4132	0.4924	0.2635	0.1206	0.4098	0.5033	0.2452	0.0975
-0.4	0.4132	0.4924	0.2177	0.0975	0.4106	0.5011	0.1854	0.0762
-0.3	0.4132	0.4924	0.1667	0.0736	0.4116	0.4989	0.1243	0.0549
-0.2	0.4132	0.4924	0.1125	0.0493	0.4128	0.4967	0.0637	0.0337
-0.1	0.4132	0.4924	0.0566	0.0247	0.4140	0.4945	0.0049	0.0129
0.0	0.4132	0.4924	-0.0001	-0.0000	0.4151	0.4923	-0.0515	-0.0076
0.1	0.4132	0.4924	-0.0566	-0.0247	0.4161	0.4902	-0.1047	-0.0276
0.2	0.4132	0.4924	-0.1125	-0.0493	0.4169	0.4880	-0.1540	-0.0470
0.3	0.4132	0.4924	-0.1667	-0.0736	0.4175	0.4858	-0.1986	-0.0658
0.4	0.4132	0.4924	-0.2177	-0.0975	0.4178	0.4837	-0.2371	-0.0837
0.5	0.4132	0.4924	-0.2635	-0.1206	0.4176	0.4814	-0.2675	-0.1007
0.6	0.4132	0.4924	-0.3007	-0.1426	0.4166	0.4791	-0.2874	-0.1165
0.7	0.4132	0.4924	-0.3250	-0.1630	0.4147	0.4768	-0.2934	-0.1306
0.8	0.4132	0.4924	-0.3303	-0.1808	0.4113	0.4742	-0.2816	-0.1425
0.9	0.4132	0.4924	-0.3089	-0.1950	0.4061	0.4715	-0.2469	-0.1513
1.0	0.4132	0.4924	-0.2509	-0.2035	0.3984	0.4684	-0.1835	-0.1558
	GAMMA=4				GAMMA=8			
-1.0	0.4155	0.5322	0.4823	0.1564	0.4070	0.5415	0.5850	0.1349
-0.9	0.4105	0.5271	0.4615	0.1462	0.4053	0.5354	0.5186	0.1255
-0.8	0.4082	0.5225	0.4165	0.1321	0.4055	0.5297	0.4413	0.1130
-0.7	0.4078	0.5183	0.3569	0.1156	0.4069	0.5244	0.3595	0.0988
-0.6	0.4085	0.5142	0.2898	0.0979	0.4090	0.5194	0.2774	0.0834
-0.5	0.4100	0.5104	0.2200	0.0795	0.4114	0.5146	0.1980	0.0675
-0.4	0.4117	0.5066	0.1508	0.0610	0.4138	0.5099	0.1231	0.0514
-0.3	0.4135	0.5029	0.0841	0.0426	0.4161	0.5053	0.0537	0.0355
-0.2	0.4154	0.4993	0.0211	0.0246	0.4181	0.5007	-0.0097	0.0199
-0.1	0.4170	0.4957	-0.0375	0.0071	0.4199	0.4963	-0.0670	0.0047
0.0	0.4185	0.4921	-0.0912	-0.0098	0.4213	0.4918	-0.1179	-0.0099
0.1	0.4196	0.4885	-0.1396	-0.0262	0.4224	0.4874	-0.1620	-0.0237
0.2	0.4205	0.4850	-0.1821	-0.0418	0.4229	0.4830	-0.1993	-0.0369
0.3	0.4209	0.4814	-0.2180	-0.0566	0.4229	0.4786	-0.2289	-0.0492
0.4	0.4206	0.4778	-0.2461	-0.0705	0.4221	0.4743	-0.2498	-0.0606
0.5	0.4196	0.4742	-0.2650	-0.0835	0.4202	0.4699	-0.2610	-0.0712
0.6	0.4174	0.4705	-0.2726	-0.0952	0.4171	0.4654	-0.2608	-0.0806
0.7	0.4137	0.4668	-0.2666	-0.1056	0.4123	0.4609	-0.2475	-0.0888
0.8	0.4081	0.4629	-0.2443	-0.1140	0.4053	0.4562	-0.2193	-0.0953
0.9	0.3998	0.4587	-0.2028	-0.1199	0.3955	0.4513	-0.1745	-0.0997
1.0	0.3883	0.4541	-0.1388	-0.1224	0.3821	0.4459	-0.1112	-0.1012

ALPHA=40 DEGREES, BETA=20

	GAMMA=1				GAMMA=2			
	TENSION		BENDING		TENSION		BENDING	
S	N	T	N	T	N	T	N	T
-1.0	0.4131	0.4924	0.3260	0.0696	0.4136	0.4937	0.4039	0.0536
-0.9	0.4131	0.4924	0.3379	0.0664	0.4132	0.4930	0.3850	0.0509
-0.8	0.4131	0.4924	0.3301	0.0610	0.4130	0.4924	0.3540	0.0468
-0.7	0.4131	0.4924	0.3080	0.0543	0.4129	0.4917	0.3149	0.0417
-0.6	0.4131	0.4924	0.2761	0.0470	0.4129	0.4911	0.2704	0.0361
-0.5	0.4131	0.4924	0.2373	0.0393	0.4129	0.4904	0.2226	0.0302
-0.4	0.4131	0.4924	0.1939	0.0315	0.4130	0.4898	0.1731	0.0242
-0.3	0.4131	0.4924	0.1475	0.0236	0.4131	0.4892	0.1229	0.0182
-0.2	0.4131	0.4924	0.0992	0.0157	0.4132	0.4990	0.0727	0.0121
-0.1	0.4131	0.4924	0.0498	0.0078	0.4133	0.4983	0.0231	0.0061
0.0	0.4131	0.4924	-0.0005	0.0000	0.4134	0.4976	-0.0257	0.0001
0.1	0.4131	0.4924	-0.0498	-0.0078	0.4135	0.4970	-0.0729	-0.0059
0.2	0.4131	0.4924	-0.0992	-0.0157	0.4136	0.4963	-0.1185	-0.0120
0.3	0.4131	0.4924	-0.1475	-0.0236	0.4136	0.4956	-0.1617	-0.0180
0.4	0.4131	0.4924	-0.1939	-0.0315	0.4137	0.4950	-0.2020	-0.0241
0.5	0.4131	0.4924	-0.2373	-0.0393	0.4136	0.4943	-0.2383	-0.0301
0.6	0.4131	0.4924	-0.2761	-0.0470	0.4135	0.4885	-0.2693	-0.0361
0.7	0.4131	0.4924	-0.3080	-0.0543	0.4133	0.4879	-0.2928	-0.0418
0.8	0.4131	0.4924	-0.3301	-0.0610	0.4129	0.4872	-0.3063	-0.0471
0.9	0.4131	0.4924	-0.3379	-0.0664	0.4124	0.4865	-0.3061	-0.0513
1.0	0.4131	0.4924	-0.3260	-0.0696	0.4115	0.4858	-0.2871	-0.0537
	GAMMA=4				GAMMA=8			
-1.0	0.4129	0.5026	0.4554	0.0432	0.4123	0.5045	0.4854	0.0372
-0.9	0.4127	0.5015	0.4149	0.0410	0.4123	0.5032	0.4320	0.0354
-0.8	0.4126	0.5005	0.3684	0.0378	0.4124	0.5020	0.3763	0.0327
-0.7	0.4127	0.4994	0.3180	0.0339	0.4126	0.5007	0.3195	0.0295
-0.6	0.4128	0.4984	0.2657	0.0296	0.4128	0.4995	0.2627	0.0259
-0.5	0.4129	0.4974	0.2125	0.0249	0.4130	0.4983	0.2065	0.0220
-0.4	0.4131	0.4964	0.1595	0.0201	0.4133	0.4971	0.1516	0.0179
-0.3	0.4133	0.4953	0.1072	0.0153	0.4135	0.4959	0.0982	0.0137
-0.2	0.4135	0.4944	0.0562	0.0103	0.4137	0.4947	0.0468	0.0095
-0.1	0.4136	0.4933	0.0067	0.0054	0.4138	0.4935	-0.0025	0.0051
0.0	0.4137	0.4923	-0.0410	0.0005	0.4140	0.4923	-0.0495	0.0008
0.1	0.4139	0.4913	-0.0865	-0.00 5	0.4141	0.4911	-0.0940	-0.0036
0.2	0.4139	0.4904	-0.1295	-0.0095	0.4142	0.4900	-0.1355	-0.0080
0.3	0.4140	0.4894	-0.1696	-0.0145	0.4142	0.4888	-0.1738	-0.0124
0.4	0.4140	0.4884	-0.2062	-0.0195	0.4141	0.4876	-0.2083	-0.0169
0.5	0.4138	0.4874	-0.2382	-0.0246	0.4139	0.4865	-0.2380	-0.0215
0.6	0.4136	0.4864	-0.2646	-0.0296	0.4136	0.4853	-0.2618	-0.0260
0.7	0.4132	0.4854	-0.2833	-0.0345	0.4131	0.4842	-0.2780	-0.0305
0.8	0.4126	0.4845	-0.2921	-0.0390	0.4124	0.4830	-0.2842	-0.0346
0.9	0.4117	0.4834	-0.2874	-0.0426	0.4113	0.4818	-0.2772	-0.0378
1.0	0.4104	0.4824	-0.2647	-0.0446	0.4097	0.4806	-0.2526	-0.0396

ALPHA=40 DEGREES, BETA=100

	GAMMA=1				GAMMA=2			
	TENSION		BENDING		TENSION		BENDING	
S	N	T	N	T	N	T	N	T
-1.0	0.4131	0.4924	0.3898	0.0164	0.4132	0.4938	0.4130	0.0120
-0.9	0.4131	0.4924	0.3628	0.0156	0.4132	0.4937	0.3763	0.0114
-0.8	0.4131	0.4924	0.3304	0.0143	0.4132	0.4936	0.3370	0.0105
-0.7	0.4131	0.4924	0.2942	0.0126	0.4132	0.4934	0.2959	0.0094
-0.6	0.4131	0.4924	0.2554	0.0109	0.4132	0.4933	0.2535	0.0082
-0.5	0.4131	0.4924	0.2148	0.0090	0.4132	0.4931	0.2104	0.0069
-0.4	0.4131	0.4924	0.1729	0.0072	0.4132	0.4930	0.1669	0.0056
-0.3	0.4131	0.4924	0.1302	0.0054	0.4132	0.4928	0.1233	0.0043
-0.2	0.4131	0.4924	0.0871	0.0035	0.4132	0.4927	0.0796	0.0029
-0.1	0.4131	0.4924	0.0436	0.0017	0.4132	0.4926	0.0361	0.0016
0.0	0.4131	0.4924	-0.0004	0.0000	0.4132	0.4924	-0.0071	0.0003
0.1	0.4131	0.4924	-0.0436	-0.0017	0.4132	0.4923	-0.0500	-0.0011
0.2	0.4131	0.4924	-0.0871	-0.0035	0.4132	0.4921	-0.0924	-0.0025
0.3	0.4131	0.4924	-0.1302	-0.0054	0.4132	0.4920	-0.1342	-0.0039
0.4	0.4131	0.4924	-0.1729	-0.0072	0.4132	0.4918	-0.1752	-0.0053
0.5	0.4131	0.4924	-0.2148	-0.0090	0.4132	0.4917	-0.2152	-0.0068
0.6	0.4131	0.4924	-0.2554	-0.0109	0.4132	0.4915	-0.2537	-0.0083
0.7	0.4131	0.4924	-0.2942	-0.0126	0.4132	0.4914	-0.2902	-0.0097
0.8	0.4131	0.4924	-0.3304	-0.0143	0.4132	0.4912	-0.3239	-0.0111
0.9	0.4131	0.4924	-0.3628	-0.0156	0.4131	0.4911	-0.3537	-0.0122
1.0	0.4131	0.4924	-0.3898	-0.0164	0.4131	0.4910	-0.3782	-0.0129

	GAMMA=4				GAMMA=8			
-1.0	0.4132	0.4946	0.4254	0.0096	0.4131	0.4950	0.4318	0.0083
-0.9	0.4132	0.4944	0.3835	0.0091	0.4131	0.4947	0.3872	0.0080
-0.8	0.4132	0.4941	0.3405	0.0085	0.4131	0.4944	0.3423	0.0074
-0.7	0.4132	0.4939	0.2967	0.0077	0.4132	0.4942	0.2971	0.0068
-0.6	0.4132	0.4937	0.2524	0.0068	0.4132	0.4939	0.2519	0.0060
-0.5	0.4132	0.4935	0.2081	0.0058	0.4132	0.4937	0.2068	0.0052
-0.4	0.4132	0.4933	0.1637	0.0048	0.4132	0.4934	0.1620	0.0043
-0.3	0.4132	0.4930	0.1196	0.0037	0.4132	0.4932	0.1176	0.0034
-0.2	0.4132	0.4928	0.0757	0.0026	0.4132	0.4929	0.0737	0.0025
-0.1	0.4132	0.4926	0.0322	0.0015	0.4132	0.4927	0.0302	0.0015
0.0	0.4132	0.4924	-0.0108	0.0004	0.4132	0.4924	-0.0127	0.0005
0.1	0.4132	0.4922	-0.0533	-0.0007	0.4132	0.4921	-0.0550	-0.0005
0.2	0.4132	0.4920	-0.0951	-0.0018	0.4132	0.4919	-0.0965	-0.0015
0.3	0.4132	0.4918	-0.1362	-0.0030	0.4132	0.4916	-0.1372	-0.0026
0.4	0.4132	0.4915	-0.1764	-0.0043	0.4132	0.4914	-0.1769	-0.0038
0.5	0.4132	0.4913	-0.2153	-0.0056	0.4132	0.4911	-0.2154	-0.0049
0.6	0.4132	0.4911	-0.2527	-0.0069	0.4132	0.4909	-0.2522	-0.0062
0.7	0.4132	0.4909	-0.2880	-0.0082	0.4132	0.4906	-0.2869	-0.0074
0.8	0.4132	0.4907	-0.3204	-0.0094	0.4131	0.4904	-0.3187	-0.0085
0.9	0.4131	0.4904	-0.3489	-0.0104	0.4131	0.4901	-0.3465	-0.0095
1.0	0.4130	0.4902	-0.3721	-0.0110	0.4130	0.4899	-0.3690	-0.0100

Table F2.--Largest values of adhesive normal stress (N_{max}). Locations may be estimated from tables of stress distributions.

		Tensile Load				Bending Load (as in Fig. 7)			
α	β	γ=1	γ=2	γ=4	γ=8	γ=1	γ=2	γ=4	γ=8
5°	4	0.00760	0.01190	0.01511	0.01630	0.00706	0.01009	0.13424	0.01545
	20	0.00760	0.01127	0.01201	0.01497	0.00695	0.00769	0.00845	0.01062
	100	0.00760	0.00913	0.01016	0.01098	0.00726	0.00787	0.01194	0.01526
10°	4	0.03016	0.03019	0.04562	0.05435	0.02523	0.03346	0.03999	0.04020
	20	0.03016	0.03510	0.03881	0.04362	0.02496	0.03180	0.04041	0.05203
	100	0.03016	0.03199	0.03293	0.03263	0.03273	0.03663	0.04181	0.04827
20°	4	0.11698	0.13870	0.15437	0.15228	0.08990	0.22051	0.14061	0.17481
	20	0.11698	0.12341	0.12285	0.12388	0.10406	0.11840	0.13622	0.16518
	100	0.11698	0.11753	0.11764	0.11779	0.09635	0.10743	0.12833	0.15520
30°	4	0.25005	0.26896	0.26706	0.26979	0.20179	0.23894	0.28570	0.36331
	20	0.25005	0.25198	0.25237	0.25295	0.20080	0.23006	0.28131	0.33353
	100	0.25005	0.25010	0.25017	0.25021	0.20763	0.24443	0.26733	0.27987
40°	4	0.41318	0.42067	0.42086	0.42297	0.33036	0.38691	0.48228	0.58501
	20	0.41318	0.41361	0.41397	0.41418	0.33800	0.40391	0.45543	0.48537
	100	0.41318	0.41320	0.41322	0.41323	0.38985	0.41300	0.42537	0.43177

Table F3.--Average difference in adhesive normal and shear stresses between polynomial solutions of orders 8 and 7, or of orders 8 and 6 (latter designated by *). Multiply all entries by 10^{-7}. See notes below.

		Tensile Loading						Bending Load					
		γ=2		γ=4		γ=8		γ=2		γ=4		γ=8	
α	β	Normal	Shear	Normal	Shear	Normal	Shear	Normal	Shear	Normal	Shear	Normal	Shear
10°	4	- 4	-71	21	-72	12	- 2	-51	-57	- 4	33	-10	- 6
	20	- 7*	-15*	-12*	- 6*	2	- 4	19*	6*	17*	1*	- 5	2
20°	4	-82	-44	-35*	-60*	17	0	- 3*	13*	- 8*	4*	11	12
	20	1*	10*	-12*	- 6*	- 8	- 7	-14*	4*	-17	0	-16	- 3
30°	4	75*	24*	-35	-11	- 6	12	- 4*	0*	-52	-19	-68	-22
	20	9	2	2*	- 1*	7	6	- 4	1	0*	5*	- 5	0
40°	4	- 3*	- 5*	16	6	-14*	- 5*	5*	20*	-19	6	-46*	- 3*
	20	0*	- 5*	- 1*	0*	- 1	0	4*	0*	2*	2*	0*	0*

Notes: 1. For β = 100; α = 10,20,30,40°; γ = 2,4,8, all values are in the range 0 to $2.0(10^{-7})$
2. Values omitted where data are not available.

Table F4.--Largest difference between 8^{th}- and 7^{th}-order, or 8^{th}- and 6^{th}-order polynomial solutions for adhesive stresses.

Please note:

1. Differences are expressed as a percentage of the 8^{th}-order results.
2. Omitted entries mean data not available--see section 3.1.4 for the only information applicable to $\alpha = 5°$ cases.
3. The combination with [8-6] is designated by (*) and is a pessimistic measure because [8-7] results are often substantially closer. [8-7] combination appears in the table without (*).
4. The first value tabulated is the largest % difference for all stresses, from the largest absolute value down to one-half of this maximum.
5. When there is a second error entry followed by a value in parentheses, it means that if we extend our consideration to values a little less than half the maximum, the error is larger, as indicated. The number in parentheses shows how far down one must go in the primary tables of Appendix F to get this larger error. Interpreting these items requires consultation of the primary tables.

Tensile Loading

		γ=2		γ=4		γ=8	
α	β	Normal	Shear	Normal	Shear	Normal	Shear
10°	4	10.4	0.24	5.7 -9.0 (.021)	-0.25	-7.8	0.50
	20	-7.1*	0.08*	-8.5*	-0.13*	-3.4 8.8 (.020)	0.07
	100	-0.89*	-0.006*	-0.57*	-0.005*	0.67*	-0.005*
20°	4	2.2	-.069	1.38*	0.23*	5.5	0.10 0.21 (.207)

Table F4 (Continued)

		Tensile Loading					
		γ=2		γ=4		γ=8	
α	β	Normal	Shear	Normal	Shear	Normal	Shear
20°	20	0.2*	0.009*	0.43*	-0.02*	0.49	-0.01
	100	0.02	-0.001	0.02*	0.002*	0.01	0.001
30°	4	0.57*	-0.06*	0.45	-0.05	0.54	-0.06
	20	0.06*	0.003*	-0.21*	0.02*	-0.08*	0.004
	100	-0.006*	0.000*	-0.03*	0.001*	-0.03*	0.002*
40°	4	0.32*	0.06*	0.14*	-0.03*	-0.41*	0.10*
	20	-0.05*	0.006*	-0.07*	0.01*	-0.03	0.004
	100	-.003*	0.000*	-0.004*	0.000*	- .005*	0.000*
		Bending Load					
10°	4	-2.6	0.15	-2.4	0.17	-9.7	0.16
		8.3	0.22	-3.6			.35
		(.016)	(.082)	(.189)			(.102)
	20	5.8*	0.77*	5.7*	0.42*	1.6	0.45
		9.1					
		(.015)					
	100	-5.24*	-0.60*	-0.66*	-0.16*	2.7*	0.50*
20°	4	7.7	0.28	-3.4*	0.37*	-3.7	-0.34
	20	1.4*	0.64*	-3.9	0.73	2.9	0.96
	100	2.5	-0.59				
30°	4	-8.64*	1.1*	-3.1	.071	-2.4	1.1
	20	-2.4	0.81	-3.7*	2.4*	0.46	0.79
		-3.1					
		(-.094)					
	100	1.3	1.5	-3.6*	5.1*	3.7*	5.4*
40°	4	-5.9*	2.6*	-1.4	1.1	-2.01*	2.9*
	20	-4.2*	-4.4*	-4.4	4.8	-1.8	1.9
	100	-1.1*	-5.7*	-1.1*	6.3*	-1.1*	6.7*

Table F5.--Root-Mean-Square values for percentage differences between 8^{th}-order and lower-order polynomial solutions. (Table added in proof for convenience of user.)

The largest value of T or N in Table F1 is located and multiplied by 0.4; stresses smaller than this "cutoff" value are ignored. The difference between the Table F1 values and the available lower-order solution (7^{th}- or 6^{th}-order) are expressed as a percentage of the Table F1 values. Then the root-mean-square quantities RMSN and RMST are formed from these larger-stress percent differences:

$$RMSN = [\sum(\text{normal stress \% differences})^2/(\text{No. differences considered})]^{1/2}$$

RMST is formed similarly. These are probably the best available indices of merit of the primary results in Table F1; Table F4 is useful but excessively conservative. Omitted cases below: no comparison solutions available.

			Tension		Bending					Tension		Bending	
α	β	γ	RMSN	RMST	RMSN	RMST	α	β	γ	RMSN	RMST	RMSN	RMST
5°	20	4	13.81	0.25	19.13	0.26							
10°	4	2	2.91	0.07	2.36	0.14	30°	4	2	0.19	0.01	2.63	0.61
		4	3.65	0.15	9.29	0.12			4	0.16	0.02	1.07	0.50
		8	3.61	0.33	3.47	0.20			8	0.20	0.03	0.99	0.68
	20	2	1.80	0.04	5.46	0.38		20	2	0.02	0.00	0.69	0.51
		4	2.44	0.08	16.12	0.64			4	0.07	0.01	1.40	1.75
		8	2.29	0.04	5.97	0.31			8	0.02	0.00	0.34	0.53
	100	2	0.22	0.00	1.95	0.33		100	2	0.00	0.00	0.44	0.85
		4	0.14	0.00	0.42	0.18			4	0.01	0.00	1.15	2.86
		8	0.17	0.00	0.31	0.12			8	0.01	0.00	1.21	2.79
20°	4	2	0.06	0.05	2.64	0.23	40°	4	2	0.11	0.03	2.36	1.67
		4	0.89	0.13	2.16	0.53			4	0.04	0.01	0.54	0.67
		8	1.37	0.08	1.42	0.24			8	0.13	0.05	1.00	1.77
	20	2	0.07	0.01	0.94	0.54		20	2	0.01	0.00	1.37	2.81
		4	0.11	0.01	1.18	0.39			4	0.02	0.00	1.38	2.87
		8	0.14	0.01	1.03	0.56			8	0.03	0.00	0.54	1.15
	100	2	0.01	0.00	0.67	0.28		100	2	0.00	0.00	0.37	3.34
		4	0.02	0.00	0.52	0.20			4	0.00	0.00	0.36	3.26
		8	0.03	0.00	0.41	0.12			8	0.00	0.00	0.36	0.34

APPENDIX G

COMPUTER PROGRAM

The main computer program used in this research is given below. It is written in Fortran for the CDC 3600 computer. The dollar sign ($) is a legal statement separator for this computer; each time you encounter it, put what follows on a new card in writing for most other computers. Because of space limitations, the various auxiliary programs used in this research have had to be omitted here. These include the program for the integral equation method, and more detailed commentary on the main program.

```
      PROGRAM RITZ
      DIMENSION X(21),Y(45,1),B(177,2),X8(177,2),XI(21),Z(45,1),C(45,1)
     1,D(45,1),SIGO(21),TAUO(21),YA(21),YB(21),XA(21),XB(21),BL(21),
     2AL(21),SIGXA(21),SIGXB(21),TAVA(21),TAVB(21),TAHLA(21),T12(21),
     3TAHUA(21),TAHLB(21),TAHUB(21),SIGYUA(21),SIGYLA(21),SIGYUB(21),
     4SIGYLB(21)
      COMMON /1/ A(16000)
C     PARAMETERS OF T8E JOINT
      READ 1,I,U1,U2,HETA,H,SIGE,EAG,SME
      READ 880,ALPHA
      READ 880,BETA
      READ 880,GAMMA
      HER=BETA    $    UJ=GAMMA
C     GEOMETRY OF THE JOINT
      CCCCC=COT(ALPHA) $ CHI=2.+CCCCC $ XDIS1=CHI+CCCCC
      G=1.    $    MJ=0
      DO 895 J=1,I
  895 MJ=J+MJ
      NG=MJ*4
      NE=MJ+I+2
      ND=MJ+I
      NC=MJ+2
      NB=MJ*4-3
      NA=MJ*2-3
      NH=MJ-1
      NI=MJ+I-2
      NO=MJ-2
      NP=MJ-3
      L=I+1
      NR=MJ*3-3
      R1=1.-U1*U1
      R2=1.-U2*U2
      R3=1.-U1
      R4=1.-U2
      CSQU=CCCCC*CCCCC
      H1=(1./BETA)*(SINF(ALPHA)**2+(COSF(ALPHA)**2/EAG))/SINF(ALPHA)
      H2=(1./BETA)*COSF(ALPHA)*(1.-(1./EAG))
      HH=(1./BETA)*(SINF(ALPHA)**2+EAG*COSF(ALPHA)**2)/(SINF(ALPHA)*EAG)
      M1=0
C     GENERATION OF RITZ MATRIX COEFFICIENTS
      DO 499 MN =1,I
      EM=MN-1
      L1 =I-MN+1
      DO 495 NM = 1,L1
      EN=NM-1
```

```
      N1=0
      DO 150 KJ = 1,I
      EK=KJ-1
      I1=KJ+MN-1
      I2=I1-1
      I3=I2-1
      CCCI2=CCCCC**I2
      CCCI3=CCCI2/CCCCC
      CI1=CHI**I3
      CI2=CI1*CHI
      CI0=CI2*CHI
      CH1=(-CHI)**I3
      CH2=-CHI*CH1
      CH11=-CH2*CHI
      L2 = I-KJ+1
      DO 100 JK = 1,L2
      MM=M1+NM
      NN = N1+JK
      MM2=MM+MJ*2-3
      MM3=MM+MJ*3-3
      NN2=NN+MJ*2-3
      NN3=NN+MJ*3-3
      L3 = KJ+JK+MN+NM-3
      L4=L3-1
      J1=NM+JK-1
      J2=J1-1
      J3=J2-1
      EJ=JK-1
      IF (2*(J2/2)-J2)  71,70,71
70    AS2=0
      GO TO 73
71    AS2=2./J2
73    CONTINUE
      IF  (2*(J3/2)-J3) 91,90,91
90    AS3=0
      GO TO 93
91    AS3=2./J3
93    CONTINUE
      IF (2*(L3/2) -L3) 81,80,81
80    AL3=0
      GO TO 83
81    AL3=2./L3
83    CONTINUE
      IF(2*(L4/2)-L4) 6,7,6
 7    AL4=0
      GO TO 8
 6    AL4=2./L4
 8    IF (2*(J1/2)-J1) 2,3,2
 2    AS1=2./J1
```

```
      GO TO 4
    3 AS1=0
    4 PHI1=AL3*CCCI2
      PHI0=AL4*CCCI3
      CHI2=AS3*CHI1
      CI6=AS3*CI0
      CI5=AS2*CI2
      CH21=AS2*CH2
      CHI1=AS1*CH1
      CI3=AS1*CI1
      IF (I3) 19,20,19
   19 EI3=1./I3
      GO TO 21
   20 EI3=0
   21 CONTINUE
      EI32=EI3*0.5
      MS=MM
      NS=NN
      MM=MM-1
      NN=NN-1
      IF(MS-1) 25,390,25
   25 IF (MS-L) 27,340,330
   27 IF (NS-1) 29,390,29
   29 IF (NS-L) 31,340,33
   31 MM1=MS+MJ-2
      NN1=NS+MJ-2
      GO TO 350
   33 MM1=MS+MJ-2
      NN1=NS+MJ-3
      GO TO 350
  340 IF(NS-1) 370,390,370
  330 MM1=MS+MJ-3
      IF (NS-1) 310,390,310
  310 IF (NS-L) 315,370,320
  315 NN1=NS+MJ-2
      IF(MM1-NN1)161,161,370
  320 NN1=NS+MJ-3
      IF(MM1-NN1) 161,161,370
  350 IF(MM1-NN1) 161,161,370
  161 MSY=IPOS(MM1,NN1)
      A(MSY)=(PHI0*CSQU-CHI2)*EN*(EJ*1./I1)+R3*EK*EM*EI32*(PHI0
     1-CHI1)+HH*PHI1
  370 IF(MM-NN) 171,171,390
  171 MSY=IPOS(MM,NN)
      A(MSY)=(PHI0-CHI1)*EK*EM*EI3+(PHI0*CSQU-CHI2)*R3*EN*EJ/(2.*
     1I1)+H1*PHI1
  390 CONTINUE
      IF(MM2-NN2) 391,391,392
  391 MSY=IPOS(MM2,NN2)
```

```
      A(MSY)=UJ*EK*EM*EI3*(CI3-PHIO)+EN*EJ*UJ*(R4*0.5/I1)*(CI6-PHIO*
     1CCCCC**2)+H1*PHI1
  392 CONTINUE
      IF(MM3-NN3) 393,393,394
  393 MSY=IPOS(MM3,NN3)
      A(MSY)=UJ*EJ*EN*(1./I1)* (CI6-PHIO*CCCCC**2)+UJ*EK*EM*(R4/2)*
     1EI3*(CI3-PHIO)+HH*PHI1
  394 CONTINUE
      IF(I2) 22,23,22
   23 EI2=0
      GO TO 24
   22 EI2=1./I2
   24 IF(MS-1) 237,53,237
  237 IF(MS-L) 239,45,47
  239 IF(NS-1) 241,53,241
  241 IF(NS-L) 43,46,48
   43 MM1=MS+MJ-2
      NN1=NS+MJ-2
      GO TO 49
   45 IF (NS-1) 44,53,44
   44 IF (NS-L) 52,53,54
   52 NN1=NS+MJ-2
      IF(MM-NN1) 291,291,53
   54 NN1=NS+MJ-3
      IF(MM-NN1) 291,291,53
   46 MM1=MS+MJ-2
      GO TO 51
   47 MM1=MS+MJ-3
      IF (NS-1) 55,53,55
   55 IF(NS-L) 56,51,57
   56 NN1=NS+MJ-2
      GO TO 49
   57 NN1=NS+MJ-3
      GO TO 49
   48 MM1=MS+MJ-2
      NN1=NS+MJ-3
   49 IF(MM-NN1)291,291,292
  291 MSY=IPOS(MM,NN1)
      A(MSY)=(PHIO*CCCCC-CH21)*(U1*EJ*EM+(R3/2)*EK*EN)*EI2-H2*PHI1
  292 CONTINUE
   51 IF(MM1-NN) 401,401,53
  401 MSY=IPOS(MM1,NN)
      A(MSY)=(PHIO*CCCCC-CH21)*(U1*EK*EN+(R3/2)*EJ*EM)*EI2-H2*PHI1
   53 CONTINUE
      IF(MM2-NN3) 353,353,354
  353 MSY=IPOS(MM2,NN3)
      A(MSY)=(CI5-PHIO*CCCCC)*(U2*UJ*EJ*EM+UJ*(R4/2)*EK*EN)*EI2-H2*PHI1
  354 CONTINUE
      IF(MM3-NN2) 355,355,356
```

```
  355 MSY=IPOS(MM3,NN2)
      A(MSY)=(UJ*U2*EK*EN+UJ*(R4/2)*EJ*EM)*EI2*(CI5-PHI0*CCCCC)-H2*PHI1
  356 CONTINUE
      IF(MS-1) 455,490,455
  455 IF(MM-NN2) 491,491,492
  491 MSY=IPOS(MM,NN2)
      A(MSY)=-H1*PHI1
  492 CONTINUE
      IF(MM-NN3) 501,501,502
  501 MSY=IPOS(MM,NN3)
      A(MSY)=H2*PHI1
  502 CONTINUE
      IF (MS-L) 460,490,465
  460 MM1=MS+MJ-2
      IF(MM1-NN2) 511,511,512
  511 MSY=IPOS(MM1,NN2)
      A(MSY)=H2*PHI1
  512 CONTINUE
      IF(MM1-NN3) 521,521,522
  521 MSY=IPOS(MM1,NN3)
      A(MSY)=-HH*PHI1
  522 CONTINUE
  465 MM1=MS+MJ-3
      IF(MM1-NN2) 531,531,532
  531 MSY=IPOS(MM1,NN2)
      A(MSY)=H2*PHI1
  532 CONTINUE
      IF(MM1-NN3) 541,541,490
  541 MSY=IPOS(MM1,NN3)
      A(MSY)=-HH*PHI1
  490 CONTINUE
  100 CONTINUE
  150 N1=N1+L2
  495 N1=0
  499 M1=M1+L1
C   LOAD TERMS FOR TENSION AND BENDING LOADING
      M1=0
      DO 600 MN =1,I
      EM=MN-1
      ME =EM
      LQ=I+1-MN
      DO 590 NM = 1,LQ
      EN1=NM
      NMP=NM+1
      NM2=NM+2
      EN2=NM2
      ENP=NMP
      MM=M1+NM
      MS=MM
```

```
      MM2=MM+MJ*2-3
      MM3=MM+MJ*3-3
      MM=MM-1
  520 C1=(-CHI)**ME
      C3=CHI**ME
      C55=(1.-(-1.)**NMP)*C1/ENP
      C77=(1.-(-1.)**NMP)*C3/ENP
      C11=(1.-(-1.)**NM )*C1/EN1
      C33=(1.-(-1.)**NM )*C3/EN1
      B(MM2,1)= R1*SME*C33
      B(MM2,2)=-R1*SME*C77
      B(MM3,1)=0
      B(MM3,2)=0
      IF(MS-1) 540,590,540
  540 IF(MS-L) 550,580,560
  550 MM1=MS+MJ-2
      GO TO 565
  560 MM1=MS+MJ-3
  565 B(MM,1)=R1*SME*C11*(-1.)
      B(MM,2)=R1*SME*C55
      B(MM1,1)=0
      B(MM1,2)=0
      GO TO 590
  580 CONTINUE
      B(MM,1)=R1*SME*C11*(-1.)
      B(MM,2)=R1*SME*C55
  590 CONTINUE
  600 M1=M1+LQ
C   RITZ COEFFICIENT SYMMETRIC MATRIX INVERSION
      CALL SYMINV(NB)
C   CALCULATION OF DISPLACEMENT FUNCTION COEFFICIENTS
      DO 631 I9=1,NB
      DO 631 K9=1,M
  631 X8(I9,K9)=0
      DO 621 I8=1,NB
      DO 621 J8=1,NB
      DO 621 K8=1,M
      II8=IPOS(I8,J8)
  621 X8(I8,K8)=X8(I8,K8)+A(II8)*B(J8,K8)
      DO 641 I7=1,NB
      DO 641 J7=1,M
  641 B(I7,J7)=X8(I7,J7)
C   CALCULATION OF ADHESIVE AND BOUNDARY STRESSES
      DO 2000 M=1,2
      Y(1,1)=0
      DO 790 J=1,NB
      IF (J-NH) 705,705,710
  705 II=J+1
      Y(II,1)=B(J,M)
```

```
      GO TO 790
  710 Z(II,1)=0
      IF (J-NI) 715,715,720
  715 II=J-NO
      GO TO 730
  720 Z(L,1)=0
      IF (J-NA) 725,725,735
  725 II=J-NP
  730 Z(II,1)=B(J,M)
      GO TO 790
  735 IF (J-NR) 740,740,745
  740 II=J-NA
      C(II,1)=B(J,M)
      GO TO 790
  745 IF (J-NB) 750,750,790
  750 II=J-NR
      D(II,1)=B(J,M)
  790 CONTINUE
      K=1
      DELX=0
      DSX=0
      DX1=0
      DI=0
      NZ=NZ+1.
  795 SIGO(K)=0
      TAUO(K)=0
      SIGXA(K)=0
      SIGXB(K)=0
      TAVA(K)=0
      TAVB(K)=0
      SIGYUA(K)=0
      SIGYUB(K)=0
      SIGYLA(K)=0
      SIGYLB(K)=0
      TAHLA(K)=0
      TAHUA(K)=0
      TAHUB(K)=0
      TAHLB(K)=0
      SIG(K)=0
      TAU(K)=0
      SIY(K)=0
      X(K)=-1.+DELX
      AL(K)=-CHI+DSX
      BL(K)=CHI-DSX
      DELX=DELX+.1
      X(11)=0.001
      YA(K)=X(K)
      YB(K)=YA(K)
      XA(K)=-CHI   +DX1
```

```
      XB(K)=CHI-DX1
      XI(K)=-CCCCC+DI
      IF(XI(K) .EQ. 0) XI(K)=0.001
      DX1=DX1+XDIS1/20.
      DSX=DSX+(CHI-CCCCC)/20.
      DI=DI+CCCCC/10.
      MM=0
      DO 825  MI=1,I
      LL=I+1-MI
      MMN=MI-1
      MT=MI-2
      EM=MI-1
      DO 825 N=1,LL
      MNN=MI+N-2
      MM=MM+1
      NN=1
      NT=N-2
      EN=N-1
      MN=MI-1
      NM=N-1
C     ADHESIVE NORMAL AND SHEAR STRESS CALCULATIONS
      XCOT=X(K)**MNN*CCCCC**MN
      SIGO(K)=SIGO(K)+((Z(MM,NN)-D(MM,NN))*COSF(ALPHA)-(Y(MM,NND-C(MM
     1,NN))*SINF(ALPHA))*XCOT/(HER*R1)
      TAUO(K)=TAUO(K)+((Z(MM,NN)-D(MM,NN))*SINF(ALPHA)+(Y(MM,NN)-C(MM
     1,NN))*COSF(ALPHA))*XCOT/(EAG*HER*R1)
C     BOUNDARY STRESS CALCULATIONS FOR BOTH ADHERENDS
      YANM=YA(K)**NM
      YBNM=YB(K)**NM
      YANT=YA(K)**NT
      YBNT=YB(K)**NT
      XIMT=YANM*XI(K)**MT
      XINT=YANT*XI(K)**MN
      XAYA=YANM*((-CHI)**MT)
      YAXA=YANT*((-CHI)**MN)
      XBYB=YBNM*(CHI**MT)
      YBXB=YBNT*(CHI**MN)
      AYA=AL(K)**MT*(-H)**NM
      YAA=(-H)**NT*AL(K)**MN
      BYB=BL(K)**MT*H**NM
      YBB=H**NT*BL(K)**MN
      XYA=XA(K)**MT*H**NM
      YXA=H**NT*XA(K)**MN
      XYB=XB(K)**MT*(-H)**NM
      YXB=(-H)**NT*XB(K)**MN
      TAVA(K)=TAVA(K)+(EN*YAXA*Y(MM,NNH+EM/G*Z(MM,NN)*XAYA)/(2.M(1.+U ))
      SIGXA(K)=SIGXA(K)+(EM*XAYA*Y(MM,NN)/G+U1*EN*YAXA*Z(MM,NN))1R1
      SIGXB(K)=SIGXB(K)+(EM*XBYB*C(MM,5N)/G+U2*EN*YBXB*D(MM,NN))*UJ/R2
```

```
     0TAVB(K)=TAVB(K)+(EN*YBXB*C(MM,NN)+EM/G*D(MM,NN)*XBYB)*UJ/(2.*(1.+U
     12))
      SIGYLB(K)=SIGYLB(K)+(EN*YXB*D(MM,NN)+U2*EM*XYB/G*C(MM,NN))*UJ/R2
      SIGYLA(K)=SIGYLA(K)+(EN*YAA * Z(MM,NN)+U1*EM*AYA *Y(MM,NN)/G)/R1
      SIGYUA(K)=SIGYUA(K)+(EN*YXA * Z(MM,NN)+U1*EM*XYA *Y(MM,NN)/G)/R1
      SIGYUB(K)=SIGYUB(K)+(EN*YBB*D(MM,NN)+U2*EM*BYB*C(MM,NN)/G)*UJ/R2
      TAHLA(K)=TAHLA(K)+(EN*YAA*Y(MM,NN)+EM*AYA*Z(MM,NN)/G)/(2.*(1.+U1))
      TAHLB(K)=TAHLB(K)+(EN*YXB*C(MM,NN)+EM*XYB*D(MM,NN)/G)*UJ/(2.
     1*(1.+U2))
      TAHUA(K)=TAHUA(K)+(EN*YXA*Y(MM,NN)+EM*XYA*Z(MM,NN)/G)/(2.*(1.+U1))
     0TAHUB(K)=TAHUB(K)+(EN*YBB*C(MM,NN)+EM*BYB*D(MM,NN)/G)*UJ/2.
     1*(1+U2))
  825 CONTINUE
      K=K+1
      IF (K-22) 795,826,826
  826 CONTINUE
      NGG=ALPHA*180./3.133
      AGG=NGG
      PRINT 912,AGG,HER,UJ,I
      DO 835 II=1,NB,7
      JJ=M
 8350PRINT 836 ,II,JJ,B(II,JJ),B(II+1,JJ),B(II+2,JJ),B(II+3,JJ),B(II+4,
     1JJ),B(II+5,JJ),B(II+6,JJ)
      PRINT 840,(X(K),SIGO(K),TAUO(K),SIGXA(K),SIGXB(K),TAVA(K),TAVB(K),
     1K=1,21)
      PRINT 845,(XA(K),TAHUA(K),SIGYUA(K),K=1,21)
      PRINT 850,(XB(K),TAHLB(K),SIGYLB(K),K=1,21)
      PRINT 855,(AL(K),TAHLA(K),SIGYLA(K),K=1,21)
      PRINT 860,(BL(K),TAHUB(K),SIGYUB(K),K=1,21)
    1 FORMAT (I2,5E14.8/2E14.8)
  836 FORMAT (2HB(,I3,H,,I2,2H)=,7E17.8)
  840 FORMAT( 3X,HX,16X,4HSIGO,16X,4HTAUO,16X,5HSIGXA,16X,5HSIGXB,16X,4H
     1TAVA,16X,4HTAVB//////////(3X,7(E17.8,2X)))
  845 FORMAT (29X,2HXA,36X,5HTAHUA,32X,6HSIGYUA,///(20X,3(E17.8,20X)))
  850 FORMAT (29X,2HXB,36X,5HTAHLB,32X,6HSIGYLB,///(20X,3(E17.8,20X)))
  855 FORMAT (29X,2HAL,36X,5HTAHLA,32X,6HSIGYLA,///(20X,3(E17.8,20X)))
  860 FORMAT (29X,2HBL,36X,5HTAHUB,32X,6HSIGYUB,///(20X,3(E17.8,20X)))
  880 FORMAT(E14.8)
  912 FORMAT(1X,6HANGLE=,F2.0,3X,5HBETA=,F3.0,3X,6HE2/E1=,F2.0,3X,6HORDE
     1R=,I2)
 2000 CONTINUE
      END
C    FUNCTION FOR CONVERTING SYMM. MATRIX TO LINEAR FORM
      FUNCTION IPOS(J,K)
      IF(J-K) 10,10,11
   10 IPOS=(K*(K-1))/2+J
      RETURN
   11 IPOS=(J*(J-1))/2+K
      END
```

```
C    SYMMETRIC MATRIX INVERSION SUBROUTINE
       SUBROUTINE SYMINV (N)
       DIMENSION P(177),Q(177),IR(177)
       COMMON/1/ A(16000)
       N4=(N*(N+1))/2
       DO 10 I=1,N
    10 IR(I)=0
C      GRAND LOOP STARTS
       DO 100 I=1,N
       BIGAJJ=0.
       DO 20 J=1,N
       IF (IR(J).NE.0)  GOTO 20
       M=(J*(J+1))/2
       Z=ABSF(A(M))
       IF (Z.LE.BIGAJJ)  GOTO 20
       BIGAJJ=Z
       K=J
    20 CONTINUE
       IF (BIGAJJ.NE.0.)  GOTO 21
       PRINT 6
     6 FORMAT (19H MATRIX IS SINGULAR)
       RETURN
C      PREPARATION OF ELIMINATION STEP 1
    21 IR(K)=1
       M=(K*(K+1))/2
       Q(K)=1./A(M)
       P(K)=1.
       A(M)=0.
       L=K-1
       IF (L.LE.0)  GOTO 35
       M=(K*(K-1))/2
       DO 30 J=1,L
       M=M+1
       P(J)=A(M)
       Q(J)=A(M)*Q(K)
       IF (IR(J).NE.0)  GOTO 30
       Q(J)=-Q(J)
    30 A(M)=0.
       IF (K+1-N.GT.0)  GOTO 50
    35 L=K+1
       DO 45 J=L,N
       M=(J*(J-1))/2+K
       P(J)=A(M)
       IF (IR(J).EQ.0)  GOTO 47
       P(J)=-P(J)
    47 Q(J)=-A(M)*Q(K)
    45 A(M)=0.
    50 DO 100 J=1,N
```

```
      DO 100 K=J,N
      M=(K*(K-1))/2+J
  100 A(M)=A(M)+P(J)*Q(K)
C     END OF GRAND LOOP
      RETURN
      END
```